UNIVERSITI TEKNOLOGI MARA

STABILITY EVALUATION AND CHARACTERIZATION OF OIL-IN-WATER EMULSION USING METHYL-α-*D*-GLUCOPYRANOSIDE AND SPAN SURFACTANT SERIES WITH MOLECULAR DYNAMIC SIMULATION

MUHAMMAD AFIF SYAZANI
BIN ROZANI

MSc

February 2026

UNIVERSITI TEKNOLOGI MARA

STABILITY EVALUATION AND CHARACTERIZATION OF OIL-IN-WATER EMULSION USING METHYL-α-*D*-GLUCOPYRANOSIDE AND SPAN SURFACTANT SERIES WITH MOLECULAR DYNAMIC SIMULATION

MUHAMMAD AFIF SYAZANI BIN ROZANI

Thesis submitted in fulfilment
of the requirements for the degree of
Master of Science
(Chemistry)

Faculty of Applied Sciences

February 2026

CONFIRMATION BY PANEL OF EXAMINERS

I certify that a Panel of Examiners has met on 17 November 2025 to conduct the final examination of Muhammad Afif Syazani Bin Rozani on his Masters of Science thesis entitled "Stability Evaluation And Characterization Of Oil-In-Water Emulsion Using Methyl-α-*D*-Glucopyranoside And Span Surfactant Series With Molecular Dynamic Simulation" in accordance with Universiti Teknologi MARA Act 1976 (Akta 173). The Panel of Examiner recommends that the student be awarded the relevant degree. The Panel of Examiners was as follows:

Noraini Hamzah, PhD
Associate Professor
Faculty of Applied Sciences
Universiti Teknologi MARA
(Chairman)

Lim Ying Chin, PhD
Associate Professor
Faculty of Applied Sciences
Universiti Teknologi MARA
(Internal Examiner)

Norzahir Sapawe, PhD
Associate Professor
Institute of Chemical and Bioengineering Technology
Universiti Kuala Lumpur
(External Examiner)

PROFESSOR DR HJH ZURAEDA IBRAHIM
Dean
Institute of Postgraduates Studies
Universiti Teknologi MARA
Date: 25 February 2026

AUTHOR'S DECLARATION

I declare that the work in this thesis was carried out in accordance with the regulations of Universiti Teknologi MARA. It is original and is the results of my own work, unless otherwise indicated or acknowledged as referenced work. This thesis has not been submitted to any other academic institution or non-academic institution for any degree or qualification.

I, hereby, acknowledge that I have been supplied with the Academic Rules and Regulations for Post Graduate, Universiti Teknologi MARA, regulating the conduct of my study and research.

Name of Student	:	Muhammad Afif Syazani Bin Rozani
Student ID. No.	:	2023732259
Programme	:	Master of Science (Chemistry) – AS756
Faculty	:	Applied Sciences
Thesis Title	:	Stability Evaluation And Characterization Of Oil-In-Water Emulsion Using Methyl-α-*D*-Glucopyranoside And Span Surfactant Series With Molecular Dynamic Simulation
Signature of Student	:	.....
Date	:	25 February 2026

ABSTRACT

Oil-in-water (O/W) emulsions are widely utilized in pharmaceutical, food, and cosmetic applications for the delivery of lipophilic compounds, yet their inherent thermodynamic instability requires the use of suitable surfactants to reduce interfacial tension and enhance structural integrity. This study investigates the formulation and stability behaviour of virgin coconut oil (VCO)-in-water emulsions prepared with methyl-α-*D*-glucopyranoside (MEG), Span 20, and Span 80 as non-ionic emulsifiers. Both single-surfactant and mixed-surfactant systems were developed and tested across five temperatures (30 °C, 35 °C, 40 °C, 45 °C, and 60 °C) to assess their robustness under thermal stress. Stability evaluations were conducted using creaming index measurement, rheological profiling, droplet size distribution via optical microscopy, FTIR spectroscopy, and molecular dynamics (MD) simulations. Results indicated clear performance differences between surfactant systems. The formulation containing a 30:40:15:15 ratio of oil: water: Span 20: MEG (Sample MS20-C) demonstrated the strongest stability profile. MS20-C recorded 0% phase separation at 30 °C after 30 days, in contrast to >20% separation observed in Span 80-based emulsions. Rheological analysis revealed pronounced shear-thinning behavior, with MS20-C exhibiting the highest viscosity among all samples, suggesting stronger droplet interactions and the formation of a more structured internal network. Microscopy confirmed uniformly distributed droplets without significant coalescence or large aggregates, reinforcing its macroscopic stability. FTIR results showed enhanced O–H and C–O stretching vibrations in MEG-containing systems, indicative of stronger hydrogen bonding and a well-organized interfacial film. MD simulations further supported these findings at the molecular level: MS20-C reached equilibrium at approximately 20 ns and maintained a stable radius of gyration (3.0–3.2 × 10^6 nm), together with a moderate eccentricity value (e = 0.308), reflecting compact molecular packing and near-spherical droplet geometry. These characteristics collectively suggest reduced shape deformation and lower susceptibility to instability mechanisms such as coalescence. Overall, the integrated experimental and simulation results confirm a strong synergistic stabilization effect between Span 20 and MEG, producing emulsions with superior thermal and structural stability. The findings highlight the potential of this mixed-surfactant system for high-performance, sustainable, and temperature-resilient formulations relevant to food, cosmetic, and pharmaceutical applications.

ACKNOWLEDGEMENT

First and foremost, all praise and gratitude be to Allah, the Most Gracious and the Most Merciful, for His blessings, strength, and guidance throughout the course of my Master's journey. Without His will, none of this would have been possible. I would like to express my deepest gratitude to my supervisor, ChM. Dr. Hairul Amani Abdul Hamid, for being the backbone of my academic journey. Her continuous support, guidance, and encouragement have been instrumental in shaping both my research and personal growth. I am truly thankful for her patience, expertise, and unwavering belief in my potential. My heartfelt appreciation also goes to my co-supervisors, ChM. Dr. Nursyamsyila Mat Hadzir and Dr. Muhammad Alif Mohammad Latif. Special thanks to Dr. Muhammad Alif, who guided me in learning molecular dynamics (MD) simulation from scratch. His technical support, dedication, and clear guidance were vital in completing this work. I am also grateful to Dr. Nursyamsyila for her thoughtful insights and constructive feedback throughout the research process. To my beloved parents, thank you for your endless prayers, love, and encouragement to pursue my Master's degree. Your support has been the foundation of my strength, and I dedicate this achievement to both of you. To my dear friends, thank you for being there through thick and thin. Your understanding, motivation, and constant presence have helped me overcome many hurdles along the way. I'm truly blessed to have you all in my life. This journey would not have been possible without the support and prayers of everyone mentioned. Thank you for being a part of it.

TABLE OF CONTENTS

		Page
CONFIRMATION BY PANEL OF EXAMINERS		**ii**
AUTHOR'S DECLARATION		**iii**
ABSTRACT		**iv**
ACKNOWLEDGEMENT		**v**
TABLE OF CONTENTS		**vi**
LIST OF TABLES		**ix**
LIST OF FIGURES		**x**
LIST OF SYMBOLS		**xiii**
LIST OF ABBREVIATIONS		**xiv**
LIST OF NOMENCLATURE		**xv**
CHAPTER 1 INTRODUCTION		**1**
1.1	Research Background	1
1.2	Problem Statement	4
1.3	Research Objectives	5
1.4	Scope of Research	5
1.5	Significance of Study	6
CHAPTER 2 LITERATURE REVIEW		**8**
2.1	Emulsion	8
	2.1.1 Oil-In-Water (O/W) Emulsion	9
	2.1.2 Water-In-Oil (W/O) Emulsion	10
2.2	Virgin Coconut Oil (VCO)	11
	2.2.1 Components in VCO	13
	2.2.2 Virgin Coconut Oil as Antiviral and Antimicrobial Properties	16
	2.2.3 Medium-Chain Fatty Acids in VCO Reduce Obesity	18
	2.2.4 Antioxidant Properties in VCO	18
2.3	Surfactant	19

2.3.1 Non-ionic Surfactant 20

2.3.1.1 Methyl-α-*D*-glucopyranoside 21

2.3.1.2 Span Series 22

2.4 Stability of Emulsion 23

2.5 Freeze-Thaw Stability 25

2.6 Effect of Temperature on Emulsion 25

2.7 Molecular Dynamic Simulation 26

CHAPTER 3 RESEARCH METHODOLOGY 30

3.1 Materials and Chemicals 30

3.2 Methods 30

3.2.1 Emulsion Preparation 30

3.2.3 Creaming Index 33

3.2.5 Rheology Test 35

3.2.6 Droplet Size and Distribution 35

3.2.7 Functional Group Measurement 36

3.2.8 Simulation Methodology 36

CHAPTER 4 RESULTS & DISCUSSION 41

4.1 Stability Evaluation of Emulsion Between Single Surfactant Versus Mixed Surfactant 41

4.1.1 Creaming Index 41

4.1.2 Freeze-Thaw Stability 46

4.1.3 Rheology Test 51

4.1.4 Droplet Size Distribution 58

4.1.5 Fourier-Transform Infrared Spectroscopy (FTIR) 69

4.2 Stability Evaluation of Emulsion Against Elevated Temperatures 77

4.2.1 Creaming Index 77

4.2.2 Freeze-Thaw Stability 81

4.2.3 Rheology Test 84

4.2.4 Droplet Size Distribution 88

4.3 Molecular Dynamic Simulation 94

4.3.1 Radius Of Gyration (Rg) Analysis 95

4.3.2 Self-Assembly And Droplet Formation 99
CHAPTER 5 CONCLUSION & RECOMMENDATIONS **103**
5.1 Conclusion 103
5.2 Recommendations 105

REFERENCES 106

APPENDIX 125

AUTHOR'S PROFILE 235

LIST OF TABLES

Tables	Title	Page
Table 2.1	Fatty Acids Found in Coconut Oil	13
Table 2.2	Antimicrobial Activities Of VCO	17
Table 3.1	Emulsion Formulation Using Different Ratios of MEG	30
Table 3.2	Emulsion Formulation Using Different Ratios of Span 20	31
Table 3.3	Emulsion Formulation Using Different Ratios of Span 80	31
Table 3.4	Emulsion Formulation Using Different Ratios of Mixed Surfactant (MEG and Span 20)	32
Table 3.5	Emulsion Formulation Using Different Ratios of Mixed Surfactant (MEG and Span 80)	32
Table 4.1	Droplet Size Analysis of Oil-in-Water Emulsion Using MEG	59
Table 4.2	Droplet Size Analysis of Oil-in-Water Emulsion Using Span 20	61
Table 4.3	Droplet Size Analysis of Oil-in-Water Emulsion Using Span 80	62
Table 4.4	Droplet Size Analysis of Oil-in-Water Emulsion Using MEG and Span 20	64
Table 4.5	Droplet Size Analysis of Oil-in-Water Emulsion Using MEG and Span 80	66
Table 4.6	Observation of Virgin Coconut Oil-in-Water Emulsion Phase Separation	69
Table 4.7	Droplet Size Analysis of Oil-in-Water Emulsion	89
Table 4.8	Summary of Sample Formulations: Molar Ratios, System Densities, and Molecular Quantities (N) Of Lauric Acid (C12:0), Span 20, Span 80 and MEG	95
Table 4.9	Eccentricity Values of Four Different Emulsion Systems	96

LIST OF FIGURES

Figures	Title	Page
Figure 2.1	Oil-in-Water (O/W) Emulsion	10
Figure 2.2	Water-in-Oil (W/O) Emulsion	11
Figure 2.3	The Chemical Structures of Medium-Chain Fatty Acids (MCFAs) in VCO	14
Figure 2.4	Methyl-α-*D*-Glucopyranoside	22
Figure 2.5	Span Surfactant Series	23
Figure 4.1	Creaming Index for Single Surfactant from Day 1 to Day 30 A) MEG B) Span 20 C) Span 80	43
Figure 4.2	Creaming Index for Mixed Surfactant Using MEG and Span 20 From Day 1 to Day 30	44
Figure 4.3	Creaming Index for Mixed Surfactant Using MEG and Span 80 From Day 1 to Day 30	45
Figure 4.4	Freeze-Thaw Analysis of Single Surfactant Emulsions	47
Figure 4.5	Freeze-Thaw Analysis of Mixed Surfactant Emulsions	50
Figure 4.6	Viscosity vs Shear Rate VCO-in-Water Emulsion Using MEG	52
Figure 4.7	Viscosity vs Shear Rate VCO-in-Water Emulsion Using Span 20	53
Figure 4.8	Viscosity vs Shear Rate VCO-in-Water Emulsion Using Span 80	54
Figure 4.9	Viscosity vs Shear Rate VCO-in-Water Emulsion Using Mixed Surfactant (MEG & Span 20)	55
Figure 4.10	Viscosity vs Shear Rate VCO-In-Water Emulsion Using Mixed Surfactant (MEG & Span 80)	57
Figure 4.11	Polarized Optical Microscopy Images of Emulsions Using MEG as Surfactant A) MEG-A B) MEG-B C) MEG-C D) MEG-D	60
Figure 4.12	Polarized Optical Microscopy Images of Emulsions Using Span 20 as Surfactant E) S20-A F) S20-B G) S20-C H) S20-D	61
Figure 4.13	Polarized Optical Microscopy Images of Emulsions Using Span 80 as Surfactant I) S80-A J) S80-B K) S80-C L) S80-D	63

Figure 4.14 Optical Polarizing Microscopy Images of Emulsions Using MEG and Span 20 as Surfactants M) MS20-A N) MS20-B O) MS20-C P) MS20-D 65
Figure 4.15 Optical Polarizing Microscopy Images of Emulsions Using MEG and Span 80 as Surfactants Q) MS80-A R) MS80-B S) MS80-C T) MS80-D 67
Figure 4.16 FTIR Spectra of Virgin Coconut Oil-in-Water Emulsion MEG 70
Figure 4.17 FTIR Spectra of Virgin Coconut Oil-in-Water Emulsion Using Span 20 71
Figure 4.18 FTIR Spectra of Virgin Coconut Oil-in-Water Emulsion Using Span 80 71
Figure 4.19 FTIR Spectra of Virgin Coconut Oil-in-Water Emulsion Using MEG & Span 20 74
Figure 4.20 FTIR Spectra of Virgin Coconut Oil-in-Water Emulsion Using MEG & Span 80 75
Figure 4.21 Creaming Index O/W Emulsion Affected by Temperatures A) 30 °C B) 35 °C C) 40 °C D) 45 °C E) 60 °C 80
Figure 4.22 Freeze-Thaw Analysis of Mixed Surfactant Emulsions Affected by Temperatures 82
Figure 4.23 Viscosity vs Shear Rate VCO-in-Water Emulsion At A) 30 °C B) 35 °C C) 40 °C D) 45 °C E) 60 °C 87
Figure 4.24 Polarized Optical Microscopy Images of Emulsions at 30 °C in 20x Magnification A) MS20-C B) MS20-D C) MS80-B D) MS80-C 89
Figure 4.25 Polarized Optical Microscopy Images of Emulsions at 35 °C in 20x Magnification A) MS20-C B) MS20-D C) MS80-B D) MS80-C 90
Figure 4.26 Polarized Optical Microscopy Images of Emulsions at 40 °C in 20x Magnification A) MS20-C B) MS20-D C) MS80-B D) MS80-C 90
Figure 4.27 Polarized Optical Microscopy Images of Emulsions at 45 °C in 20x Magnification A) MS20-C B) MS20-D C) MS80-B D) MS80-C 91
Figure 4.28 Polarized Optical Microscopy Images of Emulsions at 60 °C in 20x Magnification A) MS20-C B) MS20-D C) MS80-B D) MS80-C 91
Figure 4.29 Radius of Gyration (Rg) for Four Emulsion Systems 96

Figure 4.30 Self-Assembly and Droplet Formation for A) MS20-C B) MS20-B C) MS80-B D) MS20-D Emulsions 100

LIST OF SYMBOLS

Symbols

%	Percent
°C	Degree Celsius
α	Alpha
g	Gram
mm	Millimetre
pH	Potential hydrogen
rpm	Rotation per minute
w/w	Weight per weight

LIST OF ABBREVIATIONS

Abbreviations

CMC	Critical Micelle Concentration
HLB	Hydrophilic-Lipophilic Balance
MCFA	Medium Chain Fatty Acid
O/W	Oil-in-Water
O/W/O	Oil-in-Water-in-Oil
OPM	Optical Polarizing Microscope
VCO	Virgin Coconut Oil
W/O	Water-in-Oil

LIST OF NOMENCLATURE

Nomenclatures

APEO	Alkylphenol Ethoxylate
MEG	Methyl-α-*D*-Glucopyranoside
Span 20	Sorbitan Monolaurate
Span 80	Sorbitan Monooleate

CHAPTER 1
INTRODUCTION

1.1 Research Background

Emulsions are important systems have a long history of usage in a variety of sectors, including medicine, cosmetics, and food, as well as other practical applications such as oil recovery and the development of innovative soft materials. An emulsion is a mixture of two immiscible liquid phases, one of which is dispersed into the other. An emulsion is primarily composed of a continuous phase, known as the external phase, in which the droplets are distributed, and a dispersed phase, known as the internal or discontinuous phase.

In general, a simple emulsion is made up of either water droplets embedded in a continuous aqueous phase (water-in-oil (W/O) emulsion) or oil suspended in an aqueous phase (oil-in-water (O/W) emulsion). Surfactants (emulsifying agents) with affinities for both phases are used to stabilize emulsions, this lowers the energy needed to establish new surfaces between the two phases, which is referred to as interfacial surface tension (Bajpai, 2018). Fenton *et al.* (2021) has described that surfactants or surface- active agent, which are described as amphiphilic compounds that bind to surfaces, are required when the two phases become more compatible with one another, resulting in wetting or emulsification owing to surface tension decrease.

The interactions between surface-active agents and the water–oil interface are fundamental in governing emulsion stability. Such stability is influenced by several parameters, including the production technique, the type and concentration of emulsifiers, temperature, and the pH of the continuous medium (Zheng et al., 2020). As mentioned by Solans et al. (2016), the intrinsic immiscibility of the liquid–liquid system gives rise to interfacial tension at the boundary between the two phases, rendering emulsions thermodynamically unstable. To address this instability, emulsifying agents with dual affinities for the aqueous and oil phases are employed. These agents reduce the energy required to generate new interfacial areas, thereby lowering interfacial surface tension and contributing to the stabilization of the dispersed droplets. Despite emulsifier incorporation, emulsions remain susceptible to progressive destabilization. Emulsion aging is driven by several physicochemical processes, including interfacial

film drainage, gravity-induced separation phenomena such as creaming and sedimentation, as well as flocculation, coalescence, and Ostwald ripening or coarsening. These mechanisms, comprehensively discussed by Ravera et al. (2021), collectively determine the long-term stability and structural evolution of emulsified systems.

Non-ionic surfactants excel in emulsifying oils and surpass anionic surfactants in removing organic soils. When combined, these surfactants form versatile cleansers capable of lifting particulate soils and emulsifying greasy residues. Non-ionic surfactants exhibit superior emulsification capabilities and are resistant to the challenges posed by hard water, making them indispensable in detergent and emulsifier formulations (Kim, 2021). While anionic surfactants are effective, they come with drawbacks, such as the potential to cause skin irritation, particularly for individuals with sensitive skin. In contrast, non-ionic surfactants are gentler, making them suitable for use in personal care products (Mijaljica *et al.*, 2022). Anionic surfactants also raise environmental concerns due to lower biodegradability and compatibility issues with certain ingredients. The tendency of anionic surfactants to leave residues on surfaces further complicates their application. Striking a balance between the advantages and disadvantages of anionic surfactants requires meticulous formulation to ensure optimal performance while minimizing potential adverse effects (Badmus *et al.*, 2021).

Methyl-α-*D*-glucopyranoside (MEG), a derivative of glucose, finds common use in carbohydrate chemistry as a compound that can serve as a model for more intricate carbohydrates. While it may not function as a typical surfactant by itself, its derivatives or related compounds may exhibit surfactant properties. Glycosides, which originate from natural sources like sugars, are particularly appealing for surfactant applications due to their biocompatibility, making them suitable for inclusion in cosmetics and pharmaceutical products. Compared to certain synthetic alternatives, glycoside surfactants are generally milder, making them well-suited for use in personal care items. Additionally, the renewable sourcing of many glycosides contributes to sustainability efforts, and their tendency to biodegrade effectively further reduces environmental impact. Some glycoside surfactants also boast excellent foaming properties, making them ideal for formulations like foaming cleansers and shampoos. The choice of surfactant ultimately depends on the specific application and desired product characteristics, and glycoside surfactants offer a combination of effectiveness, mildness, and environmental friendliness in certain scenarios, as emphasized by Stubbs et al., (2022).

The term "Span series" commonly denotes a category of non-ionic surfactants recognized as Span surfactants, which are integral to the broader Span-Tween series renowned for their emulsifying capabilities, as elucidated by Jog and Burgess in 2018. Span surfactants are comprised of sorbitan fatty acid esters, arising from the esterification process of sorbitan with diverse fatty acids, giving rise to distinct members within the Span series. These surfactants typically display lipophilic properties, showcasing a pronounced attraction to oil, positioning them as a preferred lipophilic component in emulsification systems, as underscored by Zheng *et al.* (2022). A noteworthy attribute of Span surfactants lies in their adeptness at stabilizing oil-in-water emulsions. This is achieved through the formation of a monolayer at the interface between oil and water, effectively mitigating interfacial tension and impeding the coalescence of oil droplets. The applications of Span surfactants are diverse and extend across various industries, including food, pharmaceuticals, cosmetics, and textiles, where the establishment and preservation of stable emulsions are imperative, as discussed in the research by Khoee & Yaghoobian (2017).

Nebogina et al., (2020) has considered that the temperature has a significant influence on emulsion stability. Temperature influences the physical properties of oil, water, interfacial coatings, and surfactant solubilities in the oil and water phases. These, in turn, have an effect on the stability of the emulsion.

Because of its more functional activities, VCO has become widely employed in the food, pharmaceutical, and cosmetic sectors in recent years. VCO has received a lot of interest in recent years due to its medicinal potential. VCO contains biological activities such as antioxidant, anti-inflammatory, antibacterial, and antiviral properties, as well as potential therapeutic benefits on numerous chronic degenerative disorders (Mohammed *et al.*, 2021). These saturated fatty acids include a high concentration of medium chain triglycerides (MCTs), which include caprylic acid, capric acid, and lauric acid. These MCTs are 'unique' due to their physicochemical properties, which include shorter chains and a lower molecular weight compared to long-chain triglycerides (LCT) allowing them to be absorbed and hydrolyzed faster in the body, resulting in faster oxidation and higher energy production (Nurhadi *et al.*, 2022). Therefore, the purpose of this study is to determine the stability of oil-in-water emulsion using VCO as an oil phase and mixed surfactants as stabilizers.

1.1 Problem Statement

While numerous studies have explored the use of individual surfactants for oil-in-water emulsions, limited attention has been given to the stability challenges specific to virgin coconut oil (VCO) emulsions. Existing formulations often rely on single surfactants or conventional emulsifiers such as the Tween series, which may not provide optimal performance due to their high hydrophilic-lipophilic balance (HLB) values and steric limitations, especially when interacting with medium-chain triglycerides present in VCO (Rukmini *et al.*, 2012). Stabilizing virgin coconut oil (VCO)-in-water emulsions remains a major challenge due to the high interfacial tension between the oil and aqueous phases, as well as the structural complexity of VCO, which is rich in medium- chain triglycerides. The selection of an appropriate surfactant system is critical to reduce interfacial tension and form a stable interfacial film. However, the use of individual surfactants such as methyl-α-*D*-glucopyranoside (MEG), Span 20 (sorbitan monolaurate), or Span 80 (sorbitan monooleate) often results in poor droplet dispersion, large droplet sizes, and weak interfacial film formation. These issues arise due to the fixed HLB values and limited molecular adaptability of single-component systems, which are insufficient to meet the dual demands of hydrophilic and lipophilic interactions required in VCO emulsions (Ramli *et al.*, 2019).

Alternative surfactants such as the Tween series (e.g., Tween 20 or Tween 80) offer high HLB values and are commonly used in oil-in-water emulsions. However, their long polyethylene glycol (PEG) chains introduce steric bulk, which can hinder effective packing at the oil–water interface. Additionally, the high hydrophilicity of Tweens may not be ideal for medium-chain triglyceride-rich oils like VCO, often leading to unstable or loosely packed interfacial films (Mahdi *et al.*, 2011).

Amaliyah et al. (2024) have reported that employing a mixed-surfactant system provides a promising alternative to overcome these limitations. By combining surfactants with different HLB values and molecular structures such as MEG with Span 20 or Span 80, it is possible to achieve synergistic effects that enhance interfacial film strength, optimize HLB for the specific emulsion system, and improve overall droplet stability. This strategy is particularly relevant for natural oil emulsions like VCO, where both interfacial and bulk phase interactions must be carefully balanced to achieve long-term stability.

Therefore, thorough research should be done on the kind of surfactant utilized and its concentration in the emulsion system. It is essential to evaluate how temperature affects emulsion stability. To ascertain the best conditions to stabilize the emulsion, this research evaluates the effect of temperature and different surfactants on the stability of oil-in-water (O/W) emulsion.

1.2 Research Objectives

The aims of this study are as follows:

a) To determine the oil-in-water emulsion with the highest stability using methyl-α-*D*-glucopyranoside, Span 20 and Span 80 surfactants
b) To characterize the oil-in-water emulsion prepared using mixed surfactants at different temperatures (30 °C, 35 °C, 40 °C, 45 °C, and 60°C) using creaming index, rheology, droplet size and distribution and functional group measurements
c) To determine the stability of oil-in-water emulsion prepared using mixed surfactant via molecular simulation method (radius of gyration and eccentricity)

1.3 Scope of Research

This study focuses on the development and evaluation of virgin coconut oil (VCO) oil-in-water (O/W) emulsions stabilized using mixed non-ionic surfactants, specifically methyl-α-D-glucopyranoside (MEG), Span 20, and Span 80. The work is limited to the formulation of selected emulsion systems prepared using these surfactant combinations, without extending to other classes of surfactants or alternative oil phases. The characterization of emulsion stability is confined to laboratory-scale analyses conducted at controlled temperatures of 30 °C, 35 °C, 40 °C, 45 °C, and 60 °C. Stability assessment encompasses physical and structural evaluations using creaming index measurements, rheological analysis, droplet size and distribution profiling, and functional group identification. The study does not cover long-term storage stability or large-scale production behavior.

In addition to experimental work, molecular dynamics simulations are performed on selected mixed-surfactant emulsion systems to provide molecular insight into their structural stability. The simulation component is restricted to evaluating structural parameters such as radius of gyration and eccentricity, and does not attempt to model full-scale macroscopic behavior.

Overall, this study is limited to understanding how specific mixed non-ionic surfactant systems influence the stability and structural characteristics of VCO-based O/W emulsions under controlled laboratory conditions.

1.4 Significance of Study

This study contributes to the advancement of VCO-in-water emulsion formulation by investigating a mixed-surfactant system consisting of MEG, Span 20, and Span 80. VCO, which is rich in medium-chain triglycerides (MCTs), is widely applied in food, pharmaceutical, nutraceutical, and cosmetic products, yet its emulsification requires a well-tailored interfacial system. The combination of MEG with Span 20 and Span 80 provides a more flexible and synergistic approach than single-surfactant systems. MEG, although not a classical surfactant, acts as a hydrophilic co-surfactant that enhances dispersion and hydrogen bonding in the aqueous phase. Span 20 and Span 80, both non-ionic surfactants with different HLB values, contribute complementary lipophilic anchoring and interfacial flexibility. Adjusting their ratios enables fine-tuning of the overall HLB to meet the emulsification needs of VCO, resulting in improved droplet size distribution, stronger interfacial films, and enhanced emulsion stability. This approach overcomes the inherent limitations of using a single surfactant with fixed HLB characteristics.

Furthermore, this study contributes to the theoretical understanding of surfactant behavior at the molecular level through molecular dynamics (MD) simulations. These simulations provide detailed insights into the arrangement, interaction energy, and packing behavior of surfactant molecules at the oil–water interface. Such molecular-level understanding is crucial for bridging the gap between empirical formulation and mechanistic design, offering a rational basis for selecting and optimizing surfactants in complex emulsion systems.

The outcomes of this research are also of practical importance. By utilizing safe, non-ionic, and Generally Recognized As Safe (GRAS)-status surfactants, the formulation strategy aligns with regulatory and consumer safety standards. The approach proposed in this study supports the development of stable, cost-effective, and scalable emulsions, which are essential for commercial products that require consistent performance, such as creams, beverages, or therapeutic delivery systems. Moreover, given the increasing demand for natural and plant-based ingredients, particularly in Southeast Asia where VCO is abundantly produced, this study contributes to the

valorization of local resources in high-value formulations.

In summary, this study advances both the scientific and practical aspects of emulsion technology by introducing a novel surfactant combination, providing molecular insight into interfacial behavior, and offering a formulation strategy that can be adapted for industrial use. It fills an important research gap by focusing on VCO, a natural oil with specific formulation challenges, and highlights the importance of surfactant synergy in achieving stable, functional emulsions.

CHAPTER 2
LITERATURE REVIEW

2.1 Emulsion

An emulsion is a composition of two immiscible liquid phases, one of which is disseminated into the other. An emulsion is mainly composed of a continuous phase, known as the external phase, where the droplets are distributed, and a dispersed phase, known as the internal or discontinuous phase (Akbari and Nour, 2018; Zheng *et al.*, 2020). Emulsions are systems of significant interest in a wide range of applied industries, including medicines, cosmetics, and foods, as well as other practical uses such as oil recovery and the production of novel nano-structured soft materials (Ravera *et al.*, 2021). There are several types of emulsions that have been used in manufacturing industries which are oil-in-water (O/W), water-in-oil (W/O) and multiple emulsions either oil-in-water-in-oil (O/W/O) or water-in-oil-in-water (W/O/W).

Homogenization is the process of combining two immiscible liquids to form an emulsion, and a homogenizer is a mechanical device commonly employed in this process. This homogenization process is classified into two types: primary and secondary homogenization. The former is described as the conversion of two bulk liquids into an emulsion, whilst the latter is defined as the decrease of droplet size in an existing emulsion (Bakry *et al.*, 2016).

Since the emulsion is always used as a primary ingredient in a variety of food products, its consistency must be observed. According to Wiyani *et al.* (2020), when an emulsion becomes more stable, its qualities become more difficult to alter over time. It is becoming more difficult for industries to generate stable emulsions since emulsions are typically unstable systems in terms of thermodynamics. This is due to the fact that liquid/liquid immiscibility causes an interfacial tension between the two liquid phases, making these structures thermodynamically unstable. Emulsifiers have been created to improve emulsion stability and to help in the creation of emulsions. Emulsifiers in emulsions operate as a surface-active molecule, rapidly adsorbing to the surface of the droplets of the oil given during homogenization (Yani *et al.*, 2018).

A simple emulsion is composed of either water droplets embedded inside a continuous aqueous phase, referred to as a water-in-oil (W/O) emulsion, or oil suspended in an aqueous phase, referred to as an oil-in-water (O/W) emulsion. The emulsion can be diluted using the same substance that was used in the continuous phase. Mayonnaise, a W/O emulsion, is diluted with cooking oil; milk, an O/W emulsion, is diluted with milk. Emulsions are stabilized using surfactants (emulsifying agents) that have affinities for both phases; this reduces the energy required to form new surfaces between the two phases, which is referred to as the interfacial surface tension. Because of the absence of emulsifier or surfactant, the emulsion can be unstable and breakdown easily within a minute (Bajpai, 2018; Niu *et al.*, 2023).

2.1.1 Oil-In-Water (O/W) Emulsion

According to Ng *et al.* (2014), oil-in-water (O/W) emulsion is a system that composed of three parts consisting of oil phase which considered as hydrophobic fat, an aqueous phase, and a surface-active compound interface that links the two phases as shown in Figure 2.1. The chemical composition of an oil-in-water emulsion differs from that of a water in oil emulsion, each is most successfully utilized in different goods. Oil-in-water emulsions is the foundation of water-based goods, in the pharmaceutical business, they may be found in creams such as moisturizers and topical steroid treatments. Since they are simple to make, have high thermodynamic stability, and promote the solubilization of lipophilic medications, oil-in-water emulsions appear to be a good approach for improving skin penetration of lipophilic pharmaceuticals (Hiranphinyophat *et al.*, 2021).

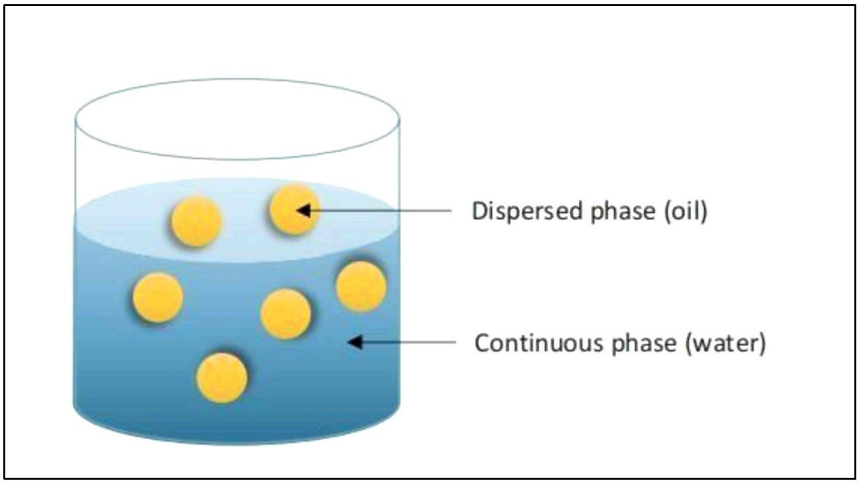

Figure 2.1 Oil-In-Water (O/W) Emulsion

2.1.2 Water-In-Oil (W/O) Emulsion

Water-in-oil (W/O) emulsion is attributed to water droplets distributing in an oil phase (Bakry *et al.*, 2016) as shown in Figure 2.2. W/O emulsion can be beneficial in some sectors such as food, pharmaceutical and cosmetic industries as this type of emulsion can be helpful in some ways. Colucci et al. (2020) has studied this form of emulsion, for example, can be used to encapsulate pharmaceuticals, immobilize enzymes, and load protein therapeutics. This structure lends itself to the transfer of hydrophilic chemicals, which can then provide various functions to the emulsified system, such as antibacterial and antioxidant activity. The primary difficulty with emulsion technology is that they are thermodynamically unstable systems.

According to Colucci *et al.* (2020), since it has high mobility of water droplets that triggers sedimentation, coalescence and flocculation, the W/O emulsion basically has lower stability than its counterpart O/W emulsion. Moreover, only steric effects can be anticipated to ensure the stability of this kind of emulsion due to the poorer electrical conductivity in oil continuous phase.

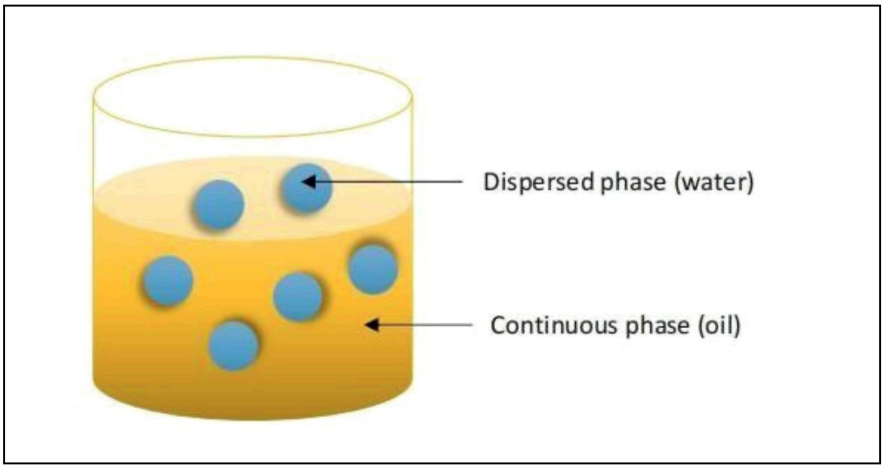

Figure 2.2 Water-In-Oil (W/O) Emulsion

2.2 Virgin Coconut Oil (VCO)

Virgin coconut oil (VCO) is an oil extracted from *Cocos nucifera L.* commonly referred to as "the tree of life" corresponds to the *Arecaceae* family (palm) (Lukić *et al.*, 2016; Srivastava *et al.*, 2018). It is one of the most essential plants, being utilized for countless purposes globally. It is the only species of the genus *Cocos* that is known to have a tall trunk that may reach a height of 30 meters, pinnate leaves that are 4-6 metres long, and pinnae that are 60-90 cm long. Old leaves easily fall off, keeping the trunk smooth (Lima *et al.*, 2015). It is also known as fresh and matured coconut kernel utilized by mechanism and natural techniques. No heating process was implicated to maintain the nature of the oil (Mathew *et al.*, 2011).

VCO was identified to be a colorless oil retained its nutritional value with a mild coconut scent by not refining, bleaching, and deodorizing. The phrase "cold extraction" refers to the process of extracting coconut oil from coconut milk without heating it (Agarwal, 2017). The high stability of the coconut milk emulsion necessitates the destabilization of coconut milk, which may be accomplished in three phases. The action of gravity force separates cream in the first step, resulting in two phases, the top phase with the creamy layer and the bottom phase with the watery layer. The second stage is flocculation and clustering, which involves the oil phase moving as a group without rupturing the interfacial coating that ordinarily covers it. The third step is the most crucial in the destabilization of coconut milk, coalescence (Rohman *et al.*, 2021).

During this stage, the interfacial regions are ruptured and reduced, which aids in the joining of oil globules. This approach looks to be more appealing due to the elimination of the solvent and refining, bleaching, and deodorizing processes, which may minimize the investment cost and energy needs, making it more ecologically friendly than solvent extraction (Agarwal, 2017).

Chilling, freezing, and thawing break the stability of the coconut milk emulsion in this process, and thawed cream is separated by centrifugation. To enable for better packing of the coconut oil globules, the emulsion was centrifuged before chilling and thawing (Raghavendra and Raghavarao, 2010). The chilling and freezing processes were carried out at temperatures of 10 °C and -4 °C, respectively, while the thawing procedure was carried out in a water bath at 40 °C until the coconut cream reached room temperature (25 °C) (Prasanna *et al.*, 2024). Furthermore, this action aids in the removal of undissolved materials during extraction. The elimination of particles present in high percentages in the dispersion of oil seed was critical for successful oil recovery by centrifugation.

Some studies have stated that because of a general prejudice against saturated fats, information about VCO has been kept hidden in medical journals. VCO has been shown to have the potential to protect against not only heart disease but a wide variety of chronic health problems including diabetes and cancer as well as a means to prevent and even treat infectious diseases (Boateng et al., 2016; DebMandal and Mandal, 2011).

2.2.1 Components in VCO

The primary triglyceride components of VCO were revealed to be dicapricmonolaurin (14.32%), dilauricmonocaprin (18.59%), trilaurin (21.88%), dilauricmonomyristin (17.20%), and dimyristicmonolaurin (9.62%) (Ghosh et al., 2014). Since medium-chain triglycerides (MCT) are completely hydrolyzed by the pancreatic enzyme lipase into glycerol, monoglycerides, and medium chain fatty acids (MCFA)s molecules are very easily absorbed by the body (Jadhav and Annapure, 2023). Medium chain monoglycerides (MCMs), such as monocaprylin, monolaurin, monocaprin, and monomyristin, are compounds with a single carbon chain length varying from 8 to 14 atoms in the acyl groups (Jack *et al.*, 2022). Caproic acid, caprylic acid, capric acid, lauric acid, and myristic acid are among the MCFAs in VCO (Gondokesumo *et al.*, 2022; Jack *et al.*, 2022). Table 2.1 and Figure 2.3 show fatty acids and their chemical structures found in coconut oil, respectively.

Table 2.1

Fatty acids found in coconut oil

	Medium-chain Fatty Acid (MCFA)	Molecular Formula	Fatty Acids Found (%)
a)	Caprylic acid (C -8:0)	$C_8H_{16}O_2$	8%
b)	Capric acid (C-10:0)	$C_{10}H_{20}O_2$	7%
c)	Lauric acid (C-12:0)	$C_{12}H_{24}O_2$	49%
d)	Myristic acid (C-14:0)	$C_{14}H_{28}O_2$	8%
e)	Palmitic acid (C-16:0)	$C_{16}H_{32}O_2$	8%
f)	Stearic acid (C-18:0)	$C_{18}H_{36}O_2$	2%
g)	Oleic acid (C-18:1)	$C_{18}H_{34}O_2$	6%
h)	Linoleic acid (C-18:2)	$C_{18}H_{32}O_2$	2%

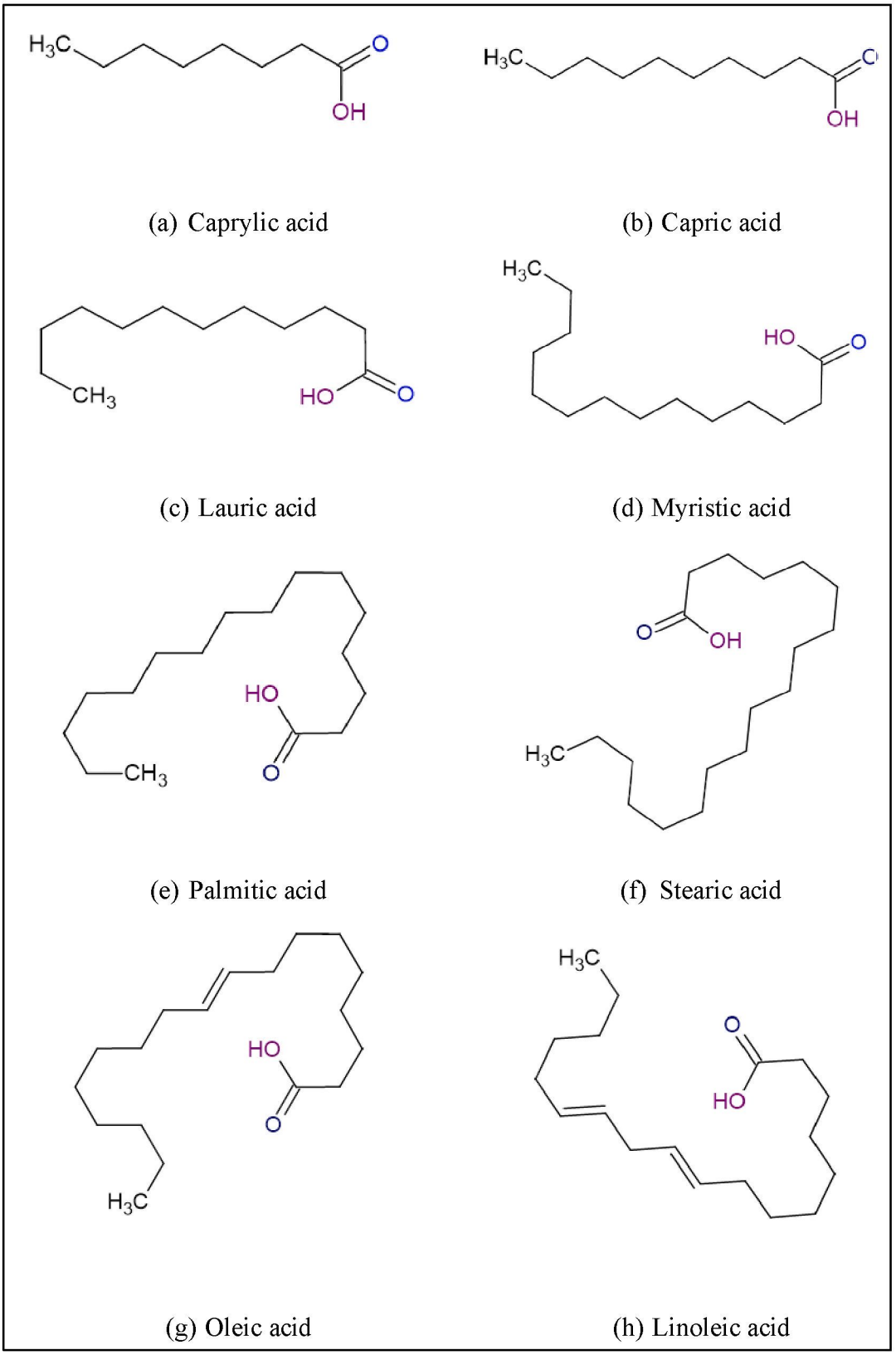

Figure 2.3 The chemical structures of medium-chain fatty acids (MCFAs) in VCO

MCMs and MCFAs are bioactive forms of MCTs with a wide range of pharmacological properties that can aid in enhancing the immune system, treating conditions like inflammatory, gastrointestinal (Parrish, 2017), and cardiovascular diseases, and having the power to combat a wide range of bacterial, fungal, and viral infections (Joshi, 2020; Subroto & Indiarto, 2020).

Since VCO contains rich medium-chain fatty acids (MCFAs), which are first digested or metabolized in the body from carbohydrates and can help reduce appetite. As a result, people consume fewer carbs and help obesity reduction by increasing metabolism rates when ingesting in the liver (Hee *et al.*, 2017; Suryani *et al.*, 2020). That MCFAs do not participate in the creation and transport of cholesterol because VCO is rich in medium chain saturated fatty acids (lauric acid), which allow them to be immediately absorbed from the intestine and transported straight to the liver to be quickly utilized for energy generation (Roopashree *et al.*, 2021). Developing nations in West Africa that are coping with the nutrition shift and its accompanying rise in chronic diet-related diseases such as obesity and heart disease might benefit from coconut oil's cardioprotective properties (Boateng *et al.*, 2016; DebMandal & Mandal, 2011).

VCO, also known for its polyphenolic content, has a cardioprotective impact that can be helpful by decreasing lipid components, enhancing antioxidant enzymes, and lowering lipid peroxide levels (Hee *et al.*, 2017). VCO can also be utilized as an antioxidant and has an effect on healing after an ovariectomy (Abujazia *et al.*, 2012). VCO can also help to lower blood pressure (Mozaffarian *et al.*, 2016; Nurul-Iman *et al.*, 2013). Moreover, VCO can be utilized as an external medicament for cosmetics, such as wound medicine, and as a probiotic (Suryani *et al.*, 2020).

Because of its therapeutic significance, VCO has sparked a lot of attention in recent years (Dumancas G *et al.*, 2016). On a daily basis, consumers are becoming more aware of the value of organic, non-chemically produced edible oils (Mohammed *et al.*, 2021). Many consumers, however, dislike the texture of VCO since it includes saturated fatty acids that are solid at ambient temperature. A revised VCO formulation was recently created to improve its appeal and stability, as well as to lessen the oily taste and texture of VCO. Such a kind is formed into VCO in the form of an emulsion, which serves both the VCO-producing industries and the VCO-consuming industries (Wiyani *et al.*, 2020).

2.2.2 Virgin coconut oil as antiviral and antimicrobial properties

VCO has been reported to have antibacterial, antiviral, antinociceptive, and anti-inflammatory properties (Varma *et al.*, 2019; Zakaria *et al.*, 2011). Lauric acid, a primary fatty acid in VCO, is responsible for its potent antiviral and antibacterial properties (Dayrit, 2015). The lipid membrane of bacteria can be destroyed by monolaurin, which can be produced from the lauric acid in VCO (Nitbani *et al.*, 2022). This feature of VCO was therefore shown to function as a natural food preservative by destroying microorganisms. According to reports, immersing chicken meat in VCO can increase the protein content and shelf life of the meat while lowering the moisture content and bacterial colony count. The shelf life of chicken meat kept at room temperature has been extended by soaking it for two hours in VCO (Srivastava *et al.*, 2018).

Three primary pathways may be used to categorize the antibacterial activity of lauric acid, monolaurin, and various ester derivatives: 1) interference with biological functions including signal transmission and transcription, 2) destruction of gramme positive bacteria and lipid-coated viral cell membranes through physicochemical mechanisms, and 3) stabilization of human cell membranes. The existence of these many pathways may be one of the factors preventing bacteria from developing a tolerance to these substances' effects (Dayrit, 2015).

Monolaurin has been demonstrated to reduce the transcription of Toxic shock syndrome toxin-1 (TSST-1) and anti-hemolysin (thus reducing virulence), and also hinders induction of beta-lactamase production (thus inhibiting antibiotic resistance) (Touaitia *et al.*, 2025). The bacterial cell membrane's surface receives signals that activate the transcription of virulence proteins and antibiotic-resistance genes (Beceiro *et al.*, 2013). Touaitia *et al.* (2025) have stated that gram-negative cell membranes are thicker because they are formed of a thick coating of lipopolysaccharide, which allows lipophilic free fatty acids (FFAs) to easily mix into them. Gram-positive cell membranes have a thinner fat layer, but monolaurin, a non-ionic surfactant with polar and hydrophobic sides, can damage and lyse them as well. Exoproteins are produced by bacterial cells through membrane-associated procedures. By disrupting the cell

membrane, monolaurin disrupts this stage (in which external metabolites activate signal transduction receptors on the cell membrane, which in turn activate exoprotein genes).

Another mechanism of action is to simply prevent biofilm formation from occurring, if that is the bacteria's mode of operation, by acting as a surfactant on the vulnerable substratum, such as a catheter/stent/prosthetic, and preventing bacteria from laying down the initial lipid-rich biofilm (Bhatt, 2021). Table 2.2 summarizes the antimicrobial activities of VCO.

Table 2.2
Antimicrobial activities of VCO

No.	Microorganism tested	Activity	References
1.	*Staphylococcus aureus*	Lactic acid has a synergistic impact in the presence of lauric acid and monolaurin, which is assumed to be owing to enhanced fatty acid absorption into the membrane, leading in membrane disruption.	(Tangwatcharin & Khopaibool, 2012)
2.	*Staphylococcus aureus, Salmonella thypi* and *Escherichia coli*	Saponification or an enzymatic process converts fat into fatty acids and monoglycerides. Hydrolysis by the enzyme lipase (lipozyme) or partial hydrolysis of VCO boost bacterial inhibition.	(Silalahi & Suryanto, 2014)
3.	*Enterococcus faecalis*	Restricting biofilm growth as indicated by fewer viable biofilm-associated microorganisms and lower biofilm biomass	(Hess *et al.*, 2015)
4.	*Clostridium diffificile*	It is metabolized by digestive lipases, releasing specific fatty acids and eventually limiting the development of microbes in vivo.	(Shilling *et al.*, 2013)
5.	*Clostridium perfringens*	N/A	(Skřivanová *et al.*, 2005)
6.	*Staphylococcus aureus, Streptococcus pneumoniae, Escherichia coli, Salmonella species* and *Mycobacterium tuberculosis.*	N/A	(Anzaku *et al.*, 2017)

2.2.3 Medium-chain fatty acids in VCO reduce obesity

A research study has stated that obesity is linked to a persistent low-grade inflammation state and is a risk factor for inflammatory and metabolic illnesses (Ströher *et al.*, 2020). Obesity is caused by a variety of variables, including genetics, lifestyle choices, environmental exposures, and microbiome, but one of the most important is still nutrition, both in terms of the quantity and type of calories ingested (Deol *et al.*, 2015). Low-fat diets, physical exercise, and medication are the most regularly employed techniques for the treatment of obesity and subsequent illnesses (Makris & Foster, 2011). Nonetheless, medication is frequently accompanied with negative side effects (Kang & Park, 2012). In this regard, it has been looking for some dietary substances, such as polyphenols and specific fatty acids, that have the ability to treat obesity-related metabolic diseases by laying down the first lipid-rich biofilm (Ströher *et al.*, 2020).

Coconut oil appears to aid in weight loss and the improvement of metabolic markers related to obesity (Vogel *et al.*, 2020). Because of its short chain length, MCFA is easily hydrolyzed and absorbed participating in cholesterol transport and providing a fast source of energy (Babu *et al.*, 2014). MCFA enters the portal circulation after absorption in the proximal intestine and is delivered to the liver bound to albumin (Schopfer *et al.*, 2025). A tiny fraction remains in the circulation and is accessible to peripheral tissues, rather than being stored in adipocytes. After being transported across the mitochondrial membrane by acyl-CoA synthetases, MCFA are mostly employed in hepatic-oxidation (He *et al.*, 2024).

2.2.4 Antioxidant properties in VCO

Coconut oil differs from other seed oils in that it contains the skin of the coconut kernel, known as 'coconut testa,' which contributes significantly to the oil's phenol content (Srivastava *et al.*, 2018). Because the solubility of polar phenolic compounds in non-polar coconut oil improves at high temperatures, VCO is projected to have higher phenolic-dependent antioxidant capabilities than copra oil (Seneviratne *et al.*, 2009). Caffeic acid, p-coumaric acid, and ferulic acid are phenolic chemicals found in VCO (Sundrasegaran & Mah, 2020), while syringic acid was not found in refined bleached deodorized coconut oil (Seneviratne & Dissanayake, 2008) .

The antioxidant capability of plants is directly related to their phenolic content. VCO has been researched for its antioxidative properties, which include impacts on many antioxidant pathways in the body. The antioxidant activity of specific compounds and extracts of natural products (such as coconut oil) is typically measured using both chemical and automated assays and technologies (Shahidi & Zhong, 2015), which include examining the scavenging properties of various free radicals/reactive oxygen species as well as chelation and reducing properties (Bhatt, 2021; Seneviratne & Dissanayake, 2008; Som *et al.*, 2019).

2.3 Surfactant

Surface-active agents, commonly known as surfactants, are amphiphilic compounds that attach to surfaces and help to reduce interfacial tension. (Fenton *et al.*, 2021). Surfactants have two different areas with distinct solubilities because they have a hydrophilic head and a lipophilic tail (Zhao *et al.*, 2021). Cationic, anionic, and amphoteric molecules make comprise the head group and are conveniently soluble in water. Alkanes, fluorocarbons, aromatic molecules, and other nonpolar groups can be found in the lipophilic area. Surfactants are divided into four categories: cationic, anionic, amphoteric, and non-ionic based on the properties of the head group region (Khoee & Yaghoobian, 2017).

Surfactant must be able to lower interfacial tension to near zero during emulsion preparation to promote dispersion of all components. Non-ionic, anionic, cationic, and zwitterionic surfactants are all possible. The nature of the surfactants influences the stability of the emulsion. Non-ionic surfactants are stabilized by dipole and hydrogen bond interactions, while ionic surfactants are sustained by electrical double layer interactions. Salt content has an effect on ionic surfactants as well. As a result of their instability and toxicity concerns, ionic surfactants are typically not preferred. Non-ionic surfactants, on the other hand, can develop harmless medicinal dosage forms, making them more desirable (Kale & Deore, 2016).

HLB is a dimensionless critical variable in the surfactant selection process for the creation of niosomes. This parameter influences the size and quantity of drug loading. Surfactants having an HLB value between 4 and 8 are vesicle-forming

compatible. Surfactants with HLB values more than 6 can scarcely form vesicles; hence, cholesterol must be added to produce niosomes. According to Kale & Deore (2016), surfactants with HLB values of 3-6 are beneficial in the development of water-in-oil emulsion, whereas surfactants with HLB values of 8-18 are useful in the preparation of oil-in-water emulsion. Surfactants with more than 20 HLB values act as co-surfactants to lower surfactant concentrations to an appropriate level and to create emulsions.

When the concentration of surfactant approaches or exceeds the critical micelle concentration (CMC), they form orderly structures called micelles. When the CMC is achieved, the surface tension does not drop any more with the addition of more surfactant. Owing to a reduction in interfacial tension, the presence of a surfactant makes the two phases more aligned with each other, resulting in wetting or emulsification. In detergency uses, this concept allows for the washing of soiled clothing and crockery (Fenton *et al.*, 2021).

2.3.1 Non-ionic Surfactant

Non-ionic surfactant-based vesicles, also known as niosomes, have gotten a lot of interest in the pharmaceutical industry because of their exceptional ability to encapsulate both hydrophilic and hydrophobic drugs. It has recently been shown that these vesicles can increase medication bioavailability and may operate as a novel technique for delivering a variety of therapeutic agents, including as chemical pharmaceuticals, protein therapeutics, and gene materials, with minimal toxicity and desirable targeting effectiveness (Ge *et al.*, 2019). Non-ionic surfactants are typically those that are not dissociated in aqueous solution, and their head groups are inherently big and bulky, pointing away from the oil droplet. These polar head groups clash and tangle with other water droplet head groups, preventing droplets from sterically colliding (Cassiday, 2014).

Non-ionic surfactants are polymeric surfactants made up of complex molecules with a high molecular weight. They form a bulky visco-elastic coating around droplets to prevent encapsulated material from escaping while also maintaining steric stability, preventing internal droplet coalescence, and thus improving stability, whereas monomeric emulsifiers are simple molecules that align at the interface but do not have optimal stability in double emulsions due to their proclivity to move from one step to

the next. Non-ionic emulsifiers may be used alone or in combination with charged emulsifiers to increase emulsion stability (Cassiday, 2014).

Alkyl esters, such as sorbitan fatty acid esters (Spans) and polyoxyethylene sorbitan fatty acid esters (Tweens), are another class of non-ionic surfactants that have been utilized extensively. They are thought to be harmless and non-irritating compounds. As the acyl chain length grows, the gel transition temperature of spans rises. At room temperature, for instance, span 20 (sorbitan monolaurate), which has a carbon chain of 9 carbon atoms, is a liquid. With 13 carbon atoms in the carbon chain, span 40 (sorbitan monopalmitate) has a gel transition temperature of around 47 °C, whereas span 60 has a gel transition temperature of roughly 58 °C. Entrapment efficiency improves with carbon-chain length, which is interesting. Tweens have a high hydrophilic-lipophilic balance (HLB) because they are generated from polyoxyethylene combined with sorbitan fatty acid esters (Spans) (Khoee & Yaghoobian, 2017).

2.3.1.1 Methyl-α-D-glucopyranoside

Methyl-α-*D*-glucopyranoside (MEG) is an anomeric α-*D*-glucopyranoside with a methyl group as illustrated in Figure 2.4. It is a methyl-*D*-glucoside and an α-*D*-glucoside. Methyl-α-*D*-glucopyranoside a white powder, is a well-known industrial chemical that is frequently used to make a variety of products, such as esterified surfactants, adhesives, coatings, cosmetics, detergents, polyether polyols, and more recently, starting polyols for use in the production of urethane foams after prior oxyalkylation. MEG are commonly synthesized in a batch method by the alcoholysis reaction of a monosaccharide (e.g., glucose) or a polysaccharide (e.g., starch) with methanol in the presence of a catalytic quantity of p-toluene sulfonic acid or sulfuric acid. The alcoholysis process produces a combination of products, the most prominent of which are α-MeG and β-MeG. The methanol can be evaporated and swapped with coolant to produce a dark solution that can be decolored using a whitening agent (e.g., activated carbon) (Yang *et al.*, 2016).

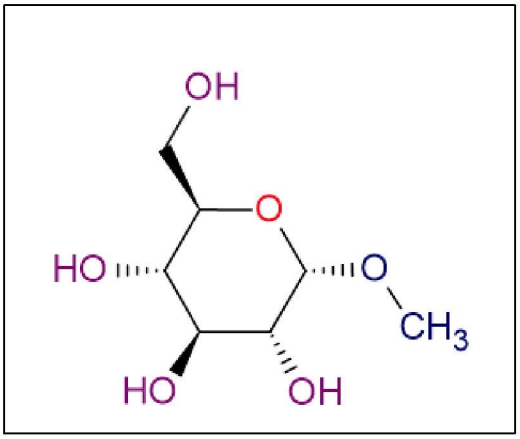

Figure 2.4 Methyl-α-*D*-glucopyranoside

2.3.1.2 Span series

Non-ionic emulsifiers titled spans (which are also referred to as sorbitan esters) serve their purpose in emulsions, creams, and ointments. The Span surfactant series is a class of non-ionic surfactants that are widely utilized, non-irritating, safe, and easily accessible. Sorbitan monolaurate (Span 20), sorbitan monopalmitate (Span 40), sorbitan monostearate (Span 60), and sorbitan monooleate (Span 80) are examples of common sorbitan monoesters. As shown in Figure 2.5, these Span surfactants are made up of various fatty acid chains and the same sorbitan group (Zheng *et al.*, 2022).

In the cases of Span 20 and Span 80, it was discovered that the added cholesterol had an impact on the preparation type, causing it to either be a proniosomal alcoholic solution or a liquid crystalline gel system. Because of the low transition temperatures of Span 20 and Span 80 (16 °C and 12 °C, respectively), these substances are liquid at ambient temperature and cannot gel with lower cholesterol concentrations. On the other hand, because they have high transition temperatures and are solids at room temperature, Span 40 (Tc = 42 °C) and Span 60 (Tc = 53 °C) operate as gelators by themselves and generate white creamy gels in the presence or absence of cholesterol. For Span 20 and Span 80, gel formation will begin at 20% and 30% (molar percent) of cholesterol, respectively. At cholesterol concentrations below 30%, Span 80 created two phases of proniosomal liquids because it is more hydrophobic than Span 20 (HLB = 8.6) (HLB = 4.3). It was discovered that the proniosomal gels were thermo-reversible. It was predicted that the prepared systems would release flurbiprofen under regulated

conditions over an extended length of time (Khoee & Yaghoobian, 2017).

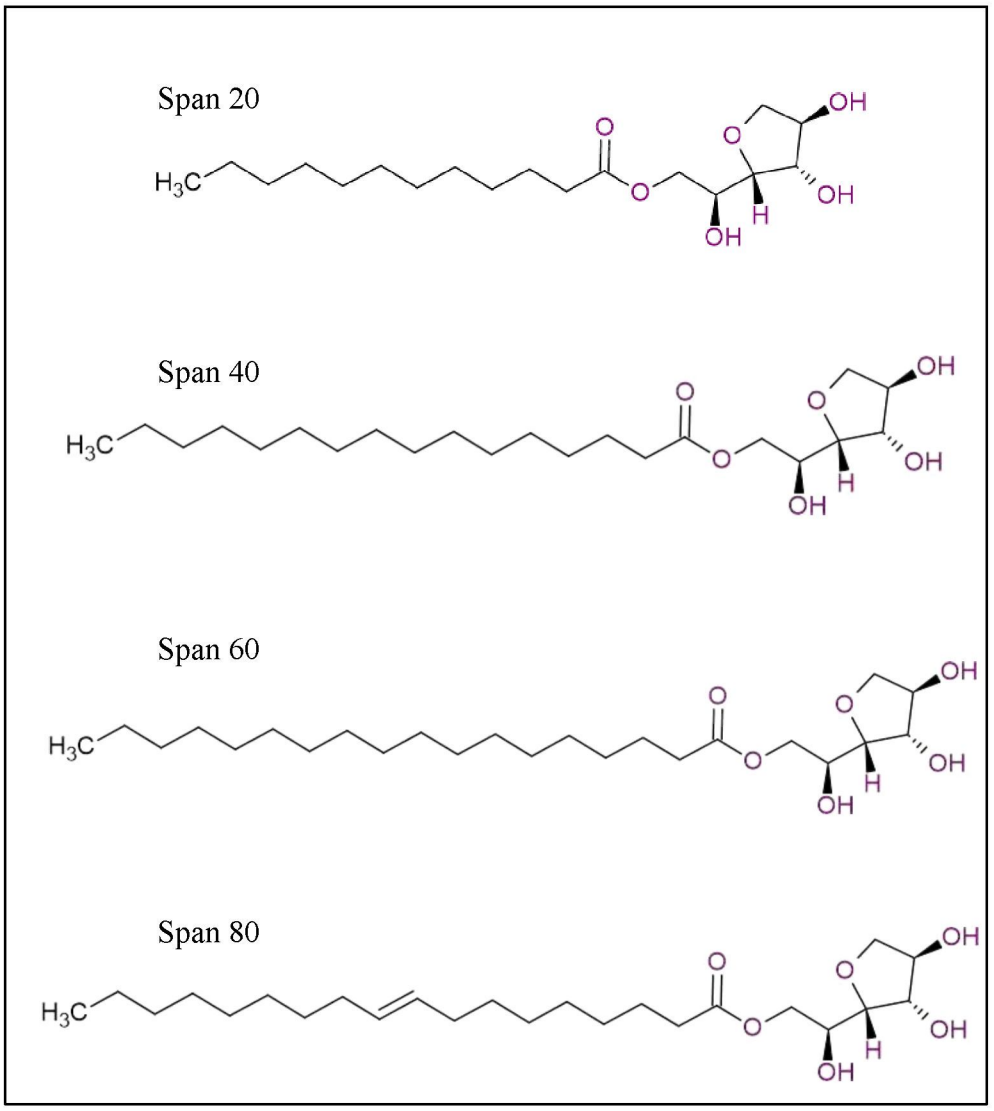

Figure 2.5 Span surfactant series

2.4 Stability of Emulsion

According to Goodarzi & Zendehboudi (2019), owing to the inherent inclination of a liquid/liquid mixture to reduce interfacial interactions, an emulsion is a thermodynamically unstable method. After a period of time, however, most emulsions display kinetic stability. The emulsion stability is largely determined by the interactions between surface-active agents and the water/oil interfaces (Goodarzi & Zendehboudi, 2019) and influenced by the technique of production, emulsifier type and concentration,

temperature, and medium pH (Maphosa & Jideani, 2018; L. Zheng *et al.*, 2020). During emulsification, emulsifying agents are adsorbed to the newly created interfacial layer, decreasing interfacial tensions and enabling the immiscible phases to partially blend. (Goodarzi & Zendehboudi, 2019).

As demonstrated in Figure 2.6, many processes such as flocculation, coalescence, sedimentation, Ostwald ripening, creaming, and phase inversion are responsible for emulsion destabilization. Flocculation is the process by which droplets in an emulsion attract each other and produce flocs without causing the stabilizing layer at the interface to burst. Droplet flocculation happens as a result of gravitational force, centrifugation, Brownian forces, and when repulsive energy is smaller than van der Waals energy. This phenomenon is undesired since it increases creaming and minimizes clouding due to bigger particle sizes, as well as promotes coalescence due to the closer proximity of droplets (Maphosa & Jideani, 2018; Ravera *et al.*, 2021).

Coalescence is the merging of two droplets into a single one produced by the thinning and rupture of the liquid coating between them and is heavily influenced by the interfacial characteristics of the adsorbed layers (Wiyani *et al.*, 2020). Coalescence in emulsions can occur when moving droplets collide with each other or as a result of flocculation (Lamba *et al.*, 2015). Ostwald ripening happens when capillary pressure induces a partial breakdown of the dispersed liquid process, resulting in a mass transition from tiny to big droplets interface. This process is impacted by the interaction of surfactants and the rheological characteristics of the interfacial membranes, but it is primarily motivated by the solubility of the dispersed substance and is strongly reliant on droplet size (Ravera *et al.*, 2021).

Gravitational separation causes creaming (upward) and sedimentation (downward). These occur when emulsion droplets combine to form larger droplets or when the droplets rise to the emulsion's surface due to buoyancy. When the density of the scattered phase is smaller than the density of the continuous phase, this is frequently caused by gravitational force. Typically, this occurrence results in a divided emulsion with a droplet-rich cream layer and a droplet-depleted watery layer.

Creaming is often a prelude to coalescence and is followed by phase separation; the creaming index may be used to describe the amount of creaming in O/W emulsions. The creaming index indicates the level of droplet aggregation; hence, the higher the index, the more droplets have agglomerated. Creaming can be measured visually or using optical imaging. The creaming index can be used to describe the amount of O/W

emulsions (Maphosa & Jideani, 2018).

2.5 Freeze-thaw Stability

O/W emulsions may be susceptible to freeze-thaw during production and storage. Freezing is often used to extend the shelf life and maintain the quality of goods that are thawed before eating. Additionally, freezing is a process used in the production of ice cream and other sweets that are intended to be eaten frozen. Bramante *et al.* (2025) stated regardless of the cause, freeze-thaw may cause o/w emulsions to become unstable by altering their microstructure. Because it affects the quality of various meals (most notably ice cream), the freeze-thaw stability of both o/w emulsions and emulsion-based foods has been studied (Muhammad Shariful *et al.*, 2018). The quality of meals based on emulsions has been shown to be affected by the fact that o/w emulsions are often unstable to freeze-thaw. A process of partial coalescence between oil droplets, followed by coalescence upon thawing, is often responsible for destabilization induced by crystallization of the dispersed phase. This might ultimately lead to emulsion breakage and the release of the emulsified oil. The impact of cooling temperature, cooling rate, and isothermal holding duration on the freeze-thaw stability of o/w emulsions has been examined in a number of studies since these factors influence the emulsion's crystallisation profile, particularly the dispersed phases (Okuro *et al.*, 2022). Ice expansion, which puts pressure on the oil droplets and causes coalescence, would encourage o/w emulsion instability when the continuous phase crystallizes.

2.6 Effect of Temperature on Emulsion

Emulsions are thermodynamically unstable systems that rapidly divide into oil and water layers. This is owing to the differing densities of the oil and aqueous phases, as well as the unfavorable interaction between oil and water molecules. An emulsion's stability may be described as its capacity to retain its qualities; that is, the ability of the emulsion's phases to remain mixed together (Maphosa & Jideani, 2018).

Temperature has a considerable impact on emulsion stability. The physical characteristics of oil, water, interfacial films, and surfactant solubilities in the oil and

water phases are all affected by temperature. They, in turn, have an impact on the emulsion's stability. According to Ismail *et al.* (2020), temperature increases often aid in the separation of emulsions. This is due to the lower viscosity of the continuous phase, which causes it to coagulate even more. Temperature rise also reduces surface viscosity, which destabilizes the surface oil coating in the water. The most important influence of temperature on emulsion viscosity is that viscosity reduces with rising temperature. This drop is mostly due to a decrease in oil viscosity (Nebogina *et al.*, 2020).

2.7 Molecular Dynamic Simulation

Computational drug discovery can help to speed up the difficult process of creating and optimizing a novel medication candidate. Because of the rapid development of faster architectures and improved algorithms for high-level calculations in a time-efficient way, the effect of computational structure-based drug design (SBDD) on drug discovery has increased in the last decade. Nowadays, classic molecular dynamics (MD) simulations enable the application of SBDD tactics that fully account for the structural flexibility of the total drug target model system. Indeed, the two major drug-binding paradigms (induced-fit and conformational selection) have largely supplanted Emil Fischer's rigid lock-and-key binding paradigm (De Vivo *et al.*, 2016).

According to De Vivo *et al.* (2016), Classical Molecular Dynamics (CMD) is a physical approach for investigating the interaction and motion of atoms and molecules using Newton's physics. A force field is used to compute the total energy of a system by estimating the forces between interacting atoms. The integration of Newton's equations of motion then provides successive configurations of the developing system during MD simulations, yielding trajectories that describe particle locations and velocities across time. A range of features, including free energy, kinetics measures, and other macroscopic variables, may be derived from these MD trajectories and compared to experimental observables. The approach was developed in theoretical physics in the late 1950s and is currently used in chemical physics, materials science, biomolecule modelling, and, more recently, drug development.

The reversible emulsification and demulsification processes were studied using molecular dynamics simulations (Liu *et al.*, 2019). MD simulations are frequently used in conjunction with experimental structural biology methods as as X-ray crystallography, cryo-electron microscopy (cryo-EM), nuclear magnetic resonance

(NMR), electron paramagnetic resonance (EPR), and Forster resonance energy transfer (FRET) (Hollingsworth & Dror, 2018). Molecular dynamics (MD) simulation is a powerful tool for studying physical processes at the microscale, such as molecule adsorption and droplet coalescence. In the case of W/O emulsion, several research have appeared in recent years to investigate the microscopic mechanisms of deformation, breakdown, and coalescence of water droplets under external electric fields at the molecular level using MD modelling. These studies mostly concentrated on the many contributing parameters, such as electric field intensity, electric field type, and ion concentration (Li *et al.*, 2022).

Based on a generic model of the physics driving interatomic interactions, molecular dynamics (MD) simulations predict how each atom in a protein or other molecular system would move over time. These simulations may capture a wide range of critical biomolecular events, such as conformational change, ligand binding, and protein folding, and disclose the locations of all atoms with femtosecond temporal resolution. Crucially, such simulations may anticipate how biomolecules will react at the atomic level to perturbations like mutation, phosphorylation, protonation, or the addition or removal of a ligand (Hollingsworth & Dror, 2018).

2.7.1 Self-assembly in emulsion

In emulsion systems, aggregation is the production of agglomerates without coalescence, that is, without the actual rupture of the interfacial layer and the consequent generation of bigger droplets. Coalescence can be avoided if contact between phases is prohibited by a sufficiently high barrier, which can be electrical or steric in nature. Aggregation may occur in these systems if attractive droplet-droplet forces prevail at long range. This long-distance attraction can be attributed to one or both of two separate origins. Bar-On & Manor (2024) has studied two droplets will attract each other noticeably (attractive energies $\geq$ kT, where k= Boltzmann's constant and T= absolute temperature) even at significant distances relative to molecular dimensions. These are the London dispersion forces amplified by the integration of molecule-molecule interactions across the volumes of the two droplets.

The second aspect to droplet-droplet attraction may occur if the interfacial film of one droplet attracts the film of the other in the area between the two particles. This is most

likely to be the case when the absorbed surfactant films on oil droplets in water expose relatively hydrophobic and/or nonionizing functional groups toward the water phase. "Soluble" surfactants that may expose an excess of hydrophilic groups to water when adsorbed onto oil droplets should, in general, not influence droplet-droplet attraction and so aggregation. On the contrary, their charges or/and hydrophilic bulk should help to the avoidance of droplet close proximity (Bar-On & Manor, 2024). If the repulsive forces (electrical or steric) are not as long ranged as the aforementioned attractive forces, the droplets may be more energetically comfortable in aggregated forms.

Abdul Rahman *et al.* (2010) mentioned the shape and size of the aggregate generated will be affected, which are intricately associated and sensitive to the composition, temperature, and solution conditions. The connection between the area of the head-group and the length of the chain and the form of the resultant aggregation and implies that the resultant structure from surfactant solubilization will vary in form, such as spherical, cylindrical, or cubical micelle, lamellar, and even inverted structures. The development of a spherical micelle, on the other hand, is most advantageous since it has the smallest surface area and size for a given volume. Table 2.5 shows several studies that indicates the shape of the aggregation that has presented in the emulsion system.

Table 2.3
Shape of the aggregation in emulsion system

No.	Shape of the aggregation	System	Surfactant	References
1.	Cylindrical, Cubical and Lamellar	Micelles	Span 20	(Abdul Rahman *et al.*, 2010)
2.	Lamellar. Hexagonal and Orthorhombic	Oil-in-water emulsion	Tween 20	(Mao *et al.*, 2014)
3.	Hollow Vesicle-like	Oil-in-water emulsion	Hexadecyltrimethylammonium Bromide	(Park *et al.*, 2016)
4.	Lamellar	Oil-in-water emulsion	Tween 80	(Moraes *et al.*, 2018)
5.	Spherical / Prolate Ellipsoid	Nanoemulsion	Benzalkonium Chloride	

The concentration of the surfactants influences the development of emulsion droplets or micelles. If the value is greater than the critical micelle concentration (CMC), enough surfactants are present to stabilize each nanoparticle and form micelles. If the value is less than the CMC, macroemulsion droplets develop, each enclosing numerous nanoparticle (Wu *et al.*, 2022). Because of the van der Waals contact between the hydrophobic capping ligands on the nanoparticle surface and the hydrophobic tails of the surfactants, the final formed structures are shielded by a layer of surfactants, allowing for excellent dispersibility in water (Akbari & Nour, 2018).

The self-assembly of colloidal nanoparticles within emulsion droplets provides numerous opportunities to precisely control the size, shape, crystal structure, and component of the assembled superstructures, allowing the exploration of new collective properties (e.g., plasmonic coupling, light absorption, and catalytic activity) and improved performance in a variety of applications (e.g., drug delivery, multimodal bioimaging, and therapeutic applications). These procedures often do not require extra processes for changing building blocks and may be carried out under mild circumstances, allowing the particle interaction to be regulated to develop new synergetic qualities while retaining the inherent features of the nanoparticles (Wu *et al.*, 2022).

CHAPTER 3
RESEARCH METHODOLOGY

3.1 Materials and Chemicals

Virgin coconut oil (VCO) was purchased from Rainforest Herbs, Malaysia. Deionized water was produced using a laboratory deionization system. Methyl-α-D-glucopyranoside (MEG) was obtained from Sigma-Aldrich, United States of America (USA). Span 20 (sorbitan monolaurate) and Span 80 (sorbitan monooleate) were purchased from Chemiz, Malaysia.

3.2 Methods

3.2.1 Emulsion Preparation

All samples were prepared at a room temperature. Emulsion was prepared with only one surfactant with different ratios of composition by referring to the work by Sanjeewani *et al.* (2013) with slight modification. VCO, deionized water and surfactant were weighed and mixed together using a vortex mixer. Based on the composition listed in Table 3.1, the emulsion mixture was produced involving MEG. The procedures were repeated using two surfactants which are Span 20 and Span 80. Tables 3.2 and 3.3 illustrate the composition of emulsion mixture using those two surfactants.

Table 3.1
Emulsion formulation using different ratios of MEG

Samples	VCO (g)	Deionized water (g)	Surfactant (g)	VCO : Deionized Water : Surfactant % (w/w)
MEG-A	2.0	6.0	2.0	20 : 60 : 20
MEG-B	2.0	4.0	4.0	20 : 40 : 40
MEG-C	3.0	4.0	3.0	30 : 40 : 30
MEG-D	1.0	6.0	3.0	10 : 60 : 30

Table 3.2
Emulsion formulation using different ratios of Span 20

Samples	VCO (g)	Deionized water (g)	Surfactant (g)	VCO : Deionized Water : Surfactant % (w/w)
S20-A	2.0	6.0	2.0	20 : 60 : 20
S20-B	2.0	4.0	4.0	20 : 40 : 40
S20-C	3.0	4.0	3.0	30 : 40 : 30
S20-D	1.0	6.0	3.0	10 : 60 : 30

Table 3.3
Emulsion formulation using different ratios of Span 80

Samples	VCO (g)	Deionized water (g)	Surfactant (g)	VCO : Deionized Water : Surfactant % (w/w)
S80-A	2.0	6.0	2.0	20 : 60 : 20
S80-B	2.0	4.0	4.0	20 : 40 : 40
S80-C	3.0	4.0	3.0	30 : 40 : 30
S80-D	1.0	6.0	3.0	10 : 60 : 30

Table 3.4 shows the composition of emulsion with VCO involving mixed surfactants consisting of MEG and Span 20. The composition was prepared with deionized water using the mixture consists of VCO and mixed surfactants. The composition was mixed together using vortex mixer.

Table 3.4
Emulsion formulation using different ratios of mixed surfactant (MEG and Span 20)

Samples	VCO (g)	Deionized water (g)	Surfactant (g)		VCO : Deionized Water : Surfactant % (w/w)
			MEG	Span 20	
MS20-A	2.0	6.0	1.0	1.0	20 : 60 : 20
MS20-B	2.0	4.0	2.0	2.0	20 : 40 : 40
MS20-C	3.0	4.0	1.5	1.5	30 : 40 : 30
MS20-D	1.0	6.0	1.5	1.5	10 : 60 : 30

***M = MEG; S20 = Span 20**

Table 3.5 illustrates the preparation of emulsion formulation using MEG and Span 80.

Table 3.5
Emulsion formulation using different ratios of mixed surfactant (MEG and Span 80)

Samples	VCO (g)	Deionized water (g)	Surfactant (g)		VCO : Deionized Water : Surfactant % (w/w)
			MEG	Span 80	
MS80-A	2.0	6.0	1.0	1.0	20 : 60 : 20
MS80-B	2.0	4.0	2.0	2.0	20 : 40 : 40
MS80-C	3.0	4.0	1.5	1.5	30 : 40 : 30
MS80-D	1.0	6.0	1.5	1.5	10 : 60 : 30

***M = MEG; S80 = Span 80**

3.2.2 Stability evaluation with different temperatures

The selected formulations were evaluated for thermal stability by subjecting the samples to five different temperatures (30, 35, 40, 45, and 60 °C) in a water bath for 10 minutes. Observations focused on emulsion stability, droplet size, and visual appearance. Specifically, the samples were monitored for phase separation or creaming, droplet coalescence, changes in viscosity, and sediment formation. These observations allowed comparison of the thermal stability of formulations containing different surfactants and compositions, thereby identifying the most stable system under varying temperature conditions.

3.2.3 Creaming Index

All of the emulsion samples were placed in a small vial tube with a tightly sealed cap and were stored for 32 days at 25 °C. During the storage period, observations were taken every four days. According to Sanjeewani & Sakeena (2013), commonly, the oil droplets have lower density than the surrounding aqueous phase, causing the droplets to move upwards while being stored, then lead to creaming. Creaming Index was calculated as shown in (3.1):

$$\text{Creaming index}\,\% = \frac{\text{Height of the droplet depleted lower layer (HD)}}{\text{Height of total emulsion (HE)}} \times 100\% \qquad (3.1)$$

3.2.4 Freeze-thaw stability

Freeze-thaw experiments for oil-in-water (O/W) emulsions and aqueous dispersions were conducted immediately following preparation in order to evaluate their stability under temperature fluctuations. All samples were pre-conditioned at 20 ± 1 °C prior to the freezing stage to ensure uniform thermal conditions (Palazolo *et al.*, 2011).

Freezing stage: Emulsions were stored isothermally at -20 °C in a still-air environment for 24 hours under airtight, leak-proof containers in order to allow for full solidification.

Thawing stage: Samples following the freezing stage were then placed at room temperature for full liquefaction.

Post-thaw, emulsions at room temperature underwent additional visual and quantitative observations. Following the freeze-thaw, some emulsions showed a state of phase separation, with an apparent development of discrete layers with a range of visual appearances, including:

- Oil layer (disengaged oil phase)
- Cream layer (coalescence of oil droplets)
- Serum layer (clear, transparent, aqueous phase)

A visual estimation of each layer's thickness with a ruler was performed to monitor the level of phase separation. To evaluate the stability of the emulsions against gravitational separation (GS), the ratio of the serum height (h_S) to the total sample height (h_T) was calculated and expressed as a percentage using the formula (3.2):

$$\text{Stability of emulsion against GS} = \frac{\text{Height of the bottom serum layer } (h_S)}{\text{Total sample height } (h_T)} \qquad (3.2)$$

where:

- h_S (Height of the serum layer): The measured height of the clear aqueous phase at the bottom, indicating the extent of phase separation.
- h_T (Total sample height): The initial total height of the emulsion before freeze-thaw treatment.

The thickness of each layer was measured using a calibrated ruler with an accuracy of ±0.1 mm. The measurements were taken from the base of the vial, ensuring consistency across all samples.

A heightened level of GS reflects a high level of gravitational separation and, therefore, reduced emulsion stability under freeze-thaw testing. In contrast, a reduced level of GS reflects increased emulsion stability, with little, if any, phase separation. Both qualitative and quantitative analysis yield a thorough evaluation of emulsions' stability in terms of freeze-thaw testing.

3.2.5 Rheology Test

The viscosity of the emulsion mixtures was determined by using rotational Physics MCR 300 rheometers, Paar Physica circulating bath and controlled Peltier system. According to Gao et al. (2021), the shear rate of the emulsion mixture was calculated using the following formula (3.3) and (3.4):

$$\text{Shear rate } (\Upsilon) = \frac{\text{Flow velocity difference (v)}}{\text{Height difference of 2 liquid levels (r)}} \quad (3.3)$$

$$\text{Flow velocity difference (v)} = \frac{\text{Flowrate (Q)}}{\text{Area (A)}} \quad (3.4)$$

The pressure was set up until the stable reading has reached and the time taken was adjusted to 5 minutes on the beginning of the operation of rheometer. Next, the 'Time-Temperature Test Constant Shear Stress' was chosen as the type of rheomode to determine the viscosity. In order to calibrate the spinning spindle, the software was used to set the parameters and the position of spinning spindle was set 0.5 mm from the stage as this is the one of the important things in parameter. The sample was placed on the stage before the analysis while the spinning spindle was slightly lifted in order to place the sample. The reading for the samples' viscosity were obtained and recorded after the spinning spindle was let to spin the mixture.

3.2.6 Droplet Size and Distribution

By using Nikon SMZ-U optical polarizing microscope (OPM) connecting with DCLR Canon Fos 550D, the droplet size of emulsion was determined. A drop of sample was dropped onto a glass microscope, which then was sealed with a glass cover slide. The sample then was examined under 10x, 20x and 50x magnifications through the objective glass. The droplet size was determined by calculating the diameter of each droplet by using a software given after the images were captured with a camera on the force applied to the plate and interpreted using the given software.

3.2.7 Functional Group Measurement

Fourier transform infrared spectroscopy (FTIR) is well known as a quick, non-destructive, and straightforward examination that does not need sample preparation or the use of organic solvents. The FTIR spectrometer utilized is a PerkinElmer Spectrum One FT-IR spectrometer housed in Faculty of Applied Science block A306. This spectrometer is very useful for determining the functional group of chemicals in liquid samples. A few drops of sample were deposited in the center of the aperture plate, and the second aperture plate was placed on top of the first. The aperture plates were fastened together and the FTIR spectrometer was used to investigate them. The spectrum one plus program was used to acquire the infrared spectrum result.

3.2.8 Simulation Methodology

GROMACS v5.0.4 software was used to perform molecular dynamics simulations (Abdul Rahman *et al.*, 2010). In all directions, periodic boundary conditions were used. Grid neighbor-searching was used at 5 integration step intervals with a cut-off radius of 1.2 nm. Using the Verlet cut-off approach, all long-ranged, non-bonded interactions were cutoff at 1.2 nm. The Particle-Mesh Ewald technique with fourth-order interpolation was used to model long-range electrostatic interactions.

To guarantee that all conceivable interactions were considered, the van der Waals interactions were addressed using a simple cut-off. The Velocity rescaling thermostat was used to keep the system temperature at 300 K, with a temperature-coupling constant of 1.0 104 ns (1.0 105 ns for pre-equilibration). While simulating in an isothermal isobaric (NPT) ensemble, Berendsen's pressure coupling approach was used.

Energy Minimization

Prior to equilibration, energy minimization was carried out to eliminate steric clashes or high-energy contacts in the initial structure. The steepest descent algorithm was used with a maximum of 50,000 steps and a step size of 0.01 nm. The minimization was considered complete once the maximum force on any atom fell below 1000.0 kJ/mol/nm.

To maintain the structure of selected molecules during minimization, position restraints were applied to 880M, LQAU, and DO6T surfactant molecules via the -DPOSRES directive.

Nonbonded interactions were computed using the Verlet cutoff scheme, with neighbor list updates every step (nstlist = 1). Electrostatic interactions were handled using the Particle Mesh Ewald (PME) method, with a short-range Coulomb cutoff of

1.2 nm, while van der Waals interactions were truncated at the same distance (1.2 nm). Periodic boundary conditions (PBC) were applied in all three spatial dimensions to mimic an infinite system.

This step ensured a stable starting structure for the subsequent NVT and NPT equilibration simulations.

NVT Equilibration

The system was subjected to constant number of particles, volume, and temperature (NVT) equilibration using the leap-frog integrator for a total of 100 ps (50,000 steps with a time step of 2 fs). To stabilize the system at the desired temperature, the V-rescale thermostat (modified Berendsen thermostat) was employed with a reference temperature of 300 K for each group of molecules (surfactants and solvent), namely 880M, LQAU, DO6T, and water. A coupling constant (τ_t) of 0.1 ps was used for all temperature groups.

Initial velocities were generated from a Maxwell-Boltzmann distribution at 300 K, with a randomly assigned seed. The system was not coupled to a barostat, as the pressure was not regulated during the NVT phase. All bonds involving hydrogen atoms were constrained using the LINCS algorithm, with an order of 4 and a single iteration to improve constraint accuracy.

Electrostatic interactions were calculated using the Particle Mesh Ewald (PME) method with a real-space cutoff of 1.2 nm, Fourier spacing of 0.16 nm, and PME interpolation order of 4. Van der Waals (vdW) interactions were also truncated at 1.2 nm, and long-range dispersion corrections to energy and pressure were applied.

Neighbor searching was based on a Verlet cutoff scheme with grid-based searching and a neighbor list update every 10 steps. Position restraints were applied to the selected surfactant molecules (880M, LQAU, and DO6T) using the -DPOSRES directive to prevent significant structural distortions during the equilibration phase. The system was simulated under periodic boundary conditions in all directions (PBC = xyz).

Trajectory output (coordinates, velocities, energies, and logs) was saved every 500 steps (equivalent to every 1 ps) for post-equilibration analysis.

NPT Equilibration

Following the NVT equilibration, the system was further equilibrated under constant number of particles, pressure, and temperature (NPT) conditions to allow density stabilization and volume relaxation. The leap-frog integrator was used over 50,000 steps (equivalent to 100 ps) with a time step of 2 fs. The simulation continued from the previous NVT state, maintaining position restraints on selected surfactant molecules (880M, LQAU, and DO6T) to preserve their structure during equilibration.

Temperature coupling was maintained using the V-rescale thermostat, with coupling groups defined individually for 880M, LQAU, DO6T, and water (SOL), each coupled to a reference temperature of 300 K with a coupling time constant of 0.1 ps. Pressure coupling was applied using the C-rescale barostat in an isotropic mode, allowing uniform scaling of all box vectors. The reference pressure was set at 1 bar with a coupling time constant of 2.0 ps and compressibility of 4.5×10^{-5} bar^{-1}, corresponding to water.

Electrostatics were handled using the Particle Mesh Ewald (PME) method, with a short-range Coulomb cutoff of 1.2 nm, PME order of 4, and Fourier spacing of 0.16 nm. Similarly, van der Waals interactions were truncated at 1.2 nm, and long-range dispersion corrections for energy and pressure were included. Hydrogen bonds were constrained using the LINCS algorithm with a higher iteration (2) and order (2) to improve stability during pressure equilibration.

Neighbor searching employed the Verlet cutoff scheme with updates every 10 steps. Periodic boundary conditions were applied in all directions (PBC = xyz). Velocity generation was turned off during NPT equilibration to maintain continuity from the NVT phase.

Simulation outputs (coordinates, velocities, energies, and logs) were recorded every 500 steps (1 ps intervals) for analysis.

Production of Molecular Dynamics (MD) Simulation

After the equilibration phases, a 20 ns production molecular dynamics (MD) simulation was performed under NPT ensemble conditions to observe the long-term behavior and stability of the emulsion system. The leap-frog integrator was used with a 2 fs time step, totaling 10,000,000 steps. No new velocities were generated, as the simulation was continued from the previous equilibration stage.

Temperature control was maintained using the V-rescale thermostat, with individual coupling groups defined for 880M, LQAU, DO6T, and water (SOL), each assigned a reference temperature of 300 K and a coupling time constant (τ_t) of 0.1 ps. Pressure coupling was applied using the C-rescale barostat in isotropic mode, with a reference pressure of 1 bar, compressibility of 4.5×10^{-5} bar^{-1}, and a pressure coupling time constant (τ_p) of 2.0 ps.

Electrostatic interactions were computed using the Particle Mesh Ewald (PME) method with a real-space cutoff of 1.0 nm, PME order of 4, and a Fourier grid spacing of 0.16 nm. Van der Waals interactions were also truncated at 1.0 nm, and long-range dispersion corrections to energy and pressure were applied to improve accuracy. Bond constraints involving hydrogen atoms were applied using the LINCS algorithm, with an order of 4 and one iteration.

Neighbor searching was handled via the Verlet cutoff scheme with updates every 10 steps. Periodic boundary conditions were enforced in all three dimensions to mimic a bulk system. Output data were optimized to reduce file size: coordinates were stored in compressed format every 10 ps, while energies and log updates were also saved at 10 ps intervals.

This production run was critical for analyzing the structural, interfacial, and dynamic properties of the emulsion system under study.

CHAPTER 4
RESULTS & DISCUSSION

4.1 Stability evaluation of emulsion between single surfactant versus mixed surfactant

4.1.1 Creaming index

Higher stability is reflected by a lower creaming index (CI), which measures the extent of phase separation in an emulsion (Som et al., 2023). A higher CI indicates that the oil phase has risen to the top (creaming) or fully separated from the aqueous phase, signaling severe instability that compromises product consistency and performance. In contrast, a low CI suggests that the dispersed oil droplets remain uniformly distributed within the continuous phase. Such uniform dispersion prevents droplet aggregation and upward migration, preserving the product's texture, appearance, and functional effectiveness throughout storage.

When methyl-α-*D*-glucopyranoside (MEG) was used as a single surfactant (Figure 4.1(a)), several formulations exhibited instability as early as Day 1. Sample MEG-C showed moderate separation with a CI of 63.16%, while MEG-D recorded the highest CI at 84.21%, indicating poor stability. These observations suggest that MEG alone provides limited ability to prevent droplet coalescence and creaming.

A different trend was observed with the Span 20 formulations (Figure 4.1(b)). All samples appeared stable on Day 1 except S20-B. However, Samples S20-B, S20-C, and S20-D displayed gradual increases in CI over the 30-day period, demonstrating reduced stability during storage. Among this group, S20-A remained the most stable, showing no creaming throughout the study.

For the Span 80 system (Figure 4.1(c)), Samples S80-A and S80-D demonstrated the highest stability, with no creaming detected from Day 1 to Day 30. In comparison, S80-B and S80-C exhibited slight creaming on Day 1 and continued to show small but progressive increases in CI at each six-day interval. Overall, Span 80 produced the lowest degree of phase separation among the three single-surfactant systems, indicating superior stabilizing performance when used alone.

These findings collectively show that MEG alone provides the weakest emulsion stability, while Span 80 offers the strongest stabilizing effect among the single-surfactant formulations. Span 20 performs moderately but displays variability depending on formulation, with only one sample maintaining full stability throughout the 30-day period.

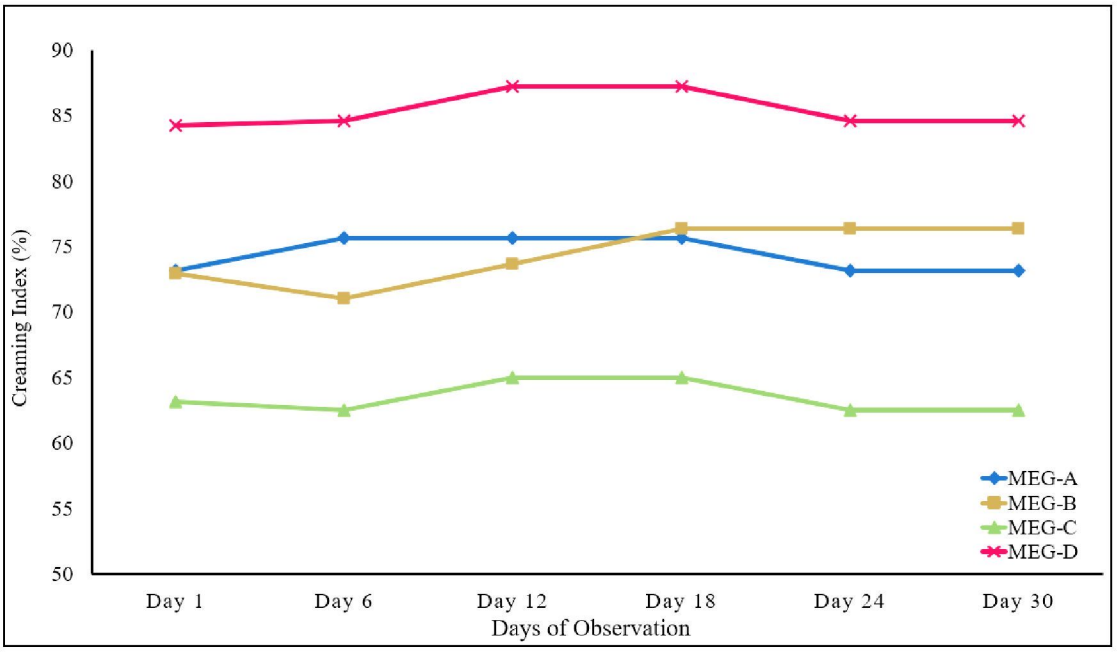

(a)

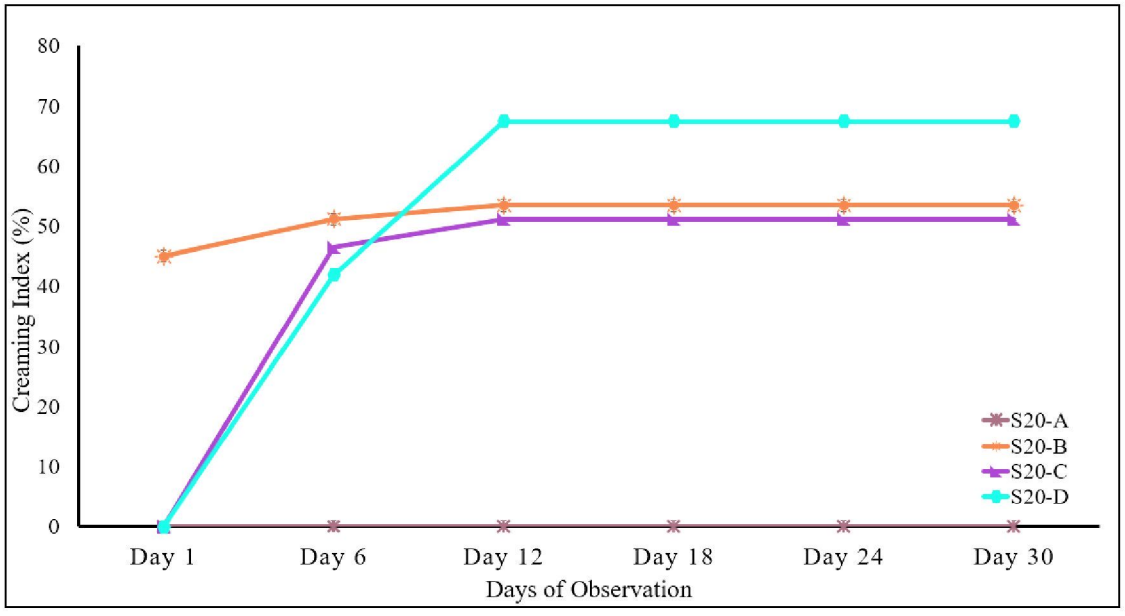

(b)

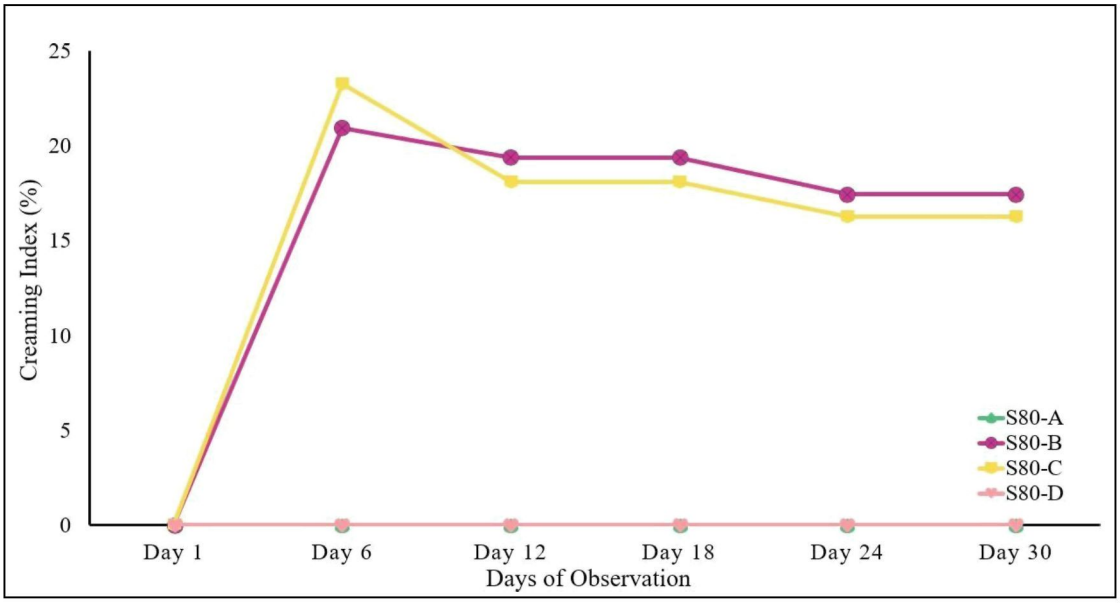

(c)

Figure 4.1 Creaming index for single surfactant from Day 1 to Day 30
a) MEG b) Span 20 c) Span 80

Among the three single-surfactant systems, the MEG-based emulsions exhibited the lowest stability. MEG, a sugar-derived compound, does not possess the strong surface tension–reducing capabilities characteristic of conventional surfactants such as those in the Span series. Although its molecular structure provides some amphiphilic properties, MEG is not optimally suited for significantly lowering interfacial tension which is a crucial mechanism for stabilizing emulsions (Posocco et al., 2016). As noted by Tian et al. (2022), highly effective emulsifiers adsorb firmly at the oil–water interface and form a protective interfacial film that shields dispersed droplets, preventing their coalescence.

MEG, however, does not sufficiently adsorb or form a robust interfacial layer around the oil droplets. This limited surface activity makes it unable to prevent droplet coalescence, leading smaller droplets to merge into larger ones and resulting in higher creaming indices over time (Lu et al., 2024). In emulsions containing virgin coconut oil, strong interfacial stabilization is essential to maintain fine droplet dispersion, but MEG alone lacks the capacity to withstand environmental or storage-related stresses.

In contrast, the Span family of surfactants demonstrates greater stabilizing performance due to their specific chemical properties and mechanisms of action. Span

molecules strongly adsorb at the oil–water interface, forming a stable interfacial film that effectively prevents droplet coalescence and enhances long-term stability (Posocco et al., 2016). Their relatively bulky molecular structures also introduce steric hindrance, physically spacing droplets apart and reducing the likelihood of aggregation or phase separation (Jiao & Burgess, 2003; Zdrali et al., 2019). These characteristics explain the significantly better performance of Span 20 and Span 80 compared to MEG when used as single surfactants.

The MEG–Span 20 (MS20) emulsions showed good initial stability on Day 1, as presented in Figure 4.2. Over the storage period, some fluctuations in creaming index were observed, but several formulations maintained strong stability throughout. In particular, MS20-C and MS20-D demonstrated the most consistent performance, exhibiting low creaming indices and retaining good homogeneity over time. In addition, MS20-A and MS20-B also displayed favorable stability compared with the corresponding MEG–Span 80 (MS80) formulations (MS80-A and MS80-B) shown in Figure 4.3.

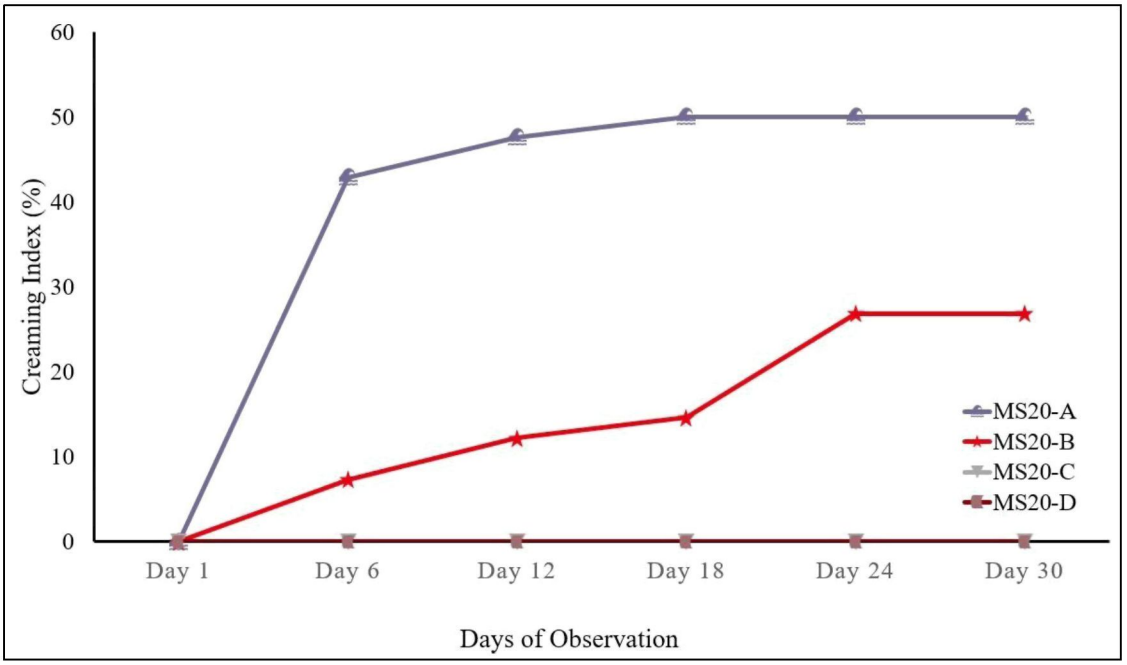

Figure 4.2 Creaming index for mixed surfactant using MEG and Span 20 from Day 1 to Day 30

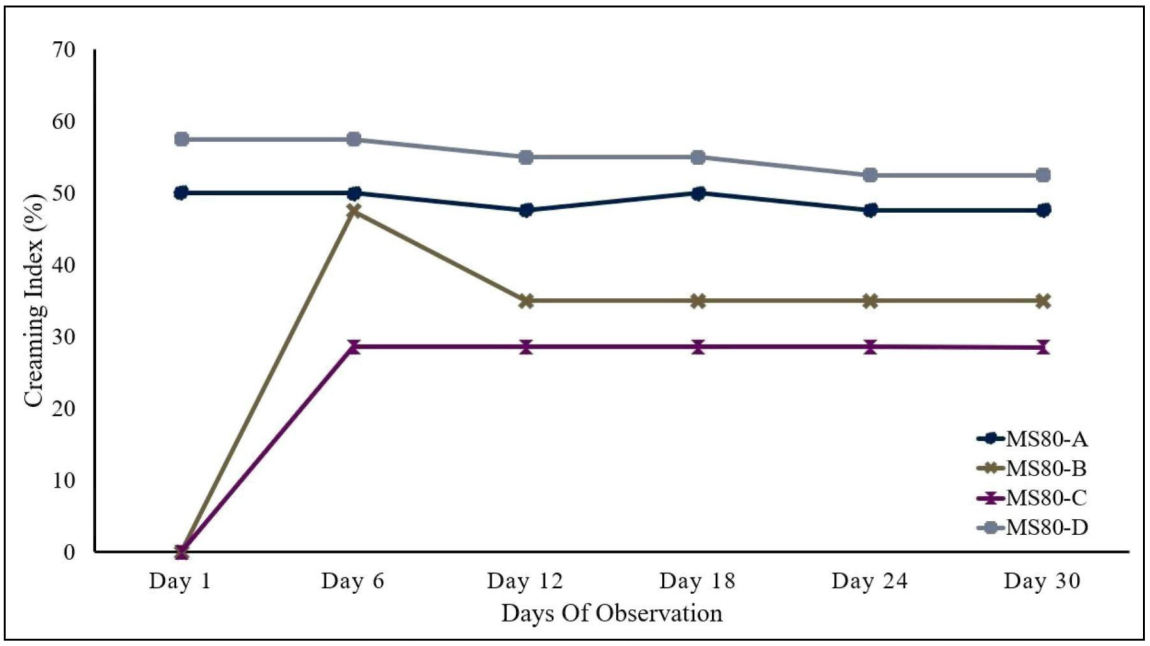

Figure 4.3 Creaming index for mixed surfactant using MEG and Span 80 from Day 1 to Day 30

MEG is a sugar-derived compound with strong hydrophilic characteristics, which enhances its compatibility with surfactants used in stabilizing oil-in-water emulsions. When MEG is combined with Span 20, the two surfactants can exhibit synergistic effects because of their complementary interactions at the interface. Synergism often arises from favourable head–group and tail–group interactions between mixed surfactants (Shah et al., 2022). Surfactants with compatible head groups can form hydrogen bonds or other attractive interactions that strengthen the interfacial film, resulting in improved emulsion stability (Stubenrauch et al., 2017).

Span surfactants contain a hydrophobic fatty acid tail and a small, non-ionic hydrophilic head. These molecular features allow Span molecules to adsorb effectively at the oil–water interface (Posocco et al., 2016). The hydrophobic tail anchors into the oil phase, while the hydrophilic head interacts with the aqueous phase. Meanwhile, the sugar-based head group of MEG interacts strongly with water due to its high hydrophilicity. When both are present, the combined system lowers interfacial tension more efficiently and forms a stronger interfacial layer that surrounds oil droplets, preventing them from coalescing. This complementary interaction enhances emulsion homogeneity and long-term stability.

In contrast, Span 80 shows a different behavior when mixed with MEG. Due to its lower HLB value and stronger affinity for the oil phase, Span 80 is better suited for water-in-oil emulsions, where oil is the continuous phase. Its more lipophilic nature means it interacts less effectively with the highly hydrophilic MEG. This mismatch in solubility preference weakens the formation of a cohesive interfacial film and reduces the overall stability of the emulsion.

This difference is reflected in the creaming index profiles. As shown in Figure 4.3, the MEG–Span 80 mixtures did not achieve the same level of stability as the MEG–Span 20 formulations. Although some MEG–Span 80 samples displayed initial stability on Day 1, variations in creaming index became apparent over time. Certain formulations exhibited progressively higher creaming indices, indicating limited interfacial protection and weaker resistance to droplet coalescence. Conversely, several MEG– Span 20 formulations showed minimal creaming throughout the 30-day storage period, confirming better performance of this combination.

These observations highlight the importance of surfactant compatibility in mixed-surfactant systems. The MEG–Span 20 system benefits from strong hydrophilic interactions and the formation of a more effective interfacial film, resulting in highly stable oil-in-water emulsions. In contrast, the MEG–Span 80 system suffers from mismatched solubility tendencies and weaker interfacial cohesion, which leads to lower stability. Overall, the findings clearly demonstrate that Span 20 is more suitable than Span 80 for blending with MEG in the stabilization of virgin coconut oil emulsions.

4.1.2 Freeze-Thaw Stability

The stability of emulsions is significantly influenced by the choice of surfactants, which help in maintaining the dispersion of one liquid within another. The stability of emulsions can be particularly challenged by environmental stresses such as freeze-thaw cycles, which can induce phase separation and compromise product quality (Ghosh & Rousseau, 2009; Thanasukarn et al., 2004). This study investigates the stability of emulsions using both single and mixed surfactants, focusing on their behavior through multiple freeze-thaw cycles. By analyzing the percentage of phase separation in various samples, this research aims to understand the impact of surfactant properties, hydrophilic-lipophilic balance (HLB), and molecular interactions on the long-term stability of emulsions. The findings provide valuable insights into optimizing

surfactant formulations for enhanced emulsion stability under challenging conditions.

The investigation of emulsion stability across freeze-thaw cycles (Figure 4.4) shows different behaviors when using a single surfactant. This approach aligns with the findings of Doutsi *et al.* (2025)., who emphasized that surfactant type and concentration are crucial in determining the emulsion stability under thermal stress conditions.

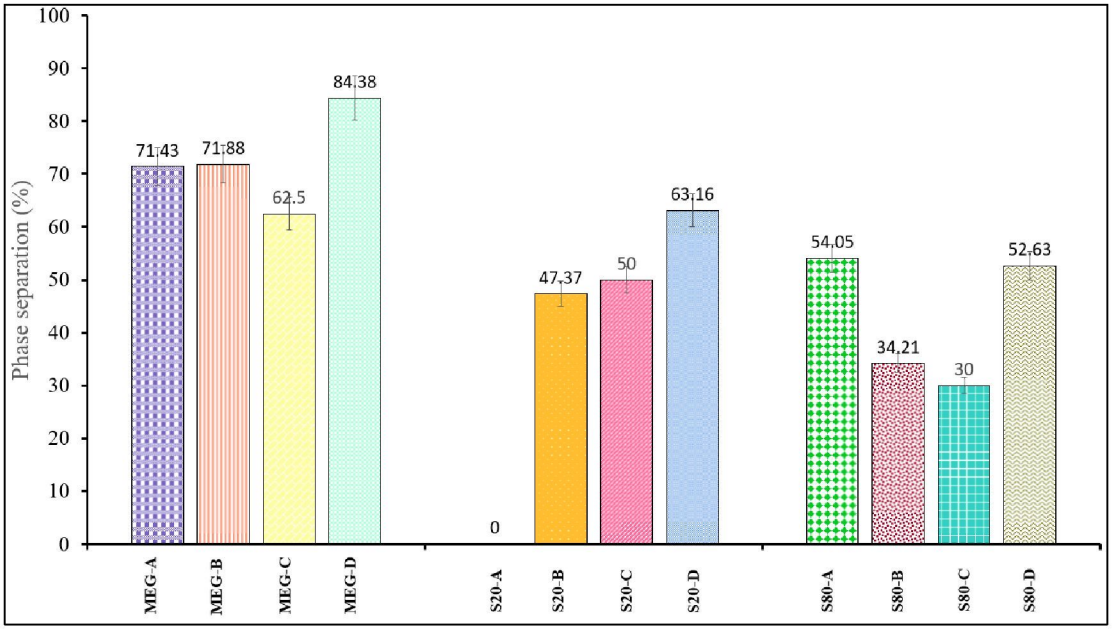

Figure 4.4 Freeze-thaw analysis of single surfactant emulsions

The stability of the emulsions clearly depended on the type of surfactant used and the specific composition of each sample. Emulsions prepared with MEG performed poorly across most samples, with high phase separation 71.43% in MEG-A, 71.88% in MEG-B, and 62.5% in MEG-C showing that MEG was not effective at keeping the emulsions intact. This likely happened because MEG could not form a strong protective layer around the oil droplets, leaving them prone to separation. On the other hand, Span 20 consistently improved stability. Phase separation dropped to 0% in S20-A, 47.37% in S20-B, and 50% in S20-C, suggesting that Span 20 interacts much more effectively with the emulsion components to create a durable interfacial film, as Peng et al. (2011) also observed. Span 80 performed better than MEG but was slightly less consistent than Span 20, showing 54.05% separation in S80-A, 34.21% in S80-B, and 30% in S80-C. This indicates that Span 80 can stabilize emulsions, but its effectiveness depends on the

sample composition and the way it interacts at the oil–water interface.

Across four formulations, sample D formulation stood out as the most inherently stable. Even with MEG, phase separation was only 15.62%, and although it increased slightly with Span 20 (36.84%) and Span 80 (47.37%), these numbers were still lower than in other samples, showing the robustness of this formulation. This suggests that the combination of virgin coconut oil, deionized water, and the surfactant blend in sample D formulation creates strong and resilient interfacial films that resist destabilization, even under challenging freeze-thaw conditions. Interestingly, in sample formulations B and C, the stability improved over successive freeze-thaw cycles, indicating that surfactants can "adapt" over time, gradually forming stronger interfacial layers that enhance the overall stability. This matches the findings of Gao et al. (2021), who noted that surfactants with intermediate HLB values tend to maintain stability better under thermal cycling.

Overall, Span 20 proved to be the most effective surfactant, while MEG was the least effective. Sample D formulation demonstrated the strongest inherent stability, highlighting how both the choice of surfactant and the precise balance of oil, water, and surfactant are critical for maintaining emulsion stability under varying temperatures. These results show that careful formulation design is key: selecting the right surfactant and composition can make the difference between an emulsion that separates quickly and one that remains stable and reliable, even under environmental stresses like freeze-thaw cycles.

The stability of emulsions prepared with mixed surfactants, especially under freeze-thaw cycles, is influenced by several factors, including the type of surfactants, their hydrophilic-lipophilic balance (HLB), molecular interactions, and the nature of the oil and water phases (Aregbe et al., 2024). In this study, a combination of MEG, a sugar-based surfactant, and Span 20 (sorbitan monolaurate) was used. Span 20, with an HLB value of approximately 8.6, is a relatively balanced surfactant well-suited for stabilizing oil-in-water emulsions. MEG enhances emulsification by forming strong hydrogen bonds with water molecules, contributing to a stable interfacial film that resists phase separation. This combination proved highly effective initially, as seen in the excellent stability of MS20-A, MS20-C, and MS20-D, which showed no phase separation, and the minimal separation observed in MS20-B (5.71%).

Replacing Span 20 with Span 80 (sorbitan monooleate) caused a marked change in emulsion behavior. Span 80 has a lower HLB value (4.3) and is more lipophilic,

which affects its ability to cover the oil droplets effectively. Its stronger hydrophobic character results in weaker steric stabilization, leading to higher separation rates in all samples during the second set of freeze-thaw cycles (56.76% for MS80-A, 50% for MS80-B, 41.67% for MS80-C, and 65.71% for MS80-D). These observations are consistent with Wang et al. (2023), who reported that surfactants with lower HLB values are less effective at stabilizing emulsions under thermal stress.

Freeze-thaw cycles impose mechanical and thermal stress on emulsions. During freezing, water expands and forms ice crystals, which can disrupt the surfactant film and promote oil droplet coalescence. Upon thawing, the destabilized emulsion becomes prone to phase separation (Ariyaprakai & Tananuwong, 2015; Donsì et al., 2011). The ability of a surfactant to restore stability after thawing depends on how quickly it can migrate to the oil-water interface and re-establish a cohesive film.

The contrasting results between Span 20 and Span 80 highlight the critical role of surfactant selection. MEG shows good compatibility with both Span 20 and Span 80, demonstrating its versatility. However, overall stability depends heavily on the co-surfactant's properties. Span 20's higher HLB supports robust initial stability, while Span 80's lower HLB compromises long-term stability under freeze-thaw conditions. Hong et al. (2018) also emphasized that surfactants with balanced HLB values provide better protection against coalescence and phase separation.

Molecular interactions between surfactants, the oil phase, and water are also pivotal. Surfactant molecules must form a cohesive, resilient film around the oil droplets to prevent coalescence. In the case of Span 80, its longer hydrophobic chain may limit efficient packing at the interface, leading to reduced stability.

Using various ratios of oil, deionized water, MEG, and surfactants specifically, Span 20 and Span 80, as revealed in Figure 4.5, the stability of emulsions was examined. For example, MS20-A exhibited excellent stability with Span 20 (0% separation), but substituting Span 80 in the same formulation led to a substantial decrease in stability (56.76% separation). Similarly, MS20-B showed good stability with Span 20 (5.71% separation) but experienced 50% separation when Span 80 was used. These results demonstrate that both surfactant selection and composition significantly influence emulsion stability under freeze-thaw conditions.

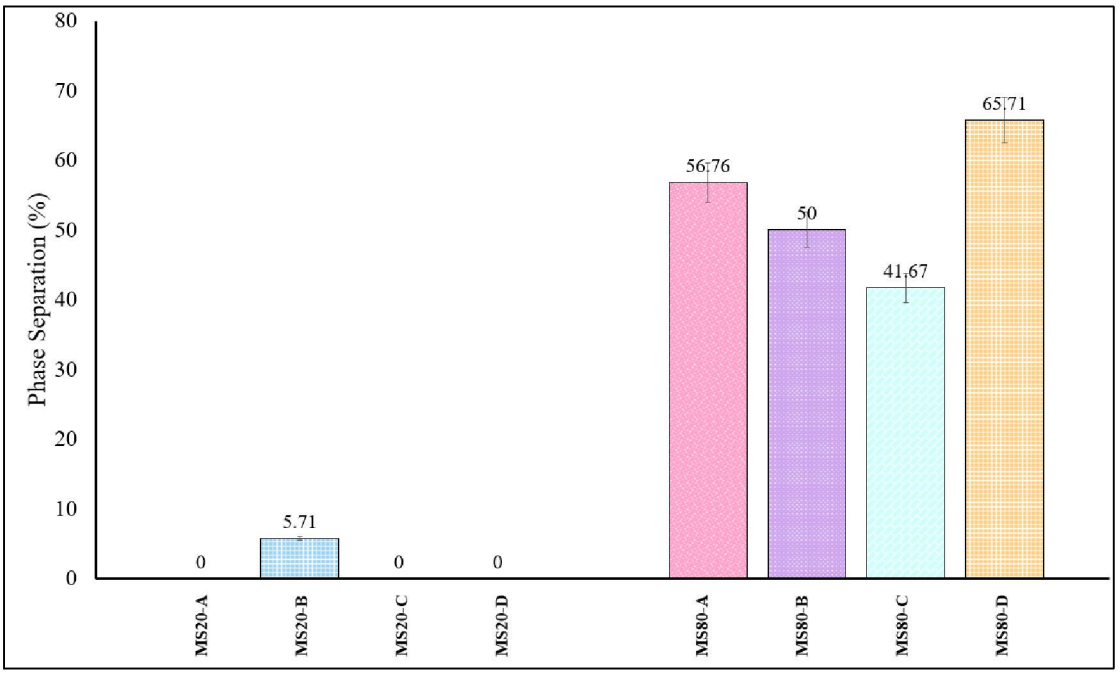

Figure 4.5 Freeze-thaw analysis of mixed surfactant emulsions

In MS20-C, the emulsion remained completely stable with Span 20 (0% separation), but stability dropped significantly to 41.67% when Span 80 was used. Similarly, MS20-D maintained excellent stability with Span 20 (0% separation), yet exhibited the highest reduction among all samples, 65.71% separation under Span 80. These results clearly demonstrate the critical role of surfactant hydrophilic-lipophilic balance (HLB) in determining emulsion stability during freeze-thaw cycles, with Span 20 consistently outperforming Span 80.

The effectiveness of a surfactant depends not only on its HLB value but also on molecular interactions and the precise ratios of oil, water, and surfactant (Thanasukarn et al., 2004). Span 20, with its balanced HLB, forms strong interfacial films that effectively stabilize emulsions, whereas Span 80's lower HLB and higher lipophilicity reduce its ability to maintain cohesion around oil droplets. These interactions are crucial for preventing coalescence and preserving emulsion integrity, as highlighted by Tesch et al., who emphasized careful selection and formulation of surfactant mixtures for optimal stability.

Analysis of both single and mixed surfactant systems across multiple freeze-thaw cycles provides further insight. Single-surfactant emulsions showed wide variability, with Span 20 achieving complete stability in S20-A, while Span 80 led to higher separation rates due to its hydrophobic nature. Sample D consistently displayed

superior stability, underscoring the importance of a well-balanced surfactant system. In mixed systems, combining MEG with Span 20 resulted in excellent initial stability, reflecting the synergy of balanced HLB values and strong molecular interactions. Replacing Span 20 with Span 80, however, caused a marked decline in stability, highlighting the challenge of maintaining emulsion integrity with more hydrophobic surfactants under repeated freeze-thaw stress.

These findings emphasize that surfactant selection and formulation design are critical for producing emulsions capable of sustaining effective interfacial tension, adapting to mechanical stress, and resisting phase separation. Optimizing surfactant mixtures and exploring novel combinations will be essential for enhancing emulsion robustness, particularly in applications such as pharmaceuticals, cosmetics, and food processing, where stability directly affects product performance and shelf life.

4.1.3 Rheology Test

Understanding the flow behavior and structural characteristics of emulsions, particularly those intended for culinary, cosmetic, or medicinal applications, requires a detailed rheological analysis. The viscosity of an emulsion reflects the extent of internal interactions between droplets and the overall stability of the dispersed phase. In this study, the flow properties and structural integrity of virgin coconut oil-in-water emulsions stabilized with different surfactant systems were examined under mechanical stress by investigating the relationship between viscosity and shear rate. Although the measurements were conducted as part of this work, previous studies provide context for interpreting the results (Khor et al., 2014). All formulations exhibited clear pseudoplastic, non-Newtonian behavior, characterized by a progressive decrease in viscosity with increasing shear rate. This shear-thinning trend was observed consistently across all samples, whether stabilized with single or mixed surfactant systems, aligning with general observations reported in the literature (da Silva Gulão et al., 2018), which further supports the interpretation of the flow behavior in similar emulsions.

For the MEG-stabilized emulsions (Figure 4.6), MEG-A exhibited the highest viscosity at low shear (0.28 Pa·s at 1 s^{-1}), indicating stronger droplet association and greater structural resistance at this surfactant concentration. MEG-B exhibited a negative viscosity value of –0.013 Pa·s at a shear rate of 1 s^{-1}, which is attributed to instrument baseline artefacts rather than a true physical property. Such apparent negative viscosity behavior has been reported in the literature and is often associated with measurement limitations and anomalous system responses rather than actual material flow characteristics (Bormashenko & Shoval, 2025).

At slightly higher shear (3.58 s^{-1}), MEG-C displayed the highest viscosity (0.102 Pa·s), followed closely by MEG-A and MEG-D, while MEG-B remained the lowest across the entire shear range. These observations suggest that MEG-C (60%) forms a network that better resists structural breakdown under shear, whereas MEG-B (40%) produces the weakest droplet interactions.

Each MEG concentration appears to create a distinct interfacial arrangement, influencing droplet packing and network formation differently. MEG-A promotes strong droplet interactions at low shear, MEG-C maintains higher viscosity under increasing shear, and MEG-D exhibits weaker structural integrity despite higher surfactant loading. These trends highlight the role of interfacial organization in determining emulsion rheology, even in single-surfactant systems.

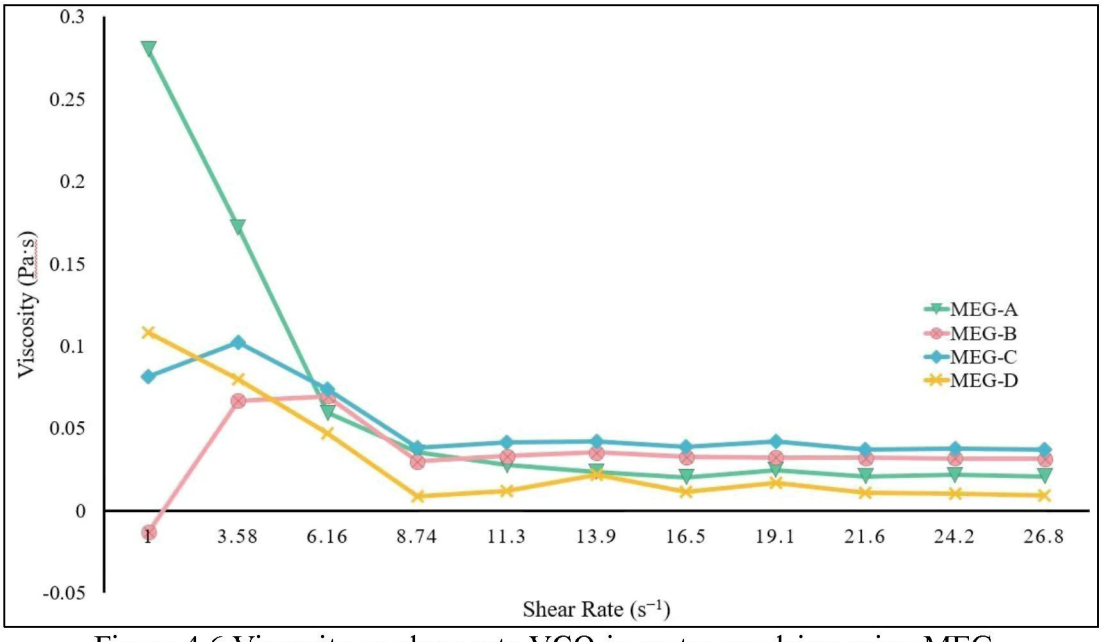

Figure 4.6 Viscosity vs shear rate VCO-in-water emulsion using MEG

Figure 4.7 shows that the Span 20–stabilized emulsions. S20-C, containing 40% surfactant, exhibited the highest viscosity at low shear (38.3 Pa·s at 1 s^{-1}), followed by a substantial decline to 1.19 Pa·s at 26.8 s^{-1}. This steep reduction reflects a highly shear-sensitive network, indicating that Span 20 promotes strong droplet flocculation and close droplet packing at rest. S20-A, S20-B, and S20-D showed lower initial viscosities (7.21, 0.965, and 4.17 Pa·s, respectively) but retained the same shear-thinning trend. The markedly higher viscosities of all Span 20 systems compared with MEG-stabilized emulsions suggest that Span 20, with its higher HLB value (~8.6), forms a more cohesive interfacial film and enables denser droplet association within an oil-in-water environment. The stronger droplet network at low shear is consistent with increased HLB promoting effective surface coverage, reduced coalescence, and enhanced droplet crowding, all of which increase resistance to deformation.

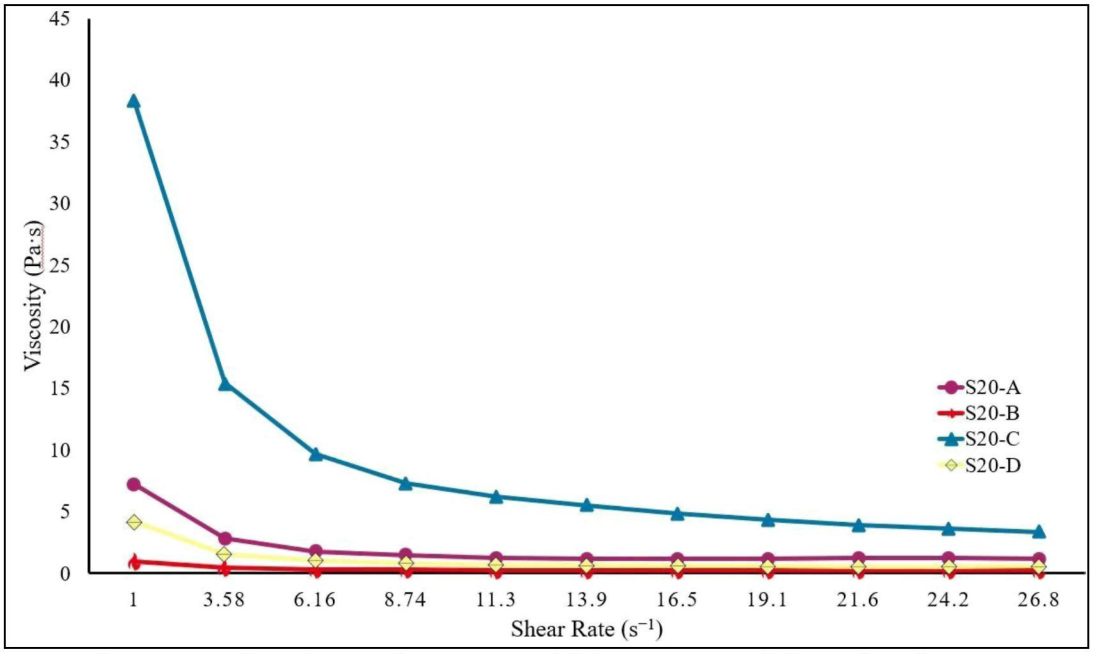

Figure 4.7 Viscosity vs shear rate VCO-in-water emulsion using Span 20

Figure 4.8 shows that the Span 80 emulsions exhibited pronounced pseudoplastic behavior, although with substantially lower viscosities compared with Span 20 systems. S80-A displayed the highest low-shear viscosity (20.3 Pa·s at 1 s^{-1}), followed by a sharp decline to 1.45 Pa·s at 26.8 s^{-1}. S80-B, S80-C, and S80-D had lower initial viscosities (0.0529, 3.55, and 3.46 Pa·s, respectively) and also decreased with increasing shear. The low viscosities indicate a weaker internal droplet network, consistent with the lipophilic nature of Span 80 (HLB ≈4.3), which limits interfacial coverage and reduces steric repulsion. As a result, droplet–droplet interactions are weaker, producing a looser structural arrangement and lower flow resistance. At high shear, all emulsions converge to low viscosities (~0.03–0.8 Pa·s), reflecting network disruption and droplet alignment under shear.

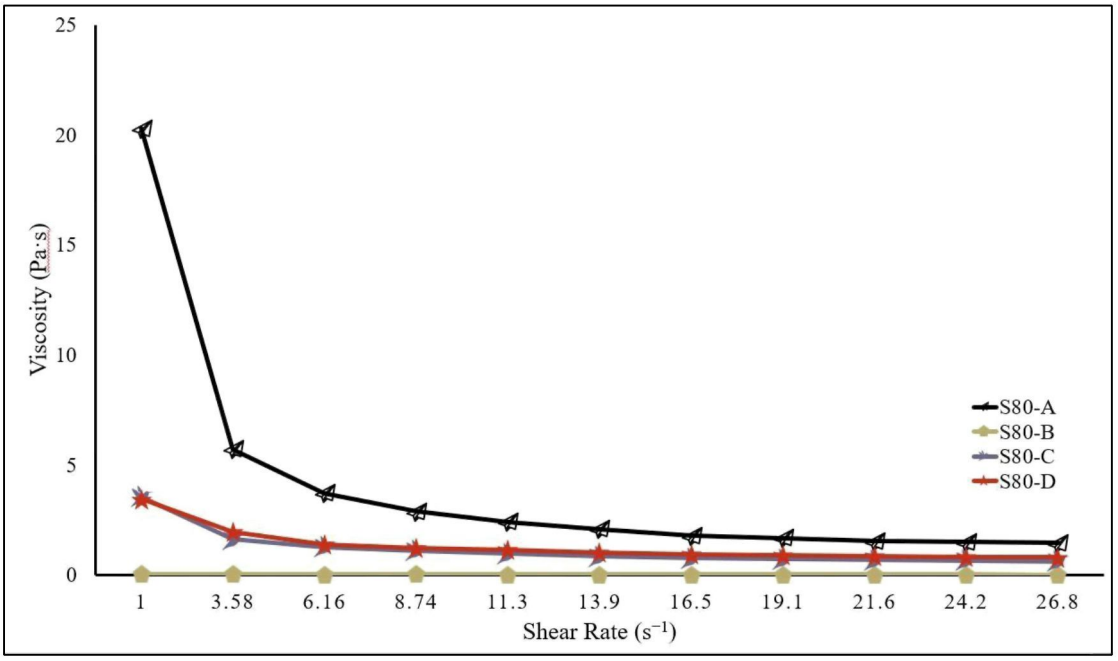

Figure 4.8 Viscosity vs shear rate VCO-in-water emulsion using Span 80

The comparison between Span 20 and Span 80 emulsions highlights the critical influence of HLB on rheological behavior. Span 20 emulsions exhibited much higher low-shear viscosities, particularly S20-C (38.3 Pa·s at 1 s^{-1}), indicating stronger droplet flocculation and denser packing due to the higher HLB (~8.6), which promotes effective surface coverage and cohesive interfacial films. In contrast, Span 80 emulsions formed weaker droplet networks, as evidenced by their lower viscosities. Both surfactants exhibited pseudoplastic (shear-thinning) behavior however, the stronger network in Span 20 systems resulted in greater resistance to deformation at low shear. These results demonstrate that surfactant HLB critically governs interfacial cohesion, droplet aggregation, and the overall rheological response of oil-in-water emulsions.

Mixed-surfactant emulsions combining MEG with Span 20 (MS20) as indicated in Figure 4.9 exhibited low-shear viscosities ranging from 0.34 Pa·s (MS20-A) to 17.7 Pa·s (MS20-C) and sharply declining to 0.088–1.51 Pa·s at 26.8 s^{-1}. The lower initial viscosities compared with single-surfactant Span 20 systems indicate that the combination promotes the formation of smaller, well-stabilized droplets rather than extensive flocculated networks.

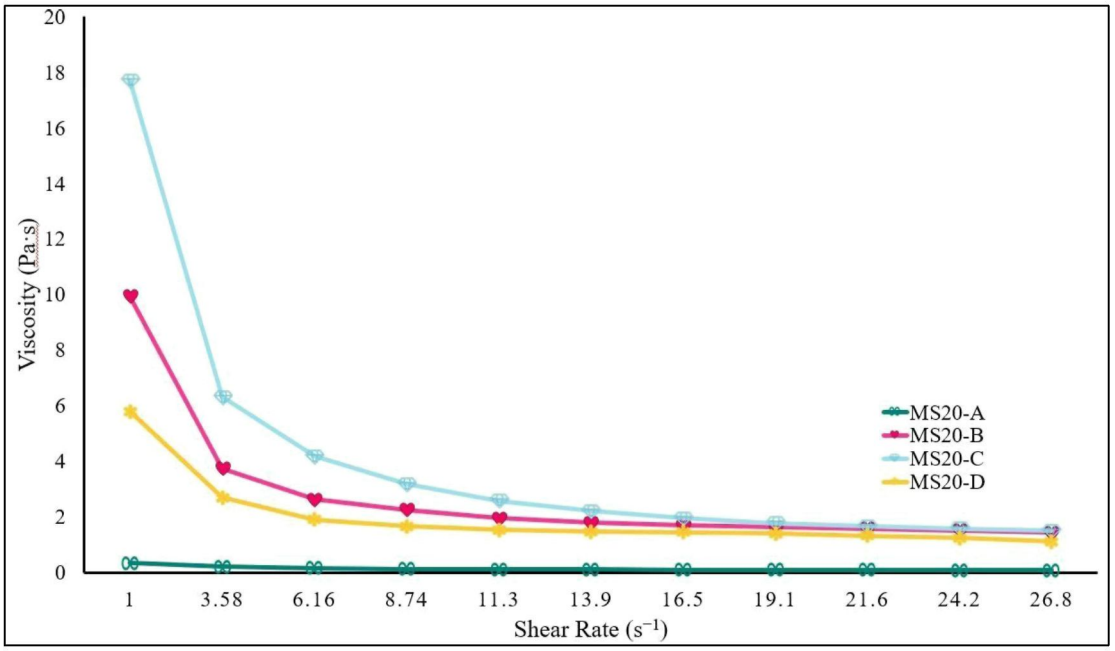

Figure 4.9 Viscosity vs shear rate VCO-in-water emulsion using mixed surfactant (MEG & Span 20)

Mechanistically, MEG contributes hydrogen bonding and short-range polar interactions that strengthen the interfacial layer on each droplet, enhancing droplet stability and preventing coalescence. Span 20 provides the hydrophobic–hydrophilic balance necessary for effective emulsification. Together, these surfactants create a flexible, elastic interface that allows droplets to remain discrete yet closely packed without forming large clusters. This structure reduces internal resistance to flow, particularly at low shear, while still retaining sufficient interfacial cohesion to resist coalescence under moderate shear.

The steep shear-thinning behavior observed across all MS20 formulations reflects the gradual alignment and deformation of droplets under increasing shear, breaking weak droplet–droplet interactions while maintaining the overall integrity of the emulsion. Differences among formulations, such as the higher low-shear viscosity of MS20-C, likely arise from variations in surfactant concentration or local packing efficiency at the interface, which enhance temporary droplet association. Overall, the MEG–Span 20 system demonstrates that combining a polar, hydrogen-bonding surfactant with a conventional emulsifier can balance droplet stability and flowability, producing a more tunable rheological profile compared with single-surfactant systems.

The MEG–Span 80 emulsions (Figure 4.10) showed low viscosities at low shear, ranging from 0.0491 Pa·s for MS80-A to 0.19 Pa·s for MS80-B, which dropped further at high shear. This behavior highlights their pseudoplastic nature, meaning the emulsions flow easily under stress but still maintain droplet stability. At the droplet level, MEG and Span 80 work together to form a flexible interfacial layer. MEG brings hydrogen bonding and polar interactions, while Span 80 anchors at the oil–water interface. The result is droplets that are individually well-stabilized but loosely packed, preventing large clusters from forming. This creates a sparse network with low internal resistance, allowing the emulsions to deform easily when sheared.

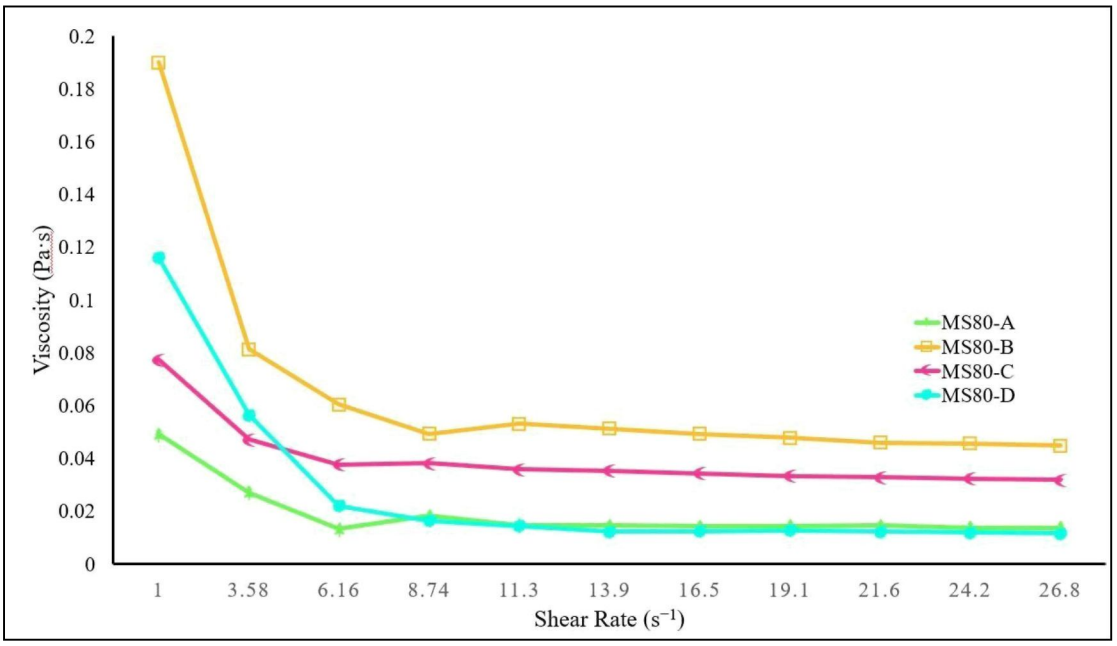

Figure 4.10 Viscosity vs shear rate VCO-in-water emulsion using mixed surfactant (MEG & Span 80)

Among the formulations, MS80-B stood out with slightly higher low-shear viscosity, suggesting a bit more droplet association, whereas MS80-A and MS80-D were the most fluid, reflecting minimal droplet interaction. Overall, the MEG–Span 80 system demonstrates how a combination of a polar surfactant and a lipophilic emulsifier can stabilize droplets effectively while keeping the emulsion highly flowable and easy to handle.

Overall, the mixed-surfactant systems demonstrate that combining MEG with either Span 20 or Span 80 results in more dispersed droplet arrangements with limited flocculation. This structure lowers low-shear viscosity while maintaining emulsion stability through efficient interfacial coverage rather than the formation of dense droplet networks. Consequently, these formulations offer reduced flow resistance while retaining enough structural integrity to withstand shear deformation.

The observed shear-thinning behavior across all systems can be attributed to the dynamic response of surfactant-coated droplets within the aqueous phase. At low shear, the droplets are stabilized by interfacial films that enable short-range interactions, including hydrogen bonding, van der Waals forces, and steric effects, forming a weakly interconnected network that resists flow. As the shear rate increases, these inter-droplet

associations gradually break, and droplets align in the direction of flow, causing a progressive decrease in viscosity. Surfactant concentration influences this behavior by modulating interfacial packing and interaction strength, while mixed surfactants enhance interfacial efficiency and elasticity through the complementary balance of hydrophilic and lipophilic functionalities (Yang and Pal, 2020).

Collectively, these results highlight the critical role of formulation composition in tailoring emulsion rheology. The behavior observed aligns with established models of non-Newtonian flow and corroborates literature reports on emulsion stability and deformation dynamics. Understanding these mechanisms is particularly valuable for applications requiring controlled flow under stress, such as pharmaceutical creams, cosmetic emulsions, and food-related dispersions.

4.1.4 Droplet Size Distribution

The analysis of droplet size in emulsions using an optical polarizing microscope reveals several factors influencing the variation in droplet size. The concentration and type of surfactants are critical determinants. Surfactants reduce the interfacial tension between the oil and water phases, facilitating the formation of smaller droplets. Higher surfactant concentrations generally lead to smaller droplet sizes due to better stabilization of the oil droplets in the continuous water phase (Fang *et al.*, 2022). Additionally, the proportion of oil to water in the emulsion significantly influences droplet size. A higher oil content can result in larger droplets because there is more oil to be dispersed within the same amount of water, while a higher water content tends to produce smaller droplets due to the higher dilution of the oil phase.

Different surfactants have varying efficiencies in stabilizing emulsions. For instance, the use of methyl-α-*D*-glucopyranoside (MEG), Span 20, and Span 80 in the provided samples affects the droplet size differently due to their distinct molecular structures and HLB values. Because of its hydrophilic nature with an HLB value of 8.6, which enables it to interact with the water phase and stabilize oil droplets more effectively, Span 20 is generally more effective at producing finer dispersions in O/W emulsions. In contrast, Span 80 which has an HLB value of 4.3 is better suited for W/O emulsions or situations where larger droplet sizes are acceptable (Bunawan *et al.*, 2023). It is possible to optimize the formulation for particular applications, such as in food goods, medicines, or cosmetics, by having a better understanding of the HLB value and

molecular properties of each surfactant. The method and intensity of mixing during emulsion preparation also play a crucial role. High-shear mixing or ultrasonication typically results in smaller droplet sizes due to the increased energy input that breaks down the oil phase more effectively.

In the single surfactant systems, MEG, Span 20, and Span 80 were used. For formulations using MEG, the mean droplet size decreased with increasing surfactant concentration as shown in Table 4.1, highlighting the ability of the surfactant to effectively reduce interfacial tension and create smaller droplets. Specifically, MEG-A had a mean droplet size of 31.11 ± 1.694 µm while MEG-B showed a smaller mean droplet size of 21.00 ± 1.850 µm. This trend aligns with the findings by (Astaraki, 2016), who reported that higher surfactant concentrations generally result in smaller droplet sizes due to enhanced reduction in interfacial tension. MEG-C exhibited a mean droplet size 31.00 µm with confidence interval ± 3.438 µm. The increasing oil content slightly increased the droplet size, suggesting a balance between oil and surfactant concentration. MEG-D showed a droplet size of 27.00 µm ± 6.796 µm. Figure 4.11 shows polarized optical microscopy images of emulsions prepared with MEG as the surfactant, supporting the observed variations in droplet size. Overall, the droplet size is influenced by both surfactant concentration and oil-to-water ratio.

Table 4.1
Droplet Size Analysis of Oil-in-Water Emulsion using MEG

Sample	**Mean (µm)**
MEG-A	31.11 ± 1.694
MEG-B	21.00 ± 1.850
MEG-C	31.00 ± 3.438
MEG-D	27.00 ± 6.796

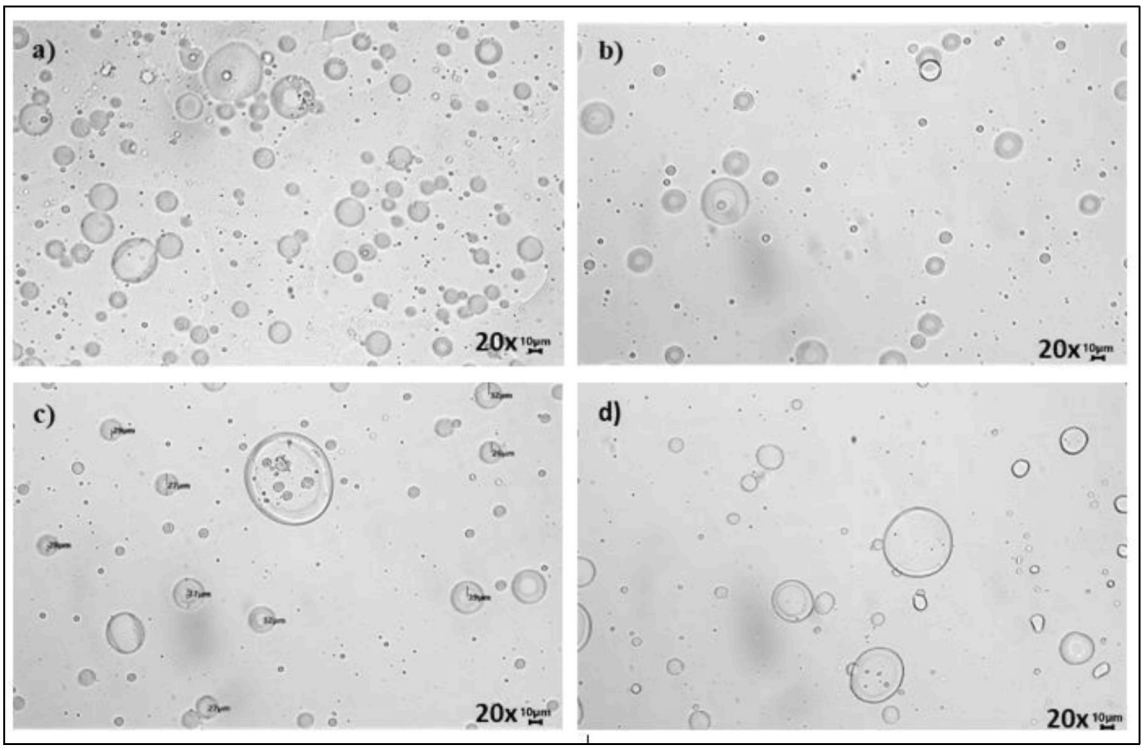

Figure 4.11 Polarized optical microscopy images of emulsions using MEG as surfactant a) MEG-A b) MEG-B c) MEG-C d) MEG-D

For the Span 20 formulations, droplet sizes were generally smaller than those observed in the MEG-stabilized emulsions. S20-A had a mean droplet size of 11.00 ± 0.477 µm, demonstrating that Span 20, with its low HLB, is effective at producing stable emulsions with relatively small droplets. S20-B, which contains the same amount of oil as S20-A but a higher surfactant content, had a larger mean droplet size (23.70 ± 1.014 µm), suggesting that increasing the surfactant proportion can influence droplet coalescence and growth under certain conditions. S20-C showed a mean droplet size of 10.44 ± 0.678 µm, indicating that the balance between oil and surfactant plays a key role in forming smaller droplets. S20-D exhibited the smallest droplets (10.20 ± 0.739 µm), where a lower oil-to-water ratio and relatively high surfactant content contributed to efficient droplet dispersion. These observations are supported by Maindarkar et al. (2013), who reported that Span 20 stabilizes emulsions effectively, producing smaller, more homogeneous droplets. Table 4.2 summarizes the particle size data, while Figure 4.12 presents polarized optical microscopy images, illustrating droplet morphology and distribution across the formulations.

Table 4.2
Droplet Size Analysis of Oil-in-Water Emulsion using Span 20

Sample	Mean (μm)
S20-A	11.00 ± 0.477
S20-B	23.70 ± 1.014
S20-C	10.44 ± 0.678
S20-D	10.20 ± 0.739

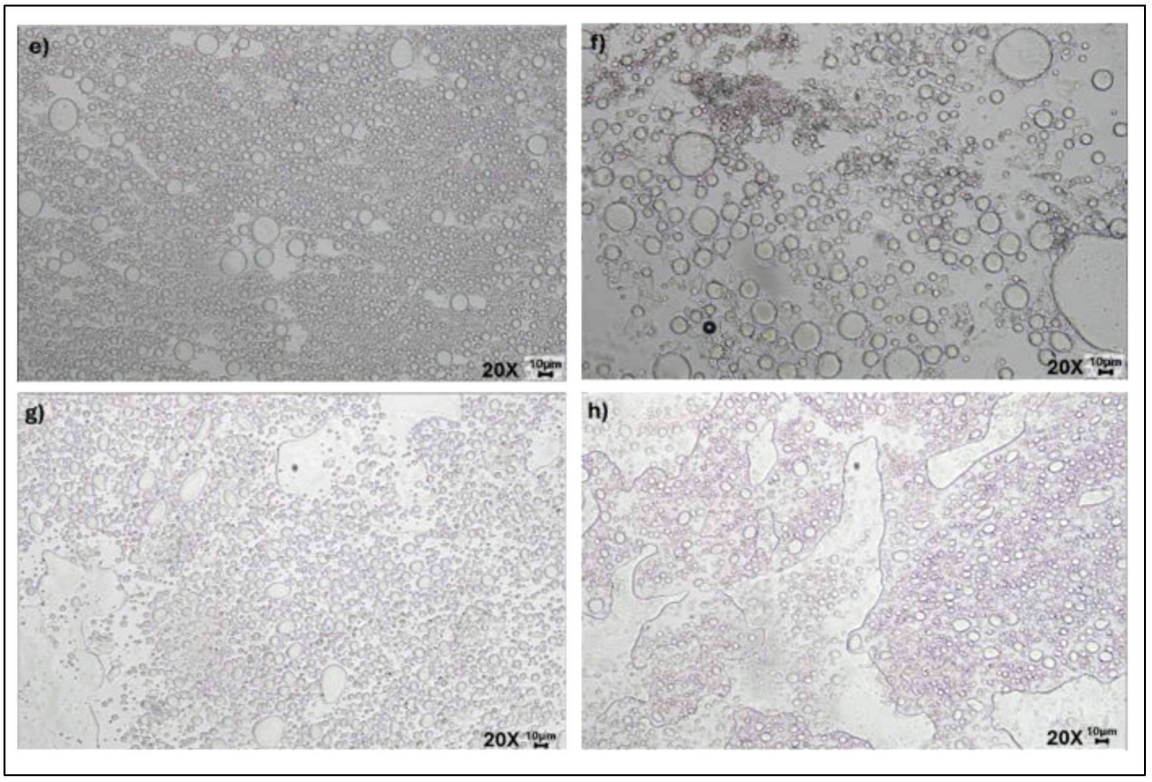

Figure 4.12 Polarized optical microscopy images of emulsions using Span 20 as surfactant e) S20-A f) S20-B g) S20-C h) S20-D

For the Span 80 formulations, droplet sizes varied more widely than in Span 20 emulsions. S80-B exhibited the largest droplets (54.80 ± 2.257 μm), reflecting that Span 80, with its relatively low HLB (≈4.3), is less suitable for stabilizing oil-in-water emulsions and reducing droplet size. Other samples also showed larger droplets compared with Span 20, indicating weaker interfacial coverage and reduced ability to prevent coalescence.

These findings align with Schramm et al. (2003), who noted that surfactants with low HLB may not always produce small droplets due to insufficient interfacial activity in O/W systems. Similarly, Hu et al. (2015) reported that lipophilic surfactants like Span 80 tend to form larger droplets because they are less effective at reducing interfacial tension in water-continuous emulsions. Table 4.3 summarizes the particle size analysis for these formulations.

Table 4.3
Droplet Size Analysis of Oil-in-Water Emulsion using Span 80

Sample	Mean (μm)
S80-A	20.70 ± 1.121
S80-B	54.80 ± 2.257
S80-C	15.00 ± 1.216
S80-D	NA

*NA: Not Available

For the Span 80 formulations, droplet sizes varied considerably. S80-A had a mean droplet size of 20.70 ± 1.121 μm, larger than emulsions stabilized with higher HLB surfactants, indicating that the relatively low HLB of Span 80 is generally less effective at reducing droplet sizes in oil-in-water systems. S80-C showed a moderate reduction in droplet size (15.00 ± 1.216 μm), suggesting that adjusting the oil-to-surfactant ratio can partially compensate for the low HLB.

In S80-D, particle size distribution could not be detected, implying a highly uniform droplet population. This formulation uses a high surfactant-to-oil ratio (30% Span 80 relative to the oil phase), which ensures sufficient interfacial coverage and reduces interfacial tension. As a result, small, evenly distributed droplets are formed despite the low HLB of Span 80. Polarized optical microscopy images (Figure 4.15) visually confirm the improved uniformity and reduced droplet size in this sample.

These observations highlight that while HLB plays a primary role in determining droplet size and emulsion stability, surfactant concentration and oil-to-surfactant ratio are equally critical, particularly for lipophilic surfactants like Span 80, where higher surfactant content can produce smaller, more uniform droplets.

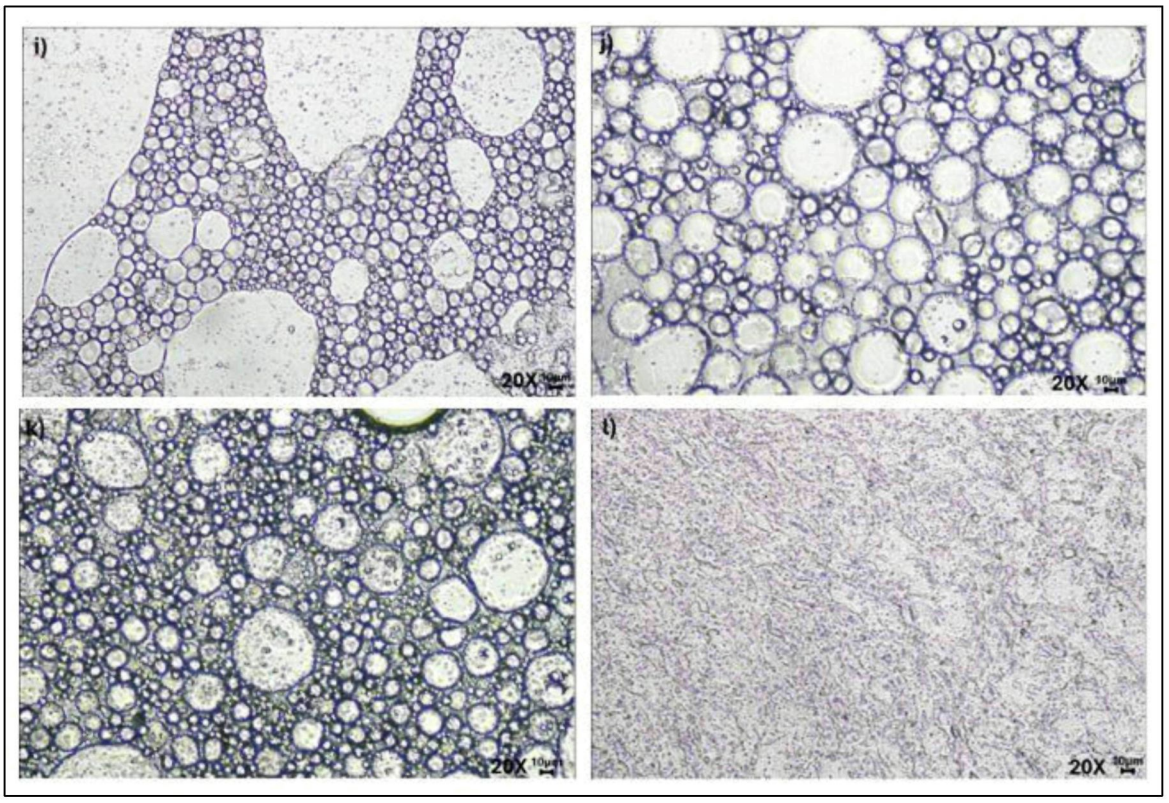

Figure 4.13 Polarized optical microscopy images of emulsions using Span 80 as surfactant i) S80-A j) S80-B k) S80-C l) S80-D

In line with previous studies, S80-D demonstrates that elevated surfactant concentrations can produce highly stable emulsions with very small, uniform droplets. Capdevila et al. (2010) reported that emulsions containing Span 80 at high levels achieve significantly reduced droplet sizes, consistent with the observations in S80-D. The relatively low oil-to-water ratio in this formulation further enhances stability, providing an abundance of continuous phase that allows the dispersed oil droplets to be thoroughly stabilized by the surfactant, resulting in a uniform dispersion.

According to Debraj et al. (2023), a combination of low oil-to-water ratio and high surfactant content promotes emulsions with minimal droplet sizes and improved stability. Similarly, Cho et al. (2008) noted that high surfactant concentrations can lead to microemulsion formation with nanometer-scale droplets, rendering the particle size distribution indistinguishable. During homogenization, high surfactant levels reduce interfacial tension, facilitating the formation of smaller droplets and a narrower particle size distribution, as also highlighted by Capdevila et al. (2010).

The high degree of homogeneity observed in S80-D can therefore be attributed to the optimized surfactant concentration and the effective stabilization provided by Span 80. This is in agreement with L'Estimé et al. (2024), who emphasized the importance of surfactant type and concentration in achieving desired emulsion properties. These results underscore that, for lipophilic surfactants like Span 80, surfactant concentration and oil-to-water ratio are key factors in controlling droplet size and uniformity, even when the surfactant's HLB is relatively low.

Synergistic effects were observed when MEG was combined with either Span 20 or Span 80 in mixed-surfactant formulations. As shown in Table 4.4, MS20-B (MEG + Span 20) had an average droplet size of 9.44 ± 0.405 μm, comparable to Span 20 alone, but the mixed system displayed improved droplet uniformity and stability. The combination of MEG and Span 20 enhances interfacial coverage through complementary interactions, creating a more flexible and cohesive interfacial layer that reduces droplet coalescence.

In contrast, formulations combining MEG with Span 80 showed a more pronounced reduction in droplet size compared with Span 80 alone, indicating that the synergistic effect is particularly beneficial when the single surfactant is less effective at stabilizing small droplets. These results demonstrate that mixed-surfactant systems can optimize both droplet size and emulsion stability by leveraging the complementary properties of polar and nonpolar surfactants.

Table 4.4
Droplet Size Analysis of Oil-in-Water Emulsion using MEG and Span 20

Sample	Mean (μm)
MS20-A	20.30 ± 1.121
MS20-B	9.44 ± 0.405
MS20-C	NA
MS20-D	10.00 ± 0.754

*NA: Not Available

The use of a combination of surfactants improves the organization of molecules at the interface between oil and water, resulting in a more effective reduction of the force between the two phases. This leads to the creation of smaller droplets and increased stability of the emulsion (Onaizi, 2022). The mean droplet size in MS20-A was 20.30 ± 1.121 μm. Figure 4.16 depicts polarized optical microscope pictures of emulsions formed by the combination of surfactants MEG and Span 20.

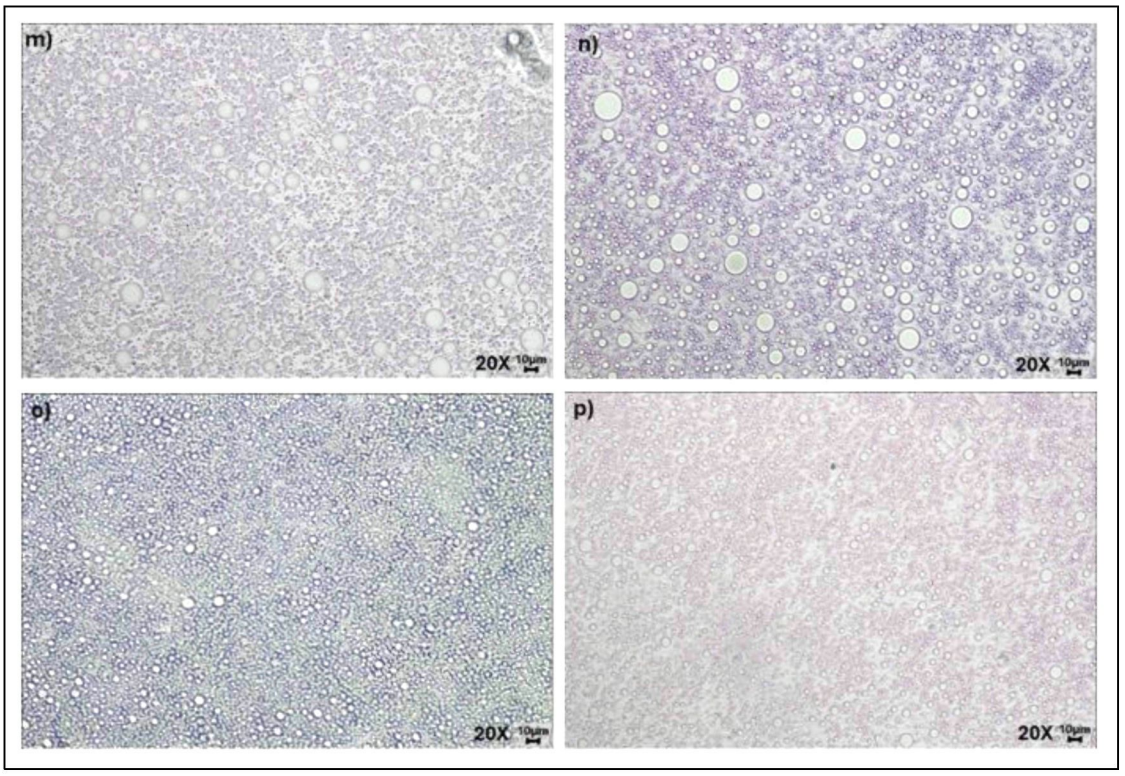

Figure 4.14 Optical polarizing microscopy images of emulsions using MEG and Span 20 as surfactants m) MS20-A n) MS20-B o) MS20-C p) MS20-D

Additionally, MS20-D exhibited a mean droplet size of 10.00 ± 0.754 µm. The lower oil content combined with mixed surfactants effectively maintains smaller droplet sizes, indicating a stable emulsion. This aligns with the studies that stated that formulations with lower oil content and mixed surfactants provide a more stable and homogenous emulsion due to the enhanced synergistic effect of the surfactants (Raya *et al.*, 2022). Overall, the data suggest that mixed surfactant formulations, particularly those combining MEG with Span 20, significantly improve the emulsion properties by reducing droplet size and increasing stability.

The inability to measure the particle size distribution for MS20-C can be attributed to several factors, despite the molecules being visibly identifiable under microscopy. One of the primary reasons is the high polydispersity index (PDI) of the emulsion, indicating a broad range of droplet sizes. This diversity often results in droplets with irregular, non-spherical shapes, which pose significant challenges for most particle size measurement techniques (Bon *et al.*, 2007). Emulsions with non- spherical droplets can be difficult to analyze accurately because standard measurement techniques typically assume spherical geometry, leading to potential size underestimation or overestimation depending on the droplet orientation.

Furthermore, manual measurement under microscopy may be required for non-spherical droplets; however, defining their boundaries precisely is challenging, which can affect accuracy. Another contributing factor could be the agglomeration of droplets within the emulsion, where partial coalescence results in clusters that are visually detectable but do not represent individual particles suitable for size analysis. These clusters form due to droplets partially merging, creating larger, irregularly shaped aggregates that distort particle size readings. Additionally, the limitations of the measurement instruments used may play a significant role. Particle size analyzers have specific detection ranges, and if the droplet sizes in MS20-C fall outside these ranges whether due to being too small, too large, or due to the sample's viscosity or dilution, it can compromise the sensitivity and accuracy of the measurements. These factors collectively highlight the complexities involved in obtaining precise particle size data for emulsions with heterogeneous characteristics.

Table 4.5 shows that the average size of droplets in Sample MS80-A is 30.90 ± 1.090 µm. The somewhat larger droplets suggest that the lower hydrophilic-lipophilic balance (HLB) value of Span 80 has an impact on the size of the droplets, in comparison to the mixture containing Span 20. Surfactants with lower HLB values typically result in larger droplet sizes in oil-in-water emulsions. The average droplet size of MS80-B was 10.80 ± 0.739 µm. The combination of MEG with Span 80 results in a notable reduction in droplet size compared to using Span 80 alone in formulations. The mean droplet size in MS80-C was 21.20 ± 0.812 µm. The benefits of mixed surfactant systems are seen in the relatively small reduction in droplet size compared to single surfactant systems. Figure 4.17 indicates the size of droplets in O/W emulsion images using MEG and Span 80 surfactants.

Table 4.5
Droplet Size Analysis of Oil-in-Water Emulsion using MEG and Span 80

Sample	**Mean (µm)**
MS80-A	30.90 ± 1.090
MS80-B	10.80 ± 0.739
MS80-C	21.20 ± 0.812
MS80-D	31.40 ± 1.562

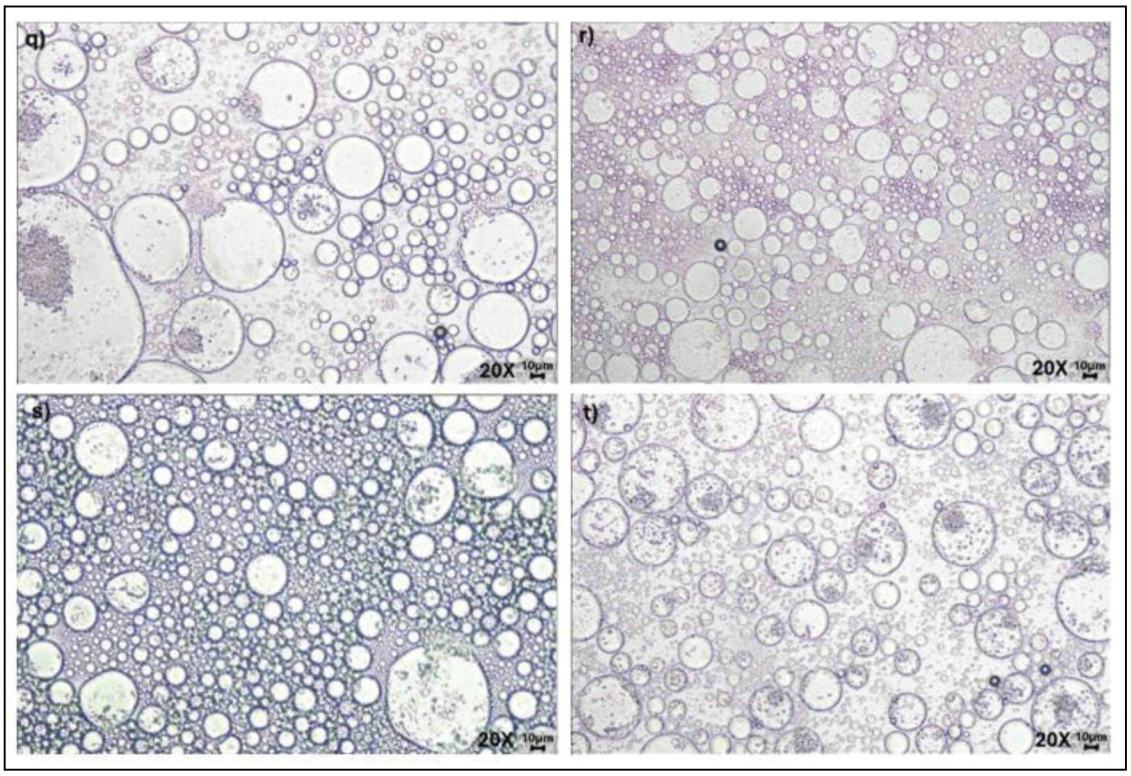

Figure 4.15 Optical polarizing microscopy images of emulsions using MEG and Span 80 as surfactants q) MS80-A r) MS80-B s) MS80-C t) MS80-D

The significance of surfactant concentration and selection in producing stable emulsions is shown by the examination of droplet sizes and confidence intervals across different formulations. Because surfactants improve stabilization by efficiently lowering interfacial tension between the water and oil phases, increasing their concentration often results in smaller droplet sizes (Hauzin *et al.*, 2024). As an example, Span 20, which is well-known for its moderate hydrophilicity and efficient lowering of interfacial tension, usually results in emulsions with smaller and more uniform droplets, particularly at higher concentrations. On the other hand, Span 80 is less successful in lowering interfacial tension in oil-in-water (O/W) systems because of its larger molecular structure and lower hydrophilic-lipophilic balance (HLB) value. Because Span 80 has a lesser capacity to stabilize the interface in comparison to Span 20, increasing its concentration often results in emulsions with bigger and less uniform droplet sizes.

While certain formulations (MS20-A, MS20-B, MS20-C, and MS20-D) showed no evidence of phase separation, suggesting stability, others (MS80-A, MS80-B, MS80-C, and MS80-D) showed physical changes that indicated instability, as Table 4.6 illustrates. These variations are explained by variations in droplet size and distribution, two important elements affecting the general characteristics of the emulsion. Because of their higher surface area, which enables surfactants to effectively inhibit droplet aggregation, smaller droplets contribute to improved stability during storage. On the other hand, the phase separation seen in MS80-A, MS80-B, MS80-C, and MS80-D indicates that the presence of bigger or more polydisperse droplets may have jeopardized their stability. Over time, creaming or sedimentation may result from larger droplets being more vulnerable to gravitational forces. To achieve the appropriate droplet size distribution, the kind of surfactant and its associated HLB value must be chosen (Ponphaiboon *et al.*, 2024). Higher HLB surfactants, such MEG, have strong hydrophilic properties and are thus better at creating smaller droplets in O/W emulsions. MEG and Span 20 together produced notably more stable emulsions with smaller droplets, indicating a synergistic interaction between the two surfactants. Increased emulsion stability and better droplet dispersion result from this synergistic interaction that improves the stabilization process.

These results highlight how crucial it is to maximize the kind and makeup of surfactants in order to get the required characteristics in emulsion systems, whether for use in food, medicine, or cosmetics. Formulators in a variety of sectors must take into account the capacity to manage droplet size via careful surfactant selection since it affects the emulsion's texture and appearance and prolongs its shelf life.

Table 4.6
Observation of virgin coconut oil-in-water emulsion phase separation

Sample	Phase separation
MS20-A	/
MS20-B	/
MS20-C	/
MS20-D	/
MS80-A	X
MS80-B	X
MS80-C	X
MS80-D	X

/ = stable or no physical changes X= not stable and physical changes occur

4.1.5 Fourier-transform infrared spectroscopy (FTIR)

Fourier-transform infrared spectroscopy (FTIR) is a powerful analytical technique used to characterize the molecular composition and interactions within materials by measuring their infrared absorption spectra. In the context of studying emulsions, FTIR provides insight into the functional groups present and can reveal how components such as oils, surfactants, and water interact at the molecular level. For example, in virgin coconut oil-in-water emulsions stabilized with surfactants like methyl-α-*D*-glucopyranoside (MEG), FTIR can help identify specific bond interactions and assess the stability and compatibility of the emulsion system (Som *et al.*, 2023). By analyzing the spectral regions associated with key functional groups, FTIR can also detect changes in the molecular environment and potential emulsification mechanisms. This information is crucial for understanding the chemical structure and potential performance of emulsions in various applications.

First, the characteristic peaks of VCO provide essential baseline information. The C–H stretching vibrations, typically found in the 2920–2850 cm^{-1} range, indicate the presence of alkanes from fatty acid chains within VCO. The prominent C=O stretching band near 1740–1750 cm^{-1} is characteristic of ester bonds found in triglycerides, the primary component of VCO (Chiplunkar and Pratap, 2016). Additionally, C–O stretching vibrations around 1160–1100 cm^{-1} are associated with the

glycerol backbone in triglycerides, further confirming the oil's structural components within the emulsion. The water content in the emulsion can be observed through the broad O–H stretching band near 3400 cm^{-1}, indicative of free and hydrogen-bonded water (Mohamed *et al.*, 2017). This peak is essential in assessing the emulsion's hydration state and any potential interactions between the water phase and surfactant or oil phase. The presence of this peak at high intensities in certain spectra, particularly for surfactants with multiple hydroxyl groups like MEG, suggests enhanced hydrophilicity and hydrogen bonding capability, which strengthen the emulsion's interfacial stability. The FTIR spectral analysis of virgin coconut oil emulsions, stabilized with single surfactants that illustrates in Figure 4.15, Figure 4.16 and Figure 4.19, reveals significant information about the chemical interactions contributing to emulsion stability.

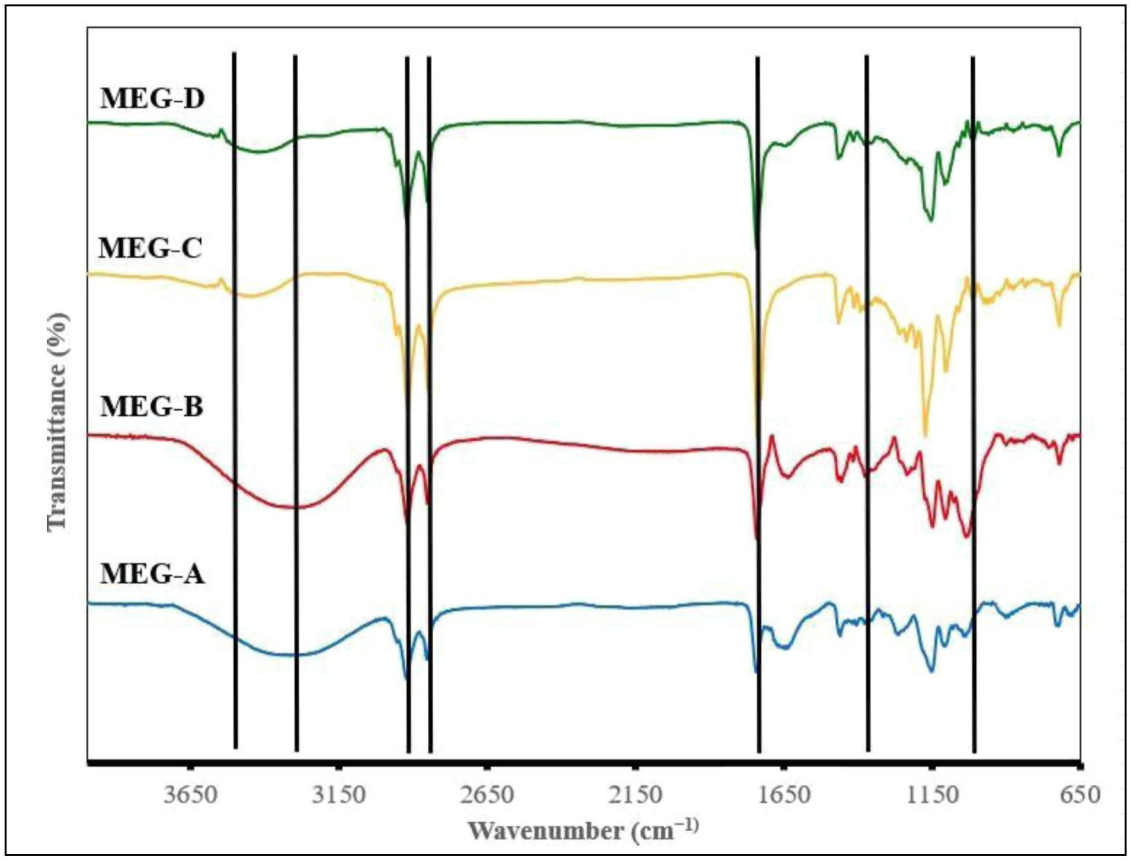

Figure 4.16 FTIR Spectra of virgin coconut oil-in-water emulsion MEG

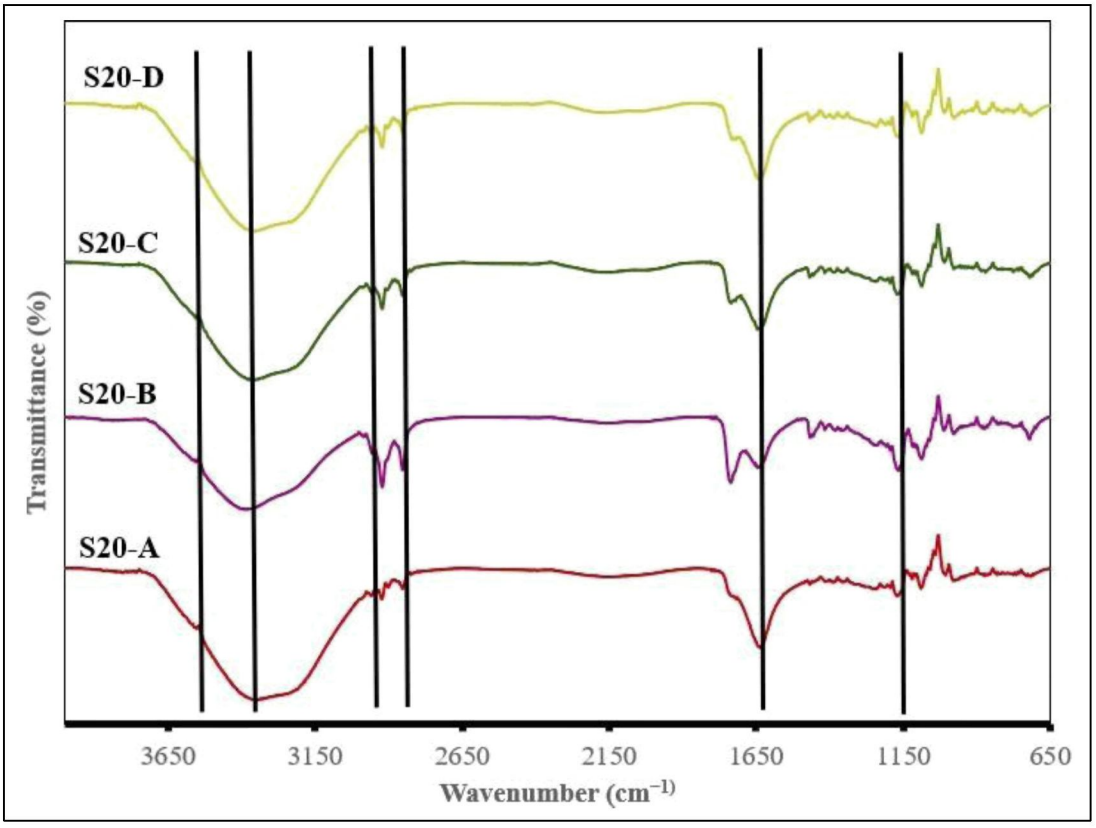

Figure 4.17 FTIR Spectra of virgin coconut oil-in-water emulsion using Span 20

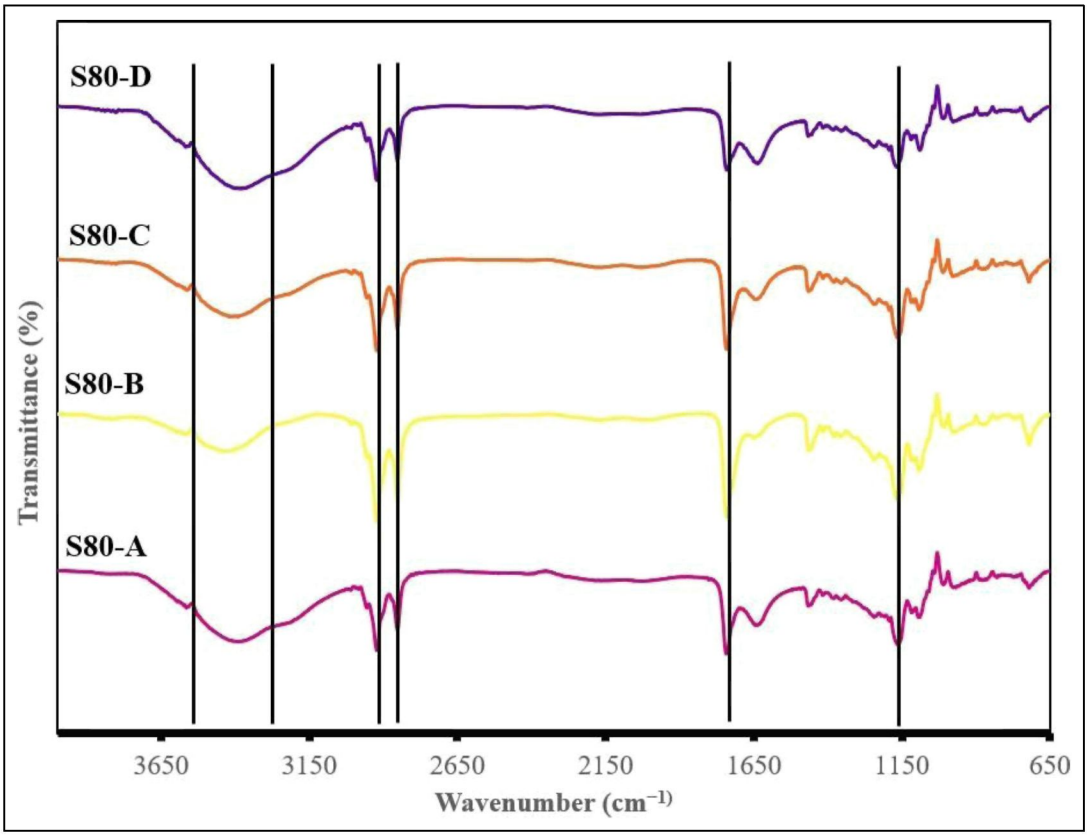

Figure 4.18 FTIR Spectra of virgin coconut oil-in-water emulsion using Span 80

The CH stretching region, spanning 2800–3000 cm^{-1}, corresponds to the C–H stretching vibrations of methyl (CH_3) and methylene (CH_2) groups, which are characteristic of the lipid chains in coconut oil. This peak region provides insight into the hydrocarbon content within the emulsion. Saturated surfactants, such as Span 20, typically display broader peaks here, reflecting the dense hydrocarbon structure. In contrast, the spectra for Span 80, which contains unsaturated chains, exhibit sharper CH peaks, indicating its distinct molecular configuration that could influence the emulsion's stability through altered hydrophobic interactions with the oil phase. Variations in the intensity or position of the C=O peak can indicate interactions between the surfactants and the lipid phase of the coconut oil, with potential implications for the hydrophilic-lipophilic balance and overall emulsion stability.

For MEG, the primary surfactant used in this emulsion, specific peaks provide insight into its integration and interactions within the emulsion. The multiple hydroxyl (O–H) groups in the glucopyranoside molecule exhibit a broad stretching band between 3300–3500 cm^{-1}, which may overlap with water's O–H signal (Nandiyanto *et al.*, 2019). This region is valuable for detecting any hydrogen bonding that occurs between the surfactant and water or VCO. Another significant peak from the surfactant is the C–O–C stretching around 1050–1100 cm^{-1}, associated with the glycosidic linkage in the surfactant structure. Additionally, a peak around 2900 cm^{-1} corresponds to C–H stretching in the methyl group attached to the glucopyranoside, indicating the presence of the surfactant within the emulsion (Rosdi *et al.*, 2024).

Both Span 20 (sorbitan monolaurate) and Span 80 (sorbitan monooleate) are non-ionic surfactants derived from sorbitol and fatty acids, and each exhibits distinct peaks in FTIR spectroscopy due to their unique molecular structures. By understanding these spectral features, you can identify their presence and interactions within emulsions.

For Span 20, which is a saturated sorbitan monolaurate ester, the CH stretching region (2800–3000 cm^{-1}) displays relatively broad peaks. These broad CH peaks reflect the dense, saturated hydrocarbon structure of Span 20, which interacts predominantly with the lipid chains in the coconut oil. The broadness in this region suggests that Span 20 contributes to a robust, albeit less flexible, interfacial layer around the dispersed water droplets, which stabilizes the emulsion through enhanced hydrophobic

interactions. Additionally, Span 20 shows a noticeable peak in the C=O stretching region (1650–1750 cm^{-1}), attributed to the ester functional group (Suneetha, 2018). This carbonyl peak highlights the potential for limited interaction with the oil phase, supporting the surfactant's role in enhancing the emulsion's hydrophobic balance.

In contrast, Span 80 (sorbitan monooleate), with its unsaturated hydrocarbon chain, exhibits sharper peaks in the CH stretching region. This sharper profile is associated with the unsaturated bonds in Span 80, which offer increased flexibility in molecular orientation and may enhance compatibility with the unsaturated fatty acids in virgin coconut oil (Fu *et al.*, 2015). This characteristic allows Span 80 to form a more flexible and cohesive interfacial layer, which can further stabilize the emulsion by increasing the strength and adaptability of the interfacial layer. The C=O peak observed for Span 80, similar to that of Span 20, indicates the presence of an ester group but may show slight shifts or changes in intensity, suggesting stronger interfacial interactions with the oil phase compared to Span 20. These interactions are essential for promoting the hydrophilic-lipophilic balance that is critical for emulsion stability.

Emulsion stability can be monitored by observing any peak shifts or changes in intensity, especially in the O–H, C=O, and C–O–C regions over time. Shifts in these bands may indicate interactions between the surfactant and the oil or water phases, which could impact the emulsion's stability. Notably, changes in the O–H stretching region could signify new hydrogen-bonding interactions, while variations in the C=O region might suggest triglyceride breakdown.

Further, oxidation and hydrolysis markers are critical for evaluating the emulsion's shelf life and quality over time. New peaks or enhanced signals near 1710–1740 cm^{-1} could indicate oxidation, pointing to aldehydes or ketones formed as VCO undergoes oxidation. Similarly, broadening around 1700 cm^{-1} might signal hydrolysis, releasing free fatty acids from triglycerides, a process that destabilizes the emulsion.

The application of FTIR in the analysis of mixed surfactants reveals crucial insights into the interactions occurring within surfactant mixtures. By examining the spectral characteristics of mixed surfactants alongside their individual components, this study elucidates how these interactions influence emulsion stability. The comparative analysis allows for a nuanced understanding of how molecular interactions change when surfactants are combined. Specific focus on peak positions, such as the shifts in the C–H stretching region, indicates alterations in the molecular environment surrounding the surfactants, suggesting that the presence of one surfactant can significantly modify the

behavior of another in a mixed system. This fundamental understanding is key in predicting the performance of emulsions and guides the selection of surfactants for various applications.

The comparison between different surfactant systems highlights potential synergistic effects when using mixed surfactants. For instance, the combination of MEG with Span 20 as shown in Figure 4.19 displays a distinctive shift in the OH region, suggesting enhanced hydrogen bonding interactions. Similarly, the mixture of MEG with Span 80 reveals in Figure 4.20 increased intensities in both CH and C=O regions, likely due to strong interactions with the lipid phase, enhancing the stability of the emulsion through more cohesive interfacial layering.

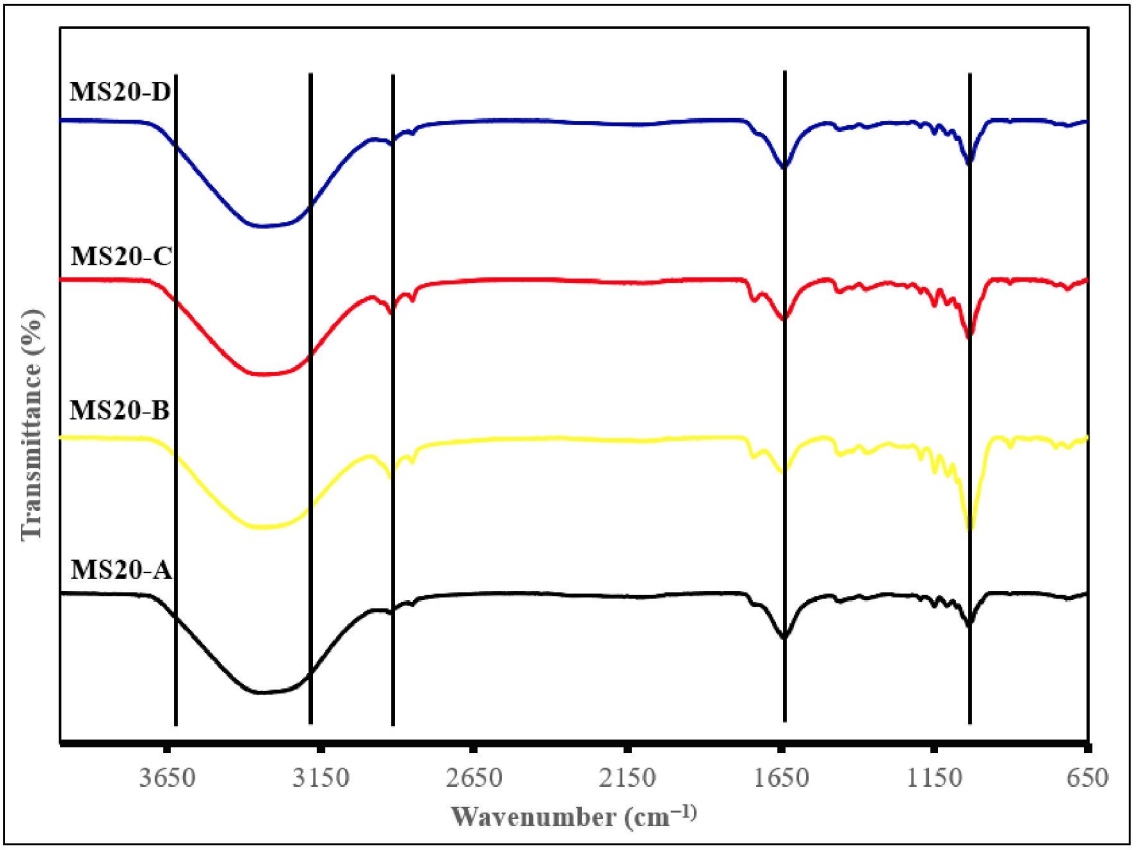

Figure 4.19 FTIR Spectra of virgin coconut oil-in-water emulsion using MEG & Span 20

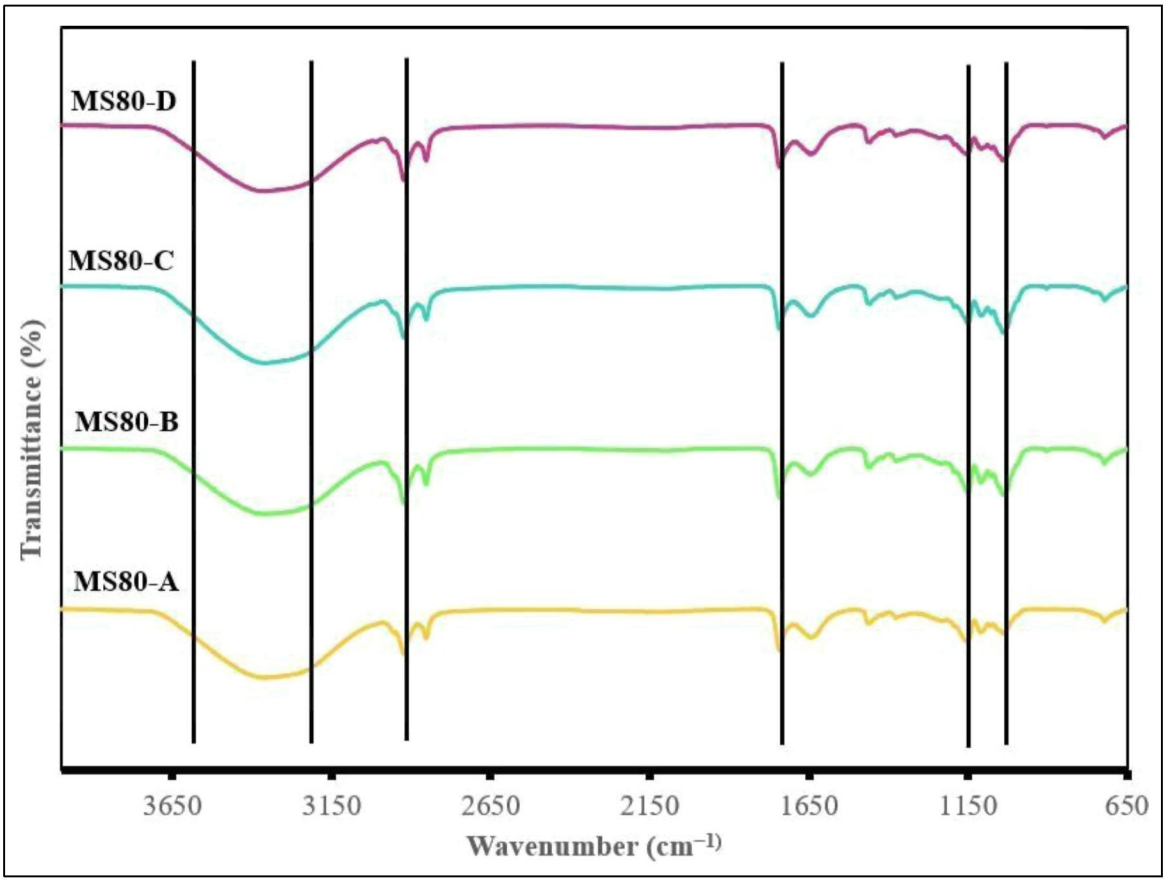

Figure 4.20 FTIR Spectra of virgin coconut oil-in-water emulsion using MEG & Span 80

The evidence for synergistic effects among mixed surfactants is particularly compelling. The pronounced changes in peak positions and intensities observed in the FTIR spectra of mixed surfactants especially in the hydroxyl (OH) stretch region indicate enhanced intermolecular interactions that are not present in the individual components. For instance, a significant increase in OH stretch intensity implies that the combination of hydrophilic and hydrophobic surfactants fosters a more robust hydrogen bonding network, which is crucial for emulsion stability. These findings are consistent with existing literature that highlights the importance of hydrogen bonding in stabilizing emulsions, reinforcing the notion that synergistic interactions can lead to enhanced stability and performance. This study demonstrates that specific combinations of surfactants can amplify the beneficial properties of each other, creating formulations with improved functionality.

The analysis of FTIR spectra for the emulsions created with virgin coconut oil in water using MEG in combination with either Span 20 (Set 1) or Span 80 (Set 2)

reveals distinct differences in molecular interactions that significantly influence emulsion stability. In Set 1, the hydroxyl (OH) stretching region between 3200–3600 cm^{-1} displays a broad peak, indicative of hydrogen-bonded hydroxyl groups from MEG and the water phase (Nandiyanto *et al.*, 2019) . A notable increase in peak intensity or a shift towards lower wavenumbers suggests enhanced hydrogen bonding within the emulsion, promoting stability. The presence of Span 20, which has a lower hydrophilic-lipophilic balance (HLB), might contribute to moderate stabilization through these hydrogen bonds, although its efficiency may be limited compared to more hydrophilic surfactants. The carbonyl (C=O) stretching peak observed in the 1700–1750 cm^{-1} region reflects interactions from Span 20, where any shifts in this peak may indicate changes at the oil-water interface, suggesting how effectively the surfactant reduces interfacial tension.

In Set 2, where Span 80 is used, the same regions are analyzed, yet the FTIR spectra may exhibit higher peak intensities and distinct shifts, particularly in the OH and C=O regions. The higher HLB value of Span 80 suggests a greater affinity for water, potentially leading to a more robust network of hydrogen bonds and improved interfacial tension reduction. This could result in smaller droplet sizes and a more stable emulsion. The C–H stretching peaks (2800–3000 cm^{-1}) in both sets indicate contributions from the virgin coconut oil and surfactants; however, in Set 2, these peaks may be more pronounced, indicating a more effective packing of surfactants at the interface, thereby enhancing stability. Furthermore, the C–O stretching region (1000–1300 cm^{-1}) reflects the interactions of the ether or alcohol groups in MEG and the surfactants.

Variations in intensity or shifts in these peaks between the two sets can provide insights into how different surfactant combinations interact with the oil and water phases, with Span 80 likely offering superior stabilization properties due to its structure and increased hydrophilicity. Overall, the comparative analysis of the FTIR peaks between the two emulsions emphasizes the critical role of surfactant selection in optimizing emulsion stability, with implications for formulation strategies across various applications in food science, pharmaceuticals, and cosmetics.

In summary, the FTIR analysis demonstrates that each surfactant and combination contribute uniquely to emulsion stability. Mixed surfactant systems, particularly those involving Span 80, show significant peak shifts and intensities in the OH, CH, and C=O regions, suggesting improved emulsion stability through complex

interfacial interactions. This study underscores the effectiveness of both single and combined surfactants in enhancing the hydrophilicity and molecular cohesion at the emulsion interface, providing valuable insights for optimizing emulsion formulations.

4.2 Stability evaluation of emulsion against elevated temperatures

4.2.1 Creaming index

When subjected to varying temperatures, these emulsions exhibit changes in CI that highlight the influence of surfactant combinations on their stability. In this case, the two mixed surfactants, MEG paired with either Span 20 or Span 80 play a central role in the stability across temperatures. As temperature rises, molecular motion within the emulsion increases. This greater kinetic energy causes droplets to collide more frequently, increasing the tendency for droplets to coalesce (Souza *et al.*, 2015). When droplets combine, they form larger droplets, which separate more readily due to gravity, resulting in a higher CI. As reflected by changes in the creaming index (CI) across the temperature range of 30 to 60 °C (Figures 4.21(a–e)). Two mixed-surfactant systems were evaluated: MEG–Span 20 (MS20-C and MS20-D) and MEG–Span 80 (MS80-B and MS80-C).

At 30 °C (Figure 4.21(a)), the emulsions stabilized with MEG and Span 20 showed excellent stability. Both MS20-C and MS20-D maintained a CI of zero throughout the 30-day storage period, indicating that no creaming occurred. This suggests that the interfacial film formed by this surfactant combination was strong enough to prevent droplet movement and phase separation. In contrast, MS80-B and MS80-C already showed measurable CI values from Day 1, indicating that creaming had begun even at this relatively low temperature. Although lower temperatures generally limit droplet collisions (Hempoonsert et al., 2010), the higher CI values observed for the MEG–Span 80 system point to weaker interfacial protection resulting in a slightly weaker emulsion structure.

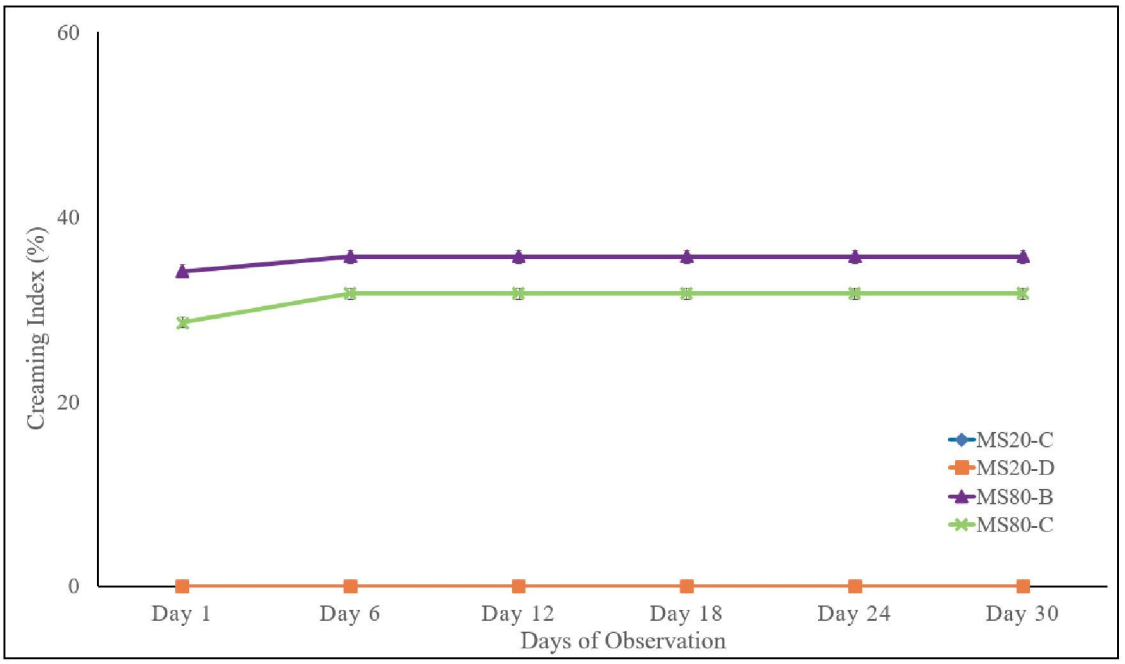
60
40
20
0
Creaming Index (%)
Day 1
Day 6
Day 12
Day 18
Day 24
Day 30
Days of Observation
MS20-C
MS20-D
MS80-B
MS80-C

(a)

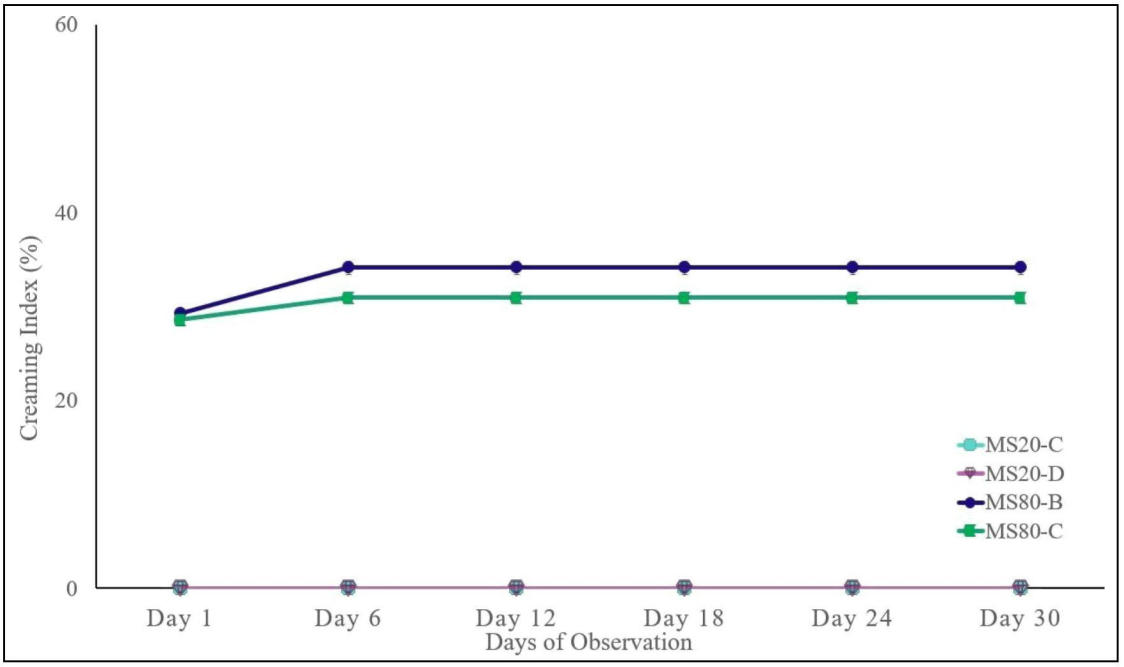
60
40
20
0
Creaming Index (%)
Day 1
Day 6
Day 12
Day 18
Day 24
Day 30
Days of Observation
MS20-C
MS20-D
MS80-B
MS80-C

(b)

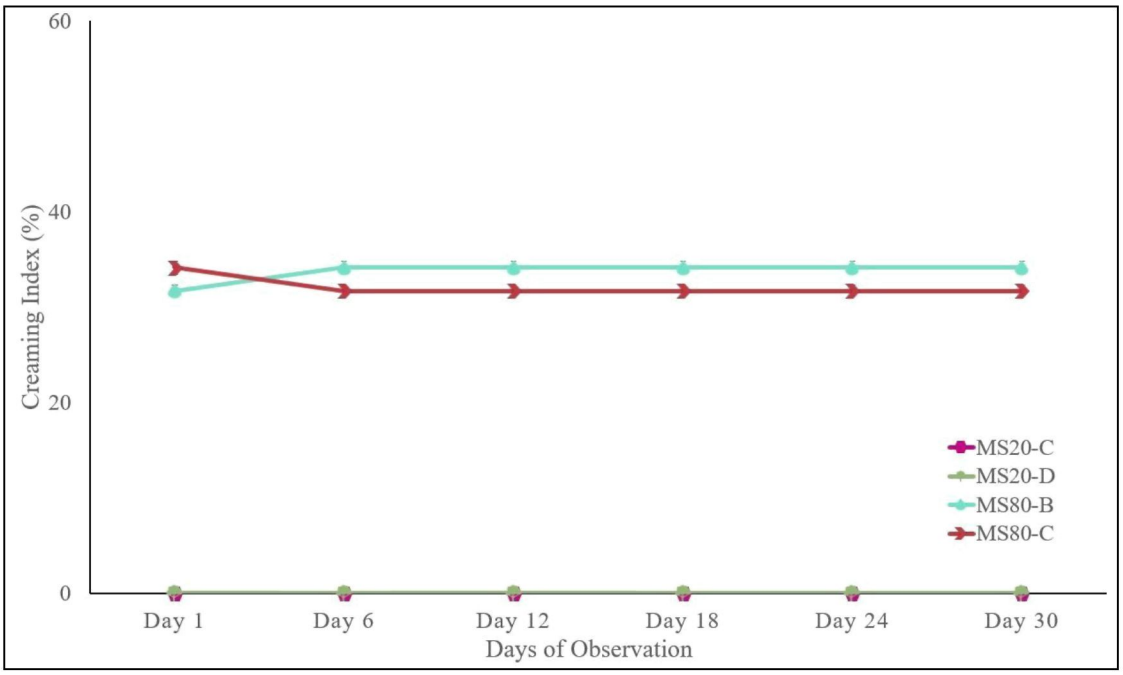
60
40
20
0
Creaming Index (%)
Day 1
Day 6
Day 12
Day 18
Day 24
Day 30
Days of Observation
MS20-C
MS20-D
MS80-B
MS80-C

(c)

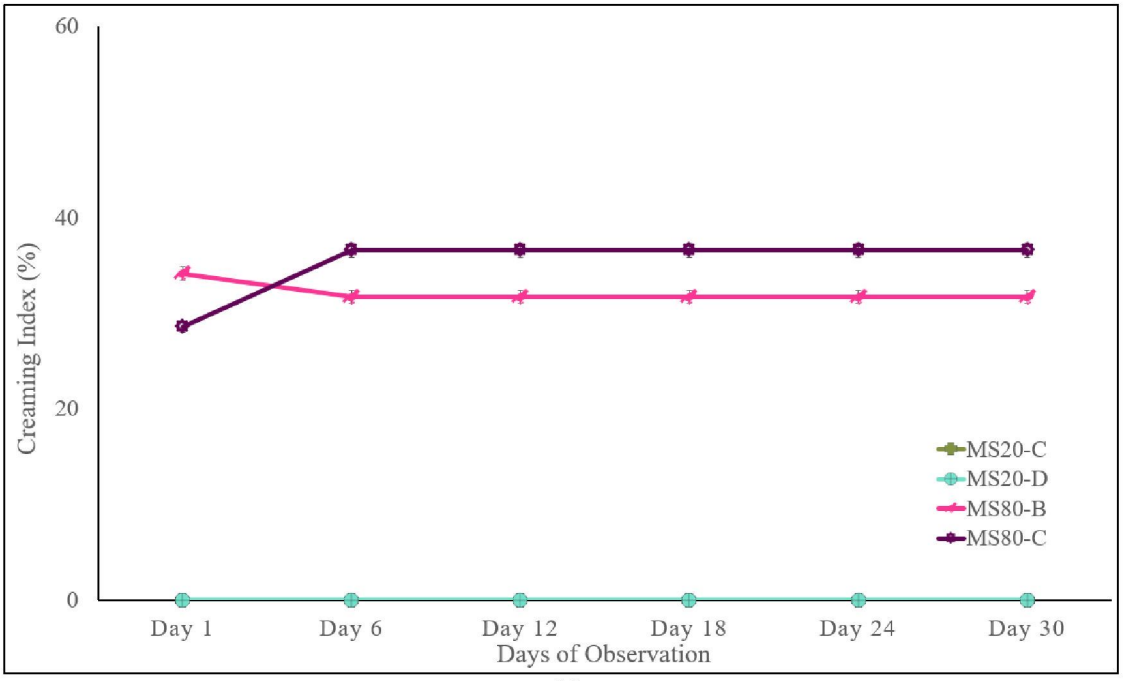
60
40
20
0
Creaming Index (%)
Day 1
Day 6
Day 12
Day 18
Day 24
Day 30
Days of Observation
MS20-C
MS20-D
MS80-B
MS80-C

(d)

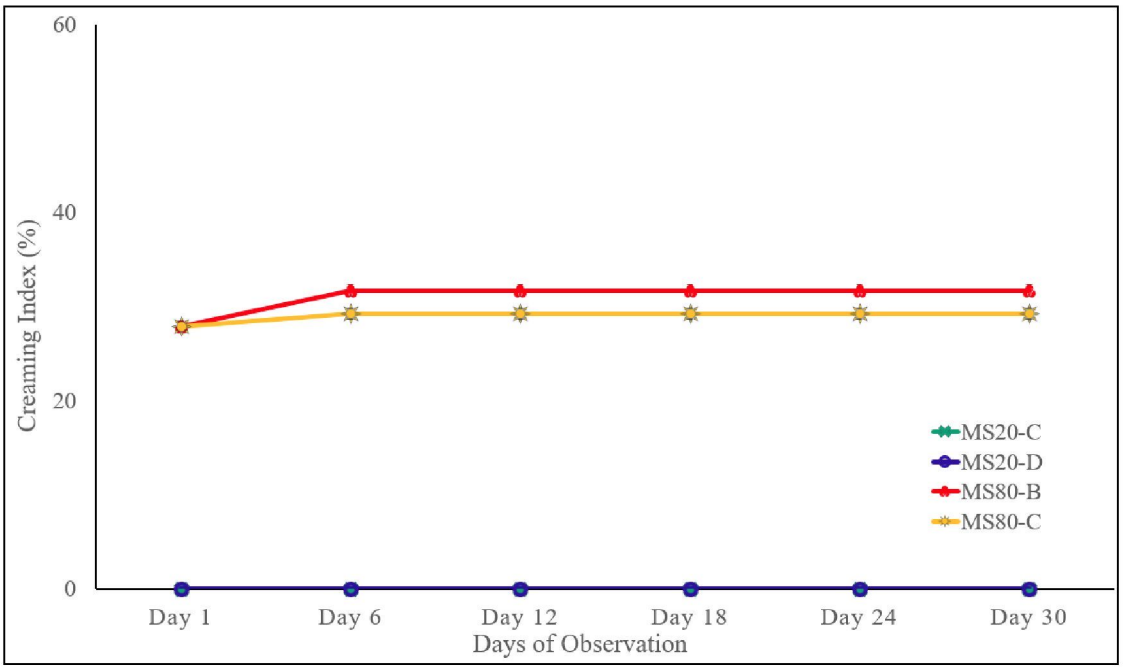

(e)

Figure 4.21 Creaming index O/W emulsion affected by temperatures a) 30 °C b) 35 °C c) 40 °C d) 45 °C e) 60 °C

When the temperature was increased to 35 °C (Figure 4.21(b)), the same trend continued. MS20-C and MS20-D remained completely stable, while MS80-B and MS80-C showed a noticeable increase in CI during the early days of storage. This increase is associated with greater molecular mobility at higher temperatures, which raises the frequency of droplet collisions and promotes coalescence (Souza et al., 2015). However, the CI values of the MEG–Span 80 samples stabilized after Day 6, suggesting that most of the destabilization occurred during the initial storage period.

At 40 °C (Figure 4.21(c)), the difference in performance between the two surfactant systems became more obvious. The CI values of MS80-B and MS80-C increased further, reflecting reduced resistance of the interfacial film to thermal stress. Meanwhile, MS20-C and MS20-D continued to show zero CI, demonstrating that the MEG–Span 20 interfacial layer remained intact even under moderate heating. This behavior highlights the importance of surfactant compatibility, as the balanced hydrophilic–lipophilic character of Span 20 allows it to interact more effectively with MEG at the oil–water interface.

More pronounced destabilization was observed at 45 °C (Figure 4.21(d)). At this temperature, MS80-C recorded the highest CI values, indicating substantial phase separation. The increased kinetic energy at elevated temperatures weakens poorly structured interfacial films, allowing droplets to merge more easily (Deng et al., 2023). In contrast, the MEG–Span 20 emulsions remained unaffected, further confirming the robustness of this surfactant combination.

At the highest temperature investigated, 60 °C (Figure 4.21(e)), all emulsions were subjected to strong thermal agitation. Despite this, MS20-C and MS20-D still showed no creaming throughout the storage period, demonstrating exceptional thermal stability. On the other hand, MS80-B and MS80-C exhibited rapid creaming during the early storage period, followed by stabilization of CI values. This suggests that high temperature mainly accelerates early-stage destabilization in the MEG–Span 80 system rather than causing continuous breakdown over time.

Overall, these results show that emulsion stability under temperature variation depends not only on temperature itself but also on how well the surfactants work together at the interface. The MEG–Span 20 system consistently provided superior stability due to its stronger interfacial cohesion and better hydrophilic–lipophilic balance. In contrast, the MEG–Span 80 system was more susceptible to temperature-induced destabilization, making it less suitable for applications that require thermal stability.

4.2.2 Freeze-Thaw Stability

Temperature significantly influences the stability of oil-in-water emulsions, particularly during freeze-thaw cycles, which stress the emulsion by subjecting it to repeated freezing and thawing conditions. This exposure can lead to phase separation, coalescence, and eventual breakdown of the emulsion structure. In this context, the choice of mixed surfactants, such as Span 20, Span 80, and MEG, reveals distinct behaviors and mechanisms at play regarding temperature's impact on emulsion stability. Figure 4.25 shows a freeze-thaw analysis of mixed surfactant emulsions at varying temperatures.

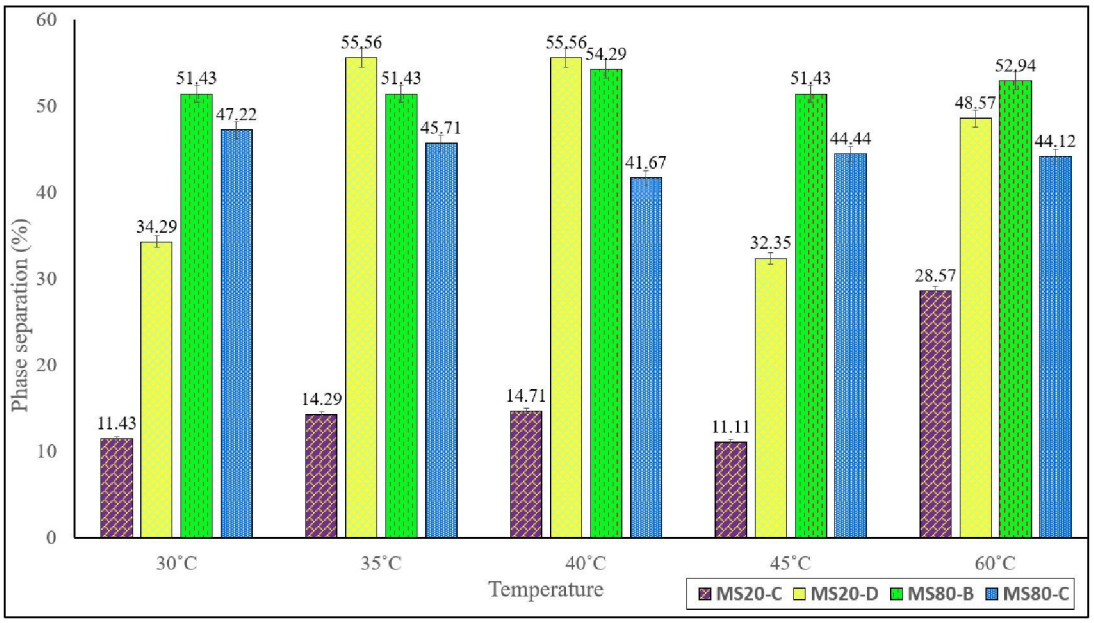

Figure 4.22 Freeze-thaw analysis of mixed surfactant emulsions affected by temperatures

The MS20 emulsions, stabilized using a combination of MEG and Span 20, show clear sensitivity to temperature variation, which can be attributed to the physicochemical characteristics of the surfactant system. Although Span 20 (sorbitan monolaurate) is commonly associated with water-in-oil emulsions, its combination with the highly hydrophilic MEG enables effective stabilization of oil-in-water emulsions through the formation of an interfacial surfactant layer around the dispersed oil droplets.

At 30 °C, relatively low phase separation was observed, with values of 11.43% for MS20-C, 34.29% for MS20-D, and 51.43% for MS80-B, indicating acceptable emulsion stability. Lower phase separation values reflect stronger resistance to droplet coalescence and phase destabilization. As the temperature increased to 35 °C and 40 °C, phase separation gradually increased, with MS20-C reaching 14.71% at 40 °C. This increase highlights the effect of temperature-induced molecular motion, which weakens interactions between surfactant molecules and oil droplets. Under these conditions, the protective surfactant layer becomes less effective as thermal energy disrupts the balance of forces stabilizing the interface.

At 45 °C, a slight reduction in phase separation for MS20-C (11.11%) suggests a temporary stabilization, possibly due to molecular rearrangement of surfactant molecules in response to thermal stress. However, when the temperature increased further to 60 °C, phase separation rose markedly to 28.50%, indicating significant emulsion destabilization. At this temperature, increased kinetic energy enables oil droplets to overcome the surfactant barrier, promoting coalescence and the formation of larger droplets, which ultimately leads to enhanced phase separation (Yonguep et al., 2022).

In contrast, the MS80 emulsions, which utilize Span 80 (sorbitan monooleate) in combination with MEG, exhibit greater resistance to temperature variation. Span 80 is more hydrophobic than Span 20 and possesses a longer hydrocarbon chain, which enhances its ability to form a stronger and more cohesive interfacial film. At 30 °C, MS80-C displayed a higher initial phase separation (47.22%) compared to MS20-C, indicating lower initial stability. However, as the temperature increased to 35 °C and 40 °C, phase separation decreased to 45.71% and 41.67%, respectively. This trend suggests that the hydrophobic character of Span 80 allows the surfactant layer to reorganize and strengthen under moderate thermal conditions.

At 45 °C, phase separation remained relatively constant (44.44%), indicating that the emulsion retained its integrity despite increased thermal stress. Even at 60 °C, only a slight change in phase separation was observed (44.12%), demonstrating the ability of Span 80 to maintain interfacial stability at elevated temperatures. This behavior is attributed to stronger hydrophobic interactions between Span 80 and the oil phase, which form a thicker and more cohesive barrier against droplet coalescence (Jiang et al., 2021).

Overall, both emulsion systems show that increasing temperature accelerates phase separation and reduces stability. However, the extent of destabilization differs significantly between the two surfactant systems. The MS20 emulsions experience more pronounced instability at high temperatures, indicating that the interfacial film formed by Span 20 is less capable of withstanding thermal stress. In contrast, the MS80 emulsions exhibit comparatively better stability across a wider temperature range, particularly at elevated temperatures, due to the stronger hydrophobic interactions provided by Span 80.

In the context of thermal and freeze–thaw stability, lower phase separation values indicate improved resistance to temperature-induced destabilization. The

relatively stable behavior of the MS80 emulsions highlights the importance of selecting surfactants with suitable hydrophobic characteristics for applications involving thermal cycling. The findings demonstrate that stronger hydrophobic interactions, as provided by Span 80, offer a more effective barrier against droplet coalescence, whereas the weaker interfacial structure formed by Span 20 becomes increasingly susceptible to breakdown under thermal stress. Understanding these mechanisms is essential for the rational design of stable emulsion formulations, particularly for applications where exposure to high temperatures or freeze–thaw conditions is unavoidable.

4.2.3 Rheology Test

Temperature has a clear influence on the viscosity and flow behavior of emulsions, as it affects molecular motion, droplet interactions, and the stability of the interfacial film. In this study, the viscosity of VCO-in-water emulsions stabilized using mixed surfactant systems was evaluated over a temperature range of 30 to 60 °C (Figures 4.23(a–e)). The discussion focuses on the main trends observed for emulsions containing MEG–Span 20 (MS20-C and MS20-D) and MEG–Span 80 (MS80-B and MS80-C).

Regardless of temperature or formulation, all emulsions exhibited a decrease in viscosity with increasing shear rate, indicating shear-thinning behavior. This behavior is typical of emulsions with an internal droplet structure, where applied shear causes the droplet network to gradually break down and align in the direction of flow (Barnes, 2004). Such behavior is beneficial in practical applications, as it allows the emulsion to remain structured at rest while becoming easier to process or spread under shear.

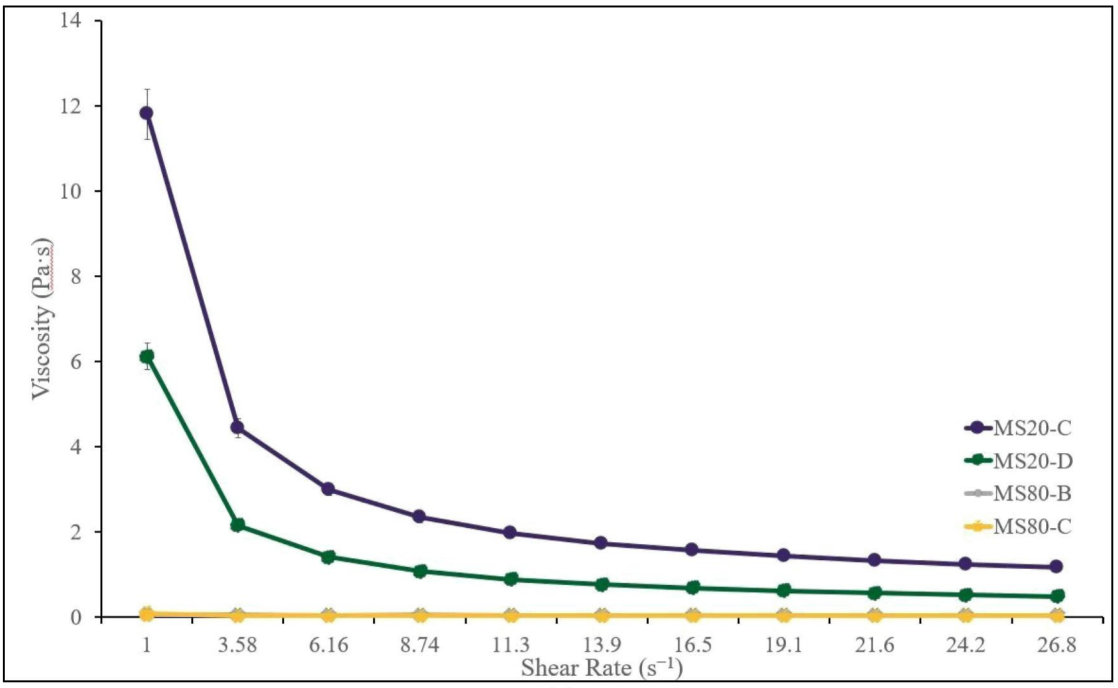
14
12
10
8
6
4
2
0
Viscosity (Pa·s)
1
3.58
6.16
8.74
11.3
13.9
16.5
19.1
21.6
24.2
26.8
Shear Rate (s⁻¹)
MS20-C
MS20-D
MS80-B
MS80-C

(a)

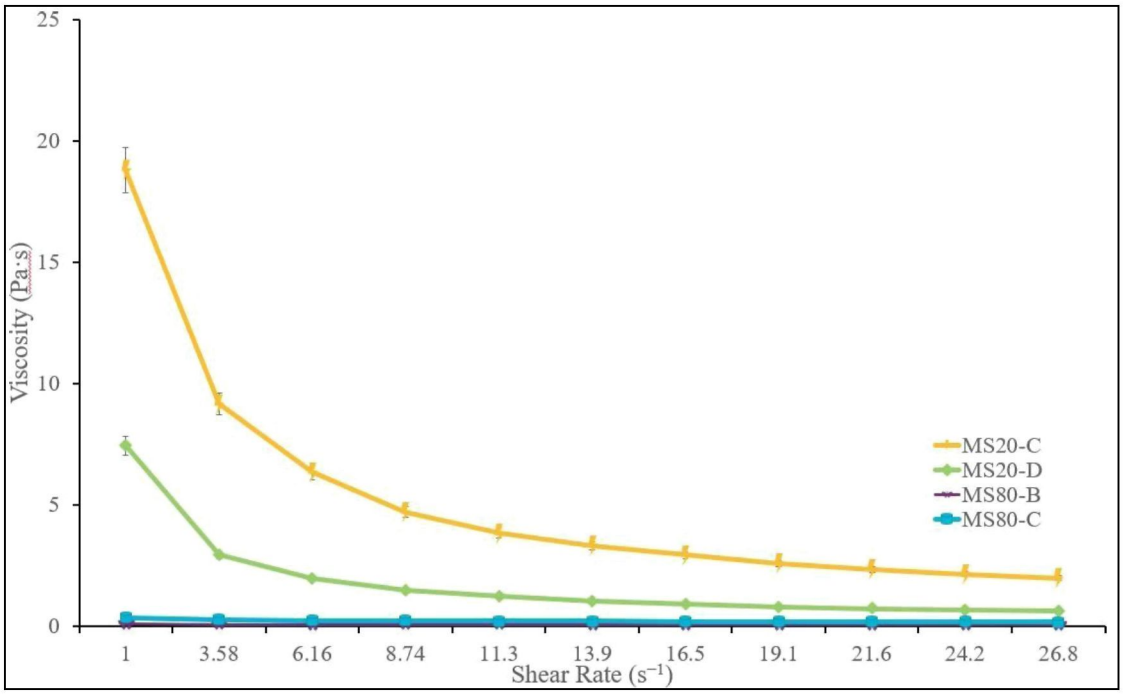
25
20
15
10
5
0
Viscosity (Pa·s)
1
3.58
6.16
8.74
11.3
13.9
16.5
19.1
21.6
24.2
26.8
Shear Rate (s⁻¹)
MS20-C
MS20-D
MS80-B
MS80-C

(b)

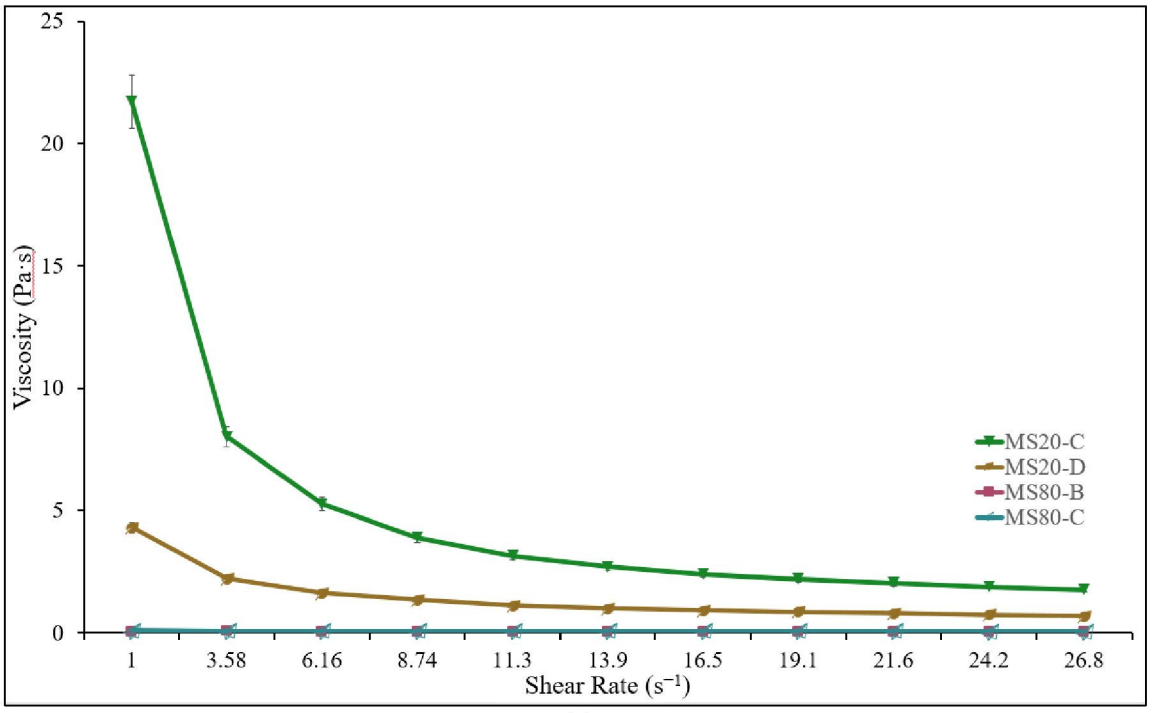
25
20
15
10
5
0
Viscosity (Pa·s)
1
3.58
6.16
8.74
11.3
13.9
16.5
19.1
21.6
24.2
26.8
Shear Rate (s⁻¹)
MS20-C
MS20-D
MS80-B
MS80-C

(c)

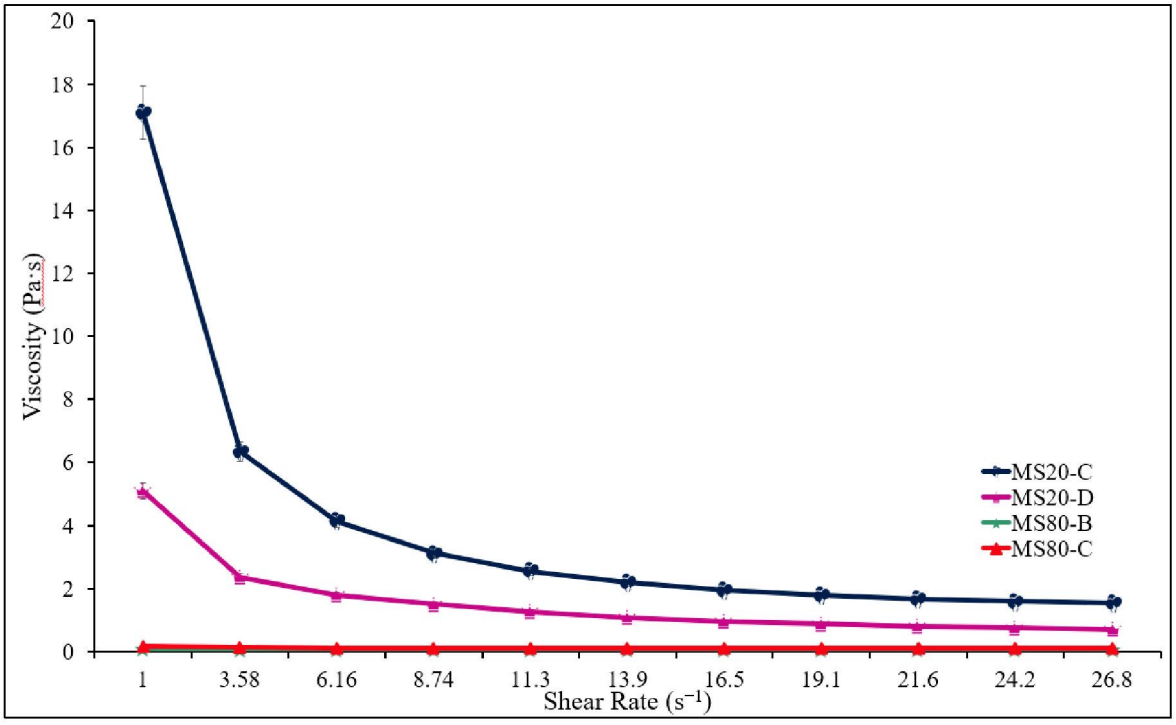
20
18
16
14
12
10
8
6
4
2
0
Viscosity (Pa·s)
1
3.58
6.16
8.74
11.3
13.9
16.5
19.1
21.6
24.2
26.8
Shear Rate (s⁻¹)
MS20-C
MS20-D
MS80-B
MS80-C

(d)

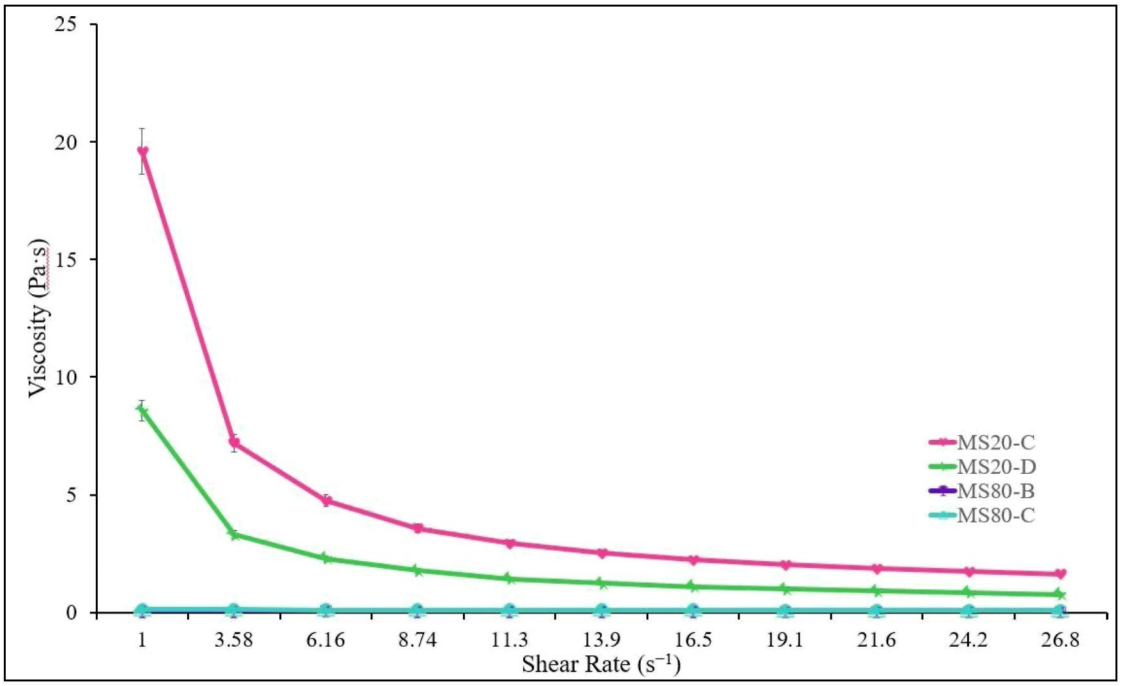

(e)

Figure 4.23 Viscosity vs shear rate VCO-in-water emulsion at a) 30 °C b) 35 °C c) 40 °C d) 45 °C e) 60 °C

At lower temperatures (30–35 °C), emulsions stabilized with Span 20 showed markedly higher viscosity compared with those containing Span 80. For example, MS20-C recorded viscosities of 11.8 Pa·s at 30 °C and 18.8 Pa·s at 35 °C at a shear rate of 1 s^{-1}, reflecting the formation of a relatively strong internal structure. At these temperatures, thermal energy is limited, allowing hydrogen bonding and intermolecular interactions between MEG, Span 20, and the aqueous phase to remain effective. As a result, the oil droplets are more strongly interconnected, leading to greater resistance to flow (Goertz et al., 2007).

As the temperature increased to 40–45 °C, a noticeable reduction in viscosity was observed for the MS20 emulsions. This change suggests that the internal droplet network became progressively weaker as thermal motion increased. Higher temperatures disrupt hydrogen bonding and reduce the strength of the interfacial film, allowing oil droplets to move more freely and decreasing resistance to shear. This explains why the MS20 system shows greater sensitivity to temperature changes compared with the MS80 system.

In contrast, the MS80 emulsions exhibited much lower viscosity values across all temperatures, but their response to temperature was more gradual. The longer hydrophobic chain of Span 80 allows it to anchor more firmly at the oil–water interface, forming a flexible yet cohesive interfacial layer that can better accommodate thermal agitation (Jiang et al., 2021). Although this system does not generate a highly viscous structure, it maintains more consistent rheological behavior as temperature increases.

At 60 °C, all emulsions showed their lowest viscosity values, indicating significant weakening of intermolecular interactions and increased droplet mobility. Under these conditions, enhanced Brownian motion and reduced interfacial resistance cause the emulsions to behave more like low-viscosity fluids (Xian et al., 2022). Even so, the MS80 emulsions displayed smoother viscosity profiles than the MS20 emulsions, suggesting better tolerance to elevated temperatures.

Overall, these findings show that viscosity is strongly influenced by both temperature and surfactant composition. The MEG–Span 20 system produces emulsions with high viscosity and a well-developed internal structure at lower temperatures but becomes increasingly sensitive as temperature rises. In contrast, the MEG–Span 80 system forms emulsions with lower viscosity but greater resistance to temperature variation. This highlights that high viscosity alone does not guarantee thermal stability and emphasizes the importance of selecting surfactant systems based on both flow behavior and stability requirements.

4.2.4 Droplet Size Distribution

The effect of temperature on droplet size distribution of oil-in-water emulsions stabilized with mixed surfactant systems was evaluated between 30 °C and 60 °C using a combined droplet size dataset (Table 4.7) and supported by optical microscopy images (Figures 4.24–4.28). The discussion focuses on the significant trends observed for emulsions stabilized with Span 20–MEG (MS20) and Span 80–MEG (MS80) systems. Overall, temperature exerted a pronounced influence on droplet size, with the extent of its effect strongly dependent on surfactant type. Emulsions stabilized with Span 20 showed a progressive reduction in droplet size as temperature increased, whereas Span 80-based emulsions displayed larger and less consistent droplet sizes, particularly at elevated temperatures.

Table 4.7
Droplet Size Analysis of Oil-in-Water Emulsion

Temperature	30 °C	35 °C	40 °C	45 °C	60 °C
Sample	**Mean (µm)**	**Mean (µm)**	**Mean (µm)**	**Mean (µm)**	**Mean (µm)**
MS20-C	NA	NA	NA	7.60 ± 0.691	8.00 ± 0.477
MS20-D	12.30 ± 1.069	9.40 ± 0.500	8.20 ± 0.302	7.90 ± 0.787	7.80 ± 0.657
MS80-B	18.80 ± 1.961	21.22 ± 0.942	17.00 ± 0.674	23.7 ± 0.829	19.40 ± 1.023
MS80-C	36.5 ± 1.0256	15.40 ± 1.225	13.70 ± 0.895	14.80 ± 0.739	18.80 ± 1.108

*NA: Not Available

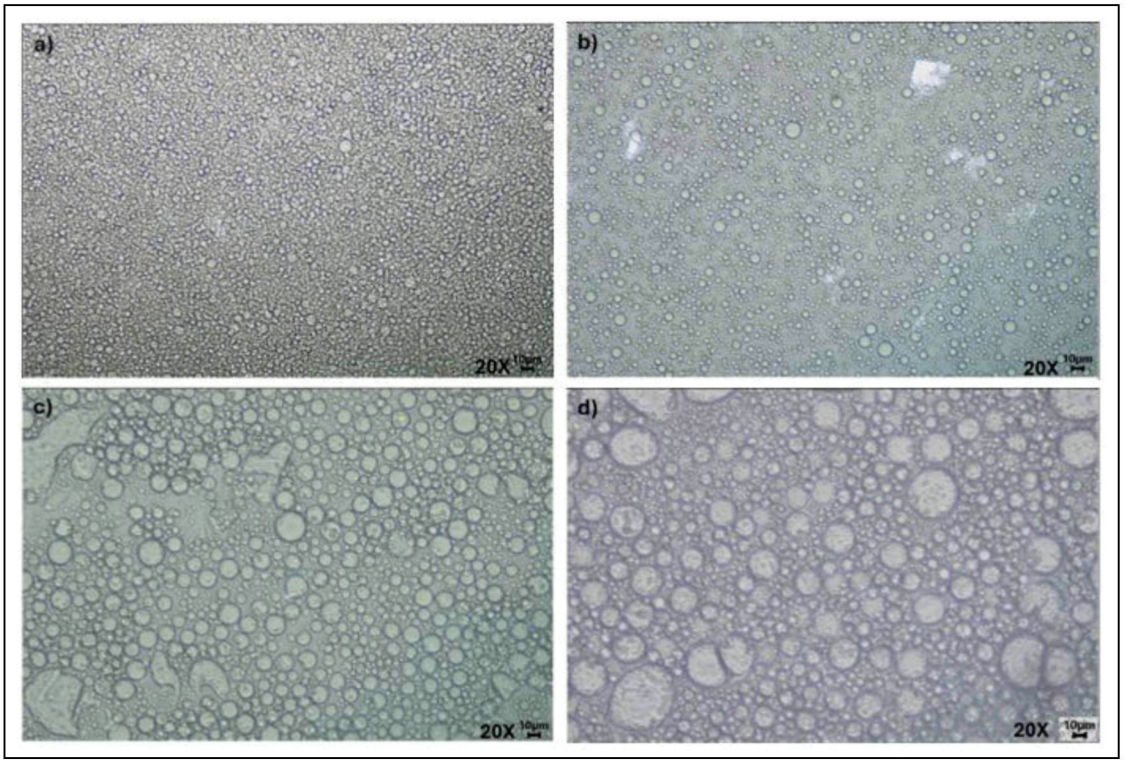

Figure 4.24 Polarized optical microscopy images of emulsions at 30 ˚C in 20x magnification a) MS20-C b) MS20-D c) MS80-B d) MS80-C

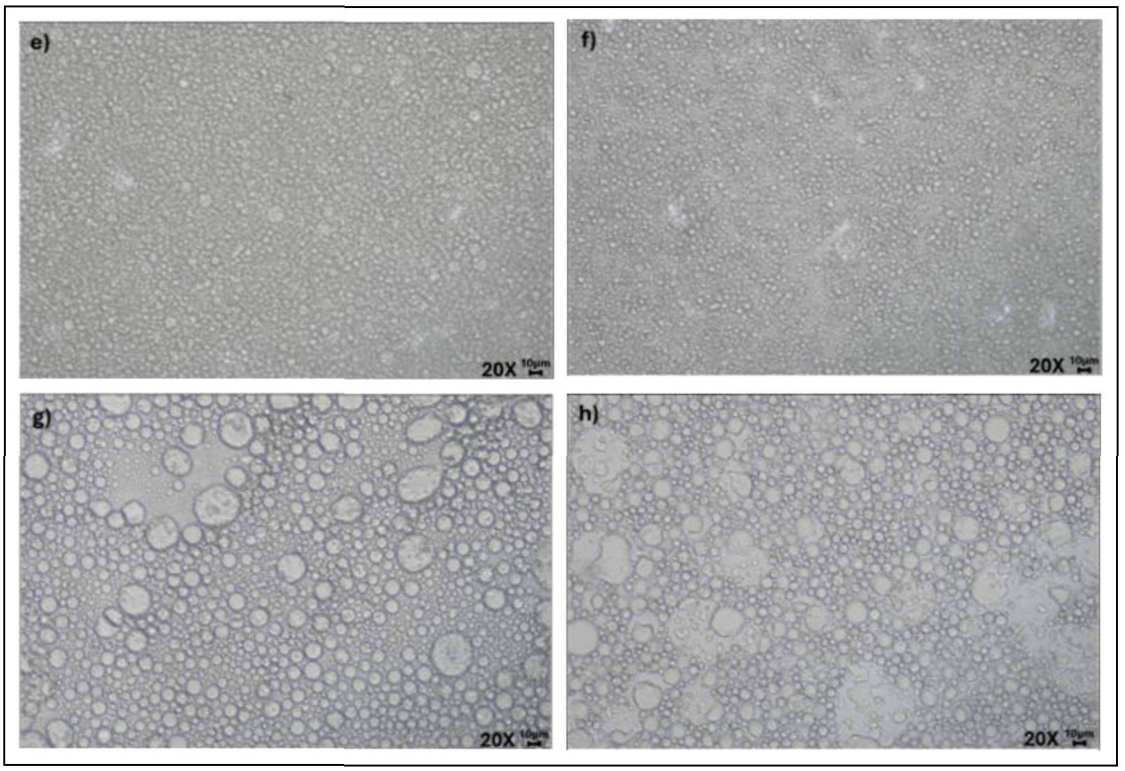

Figure 4.25 Polarized optical microscopy images of emulsions at 35 °C in 20x magnification a) MS20-C b) MS20-D c) MS80-B d) MS80-C

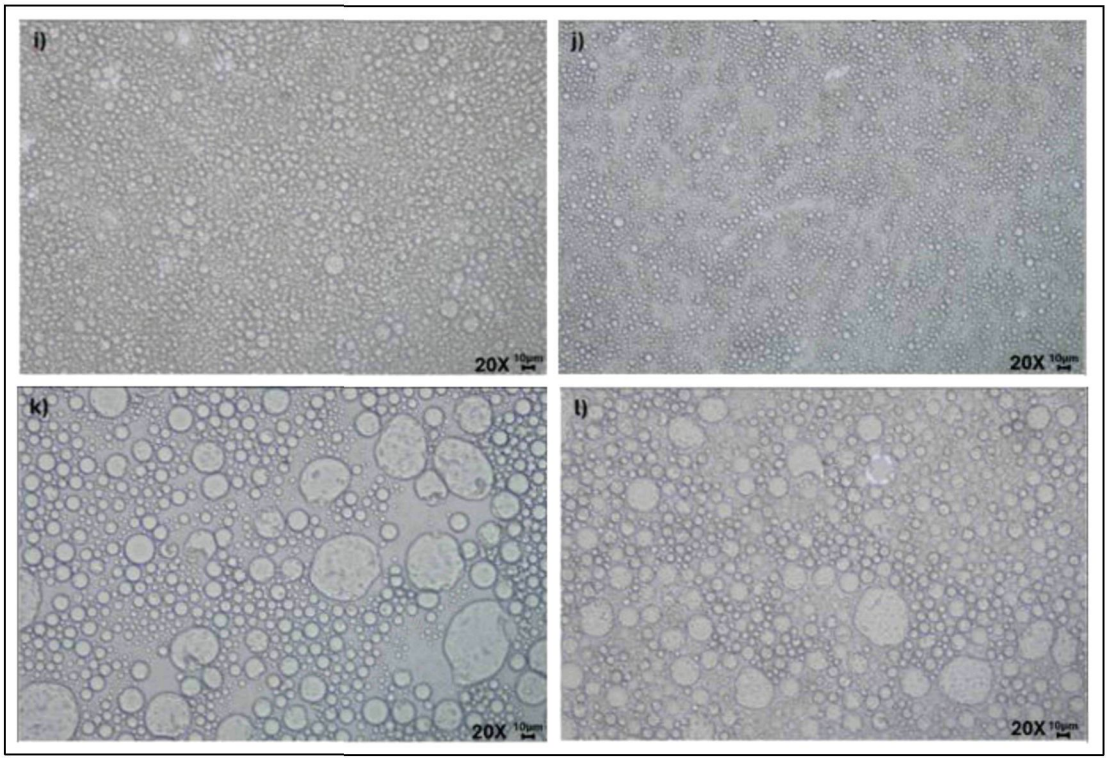

Figure 4.26 Polarized optical microscopy images of emulsions at 40 °C in 20x magnification a) MS20-C b) MS20-D c) MS80-B d) MS80-C

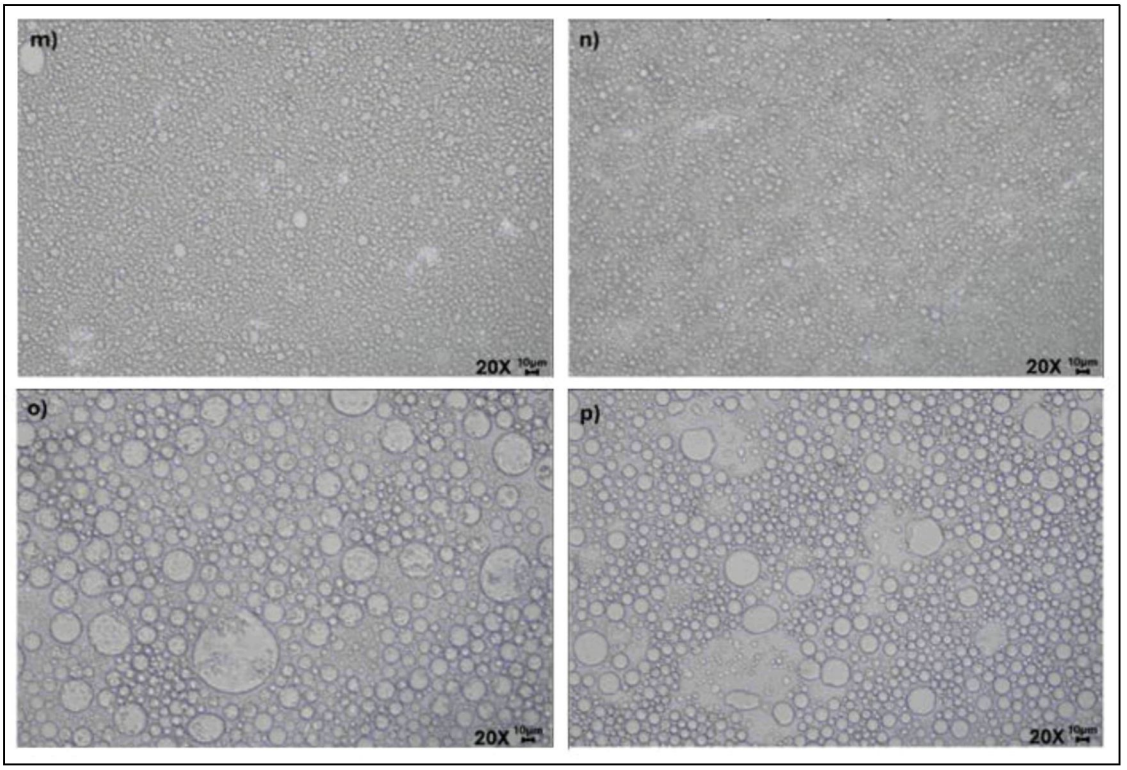

Figure 4.27 Polarized optical microscopy images of emulsions at 45 °C in 20x magnification a) MS20-C b) MS20-D c) MS80-B d) MS80-C

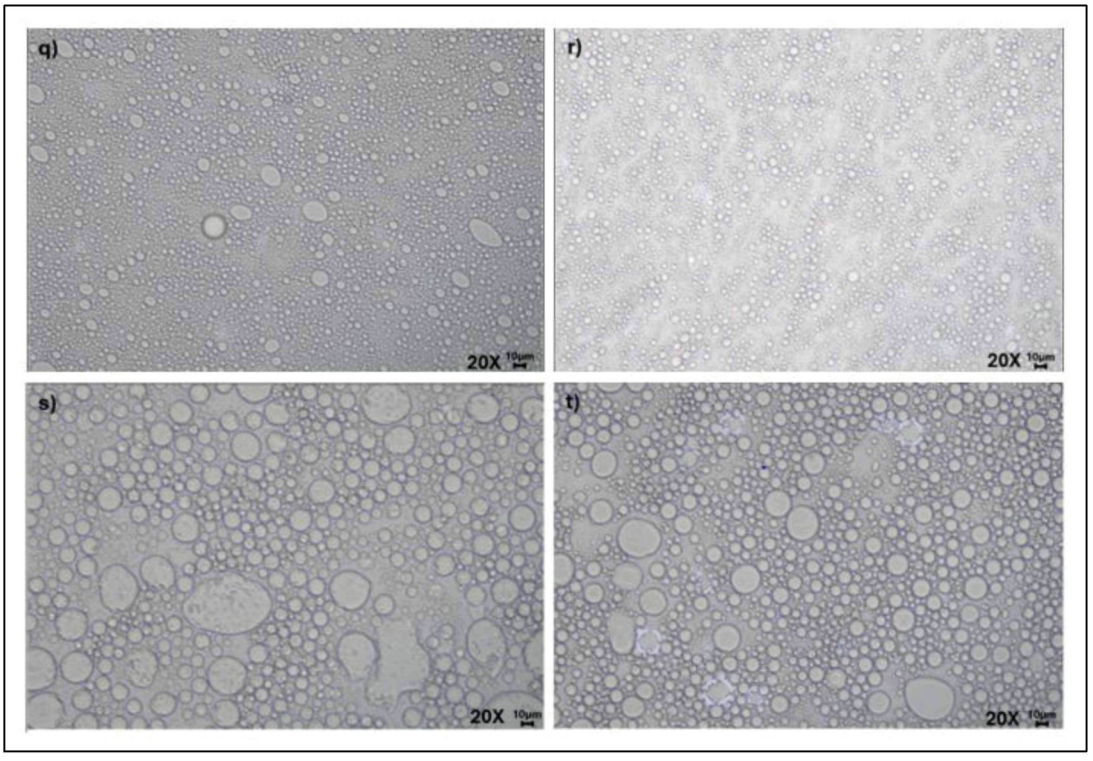

Figure 4.28 Polarized optical microscopy images of emulsions at 60 °C in 20x magnification a) MS20-C b) MS20-D c) MS80-B d) MS80-C

At 30 °C and 35 °C, MS20 emulsions exhibited relatively small and uniform droplet sizes, indicating that effective emulsification had already been achieved under mild thermal conditions. For example, the droplet size of MS20-D decreased from 12.30 μm at 30 °C to 9.40 μm at 35 °C, suggesting improved droplet disruption with a slight increase in temperature. In contrast, MS80 emulsions produced noticeably larger droplets at the same temperatures, with MS80-C reaching 36.50 μm at 30 °C, which reflects less efficient interfacial stabilization at lower temperatures. The challenges in determining the particle size distribution for MS20-C stem from several factors, even though the droplets are visible under the microscope. One major issue is the emulsion's high polydispersity index (PDI), which signifies a broad range of droplet sizes. This variation often results in irregular, non-spherical droplet shapes that are difficult to analyze using standard particle size measurement methods, which typically assume spherical geometry. As a result, droplet orientation can lead to inaccurate size estimations, either underestimating or overestimating the actual dimensions (Bon et al., 2007).

As the temperature increased to 40 °C and 45 °C, distinct differences in droplet size behavior between the two surfactant systems became more apparent. Droplet sizes in MS20 emulsions continued to decrease, reaching approximately 7.60–7.90 μm, indicating that increased thermal energy promoted further droplet breakup while the interfacial film remained sufficiently stable to limit recoalescence. Conversely, MS80 emulsions showed signs of droplet growth, with MS80-B increasing to 23.70 μm at 45 °C, suggesting the onset of partial coalescence and a reduction in interfacial stability under elevated temperature conditions.

At 60 °C, MS20-stabilized emulsions maintained relatively small droplet sizes of approximately 8 μm, demonstrating good resistance to temperature-induced droplet growth. In contrast, MS80 emulsions remained characterized by larger droplets, with sizes of approximately 18–19 μm, indicating a greater tendency toward coalescence at high temperatures. These observations suggest that the interfacial film formed in the MS80 system was less effective in restraining droplet enlargement when exposed to increased thermal stress.

The observed droplet size trends can be related to differences in the hydrophilic–lipophilic balance (HLB) of the surfactants. Span 20, with a higher HLB value, is more suitable for oil-in-water emulsions and can adsorb efficiently at the oil–water interface as temperature increases (Hauzin et al., 2024). The presence of MEG contributes to

interfacial stabilization by reducing interfacial tension and promoting finer droplet dispersion through synergistic interactions between surfactant molecules. Similar temperature-dependent droplet size behavior has been reported in previous studies, where surfactants with appropriate HLB values produced smaller droplets and improved resistance to thermal destabilization (Wang et al., 2023).

In contrast, the lower HLB value and higher lipophilicity of Span 80 limit its effectiveness in stabilizing oil-in-water emulsions, particularly at elevated temperatures. Even in the presence of MEG, the Span 80 system showed a greater tendency toward droplet growth and partial coalescence, indicating less favorable interfacial interactions under thermal stress.

Overall, the results demonstrate that surfactant type plays a key role in governing droplet size evolution and thermal stability in the formulated emulsions. Clear relationships were observed between droplet size distribution, viscosity behavior, and creaming index, indicating that emulsion stability is controlled by the combined effects of interfacial properties and bulk rheology rather than by a single parameter.

Emulsions stabilized with the Span 20–MEG system consistently exhibited smaller droplet sizes, higher viscosity, and lower creaming indices across the investigated temperature range. The formation of finer droplets increased the total interfacial area, while the higher viscosity of the continuous phase reduced droplet mobility. These combined effects effectively slowed gravitational separation and limited droplet coalescence during storage and thermal exposure. This behavior suggests the formation of a compact and cohesive interfacial film, which enhanced resistance to temperature-induced destabilization.

In contrast, emulsions stabilized with the Span 80–MEG system were characterized by larger droplet sizes and lower viscosity, leading to increased droplet mobility and a higher tendency for creaming. Although Span 80 showed relatively moderate changes in viscosity with increasing temperature, its lower hydrophilic–lipophilic balance limited its effectiveness in stabilizing oil-in-water emulsions. Consequently, the interfacial structure formed was less capable of preventing droplet aggregation and upward migration, particularly during the early stages of storage.

Taken together, these findings confirm that stable oil-in-water emulsions are achieved when small droplet size and sufficient continuous-phase viscosity act simultaneously to suppress coalescence and creaming. The observed consistency between droplet size distribution, viscosity, and creaming index highlights the

importance of selecting surfactant systems with appropriate interfacial activity and synergistic interactions, especially for formulations exposed to temperature variation.

4.3 Molecular Dynamic Simulation

The molecular dynamics (MD) simulations in this study were performed on four emulsion systems, namely MS20-C, MS20-D, MS80-B, and MS80-C, each composed of virgin coconut oil (represented by lauric acid), deionized water, and a mixed-surfactant system consisting of either Span 20 or Span 80 in combination with methyl-α-D-glucopyranoside (MEG). These systems were formulated with varying oil–water–surfactant ratios to represent different emulsification conditions and to examine how surfactant type and composition influence emulsion structure at the molecular level.

The MS20-C formulation consisted of 30 wt% lauric acid, 40 wt% deionized water, and a total surfactant content of 30 wt%, equally divided between Span 20 and MEG. In contrast, MS20-D was formulated with a lower oil content (10 wt% lauric acid) and higher water content (60 wt%), while maintaining the same surfactant ratio. This system was designed to represent a more dilute oil-in-water emulsion.

The MS80-B system differed in surfactant type, employing Span 80 instead of Span 20, with 20 wt% lauric acid, 40 wt% water, and 40 wt% total surfactants, equally divided between Span 80 and MEG. Lastly, MS80-C mirrored the composition of MS20-C but substituted Span 20 with Span 80, enabling a direct comparison of the influence of surfactant molecular structure on emulsion behavior.

The densities of each emulsion system were calculated based on experimental measurements and are presented in Table 4.8. These values were used to estimate the total mass of each system within a fixed simulation box volume of 1000 nm^3 (1×10^{-24} m^3). The calculated densities were 2448.5 kg/m^3 for MS20-C, 2436.0 kg/m^3 for MS20-D, 2217.5 kg/m^3 for MS80-B, and 2228.6 kg/m^3 for MS80-C. The corresponding molecular quantities of lauric acid, surfactants, and MEG used to construct each simulation model are summarized in Table 4.8, providing a clear overview of the molecular inputs for the MD simulations.

Table 4.8
Summary of sample formulations: molar ratios, system densities, and molecular quantities (N) of lauric acid (C12:0), Span 20, Span 80, and MEG.

Sample	Ratio	Density (kg/m^3)	$N_{C12:0}$	N_{S20}	N_{S80}	N_{MEG}
MS20-C	30: 40: 30	2448.5	2208	638		1139
MS20-D	10: 60: 30	2436.0	732	635		1113
MS80-B	20: 40: 40	2217.5	1333		623	1375
MS80-C	30: 40: 30	2228.6	2010		470	1037

Variations in the number of molecules across the systems were intentional and directly reflect differences in formulation composition and surfactant type. In addition, the structural differences between Span 20 (sorbitan monolaurate) and Span 80 (sorbitan monooleate) particularly in terms of hydrophobic chain saturation and molecular flexibility were expected to influence interfacial packing, molecular organization, and dynamic behavior within the emulsion systems.

These constructed molecular assemblies formed the basis for subsequent analyses of key dynamic and structural parameters, including radius of gyration (Rg) and visual observations of self-assembly and droplet formation throughout the 6-nanosecond simulation period. The outcomes of these analyses are discussed in the following sections, providing molecular-level insight into the stabilization mechanisms of emulsions formed using mixed-surfactant systems under different compositional conditions.

4.3.1 Radius of Gyration (Rg) Analysis

The radius of gyration (Rg) was analyzed to assess the structural compactness and distribution of mass within each emulsion system throughout molecular dynamics (MD) simulation. Rg provides a quantitative measure of how tightly or loosely the molecular components are arranged in space and is thus a useful parameter for evaluating emulsion stability at the molecular level (Niu *et al.*, 2023). The values of Rg over time for all four systems (MS20-C, MS20-D, MS80-B, and MS80-C) are presented

in Figures 4.33. In addition, the eccentricity (*e*) values of the same systems were also determined (Table 4.13) to provide complementary insight into shape anisotropy. While Rg describes the spatial spread of the system, eccentricity reveals whether the structure is more spherical (*e* near 0) or elongated (*e* approaching 1) (Ragusa *et al*., 2024).

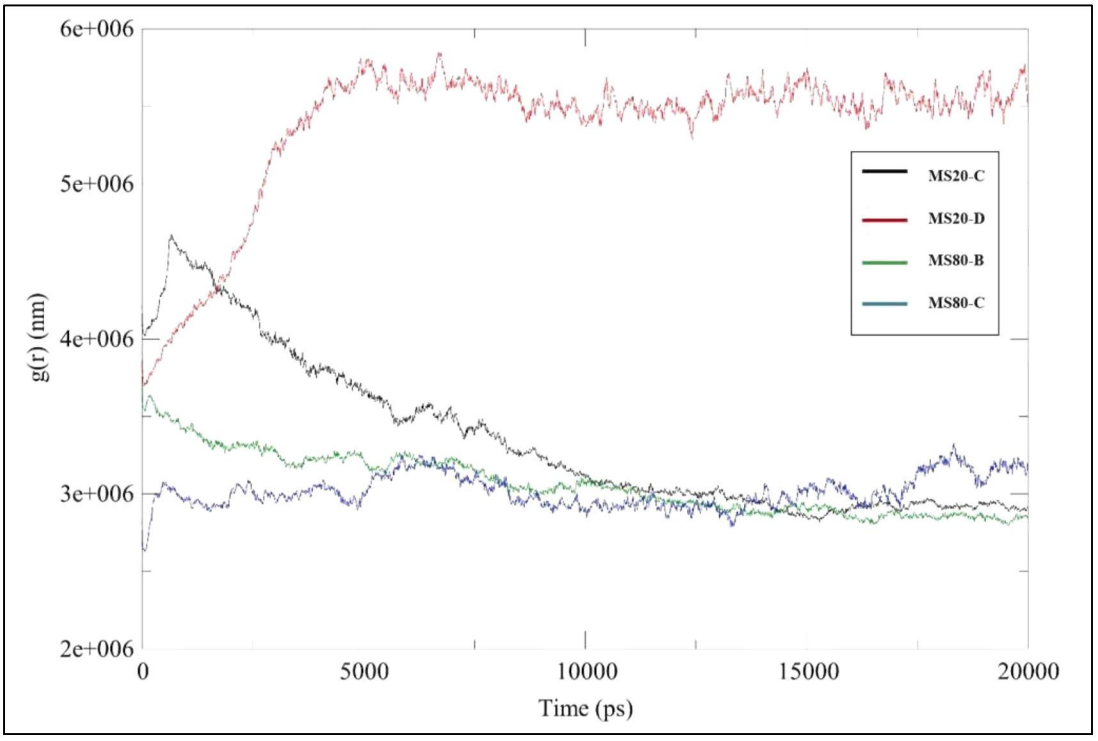

Figure 4.29 Radius of gyration (Rg) for four emulsion systems

Table 4.9

Eccentricity values of four different emulsion systems.

Structure	Eccentricity (*e*)
MS20-C	0.308
MS20-D	0.282
MS80-B	0.412
MS80-C	0.285

Note: The zero value indicates a perfect spherical shape.

During the first few nanoseconds, MS20-C showed relatively high Rg values (> 4.0×10^6 nm), reflecting an initial reorganization phase where oil and surfactant molecules underwent conformational adjustments to minimize interfacial free energy. As the simulation progressed, the system gradually reorganized into a denser configuration, stabilizing after ~10 ns at ~$3.0–3.2 \times 10^6$ nm. This compaction is characteristic of effective surfactant alignment at the oil–water boundary, where Span 20 and MEG jointly formed a cohesive interfacial film (Esposito *et al.*, 2021). The associated eccentricity value (e = 0.308) indicates that this compact arrangement also maintained a near-spherical geometry, resulting in both isotropy and stability (Toonen et al., 2016). These structural features correlate strongly with experimental results for MS20-C, which exhibited uniform droplet sizes, low creaming index, and enhanced viscosity. The behavior is consistent with the structural nature of Span 20: its short, saturated laurate tail reduces conformational mobility, thereby promoting denser and more ordered molecular packing.

MS20-D, formulated with the same surfactant mixture as MS20-C but with a reduced oil fraction (10% instead of 30%), demonstrated the lowest and most stable Rg trajectory (~$2.9–3.1 \times 10^6$ nm) with minimal fluctuations. This suggests that the lower oil content allowed more efficient dispersion of surfactant molecules across the droplet surfaces, minimizing steric congestion at the interface and facilitating stronger interfacial film formation (Debraj *et al.*, 2023; Karjiban *et al.*, 2012). Its eccentricity (e = 0.282) further highlights the spherical and isotropic nature of the aggregate. The combination of low Rg and low eccentricity in MS20-D reflects a highly compact and spherical molecular organization, which is consistent with its experimentally observed superior stability and homogeneous droplet size distribution (Hou and Shen, 2024). In this system, the synergy of Span 20's saturated structure with favorable oil-to-water composition optimized interfacial packing and stability.

In contrast, MS80-B, where Span 20 was replaced by Span 80, exhibited consistently higher Rg values (~$3.3–3.5 \times 10^6$ nm), indicative of looser molecular organization. This behavior is explained by the structural properties of Span 80, which possesses a longer, unsaturated oleate chain. The cis-double bond introduces kinks in the hydrophobic tail, increasing molecular flexibility and steric hindrance while reducing packing efficiency (Parreidt *et al.*, 2018). These structural disruptions lead to

less compact droplet assemblies, which is further confirmed by its high eccentricity (e = 0.412), reflecting elongated or irregular geometries. Such anisotropy increases interfacial energy and makes droplets more prone to deformation and coalescence. Experimentally, this is consistent with MS80-B larger droplet size distribution, higher creaming index, and reduced viscosity. The weak internal structural organization seen in the Rg–eccentricity analysis thus provides a molecular explanation for the poor macroscopic stability of MS80-B (Liu *et al.*, 2025).

Sample MS80-C displayed the most distinct behavior, with Rg values rapidly increasing during the first 5 ns and plateauing at the highest value of all systems (~5.5 × 10^6 nm). This indicates the formation of a large, expanded molecular configuration with low compactness (Debraj *et al.*, 2023). Surprisingly, its eccentricity was relatively low (e = 0.285), suggesting that despite the expanded structure, the droplet aggregates remained nearly spherical. This paradox reveals an important structural nuance: spherical geometry alone (low e) is not sufficient for stability if compactness (low Rg) is absent. MS80-C, which shares the same composition as MS20-C but with Span 80 instead of Span 20, therefore demonstrates that surfactant molecular structure can override compositional effects. While Span 20 favors compact, tightly packed assemblies, Span 80 drives the formation of expanded but isotropic aggregates (Liu *et al.*, 2025). This explains why MS80-C showed moderate but inferior stability compared to Span 20 systems, despite its spherical droplet shape.

Taken together, the combined interpretation of radius of gyration and eccentricity provides a comprehensive picture of the molecular organization within the emulsion systems. Emulsions exhibiting low Rg values together with low eccentricity, such as MS20-C and MS20-D, formed compact and near-spherical aggregates that are favorable for structural stability. In contrast, systems characterized by higher Rg values and increased eccentricity, such as MS80-B, displayed looser and more anisotropic molecular arrangements, which are more susceptible to deformation and coalescence.

The behavior of MS80-C highlights an important structural distinction, where a relatively low eccentricity was observed despite the highest Rg among all systems. This indicates that spherical geometry alone is insufficient to ensure stability if molecular compactness is lacking. Although MS80-C formed isotropic aggregates, the expanded internal structure suggests inefficient interfacial packing, which limits resistance to coalescence. This observation demonstrates that both compactness and isotropy must be achieved simultaneously to support stable emulsion structures.

These differences can be attributed to the molecular characteristics of the surfactants and formulation composition. Span 20, with its saturated laurate chain, promotes tighter and more ordered interfacial packing, whereas Span 80, containing an unsaturated oleate chain, introduces conformational flexibility that restricts compact molecular assembly. When combined with appropriate oil-to-water ratios and MEG, Span 20-based systems favor cohesive interfacial films that correspond well with experimentally observed smaller droplet sizes, higher viscosity, and lower creaming indices. Conversely, Span 80-based systems tend to form more expanded molecular arrangements, which are associated with larger droplet sizes and reduced resistance to long-term destabilization.

4.3.2 Self-assembly and droplet formation

Molecular dynamics (MD) simulations were conducted to visualize the self-assembly process and droplet formation in virgin coconut oil-in-water emulsions stabilized by mixed surfactant systems. The simulation snapshots provide qualitative insight into droplet morphology, interfacial arrangement, and surfactant packing at the oil–water interface, all of which play a critical role in determining emulsion stability. Visual analysis is particularly useful in explaining the molecular origin of experimentally observed stability trends, as it reveals how surfactant molecules organize and interact under different compositional conditions. These observations complement the quantitative analyses of radius of gyration (Rg) and eccentricity discussed earlier, which describe the compactness and shape anisotropy of the molecular assemblies (Ragusa et al., 2024).

For MS20-C, the simulation snapshots showed the formation of relatively uniform droplets with clearly defined and continuous interfacial boundaries (Figure 4.30a). Span 20 and MEG molecules were homogeneously distributed around the oil phase, forming a coherent interfacial layer that effectively encapsulated the lauric acid molecules. This uniform coverage indicates strong adsorption of the mixed surfactant system at the oil–water interface, facilitating efficient reduction of interfacial tension and limiting droplet coalescence during the simulation. In addition, the stable potential energy profile suggests that the system rapidly reached an energetically favorable

configuration with minimal large-scale molecular rearrangement (Esposito et al., 2021). These visual features are in good agreement with the compact Rg values (~3.0–3.2 × 10^6 nm) and low eccentricity (e = 0.308), confirming the formation of dense and near-spherical molecular assemblies (Toonen et al., 2016). The saturated laurate chain of Span 20 further promotes ordered packing and reduced conformational flexibility, contributing to the formation of a cohesive and mechanically stable interfacial film.

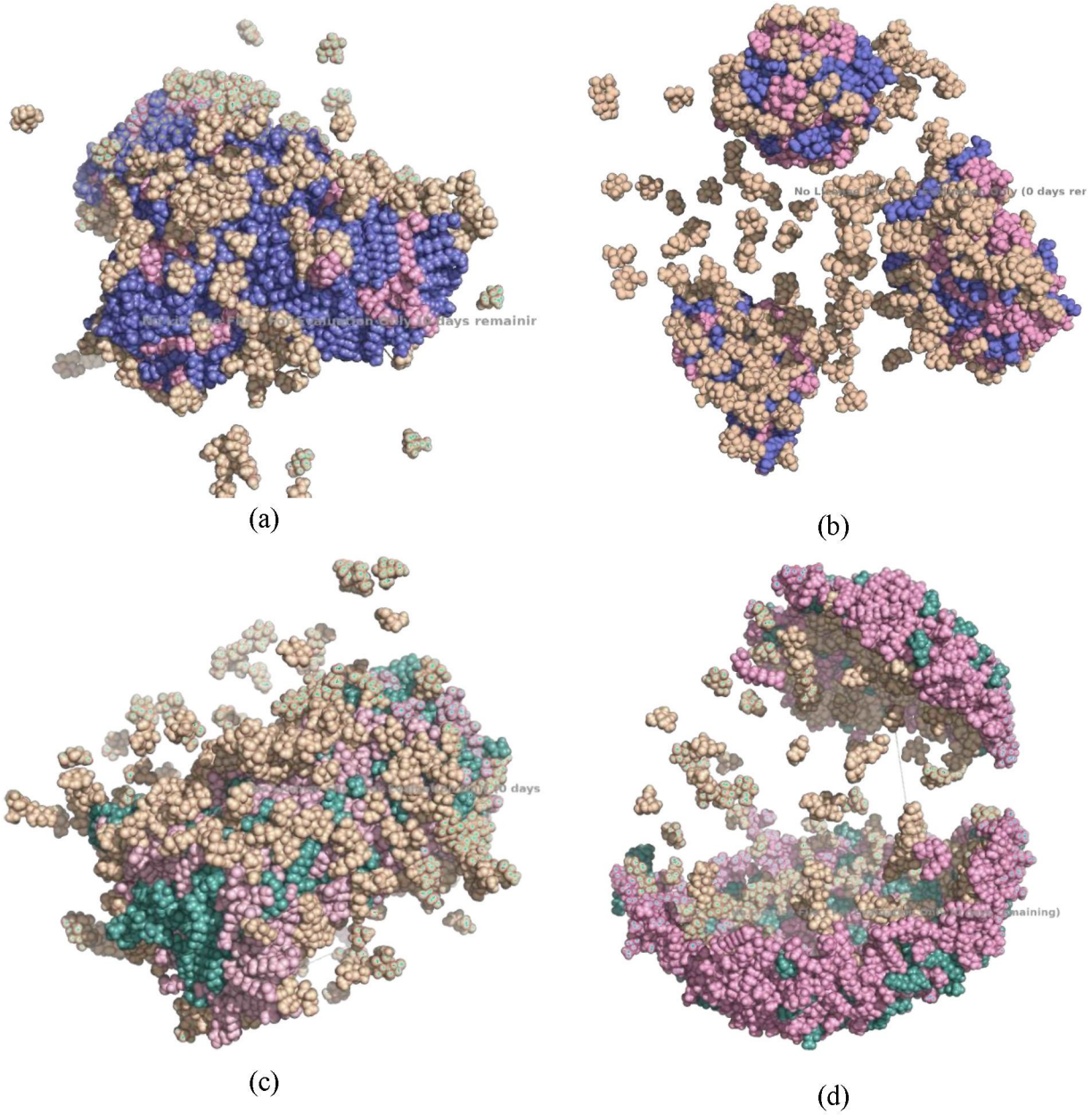

(a) (b) (c) (d)

Figure 4.30 Self-assembly and droplet formation for a) MS20-C b) MS20-B c) MS80-B d) MS20-D emulsions

In the case of MS20-D, the droplets appeared generally compact but exhibited localized aggregation and minor shape irregularities. These features suggest the occurrence of transient interfacial rearrangements rather than extensive droplet coalescence. The reduced oil fraction in this formulation alters the oil-to-surfactant ratio, resulting in a larger relative availability of surfactant molecules at the interface. While this promotes effective droplet coverage, it may also lead to localized surfactant crowding and momentary structural heterogeneity. Despite these visual irregularities, the Rg values remained low and stable (~2.9–3.1 × 10^6 nm), and the eccentricity value was minimal (e = 0.282), indicating that the overall molecular assembly retained a compact and isotropic structure. This molecular behavior aligns with experimental observations of narrow droplet size distribution and good resistance to creaming, suggesting that MS20-D maintained sufficient interfacial integrity even under diluted oil conditions (Hou and Shen, 2024).

In contrast, MS80-B exhibited noticeably larger droplets with irregular shapes and poorly defined interfacial boundaries (Figure 4.30c). The surfactant layer appeared discontinuous, reflecting weaker adsorption and less efficient packing of Span 80 and MEG molecules at the oil–water interface. The unsaturated oleate chain of Span 80 contains a cis-double bond that introduces kinks into the hydrophobic tail, increasing molecular flexibility while simultaneously reducing packing efficiency (Parreidt et al., 2018). This structural feature limits the formation of a compact interfacial film and promotes looser molecular organization. Consequently, MS80-B showed higher Rg values (~3.3–3.5 × 10^6 nm) and elevated eccentricity (e = 0.412), indicating expanded and anisotropic assemblies. Such anisotropy increases interfacial energy and enhances susceptibility to droplet deformation and coalescence, which is consistent with the experimentally observed lower viscosity and higher creaming tendency (Liu et al., 2025).

Meanwhile, MS80-C displayed visually homogeneous and well-separated droplets with predominantly spherical geometry (Figure 4.30d). The smooth interfacial boundaries suggest that surfactant molecules were able to uniformly surround the oil phase, resulting in droplets with minimal shape distortion. This observation is supported by the stable potential energy profile and pronounced peaks in the radial distribution function, indicating an ordered interfacial arrangement (Debraj et al., 2023). However, despite the spherical droplet appearance, MS80-C exhibited the highest Rg value (~5.5

$\times 10^6$ nm), while maintaining a low eccentricity (e = 0.285). This combination indicates that although the droplets were isotropic, the internal molecular structure was relatively expanded and loosely packed. This behavior highlights an important distinction between droplet shape and molecular compactness, demonstrating that spherical geometry alone does not guarantee structural stability. The flexible unsaturated chain of Span 80 allows isotropic arrangement but restricts dense packing, leading to expanded molecular assemblies (Liu et al., 2025).

Overall, the integrated interpretation of MD visualization, radius of gyration, and eccentricity analyses demonstrates that effective emulsion stabilization requires both isotropic droplet geometry and compact molecular packing at the oil–water interface. Systems that form dense and cohesive interfacial films exhibit enhanced resistance to droplet deformation, coalescence, and gravitational separation, whereas expanded or anisotropic molecular assemblies are more prone to destabilization. These findings further reinforce that surfactant molecular structure and formulation composition jointly govern self-assembly behavior and stability in virgin coconut oil- in-water emulsions. The insights gained from MD simulations provide a molecular- level explanation for the experimentally observed trends in droplet size distribution, viscosity, and creaming behavior.

CHAPTER 5
CONCLUSION & RECOMMENDATIONS

5.1 Conclusion

Assessing the stability and characterizing an oil-in-water emulsion utilizing a combination of the MEG and Span surfactant series were the main goals of this study. In addition to the experimental effort, the research sought to give a better understanding of the molecular interactions influencing emulsion stability by using molecular dynamics (MD) simulations. The characterization verified the impact of surfactant concentration and ratio on important stability parameters, and the experimental findings effectively illustrated the creation of a stable oil-in-water emulsion system utilizing virgin coconut oil. Significant variations in the stabilizing properties of MEG, Span 20, and Span 80, either separately or in different combinations, were found when the 20 samples were compared. While emulsions stabilized with Span 20 and MEG alone also performed less than optimally, those stabilized with a single surfactant, such as Span 80 with its low HLB value, displayed inconsistent stability and a propensity for phase separation. The combined surfactant systems, on the other hand, showed a definite synergistic impact that resulted in a much greater degree of stability.

Five distinct analytical techniques (creaming index, freeze-thaw, rheology, optical polarizing microscopy and FTIR) were utilized to investigate and confirm the most stable formulation. Among all samples, MS20-C, formulated with 30 wt% oil, 40 wt% water, and a total surfactant content of 30 wt% consisting of an equal ratio of Span 20 (15 wt%) and MEG (15 wt%), even across a range of temperatures (30 °C to 60 °C). According to the findings of the creaming index, MS20-C showed very little phase separation over the observation period, indicating that it was quite resistant to gravity. The freeze-thaw cycle test offered a thorough evaluation of the emulsion's resistance to temperature stress; MS20-C further demonstrated its exceptional stability by retaining its integrity and physical appearance after many cycles. The viscosity and viscoelastic characteristics of the emulsions were finally quantified by rheological analysis as MS20-C showed more structured, non-Newtonian behaviour, which was directly connected to its increased stability against external pressures. Additionally, compared to other formulations, MS20-C generated the smallest and most monodisperse droplets,

according to droplet size analysis, a crucial sign of kinetic stability. In contrast to the bigger or irregularly shaped droplets detected in less stable samples (MS80-B and MS80-C), polarized light microscopy visually confirmed these quantitative findings by revealing a homogenous emulsion with consistently sized, non-coalesced droplets. The FTIR spectra confirmed the absence of new peaks, demonstrating that no chemical degradation or by-product formation occurred during emulsification. Characteristic absorption bands of the virgin coconut oil (C=O stretching at ~1743 cm^{-1} and C–H stretching at ~2922 and 2853 cm^{-1}) were retained, while slight shifts and intensity changes in the O–H stretching region (~3300–3400 cm^{-1}) and C–O stretching (~1050–1150 cm^{-1}) indicated hydrogen bonding and interfacial interactions between the oil, water, and surfactant molecules.

The GROMACS software was used to perform molecular dynamics (MD) simulations on four chosen emulsion formulations (MS20-C, MS20-D, MS80-B, and MS80-C) in order to confirm and expand on the experimental results. The importance of surfactant interactions at the oil-water interface was shown by the simulations at the atomistic level. Radius of gyration (Rg) analysis indicated that MS20-C achieved the most compact and stable configuration, stabilizing at ~$3.0–3.2\times10^{6}$ nm after the initial equilibration phase, whereas MS80-B, and MS80-C (MEG and Span 80) displayed greater fluctuations, suggesting less stable molecular packing. Eccentricity analysis further revealed that MS20-C maintained a near-spherical droplet morphology, while the other samples showed higher eccentricity values, reflecting elongated or irregular shapes prone to instability.

5.2 Recommendations

For future work, it is recommended to investigate the influence of pH, ionic strength, and the incorporation of co-surfactants or polymers to enhance emulsion stability under a wider range of environmental conditions. Extending MD simulations to longer timescales and incorporating coarse-grained models could provide deeper insights into long-term stability and molecular self-assembly dynamics. Additionally, integrating eccentricity as a complementary parameter alongside radius of gyration in future simulations would allow for a more comprehensive evaluation of droplet geometry and structural compactness, particularly in response to formulation changes and processing conditions. Such combined structural metrics could be valuable in predicting performance during scale-up and in tailoring formulations for specific pharmaceutical, cosmetic, or food applications.

REFERENCES

Abdul Rahman, M. B., Latif, M. A. M., Basri, M., Salleh, A. B., & Abdul Rahman, R. N. Z. (2010). Molecular dynamics simulation of oleyl oleate swollen micelles system. *Molecular Simulation*, *36*(5), 403–407. https://doi.org/10.1080/08927020903544535

Abujazia, M. A., Muhammad, N., Shuid, A. N., & Soelaiman, I. N. (2012). The effects of virgin coconut oil on bone oxidative status in ovariectomised rat. *Evidence-based Complementary and Alternative Medicine*, 2012, 1–6. https://doi.org/10.1155/2012/525079

Agarwal, R. K. (2017). Extraction processes of virgin coconut oil. MOJ Food Processing & Technology, 4(2), 1-3. https://doi.org/10.15406/mojfpt.2017.04.00087

Ajao, A., Kannan, M., Krishna, R., Yakubu, S., Umoh, V., & Ameh, J. (2012). Homology modeling, simulation and molecular docking studies of catechol-2, 3-Dioxygenase from Burkholderia cepacia: Involved in degradation of petroleum hydrocarbons. *Bioinformation*, *8*(18), 848–854. https://doi.org/10.6026/97320630008848

Akbari, S., & Nour, A. H. (2018). Emulsion types, stability mechanisms and rheology: A review. *International Journal of Innovative Research and Scientific Studies*, 1(1), 11–17. https://doi.org/10.53894/ijirss.v1i1.4

Amaliyah, P. R., Mardawati, E., Macklin, B., & Prawiranegara, P. (2024). Formulation and evaluation of virgin coconut oil (VCO) lotion: Effect of variation in emulsifier type and concentration. *Advances in Food Science, Sustainable Agriculture and Agroindustrial Engineering*, *7*(1), 109–118. https://doi.org/https://doi.org/10.21776/ub.afssaae.2024.007.01.10

Anzaku, A. A., Akyala, J. I., Juliet, A., & Obianuju, E. C. (2017). Antibacterial activity of lauric acid on some selected clinical isolates. *Annals of Clinical and Laboratory Research*, 5(2), 1–5. https://doi.org/10.21767/2386-5180.1000170

Aregbe, A. G., Hsia, T., Krasowska, M., Thang, S. H., & Franks, G. V. (2024). Stability and characteristics of kerosene-in-water emulsions with xanthate surfactants: Influence of hydrophilic-lipophilic balance and molecular weight. *Colloids and Surfaces a Physicochemical and Engineering Aspects*, 700, 134818. https://doi.org/10.1016/j.colsurfa.2024.134818

Ariyaprakai, S., & Tananuwong, K. (2015). Freeze-thaw stability of edible oil-in-water emulsions stabilized by sucrose esters and Tweens. *Journal of Food Engineering*, *152*, 57–64. https://doi.org/10.1016/j.jfoodeng.2014.11.023

Astaraki, A. M. (2016). The effect of concentration of surfactant and electrolyte on the pit and droplet sizes nanoemulsions of n-dodecane in water. *Russian Journal of Applied Chemistry*, *89*(1), 84–89. https://doi.org/10.1134/S10704272160010134

Babu, A. S., Veluswamy, S. K., Arena, R., Guazzi, M., & Lavie, C. J. (2014). Virgin coconut oil and its potential cardioprotective effects. *Postgraduate Medicine*, *126*(7), 76–83. https://doi.org/10.3810/pgm.2014.11.2835

Badmus, S. O., Amusa, H. K., Oyehan, T. A., & Saleh, T. A. (2021). Environmental risks and toxicity of surfactants: overview of analysis, assessment, and remediation techniques. *Environmental Science and Pollution Research*, *28*(44), 62085–62104. https://doi.org/10.1007/s11356-021-16483-w/Published

Bajpai, P. (2018). *Colloid and surface chemistry*. In *Colloid and surface chemistry* (pp. 381–400). Elsevier. https://doi.org/10.1016/b978-0-12-814238-7.00019-2

Bakry, A. M., Abbas, S., Ali, B., Majeed, H., Abouelwafa, M. Y., Mousa, A., & Liang, L. (2016). Microencapsulation of Oils: A Comprehensive Review of Benefits, Techniques, and Applications. *Comprehensive Reviews in Food Science and Food Safety*, *15*(1), 143–182. https://doi.org/10.1111/1541-4337.12179

Barnes, H. A. (2004). The rheology of emulsions (Chapter 18). In D. N. Petsev (Ed.), *Interface science and technology*. 4, (pp. 721–759). Elsevier. https://doi.org/10.1016/S1573-4285(04)80020-6

Bar-On, R., & Manor, O. (2024). Contributions of Colloidal Forces to the Heterogeneous Separation of Stable Oil-In-Water Emulsions. *Langmuir*, *40*(44), 23458–23464. https://doi.org/10.1021/acs.langmuir.4c03056

Beceiro, A., Tomás, M., & Bou, G. (2013). Antimicrobial resistance and virulence: A successful or deleterious association in the bacterial world? *Clinical Microbiology Reviews*, 26(2), 185–230. https://doi.org/10.1128/CMR.00059-12

Bhatt, K. P., Pulickal, A. V., Agolli, A., Patel, M. H., Thevuthasan, S., Haight, R., Agatep, D., DeAngelo, O., Prado, L. D., Desimone, A., Garcia, E., & Gelovich, S. (2021). Antioxidant, antibacterial, antiviral and antifungal properties of virgin coconut oil (VCO). *Journal of Nutritional Biology*, 7(1), 458–471. https://doi.org/10.18314/jnb.v7i1.2090

Boateng, L., Ansong, R., Owusu, W. B., & Steiner-Asiedu, M. (2016). Coconut oil and palm oil's role in nutrition, health and national development: A review. *Ghana medical journal* 50(3), 189–196. https://doi.org/10.4314/gmj.v50i3.11

Bon, S. A. F., Mookhoek, S. D., Colver, P. J., Fischer, H. R., & van der Zwaag, S. (2007). Route to stable non-spherical emulsion droplets. *European Polymer Journal*, *43*(11), 4839–4842. https://doi.org/10.1016/j.eurpolymj.2007.09.001

Bormashenko, E., & Shoval, S. (2025). Negative-Viscosity Materials: Exploiting the Effect of Negative Mass. *Materials*, *18*(6), 1199. https://doi.org/10.3390/ma18061199

Bramante, F., Di Bari, V., Adams, G., Beaudoin, F., Waschatko, G., Jakobi, R., Billecke, N., & Gray, D. (2025). Freeze-thaw stability of oilseed rape oleosome emulsions. *Journal of Food Engineering*, 392, 112471. https://doi.org/10.1016/j.jfoodeng.2025.112471

Bunawan, N. S. N., Masdor, N. N. A., Yasid, N. N. A., Halmi, N. M. I. E., & Shukor, N. M. Y. A. (2023). Effect of different hydrophilic-lipophilic balance (HLB) on droplet size, polydispersity index and stability of Lemon Myrtle nanoemulsion. *International Journal of Nanoelectronics and Materials (IJNeaM)*, 16(12), 431–440. https://doi.org/10.58915/ijneam.v16idecember.423

Capdevila, M., Maestro, A., Porras, M., & Gutiérrez, J. M. (2010). Preparation of Span 80/oil/water highly concentrated emulsions: Influence of composition and formation variables and scale-up. *Journal of Colloid and Interface Science*, *345*(1), 27–33. https://doi.org/10.1016/j.jcis.2010.01.045

Cassiday, L. (2014). Emulsions: Making oil and water mix. *International News on Fats, Oils and Related Materials*, *25*(4), 200–208.

Chiplunkar, P. P., & Pratap, A. P. (2016). Utilization of sunflower acid oil for synthesis of alkyd resin. *Progress in Organic Coatings*, *93*, 61–67. https://doi.org/10.1016/j.porgcoat.2016.01.002

Cho, Y., Kim, S., Bae, E., Mok, C., & Park, J. (2008). Formulation of a Cosurfactant-Free O/W microemulsion using nonionic surfactant mixtures. *Journal of Food Science*, 73(3), E115-21. https://doi.org/10.1111/j.1750-3841.2008.00688.x

Clavier, A., Carnal, F., & Stoll, S. (2016). Effect of Surface and Salt Properties on the Ion Distribution around Spherical Nanoparticles: Monte Carlo Simulations. *Journal of Physical Chemistry B*, *120*(32), 7988–7997. https://doi.org/10.1021/acs.jpcb.6b05104

Colucci, G., Santamaria-Echart, A., Silva, S. C., Fernandes, I. P. M., Sipoli, C. C., & Barreiro, M. F. (2020). Development of Water-in-Oil Emulsions as Delivery Vehicles and Testing with a Natural Antimicrobial Extract. *Molecules*, *25*(9), 2105. https://doi.org/10.3390/molecules25092105

da Silva Gulão, E., de Souza, C. J. F., da Costa, A. R., da Rocha-Leão, M. H. M., & Garcia-Rojas, E. E. (2018). Stability and rheological behavior of coconut oil-in-water emulsions formed by biopolymers. *Polimeros*, *28*(5), 413–421. https://doi.org/10.1590/0104-1428.08017

Dayrit, F. M. (2015). The Properties of Lauric Acid and Their Significance in Coconut Oil. *Journal of the American Oil Chemists' Society*, *92*(1), 1–15. https://doi.org/10.1007/s11746-014-2562-7

De Vivo, M., Masetti, M., Bottegoni, G., & Cavalli, A. (2016). Role of Molecular Dynamics and Related Methods in Drug Discovery. *Journal of Medicinal Chemistry* 59(9), 4035–4061. https://doi.org/10.1021/acs.jmedchem.5b01684

DebMandal, M., & Mandal, S. (2011). Coconut (Cocos nucifera L.: Arecaceae): In health promotion and disease prevention. *Asian Pacific Journal of Tropical Medicine*, *4*(3), 241–247. https://doi.org/10.1016/S1995-7645(11)60078-3

Debraj, D., Carpenter, J., & Vatti, A. K. (2023). Understanding the Effect of the Oil-to-Surfactant Ratio on Eugenol Oil-in-Water Nanoemulsions Using Experimental and Molecular Dynamics Investigations. *Industrial and Engineering Chemistry Research*, *62*(41), 16766–16776. https://doi.org/10.1021/acs.iecr.3c02345

Deng, W., Zheng, H., Zhu, Z., Deng, Y., Shi, Y., Wang, D., & Zhong, Y. (2023). Effect of surfactant formula on the film forming capacity, wettability, and preservation properties of electrically sprayed sodium alginate coats. *Foods*, *12*(11), 2197. https://doi.org/10.3390/foods12112197

Donsì, F., Wang, Y., & Huang, Q. (2011). Freeze-thaw stability of lecithin and modified starch-based nanoemulsions. *Food Hydrocolloids*, *25*(5), 1327–1336. https://doi.org/10.1016/j.foodhyd.2010.12.008

Doutsi, M., Vlachou, M. C., Koukiotis, C., Kostoglou, M., & Karapantsios, T. D. (2025). Experimental investigation of stability of emulsions produced by catastrophic phase inversion using Non-Ionic surfactants. *Colloids and Interfaces*, *9*(1), 6. https://doi.org/10.3390/colloids9010006

Duan, Q., Xie, J., Xia, G., Xiao, C., Yang, X., Xie, Q., & Huang, Z. (2021). Molecular Dynamics simulation for the effect of fluorinated graphene oxide layer spacing

on the thermal and mechanical properties of fluorinated epoxy resin. *Nanomaterials*, *11*(5), 1344. https://doi.org/10.3390/nano11051344

Dumancas, G. G., Kasi Viswanath, L. C., de Leon, A. R., Ramasahayam, S., Maples, R., Hikkaduwa Koralege, R., Perera, U. D. N., Langford, J., Shakir, A., & Castles, S. (2016). *Health benefits of virgin coconut oil*. In B. Holt (Ed.), *Vegetable oil: Properties, uses, and benefits* (pp. 161–194). Nova Science Publishers, Inc.

El-Sayed, W., & Mohammad, T. G. M. (2020). Effect of hydrophilic-lipophilic balance (HLB) values of surfactant mixtures on the physicochemical properties of emulsifiable concentrate formulations of difenoconazole. *Journal of Applied Life Sciences International*, 22(4), 1–10. https://doi.org/10.9734/jalsi/2019/v22i430135

Esposito, R., Cavasso, D., Niccoli, M., & D'errico, G. (2021). Phase inversion and interfacial layer microstructure in emulsions stabilized by glycosurfactant mixtures. *Nanomaterials*, *11*(2), 1–14. https://doi.org/10.3390/nano11020331

Fang, Q., Zhao, X., Li, S., Qiu, Z., Wang, Z., & Geng, Q. (2022). Effect of Surfactants with Different Hydrophilic–Lipophilic Balance on the Cohesive Force between Cyclopentane Hydrate Particles. *Journal of Marine Science and Engineering*, *10*(9), 1255. https://doi.org/10.3390/jmse10091255

Fenton, T., Kanyuck, K., Mills, T., & Pelan, E. (2021). Formulation and characterisation of kappa-carrageenan gels with non-ionic surfactant for melting-triggered controlled release. *Carbohydrate Polymer Technologies and Applications*, *2*, 100060. https://doi.org/10.1016/j.carpta.2021.100060

Fu, X., Kong, W., Zhang, Y., Jiang, L., Wang, J., & Lei, J. (2015). Novel solid-solid phase change materials with biodegradable trihydroxy surfactants for thermal energy storage. *RSC Advances*, *5*(84), 68881–68889. https://doi.org/10.1039/c5ra11842e

Gao, Y., Lei, Y., Wu, Y., Liang, H., Li, J., Pei, Y., Li, Y., Li, B., Luo, X., & Liu, S. (2021). Beeswax: A potential self-emulsifying agent for the construction of thermal-sensitive food W/O emulsion. *Food Chemistry*, *349*, 129203. https://doi.org/10.1016/j.foodchem.2021.129203

Ge, X., Wei, M., He, S., & Yuan, W. (2019). Advances of Non-Ionic Surfactant vesicles (Niosomes) and their application in drug delivery. *Pharmaceutics*, *11*(2), 55. https://doi.org/10.3390/pharmaceutics11020055

Ghosh, P. K., Bhattacharjee, P., Mitra, S., & Poddar-Sarkar, M. (2014). Physicochemical and phytochemical analyses of COPRA and oil ofCocos NuciferaL. (West Coast Tall Variety). *International Journal of Food Science, 2014*, 1–8. https://doi.org/10.1155/2014/310852

Ghosh, S., & Rousseau, D. (2009). Freeze-thaw stability of water-in-oil emulsions. *Journal of Colloid and Interface Science*, *339*(1), 91–102. https://doi.org/10.1016/j.jcis.2009.07.047

Goertz, M. P., Houston, J. E., & Zhu, X. Y. (2007). Hydrophilicity and the viscosity of interfacial water. *Langmuir*, *23*(10), 5491–5497. https://doi.org/10.1021/la062299q

Gondokesumo, M. E., Sapei, L., Wahjudi, M., Suseno, N., & Adiarto, T. (2022). *Molecular mechanism of virgin coconut oil as a Nsp-3 inhibitor of SARS-CoV-2. Asia-Pacific Journal of Molecular Biology and Biotechnology, 30*(4), 9–19. https://doi.org/10.35118/apjmbb.2022.030.4.02

Goodarzi, F., & Zendehboudi, S. (2019). A Comprehensive Review on Emulsions and Emulsion Stability in Chemical and Energy Industries. *Canadian Journal of Chemical Engineering*, *97*(1), 281–309. https://doi.org/10.1002/cjce.23336

Hauzin, N., Mat Hadzir, N., Amani, H., Hamid, A., Hasham@Hisam, R., Nazihah, W., & Ibrahim, W. (2024). Fabrication and characterization of water-in-palm oil nanoemulsion as a carrier for catechin (Fabrikasi dan sifat nanoemulsi air dalam minyak kelapa sawit sebagai pembawa katekin). *Malaysian Journal of Analytical Sciences*, 28(2), 247-256.

He, H., Liu, K., Liu, M., Yang, A. J., Cheng, K. W., Lu, L. W., Liu, B., & Chen, J. H. (2024). The impact of medium-chain triglycerides on weight loss and metabolic health in individuals with overweight or obesity: A systematic review and meta-analysis. *Clinical Nutrition*, *43*(8), 1755–1768. https://doi.org/10.1016/j.clnu.2024.06.016

Hee, Y. Y., Tan, C. P., Rahman, R. A., Noranizan, M., Smith, R. L., & Chong, G. H. (2017). Production of virgin coconut oil microcapsules from oil-in-water emulsion with supercritical carbon dioxide spray drying. *Journal of Supercritical Fluids*, *130*, 118–124. https://doi.org/10.1016/j.supflu.2017.07.037

Hempoonsert, J., Tansel, B., & Laha, S. (2010). Effect of temperature and pH on droplet aggregation and phase separation characteristics of flocs formed in oil-water

emulsions after coagulation. *Colloids and Surfaces A: Physicochemical and Engineering Aspects*, *353*(1), 37–42. https://doi.org/10.1016/j.colsurfa.2009.10.016

Hess, D. J., Henry-Stanley, M. J., & Wells, C. L. (2015). The Natural Surfactant Glycerol Monolaurate Significantly Reduces Development of Staphylococcus aureus and Enterococcus faecalis Biofilms. *Surgical Infections*, *16*(5), 538–542. https://doi.org/10.1089/sur.2014.162

Hewlings, S. (2020). Coconuts and health: Different chain lengths of saturated fats require different consideration. *Journal of Cardiovascular Development and Disease* 7(4), 1–15. https://doi.org/10.3390/jcdd7040059

Hiranphinyophat, S., Otaka, A., Asaumi, Y., Fujii, S., & Iwasaki, Y. (2020). Particle-stabilized oil-in-water emulsions as a platform for topical lipophilic drug delivery. *Colloids and Surfaces B Biointerfaces*, *197*, 111423. https://doi.org/10.1016/j.colsurfb.2020.111423

Hollingsworth, S. A., & Dror, R. O. (2018). Molecular Dynamics Simulation for All. *Neuron* 99(6), 1129–1143. https://doi.org/10.1016/j.neuron.2018.08.011

Hong, I. K., Kim, S. I., & Lee, S. B. (2018). Effects of HLB value on oil-in-water emulsions: Droplet size, rheological behavior, zeta-potential, and creaming index. *Journal of Industrial and Engineering Chemistry*, *67*, 123–131. https://doi.org/10.1016/j.jiec.2018.06.022

Hou, C., Zhao, H., & Shen, Y. (2024). Learning biophysical dynamics with protein language models [Preprint]. *bioRxiv*. https://doi.org/10.1101/2024.10.11.617911

Ismail, I., Kazemzadeh, Y., Sharifi, M., Riazi, M., Malayeri, M. R., & Cortés, F. (2019). Formation and stability of W/O emulsions in presence of asphaltene at reservoir thermodynamic conditions. *Journal of Molecular Liquids*, *299*, 112125. https://doi.org/10.1016/j.molliq.2019.112125

Jack, K. S., Asaruddin, M. R. B., & Bhawani, S. A. (2022). Pharmacophore study, molecular docking and molecular dynamic simulation of virgin coconut oil derivatives as anti-inflammatory agent against COX-2. *Chemical and Biological Technologies in Agriculture*, *9*(1), 73. https://doi.org/10.1186/s40538-022-00340-0

Jadhav, H. B., & Annapure, U. S. (2023). Triglycerides of medium-chain fatty acids: a concise review. *Journal of Food Science and Technology* 60(8), 2143–2152.

https://doi.org/10.1007/s13197-022-05499-w

Jiang, X., Liu, M., Li, X., Wang, L., Liang, S., & Guo, X. (2021). Effects of surfactant and hydrophobic nanoparticles on the crude Oil-Water interfacial tension. *Energies*, *14*(19), 6234. https://doi.org/10.3390/en14196234

Jiao, J., & Burgess, D. J. (2003). Rheology and stability of water-in-oil-in-water multiple emulsions containing Span 83 and Tween 80. *AAPS PharmSci*, *5*(1), 62–73. https://doi.org/10.1208/ps050107

Joshi, S. (2020). Coconut Oil and Immunity: What do we really know about it so far? SITE-Screening India's Twin Epidemic View project. *Article in The Journal of the Association of Physicians of India*. 68, 67-72.

Kale, S. N., & Deore, S. L. (2016). Emulsion micro emulsion and nano emulsion: A review. *Systematic Reviews in Pharmacy* 8(1), 39–47. https://doi.org/10.5530/srp.2017.1.8

Karjiban, R. A., Basri, M., Rahman, M. B. A., & Salleh, A. B. (2012). Structural Properties of Nonionic Tween80 Micelle in Water Elucidated by Molecular Dynamics Simulation. *APCBEE Procedia*, *3*, 287–297. https://doi.org/10.1016/j.apcbee.2012.06.084

Khoee, S., & Yaghoobian, M. (2017). Niosomes: a novel approach in modern drug delivery systems. *Elsevier eBooks*. 207–237. https://doi.org/10.1016/b978-0-323-46143-6.00006-3

Khor, Y. P., Koh, S. P., Long, K., Long, S., Ahmad, S. Z. S., & Tan, C. P. (2014). A comparative study of the physicochemical properties of a virgin coconut oil emulsion and commercial food supplement emulsions. *Molecules*, *19*(7), 9187–9202. https://doi.org/10.3390/molecules19079187

Kim, D. D. (2021). *Structure and property correlations of surface-active agents in the control of colloidal behavior in home/personal care and biochemical systems* (Doctoral dissertation). Columbia University.

Kregiel, D., Berlowska, J., Witonska, I., Antolak, H., Proestos, C., Babic, M., Babic, L., & Zhang, B. (2017). Saponin-Based, Biological-Active Surfactants from Plants. In InTech eBooks. https://doi.org/10.5772/68062

Lamba, H., Sathish, K., & Sabikhi, L. (2015). Double Emulsions: Emerging Delivery System for Plant Bioactives. *Food and Bioprocess Technology*, *8*(4), 709–728. https://doi.org/10.1007/s11947-014-1468-6

L'Estimé, M., Schindler, M., Shahidzadeh, N., & Bonn, D. (2024). Droplet Size

Distribution in Emulsions. *Langmuir*, *40*(1), 275–281. https://doi.org/10.1021/acs.langmuir.3c02463

Li, S., Yuan, S., Zhang, Y., Guo, H., Liu, S., Wang, D., & Wang, Y. (2022). Molecular Dynamics Study on the Demulsification Mechanism of Water-In-Oil Emulsion with SDS Surfactant under a DC Electric Field. *Langmuir*, *38*(41), 12717–12730. https://doi.org/10.1021/acs.langmuir.2c02364

Lima, E. B. C., Sousa, C. N. S., Meneses, L. N., Ximenes, N. C., Santos Júnior, M. A., Vasconcelos, G. S., Lima, N. B. C., Patrocínio, M. C. A., Macedo, D., & Vasconcelos, S. M. M. (2015). Cocos nucifera (L.) (arecaceae): A phytochemical and pharmacological review. In *Brazilian Journal of Medical and Biological Research* 48(11), 953–964. https://doi.org/10.1590/1414-431X20154773

Liu, W., Cao, J., Zhang, Q., Wang, W., Ye, Y., Zhang, S., & Wu, L. (2024). Interfacial properties and structure of emulsions and foams Co-Stabilized by span emulsifiers of varying carbon chain lengths and egg yolk granules. *Foods*, *14*(1), 35. https://doi.org/10.3390/foods14010035

Liu, X., Li, Y., Tian, S., & Yan, H. (2019). Molecular Dynamics Simulation of Emulsification/Demulsification with a Gas Switchable Surfactant. *Journal of Physical Chemistry C*, *123*(41), 25246–25254. https://doi.org/10.1021/acs.jpcc.9b07652

Lu, H., Pourceau, G., Briou, B., Wadouachi, A., Gaudin, T., Pezron, I., & Drelich, A. (2024). Sugar-Based Surfactants: Effects of structural features on the physicochemical properties of sugar esters and their comparison to commercial octyl glycosides. *Molecules*, *29*(10), 2338. https://doi.org/10.3390/molecules29102338

Lukić, I., Kesić, Ž., Zdujić, M., & Skala, D. (2016). *Vegetable oil as a feedstock for biodiesel synthesis*. In B. Holt (Ed.), *Vegetable oil: Properties, uses and benefits*, (pp. 83–128). Nova Science Publishers. https://doi.org/10.5772/68062

Mahdi, E. S., Sakeena, M. H., Abdulkarim, M. F., Abdullah, G. Z., Sattar, M. A., & Noor, A. M. (2011). Effect of surfactant and surfactant blends on pseudoternary phase diagram behavior of newly synthesized palm kernel oil esters. *Drug Design, Development and Therapy*, *5*, 311–323. https://doi.org/10.2147/DDDT.S15698

Mao, L., Calligaris, S., Barba, L., & Miao, S. (2014). Monoglyceride self-assembled

structure in O/W emulsion: Formation, characterization and its effect on emulsion properties. *Food Research International*, *58*, 81–88. https://doi.org/10.1016/j.foodres.2014.01.042

Maphosa, Y., & Jideani, V. A. (2018). *Factors affecting the stability of emulsions stabilised by biopolymers*. In S. Karakuş (Ed.), *Science and technology behind nanoemulsions*, (pp. 65–80). InTech. https://doi.org/10.5772/intechopen.75308

Mathew, T. M., & Baby, P. O. (2011). *Global competitiveness of Indian coconut oil – an outlook. Indian Coconut Journal, 51*(6), 5–13.

Mijaljica, D., Spada, F., & Harrison, I. P. (2022). Skin Cleansing without or with Compromise: Soaps and Syndets. *Molecules*, *27*(6), 2010. https://doi.org/10.3390/molecules27062010

Mohamed, M., Jaafar, J., Ismail, A., Othman, M., & Rahman, M. (2017). Fourier transform infrared (FTIR) spectroscopy. In *Elsevier eBooks* (pp. 3–29). Elsevier. https://doi.org/10.1016/b978-0-444-63776-5.00001-2

Mohammed, N. K., Samir, Z. T., Jassim, M. A., & Saeed, S. K. (2021). Effect of different extraction methods on physicochemical properties, antioxidant activity, of virgin coconut oil. *Materials Today: Proceedings*, *42*, 2000–2005. https://doi.org/10.1016/j.matpr.2020.12.248

Moraes, C., L.V. Anjos, J., Maruno, M., Alonso, A., & Rocha-Filho, P. (2018). Development of lamellar gel phase emulsion containing baru oil (Dipteryx alata Vog.) as a prospective delivery system for cutaneous application. *Asian Journal of Pharmaceutical Sciences*, *13*(2), 183–190. https://doi.org/10.1016/j.ajps.2017.09.003

Mozaffarian, D., Benjamin, E. J., Go, A. S., Arnett, D. K., Blaha, M. J., Cushman, M., Das, S. R., De Ferranti, S., Després, J., Fullerton, H. J., Howard, V. J., Huffman, M. D., Isasi, C. R., Jiménez, M. C., Judd, S. E., Kissela, B. M., Lichtman, J. H., Lisabeth, L. D., Liu, S., . . . Turner, M. B. (2015). Heart Disease and Stroke Statistics—2016 update. *Circulation*, *133*(4), e38-360. https://doi.org/10.1161/cir.0000000000000350

Shariful, I. M., Katsuno, N., & Nishizu, T. (2018). Kinetic Analysis of Freeze-Thaw stability of mayonnaise. *Foods*, *7*(5), 75. https://doi.org/10.3390/foods7050075

Nandiyanto, A. B. D., Oktiani, R., & Ragadhita, R. (2019). How to read and interpret ftir spectroscope of organic material. *Indonesian Journal of Science and Technology*, *4*(1), 97–118. https://doi.org/10.17509/ijost.v4i1.15806

Nebogina, N. A., Prozorova, I. V., & Yudina, N. V. (2020). The influence of the temperature of formation of water-oil emulsions on their dispersion. *AIP Conference Proceedings*, *2310*, 020221. https://doi.org/10.1063/5.0035207

Ng, S. P., Lai, O. M., Abas, F., Lim, H. K., & Tan, C. P. (2014). Stability of a concentrated oil-in-water emulsion model prepared using palm olein-based diacylglycerol/virgin coconut oil blends: Effects of the rheological properties, droplet size distribution and microstructure. *Food Research International*, *64*, 919–930. https://doi.org/10.1016/j.foodres.2014.08.045

Niu, H., Wang, W., Dou, Z., Chen, X., Chen, X., Chen, H., & Fu, X. (2022). Multiscale combined techniques for evaluating emulsion stability: A critical review. *Advances in Colloid and Interface Science*, *311*, 102813. https://doi.org/10.1016/j.cis.2022.102813

Nurhadi, B., Selly, S., Nurhasanah, S., Saputra, R. A., & Arifin, H. R. (2022). The virgin coconut oil (VCO) emulsion powder characteristics: Effect of pickering emulsion with microcrystalline cellulose (MCC) and different drying techniques. *Italian Journal of Food Science*, *34*(1), 67–85. https://doi.org/10.15586/ijfs.v34i1.2111

Nurul-Iman, B. S., Kamisah, Y., Jaarin, K., & Qodriyah, H. M. S. (2013). Virgin Coconut Oil Prevents Blood Pressure Elevation and Improves Endothelial Functions in Rats Fed with Repeatedly Heated Palm Oil. *Evidence-based Complementary and Alternative Medicine*, *2013*, 1–7. https://doi.org/10.1155/2013/629329

Kannaian, U. P. N., Edwin, J. B., Rajagopal, V., Shankar, S. N., & Srinivasan, B. (2020). Phytochemical composition and antioxidant activity of coconut cotyledon. *Heliyon*, *6*(2), e03411. https://doi.org/10.1016/j.heliyon.2020.e03411

Obidoa, O., Onyechi, T. O., Joshua, P. E., & Eze, N. J. (2009). *Phytochemical analysis of Cocos nucifera L. Journal of Pharmacy Research, 1*(1), 87–96.

Okuro, P. K., Viau, M., Kermarrec, A., Cunha, R. L., Meynier, A., & Berton-Carabin, C. C. (2022). *Lipid recovery from concentrated emulsions by freezing–thawing as an alternative to solvent-based extraction: A case study on mayonnaise*. *European Journal of Lipid Science and Technology, 124*(11), 1-10. https://doi.org/10.1002/ejlt.202200101

Onaizi, S. A. (2021). Effect of oil/water ratio on rheological behavior, droplet size, zeta

potential, long-term stability, and acid-induced demulsification of crude oil/water nanoemulsions. *Journal of Petroleum Science and Engineering*, *209*, 109857. https://doi.org/10.1016/j.petrol.2021.109857

Palazolo, G. G., Sobral, P. A., & Wagner, J. R. (2011). Freeze-thaw stability of oil-in-water emulsions prepared with native and thermally-denatured soybean isolates. *Food Hydrocolloids*, *25*(3), 398–409. https://doi.org/10.1016/j.foodhyd.2010.07.008

Park, J. E., Hickey, D. R., Jun, S., Kang, S., Hu, X., Chen, X. J., & Park, S. J. (2016). Surfactant-Assisted Emulsion Self-Assembly of Nanoparticles into Hollow Vesicle-Like Structures and 2D Plates. *Advanced Functional Materials*, *26*(43), 7791–7798. https://doi.org/10.1002/adfm.201603971

Parreidt, T. S., Schott, M., Schmid, M., & Müller, K. (2018). Effect of presence and concentration of plasticizers, vegetable oils, and surfactants on the properties of Sodium-Alginate-Based edible coatings. *International Journal of Molecular Sciences*, *19*(3), 742. https://doi.org/10.3390/ijms19030742

Pencer, J., Torres, E., Alexander, J., & Radford, D. D. (2016). Applicability of 2NN-MEAM potentials in the prediction of temperature and oxygen-dependent elastic properties of titanium. *Computational Materials Science*, *125*, 110–116. https://doi.org/10.1016/j.commatsci.2016.08.007

Peng, B. Z., Chen, G. J., Sun, C. Y., Liu, B., Zhang, Y. Q., & Zhang, Q. (2011). Dynamic interfacial tension between water and n -octane plus sorbitan monolaurate at (274.2 to 293.2) K. *Journal of Chemical and Engineering Data*, *56*(4), 1617–1621. https://doi.org/10.1021/je101094u

Ponphaiboon, J., Limmatvapirat, S., & Limmatvapirat, C. (2024). Development and Evaluation of a Stable Oil-in-Water Emulsion with High Ostrich Oil Concentration for Skincare Applications. *Molecules*, *29*(5), 982. https://doi.org/10.3390/molecules29050982

Posocco, P., Perazzo, A., Preziosi, V., Laurini, E., Pricl, S., & Guido, S. (2016). Interfacial tension of oil/water emulsions with mixed non-ionic surfactants: Comparison between experiments and molecular simulations. *RSC Advances*, *6*(6), 4723–4729. https://doi.org/10.1039/c5ra24262b

Prasanna, N. S., Selvakumar, M., Choudhary, N., & Raghavarao, K. S. M. S. (2024). Virgin coconut oil: wet production methods and food applications - a review. *Sustainable Food Technology* 2(5), 1391–1408.

https://doi.org/10.1039/d4fb00093e

Raghavendra, S. N., & Raghavarao, K. S. M. S. (2010). Effect of different treatments for the destabilization of coconut milk emulsion. *Journal of Food Engineering*, *97*(3), 341–347. https://doi.org/10.1016/j.jfoodeng.2009.10.027

Ragusa, E., Lynch, E., Laibe, G., Longarini, C., & Ceppi, S. (2024). Probing the eccentricity in protostellar discs: Modelling kinematics and morphologies. *Astronomy and Astrophysics*, *686*, 264. https://doi.org/10.1051/0004-6361/202449583

Ramli, S., Chyi, K. T., Zainuddin, N., Mokhtar, W. N. A. W., & Abdul Rahman, I. (2019). The influence of surfactant/co-surfactant hydrophilic-lipophilic balance on the formation of limonene-based microemulsion as Vitamin C carrier. *Sains Malaysiana*, *48*(5), 1035–1042. https://doi.org/10.17576/jsm-2019-4805-12

Ravera, F., Dziza, K., Santini, E., Cristofolini, L., & Liggieri, L. (2020). Emulsification and emulsion stability: The role of the interfacial properties. *Advances in Colloid and Interface Science*, 288, 102344. https://doi.org/10.1016/j.cis.2020.102344

Raya, S. A., Saaid, I. M., Mohd Aji, A. Q., & A Razak, A. A. (2022). Investigation of the synergistic effect of nonionic surfactants on emulsion resolution using response surface methodology. *RSC Advances*, *12*(48), 30952–30961. https://doi.org/10.1039/d2ra04816g

Rohman, A., Irnawati, Erwanto, Y., Lukitaningsih, E., Rafi, M., Fadzilah, N. A., Windarsih, A., Sulaiman, A., & Zakaria, Z. (2021). Virgin Coconut Oil: Extraction, Physicochemical Properties, Biological Activities and Its Authentication Analysis. *Food Reviews International* 37(1), 46–66. https://doi.org/10.1080/87559129.2019.1687515

Roopashree, P., Shetty, S. S., & Kumari, N. S. (2021). Effect of medium chain fatty acid in human health and disease. *Journal of Functional Foods*, *87*, 104724. https://doi.org/10.1016/j.jff.2021.104724

Rosdi, N. A., Sha'ary, A. R., Nor, Y. A., Jimat, N. D. N., & Tshai, N. K. Y. (2024). Stability analysis of immobilized ozonated vegetable oil on silica nanoparticles. *Chemical and Natural Resources Engineering Journal (Formally Known as Biological and Natural Resources Engineering Journal)*, *8*(2), 78–91. https://doi.org/10.31436/cnrej.v8i2.108

Rukmini, A., Raharjo, S., Hastuti, P., & Supriyadi, S. (2012). Formulation and stability of water-in-virgin coconut oil microemulsion using ternary food grade nonionic

surfactants. *International Food Research Journal*, *19*(1), 259–264.

Sanjeewani, N. A., & Sakeena, M. H. F. (2013). Formulation and characterization of virgin coconut oil (VCO) based emulsion. *International Journal of Scientific and Research Publications, 3*(12), 1–6.

Schopfer, F. J., Teng, L., Sekandari, A., Ekhator, E. S., Kohan, A. B., Freeman, B. A., & Fazzari, M. (2025). Fatty acid nitroalkenes regulate intestinal lipid absorption. *Journal of Lipid Research*, *66*(8), 100855. https://doi.org/10.1016/j.jlr.2025.100855

Seneviratne, K. N., HapuarachchI, C. D., & Ekanayake, S. (2009). Comparison of the phenolic-dependent antioxidant properties of coconut oil extracted under cold and hot conditions. *Food Chemistry*, *114*(4), 1444–1449. https://doi.org/10.1016/j.foodchem.2008.11.038

Seneviratne, K. N., & Sudarshana Dissanayake, D. M. (2008). Variation of phenolic content in coconut oil extracted by two conventional methods. *International Journal of Food Science and Technology*, *43*(4), 597–602. https://doi.org/10.1111/j.1365-2621.2006.01493.x

Shah, N. D., & Limketkai, B. N. (2017). *The use of medium-chain triglycerides in gastrointestinal disorders*. *Practical Gastroenterology, 41*(2), 20–28.

Shah, S. K., Chakraborty, G., Bhattarai, A., & De, R. (2022). Synergistic and antagonistic effects in micellization of mixed surfactants. *Journal of Molecular Liquids*, *368*, 120678. https://doi.org/10.1016/j.molliq.2022.120678

Shahidi, F., & Zhong, Y. (2015). Measurement of antioxidant activity. *Journal of Functional Foods* 18, 757–781. https://doi.org/10.1016/j.jff.2015.01.047

Shalu, S., Dasgupta, K., Roy, S., Kar, P., Bal, T., & Dasgupta Ghosh, B. (2021). Thermal, mechanical, and dielectric properties of low loss PbZr0.3Ti0.7O3/polystyrene composites prepared by hot-press method. *Polymer Composites*, *42*(3), 1420–1428. https://doi.org/10.1002/pc.25912

Shilling, M., Matt, L., Rubin, E., Visitacion, M. P., Haller, N. A., Grey, S. F., & Woolverton, C. J. (2013). Antimicrobial effects of virgin coconut oil and its medium-chain fatty acids on clostridium difficile. *Journal of Medicinal Food*, *16*(12), 1079–1085. https://doi.org/10.1089/jmf.2012.0303

Sihombing, N. T. M., Silalahi, J., & Suryanto, D. (2014). *Antibacterial activity of aqueous garlic (Allium sativum) extracts and virgin coconut oil and their combination against Bacillus cereus ATCC 14579 and Escherichia coli ATCC*

8939. International Journal of ChemTech Research, 6(5), 2774–2782.

Skřivanová, E., Marounek, M., Dlouhá, G., & Kaňka, J. (2005). Susceptibility of Clostridium perfringens to C2-C18 fatty acids. *Letters in Applied Microbiology, 41*(1), 77–81. https://doi.org/10.1111/j.1472-765X.2005.01709.x

Solans, C., Morales, D., & Homs, M. (2016). Spontaneous emulsification. *Current Opinion in Colloid and Interface Science* 22, 88–93. https://doi.org/10.1016/j.cocis.2016.03.002

Som, A. M., Ahmat, N., Abdul Hamid, H. A., & Azizuddin, N. (2019). A comparative study on foliage and peels of Hylocereus undatus (white dragon fruit) regarding their antioxidant activity and phenolic content. *Heliyon, 5*(2), e01244. https://doi.org/10.1016/j.heliyon.2019.e01244

Som, A. M., Balang, E. M., & Hamid, H. A. A. (2023). Comparative Study and Performance Evaluation of Chemical and Biosurfactants in Water-In-Oil Emulsification Process. In *Key Engineering Materials* 939, 93–102. https://doi.org/10.4028/p-y8fry2

Souza, W. J., Santos, K. M. C., Cruz, A. A., Franceschi, E., Dariva, C., Santos, A. F., & Santana, C. C. (2015). Effect of water content, temperature and average droplet size on the settling velocity of water-in-oil emulsions. *Brazilian Journal of Chemical Engineering, 32*(2), 455–464. https://doi.org/10.1590/0104-6632.20150322s00003323

Srivastava, Y., Semwal, A. D., & Sharma, G. K. (2018). Virgin coconut oil as functional oil. *Elsevier eBooks*, (pp. 291–301). https://doi.org/10.1016/b978-0-12-814625-5.00015-7

Stubbs, S., Yousaf, S., & Khan, I. (2022). A review on the synthesis of bio-based surfactants using green chemistry principles. *Journal of Pharmaceutical Sciences* 30(2), 407–426. https://doi.org/10.1007/s40199-022-00450-y

Stubenrauch, C., Hamann, M., Preisig, N., Chauhan, V., & Bordes, R. (2017). On how hydrogen bonds affect foam stability. *Advances in Colloid and Interface Science* 247, 435–443. https://doi.org/10.1016/j.cis.2017.02.002

Subroto, E., & Indiarto, R. (2020). Bioactive monolaurin as an antimicrobial and its potential to improve the immune system and against covid-19: A review. In *Food Research* 4(6), 2355–2365. https://doi.org/10.26656/fr.2017.4(6).324

Sundrasegaran, S., & Mah, S. H. (2020). Extraction Methods of Virgin Coconut Oil and Palm-pressed Mesocarp Oil and their Phytonutrients. *EFood, 1*(6), 381–391.

https://doi.org/10.2991/efood.k.201106.001

Suneetha, R. B. (2018). Spectral, Thermal and Morphological Characterization of Biodegradable Graphene Oxide-Chitosan Nanocomposites. *Journal of Nanoscience and Technology*, *04*(02), 342–344. https://doi.org/10.30799/jnst.sp208.18040201

Suryani, S., Sariani, S., Earnestly, F., Marganof, M., Rahmawati, R., Sevindrajuta, S., Mahlia, T. M. I., & Fudholi, A. (2020). A comparative study of virgin coconut oil, coconut oil and palm oil in terms of their active ingredients. *Processes*, *8*(4), 402. https://doi.org/10.3390/pr8040402

Tamura, Y., Miyakoshi, M., & Yamamoto, M. (2012). *Application of saponin-containing plants in foods and cosmetics*. In H. Sakagami (Ed.), *Alternative Medicine* (pp. 85–101). InTech. https://doi.org/10.5772/53333

Tangwatcharin, P., & Khopaibool, P. (2012). *Activity of virgin coconut oil, lauric acid or monolaurin in combination with lactic acid against Staphylococcus aureus. Southeast Asian Journal of Tropical Medicine and Public Health, 43*(4), 969–985. Thanasukarn, P., Pongsawatmanit, R., & McClements, D. J. (2004). Influence of emulsifier type on freeze-thaw stability of hydrogenated palm oil-in-water emulsions. *Food Hydrocolloids*, *18*(6), 1033–1043. https://doi.org/10.1016/j.foodhyd.2004.04.010

Tian, Y., Zhou, J., He, C., He, L., Li, X., & Sui, H. (2022). The Formation, Stabilization and Separation of Oil–Water Emulsions: A review. *Processes*, *10*(4), 738. https://doi.org/10.3390/pr10040738

Toonen, S., Hamers, A., & Portegies Zwart, S. (2016). *The evolution of hierarchical triple star-systems. Computational Astrophysics and Cosmology, 3*(1), 6. https://doi.org/10.1186/s40668-016-0019-0

Touaitia, R., Ibrahim, N. A., Almuqri, E. A., Basher, N. S., Idres, T., & Touati, A. (2025). Toxic Shock Syndrome Toxin-1 (TSST-1) in Staphylococcus aureus: Prevalence, Molecular Mechanisms, and Public Health Implications. *Toxins*, *17*(7), 323. https://doi.org/10.3390/toxins17070323

Vogel, C. É., Crovesy, L., Rosado, E. L., & Soares-Mota, M. (2020). Effect of coconut oil on weight loss and metabolic parameters in men with obesity: A randomized controlled clinical trial. *Food and Function*, *11*(7), 6588–6594. https://doi.org/10.1039/d0fo00872a

Wang, Q., Zhang, H., Han, Y., Cui, Y., & Han, X. (2023). Study on the relationships

between the oil HLB value and emulsion stabilization. *RSC Advances*, *13*(35), 24692–24698. https://doi.org/10.1039/d3ra04592g

Wiyani, L., Aladin, A., Mustafiah, A., Abriana, A., & Rahmawati. (2020). *Characteristics of virgin coconut oil emulsion with honey and citric acid. Proceedings of the 5th International Conference on Food, Agriculture and Natural Resources (FANRes 2019)*, 194, 246–250. https://doi.org/10.2991/aer.k.200325.048

Wu, C., Fan, Q., & Yin, Y. (2022). Emulsion-confined self-assembly of colloidal nanoparticles into 3D superstructures. *Cell Reports Physical Science*, *3*(12), 101162. https://doi.org/10.1016/j.xcrp.2022.101162

Xian, H. W., Saidur, R., Sidik, N. A. C., & Asako, Y. (2022). Viscosity Of CuO Nanofluid Due to Nanoparticles Size and Concentration. *Journal of Advanced Research in Applied Sciences and Engineering Technology*, *28*(1), 161–167. https://doi.org/10.37934/araset.28.1.161167

Xu, X., Bo, G., He, X., Tian, X., & Yan, Y. (2020). Structural effects of dimensional nano-fillers on the properties of Sapium sebiferum oil-based polyurethane matrix: Experiments and molecular dynamics simulation. *Polymer*, *202*, 122709. https://doi.org/10.1016/j.polymer.2020.122709

Yang, J., & Pal, R. (2020). Investigation of surfactant-polymer interactions using rheology and surface tension measurements. *Polymers*, *12*(10), 1–20. https://doi.org/10.3390/polym12102302

Yang, X., Wang, J., Song, H., & Zou, W. (2016). Thermal properties and solubility of methyl α-d-glucopyranoside in methanol at different temperatures. *Fluid Phase Equilibria*, *409*, 417–424. https://doi.org/10.1016/j.fluid.2015.10.047

Yonguep, E., Kapiamba, K. F., Kabamba, K. J., & Chowdhury, M. (2022). Formation, stabilization and chemical demulsification of crude oil-in-water emulsions: A review. In *Petroleum Research* 7(4), 459–472). https://doi.org/10.1016/j.ptlrs.2022.01.007

Zdrali, E., Etienne, G., Smolentsev, N., Amstad, E., & Roke, S. (2019). The interfacial structure of nano- and micron-sized oil and water droplets stabilized with SDS and Span80. *The Journal of Chemical Physics*, *150*(20), 204704. https://doi.org/10.1063/1.5083844

Zhao, H., Kang, W., Yang, H., Huang, Z., Zhou, B., & Sarsenbekuly, B. (2020). Emulsification and stabilization mechanism of crude oil emulsion by surfactant

synergistic amphiphilic polymer system. *Colloids and Surfaces a Physicochemical and Engineering Aspects*, *609*, 125726. https://doi.org/10.1016/j.colsurfa.2020.125726

Zheng, L., Cao, C., Chen, Z., Cao, L., Huang, Q., & Song, B. (2020). Evaluation of emulsion stability by monitoring the interaction between droplets. *LWT*, *132*, 109804. https://doi.org/10.1016/j.lwt.2020.109804

Zheng, Y., Zi, Y., Tao, L., Xu, J., Chen, J., Yang, M., Wang, X., & Zhong, J. (2022). Effects of Span surfactants on the preparation and properties of fish oil-loaded sodium alginate-stabilized emulsions and calcium alginate-stabilized capsules. *International Journal of Biological Macromolecules*, *221*, 831–841. https://doi.org/10.1016/j.ijbiomac.2022.08.187

APPENDICES

APPENDIX A

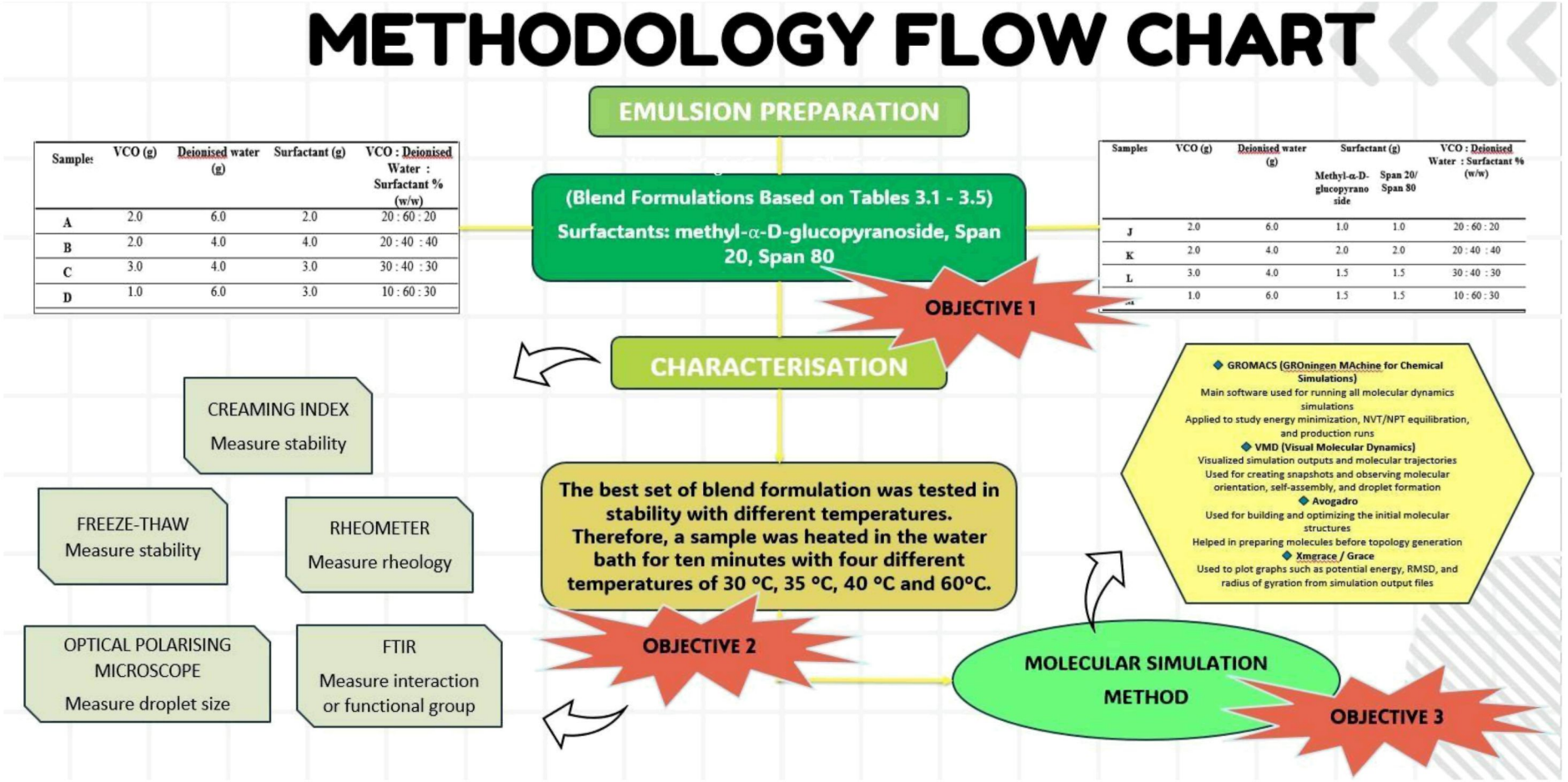

Sample	VCO (g)	Deionised water (g)	Surfactant (g)	VCO : Deionised Water : Surfactant % (w/w)
A	2.0	6.0	2.0	20 : 60 : 20
B	2.0	4.0	4.0	20 : 40 : 40
C	3.0	4.0	3.0	30 : 40 : 30
D	1.0	6.0	3.0	10 : 60 : 30

Samples	VCO (g)	Deionised water (g)	Surfactant (g)		VCO : Deionised Water : Surfactant % (w/w)
			Methyl-α-D-glucopyranoside	Span 20/ Span 80	
J	2.0	6.0	1.0	1.0	20 : 60 : 20
K	2.0	4.0	2.0	2.0	20 : 40 : 40
L	3.0	4.0	1.5	1.5	30 : 40 : 30
	1.0	6.0	1.5	1.5	10 : 60 : 30

APPENDIX B

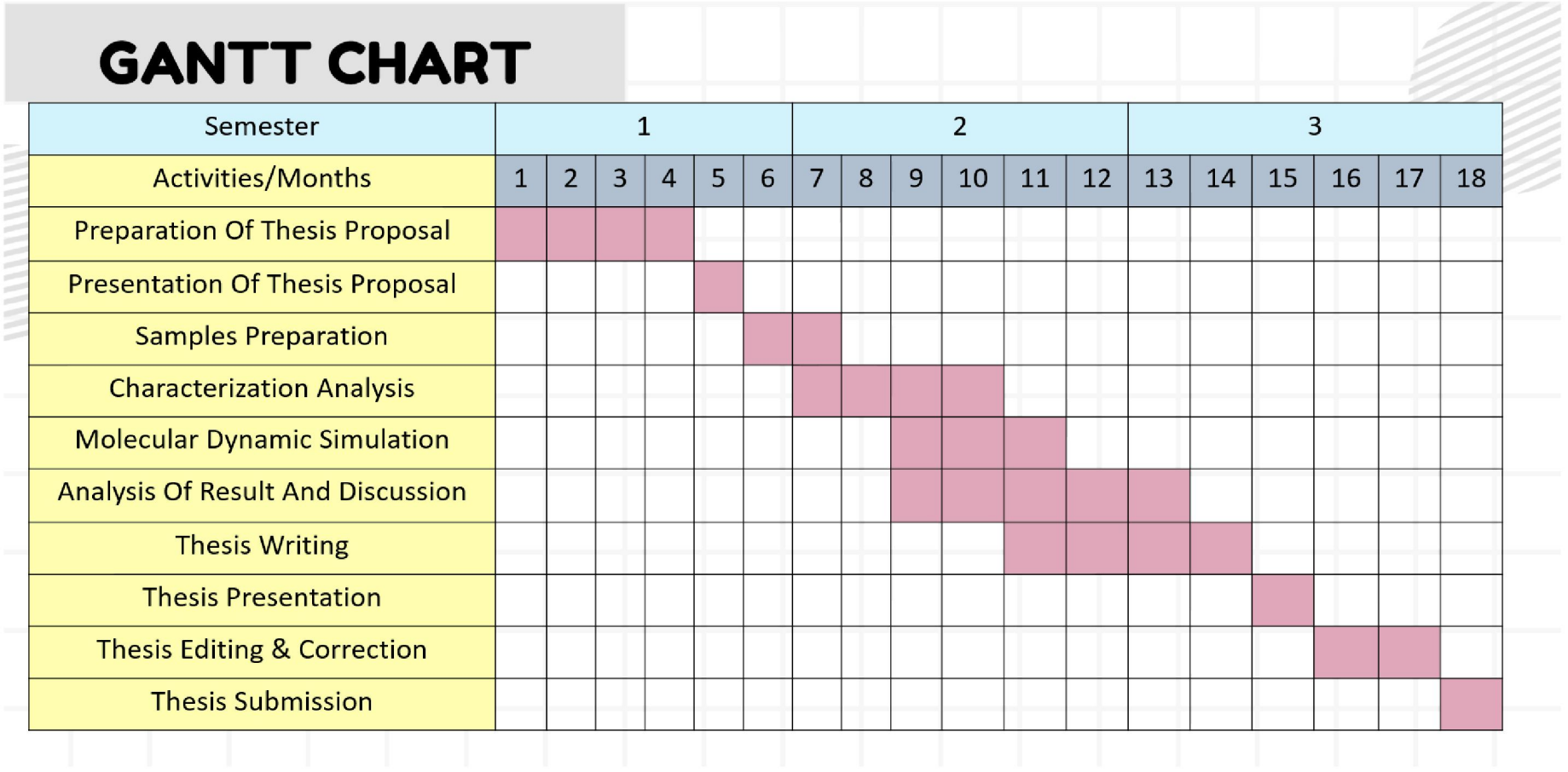
GANTT CHART
Semester
1
2
3
Activities/Months
1 2 3 4 5 6 7 8 9 10 11 12 13 14 15 16 17 18
Preparation Of Thesis Proposal
Presentation Of Thesis Proposal
Samples Preparation
Characterization Analysis
Molecular Dynamic Simulation
Analysis Of Result And Discussion
Thesis Writing
Thesis Presentation
Thesis Editing & Correction
Thesis Submission

APPENDIX C

Set 1 (Methyl-α-*D*-glucopyranoside)						
Day	1	6	12	18	24	30
SAMPLE A1			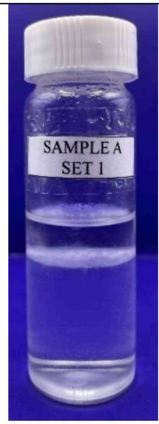			

SAMPLE B1		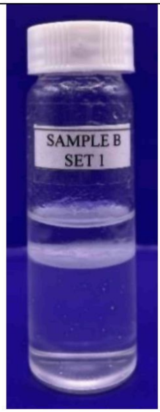				
SAMPLE C1						

SAMPLE D1	 SAMPLE D SET 1	 SAMPLE D SET 1	 SAMPLE D SET 1	 SAMPLE D SET 1	 SAMPLE D SET 1	 SAMPLE D SET 1

Set 1 (Span 20)						
Day	1	6	12	18	24	30
SAMPLE A2						
SAMPLE B2						

SAMPLE C2						
SAMPLE D2						

Set 1 (Span 80)						
Day	1	6	12	18	24	30
SAMPLE A3						
SAMPLE B3						

SAMPLE C3	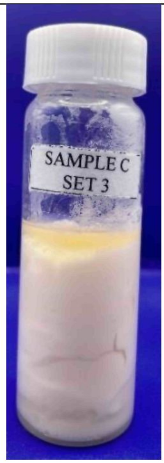					
SAMPLE D3		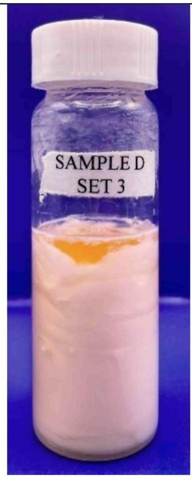				

Set 1 (Methyl-α-*D*-glucopyranoside + Span 20)						
Day	1	6	12	18	24	30
SAMPLE J1						
SAMPLE K1						

SAMPLE L1						
SAMPLE M1						

Set 2 (Methyl-α-*D*-glucopyranoside + Span 80)						
Day	1	6	12	18	24	30
SAMPLE J2						
SAMPLE K2						

SAMPLE L2						
SAMPLE M2		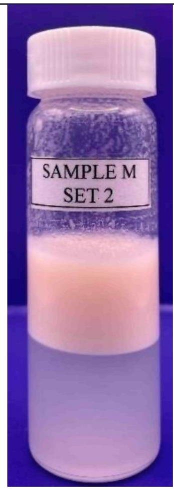				

APPENDIX D

Set 1 (Methyl-α-*D*-glucopyranoside)							
SAMPLE A1		SAMPLE B1		SAMPLE C1		SAMPLE D1	
Before	After	Before	After	Before	After	Before	After
							

Set 2 (Span 20)							
SAMPLE A2		SAMPLE B2		SAMPLE C2		SAMPLE D2	
Before	After	Before	After	Before	After	Before	After
							

Set 3 (Span 80)							
SAMPLE A3		SAMPLE B3		SAMPLE C3		SAMPLE D3	
Before	After	Before	After	Before	After	Before	After
							

Set 1 (Methyl-α-*D*-glucopyranoside + Span 20)							
SAMPLE J1		SAMPLE K1		SAMPLE L1		SAMPLE M1	
Before	After	Before	After	Before	After	Before	After
							

Set 2 (Methyl-α-*D*-glucopyranoside + Span 80)							
SAMPLE J2		SAMPLE K2		SAMPLE L2		SAMPLE M2	
Before	After	Before	After	Before	After	Before	After
							

APPENDIX E

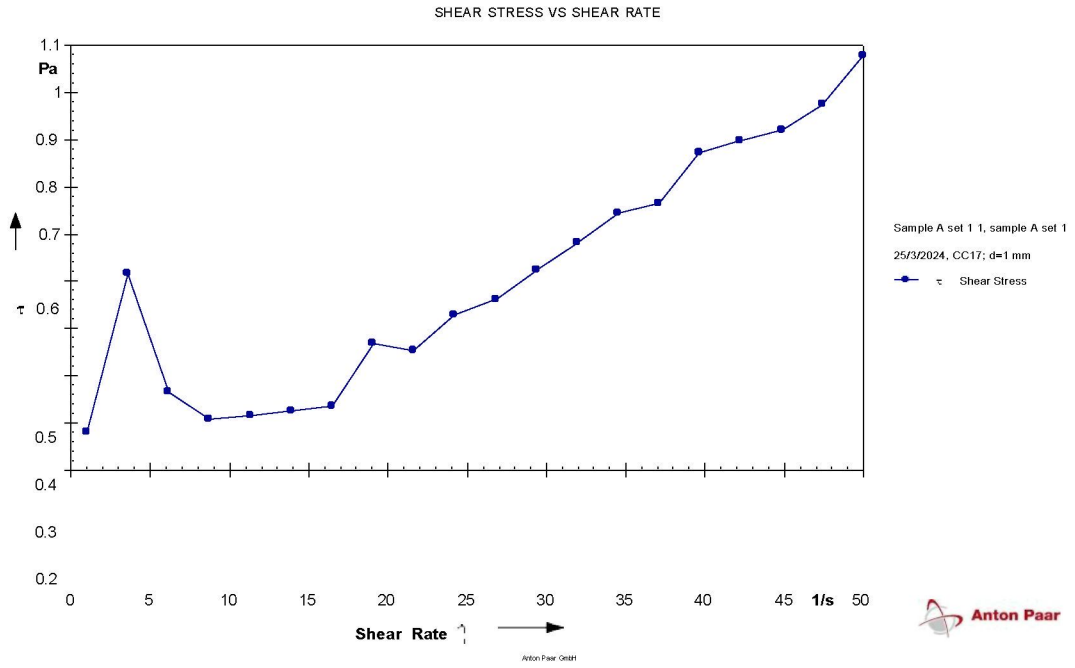

Sample A1

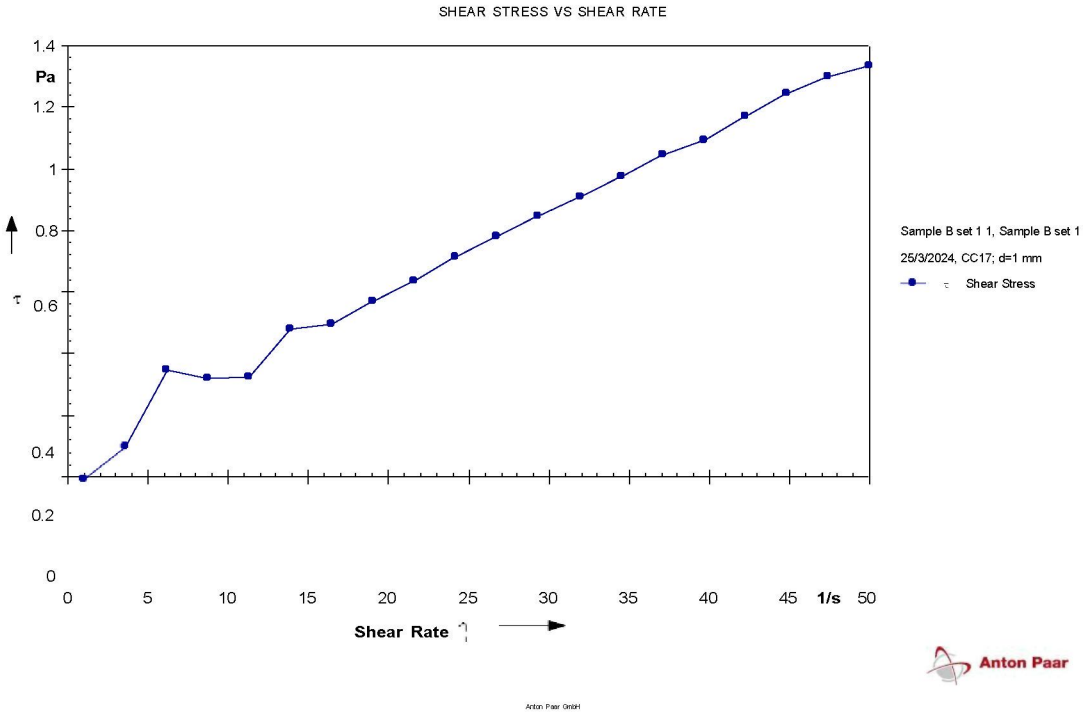

Sample B1

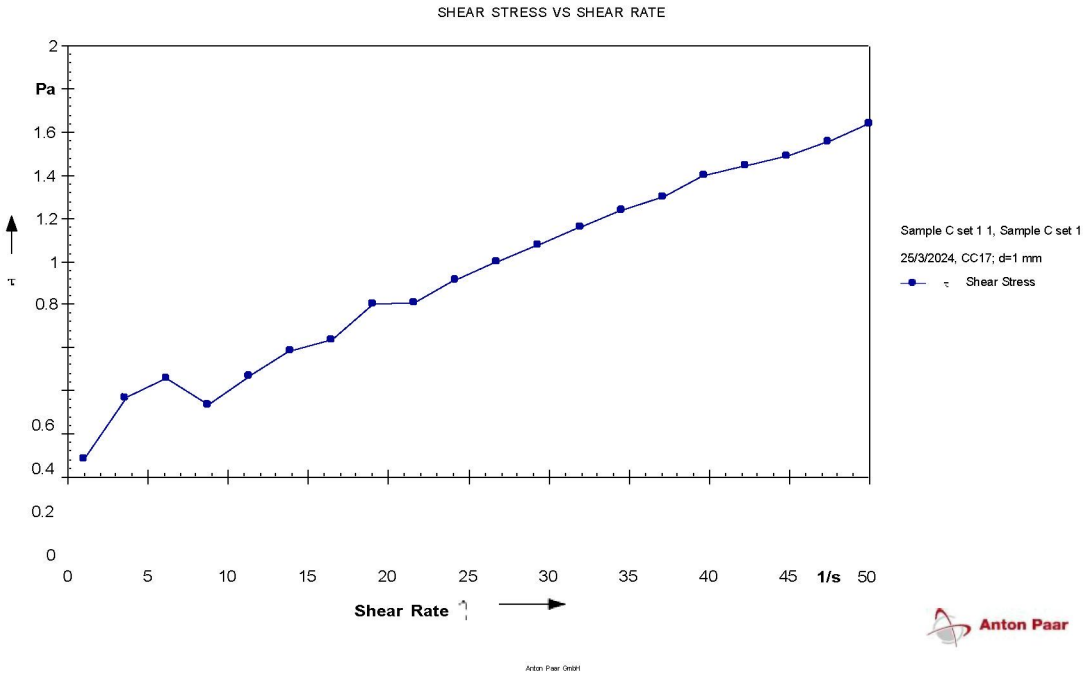

Sample C1

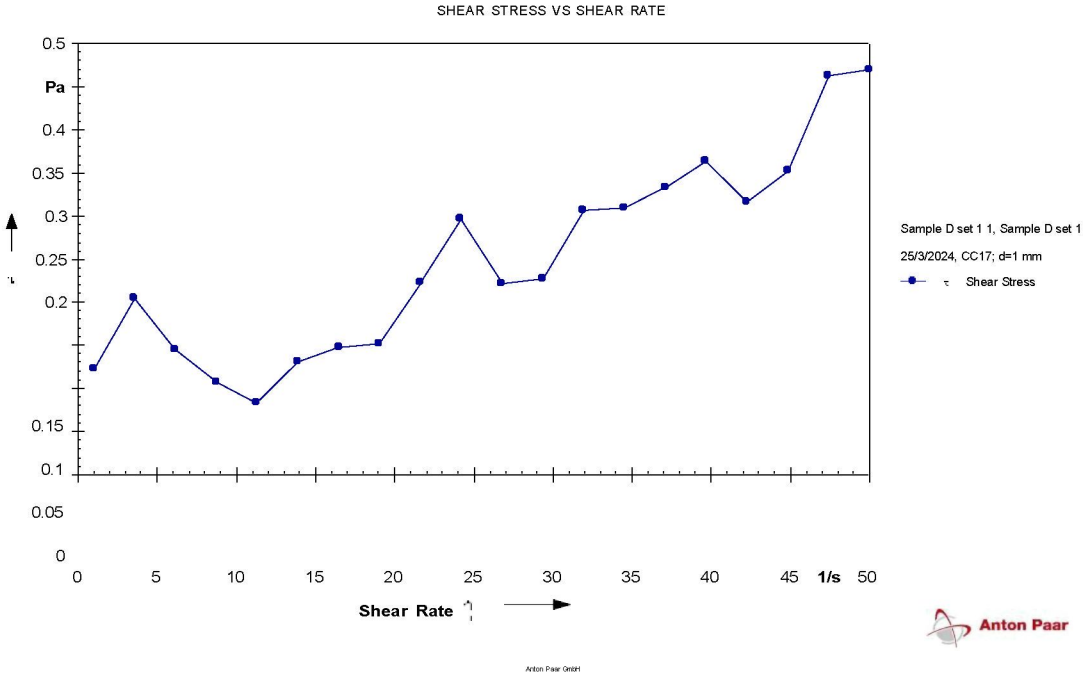

Sample D1

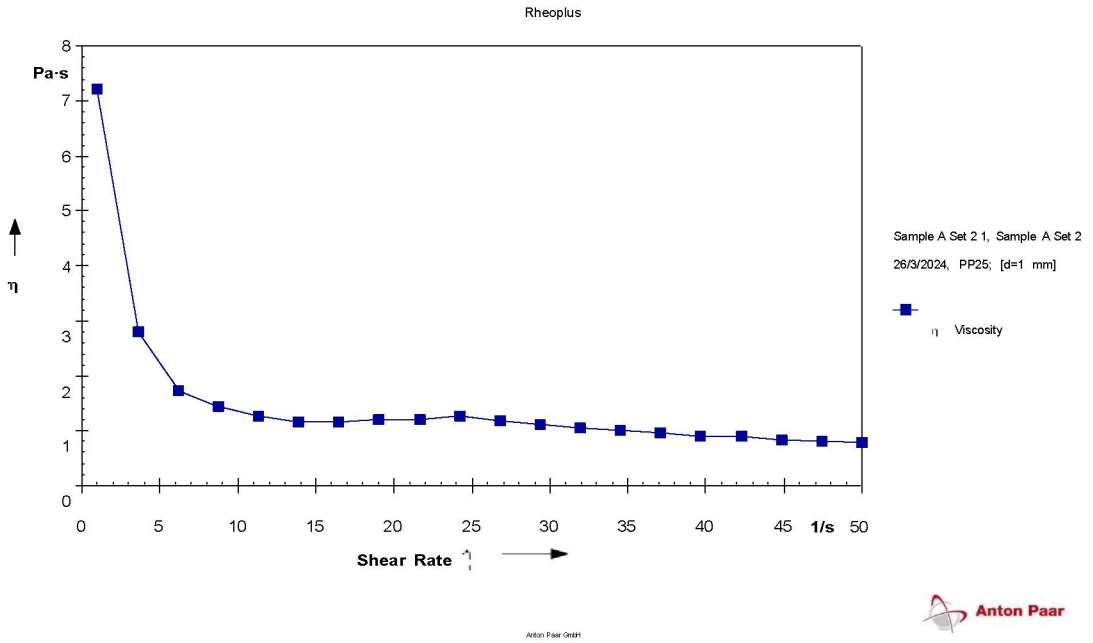

Sample A2

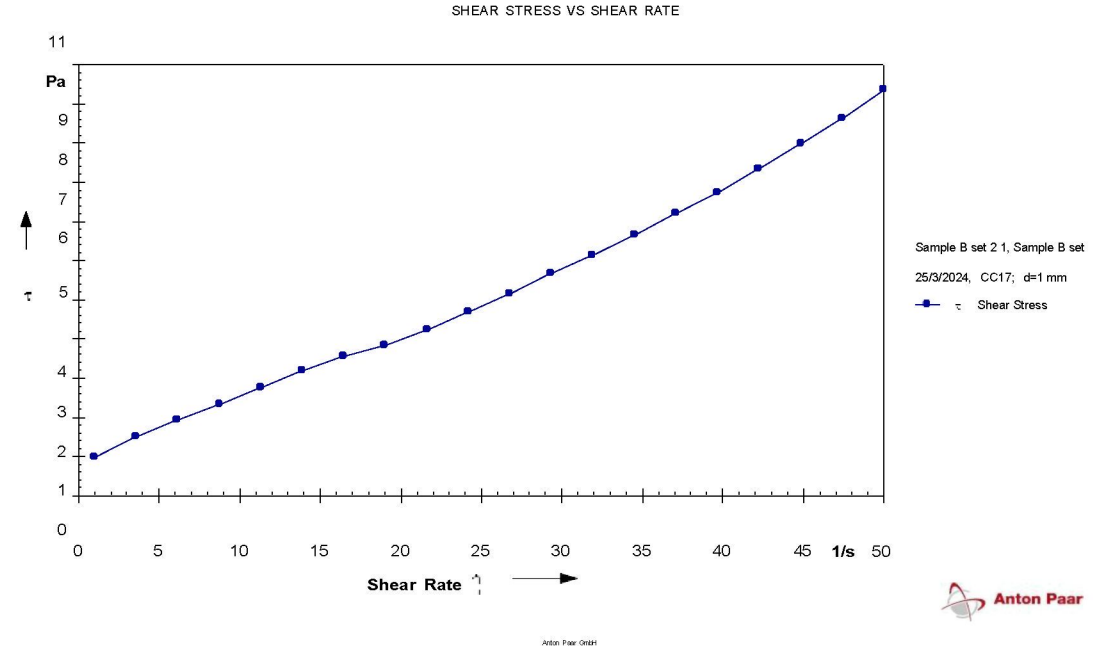

Sample B2

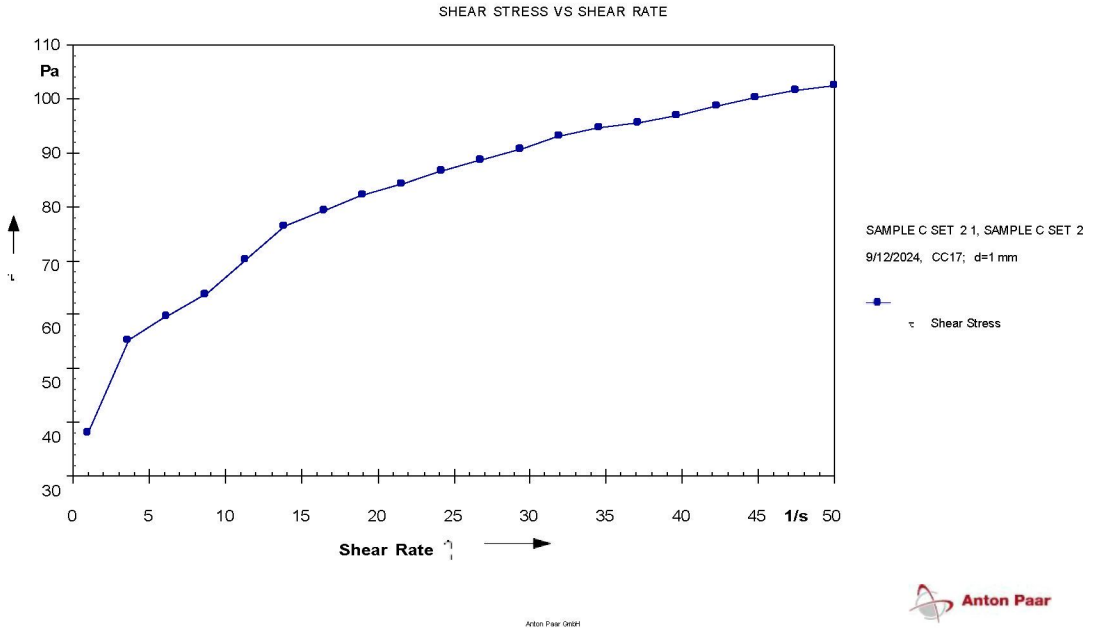

Sample C2

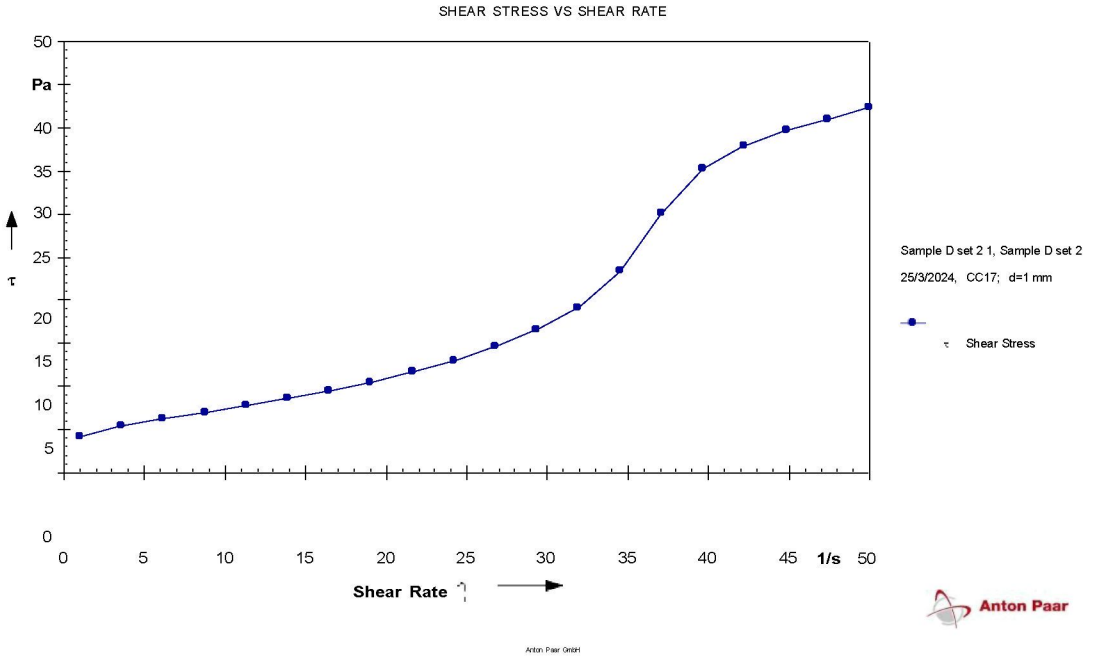

Sample D2

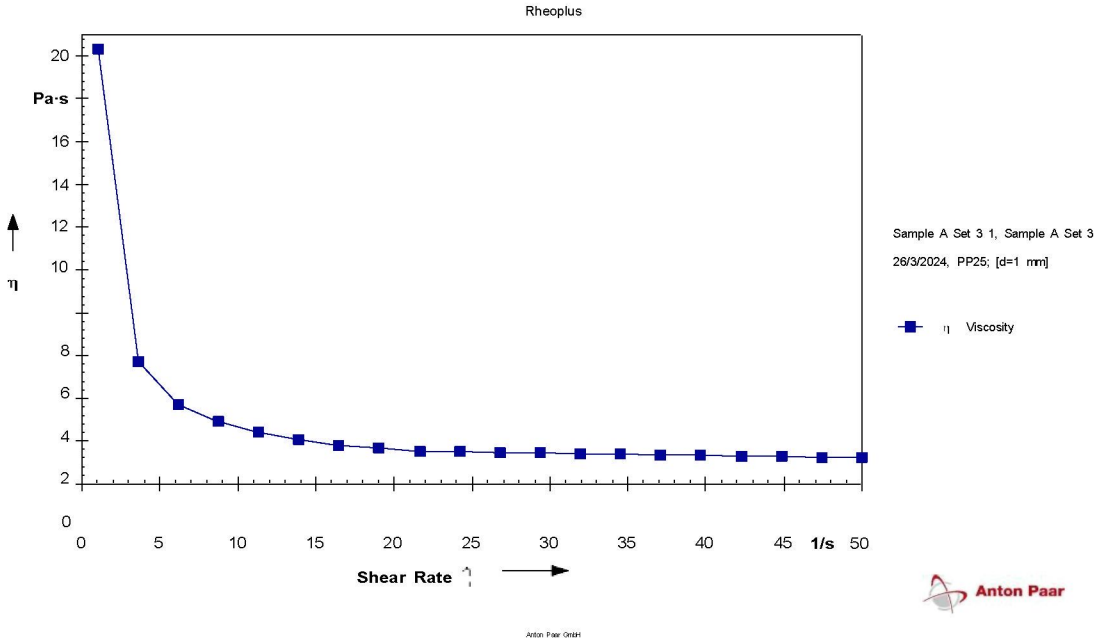

Sample A3

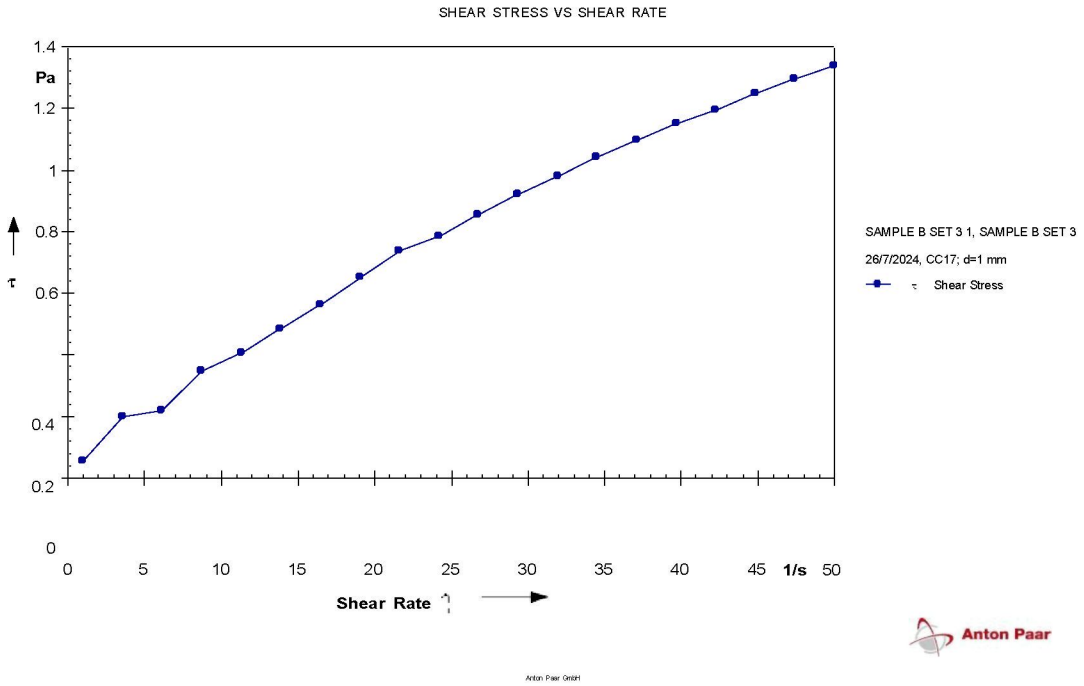

Sample B3

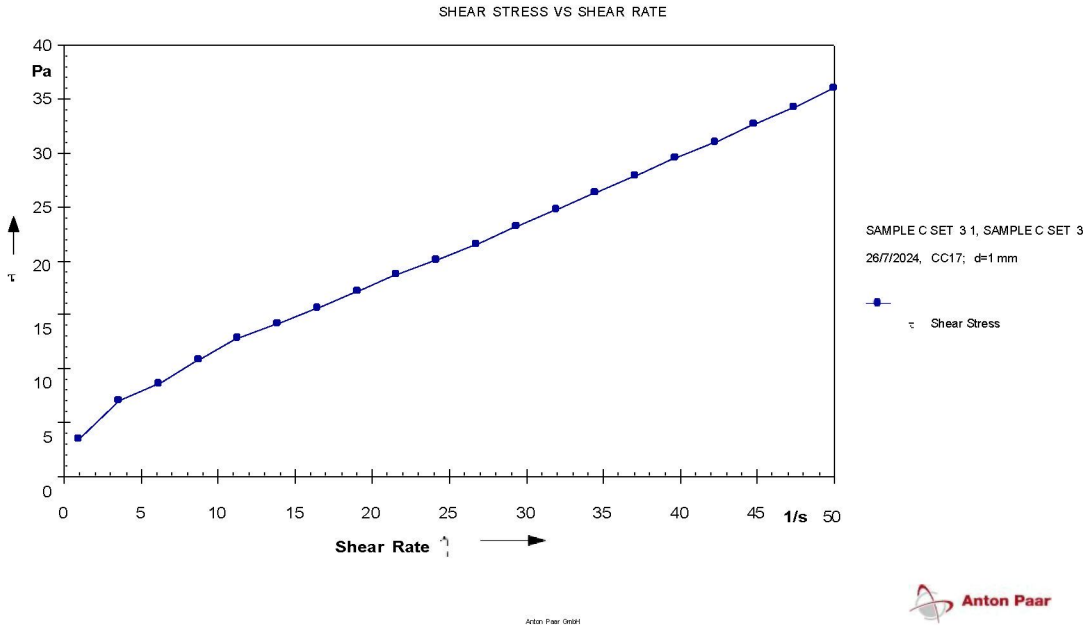

Sample C3

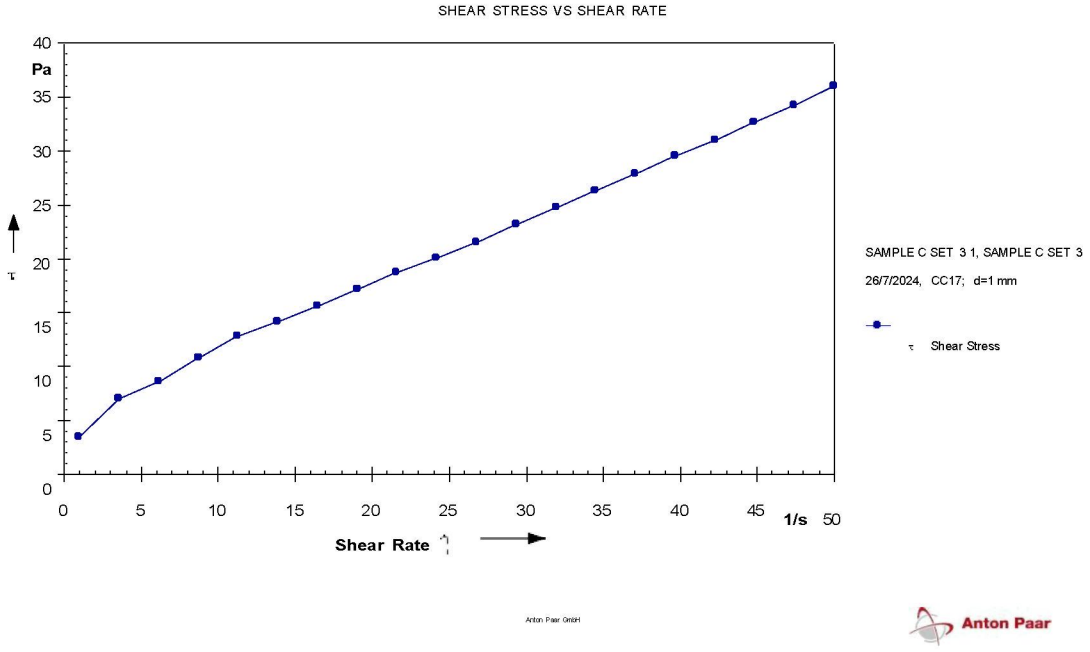

Sample D3

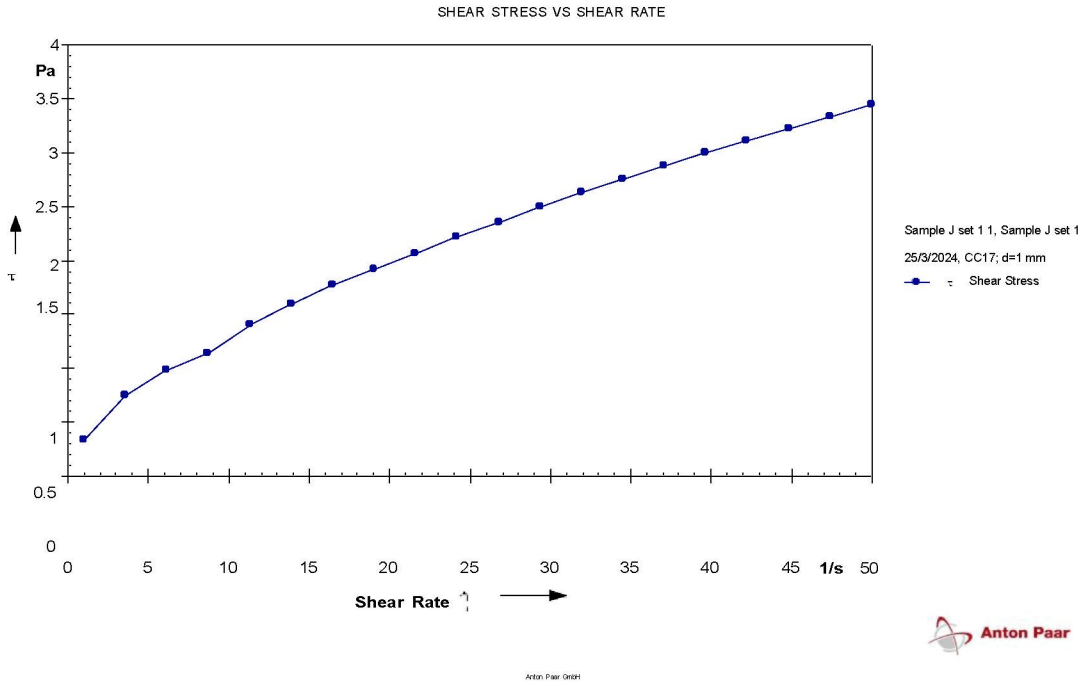

Sample J1

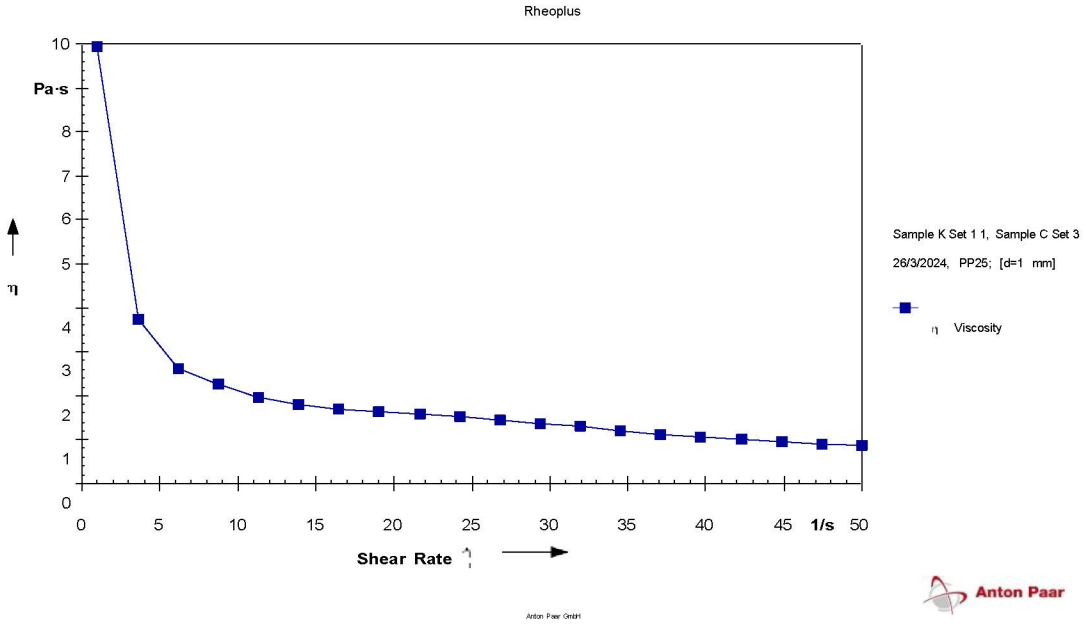

Sample K1

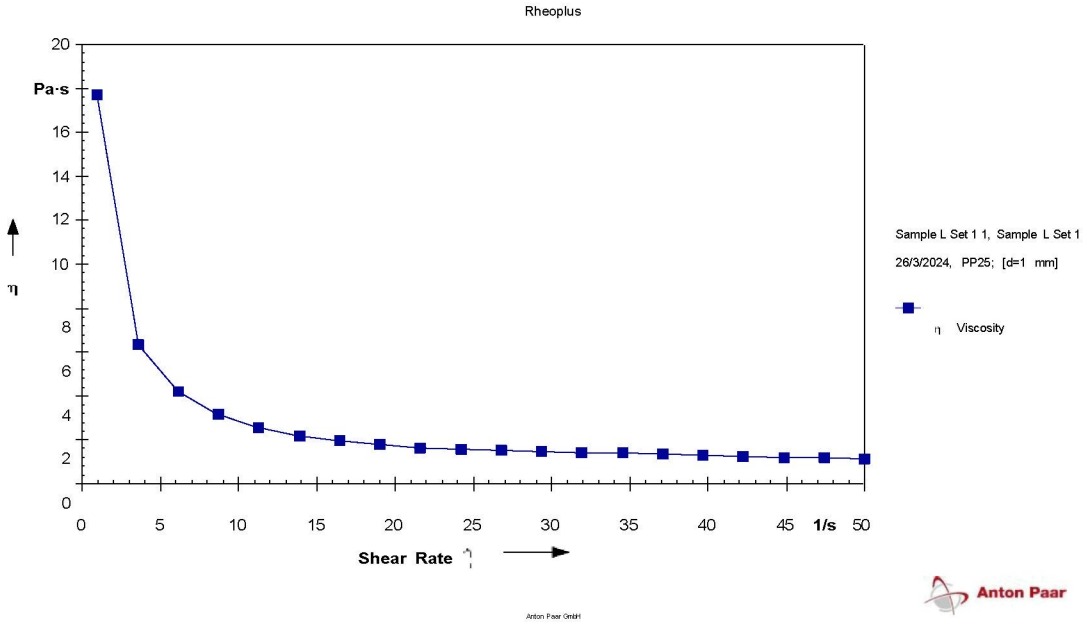

Sample L1

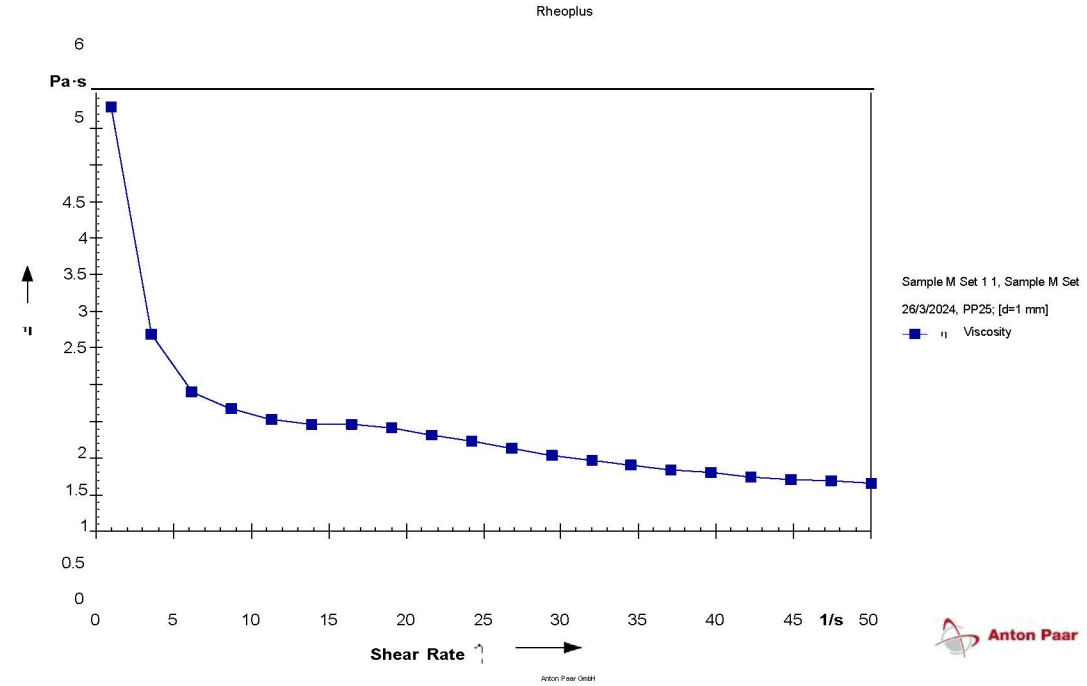

Sample M1

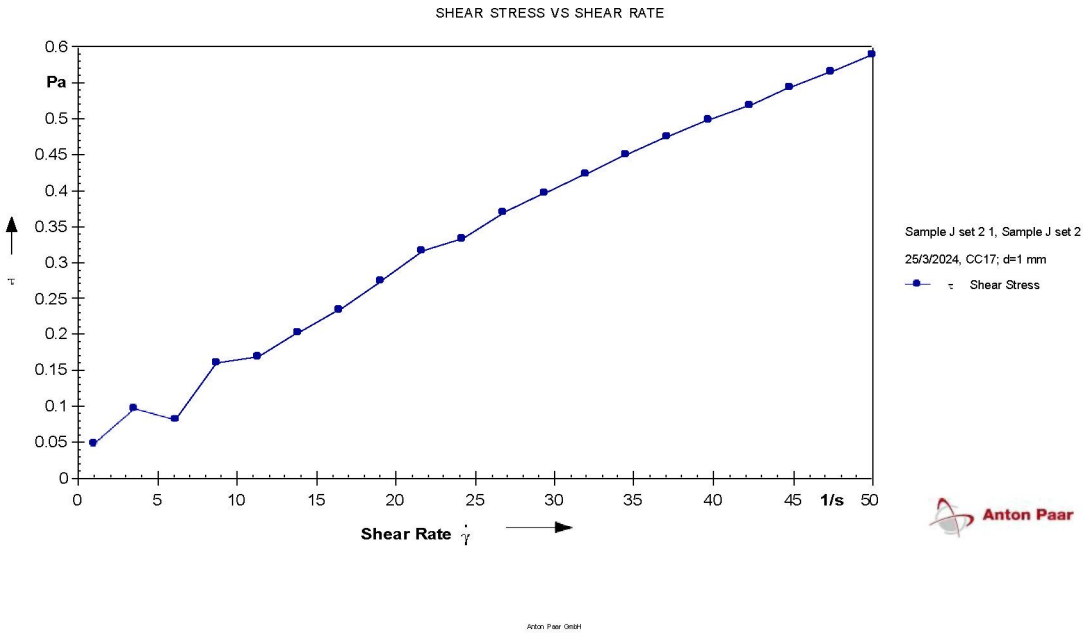

Sample J2

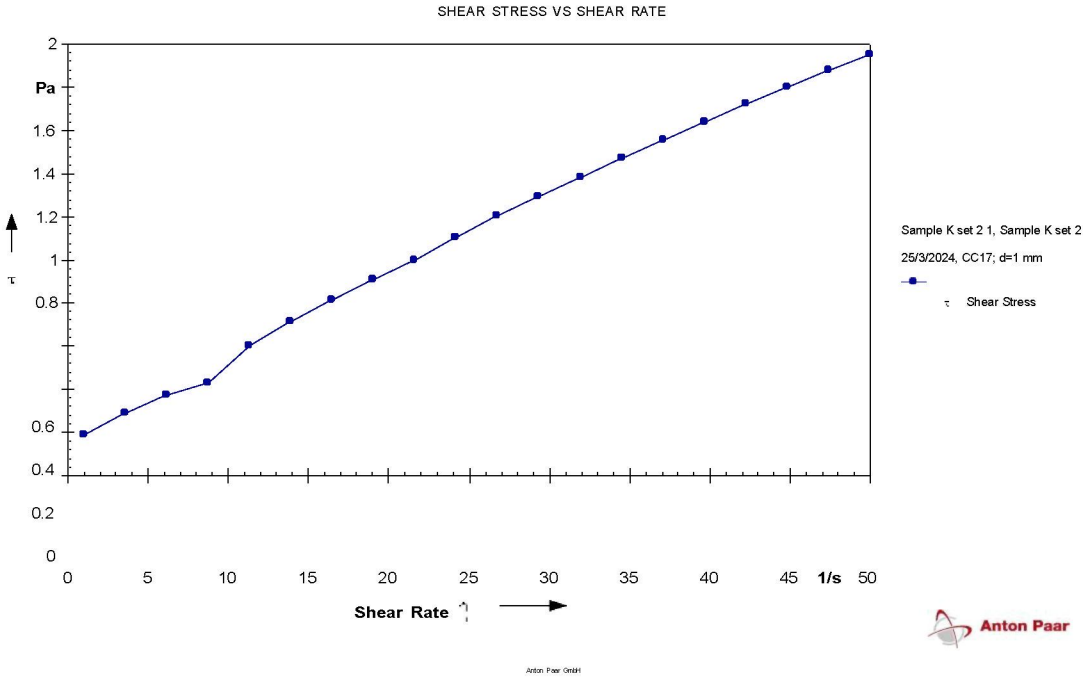

Sample K2

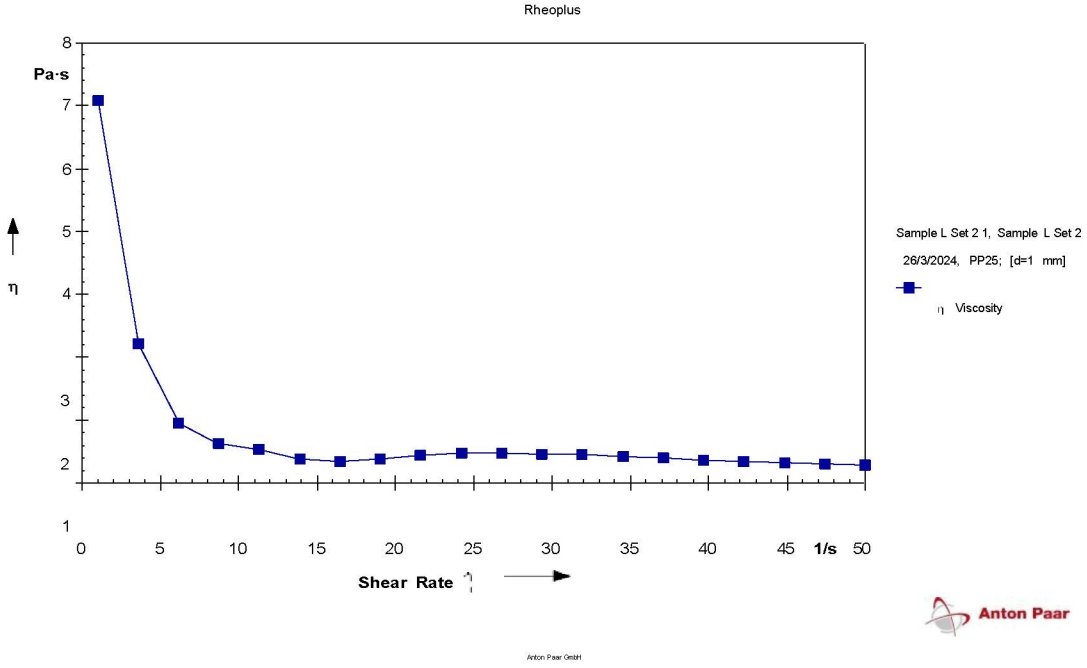

Sample L2

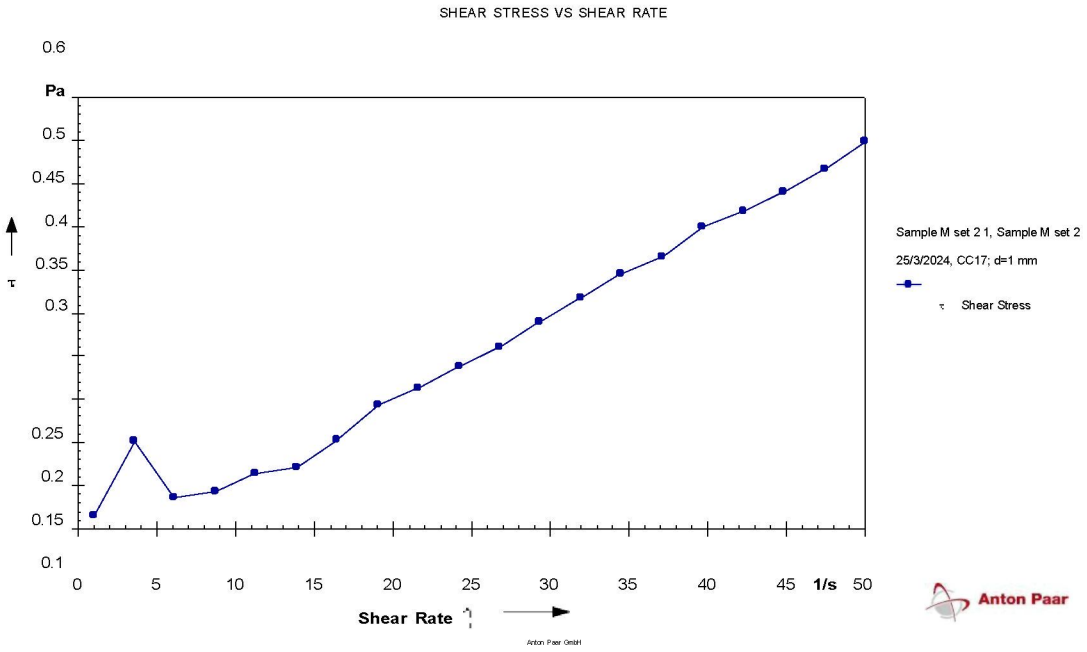

Sample M2

APPENDIX F

1) Mean, $\bar{x}$

$$x = \frac{\sum x_i}{n}$$

2) Standard deviation, s

$$s = \sqrt{\frac{\sum (x_i - \bar{x})^2}{N - 1}}$$

3) Confidence Interval, CI

$$CI = \bar{x} \pm \frac{ts}{\sqrt{N}}$$

Sample A1

1) **Mean,** $\bar{x}$

$$\frac{30+30+28+33+28+32+32+34+33}{9} = 31.11$$

2) **Standard deviation,** s

$$\sqrt{\frac{(30-31.11)^2+(30-31.11)^2+(28-31.11)^2+(33-31.11)^2+(28-31.11)^2+(32-31.11)^2+(32-31.11)^2+(34-31.11)^2+(33-31.11)^2}{8}}$$

$$= 2.205$$

3) **Confidence Interval,** CI

$$31.11 \pm \frac{(2.306)(2.205)}{\sqrt{9}} = 1.695$$

Sample B1

1) **Mean,** $\bar{x}$

$$\frac{22+18+19+21+22+21+24}{7} = 21.00$$

2) **Standard deviation,** s

$$\frac{}{\sqrt{\frac{(22-21)^2+(18-21)^2+(19-21)^2+(21-21)^2+(22-21)^2+(21-21)^2+(24-21)^2}{7-1}}}$$

$$= 2.000$$

3) **Confidence Interval,** CI

$$21.00 \pm \frac{(2.447)(2)}{\sqrt{7}} = 1.850$$

Sample C1

1) **Mean,** $\bar{x}$

$$\frac{32+26+39+32+27+37+28+29+29}{9} = 31.00$$

2) **Standard deviation,** s

$$\frac{}{\sqrt{\frac{(32-31)^2+(26-31)^2+(39-31)^2+(32-31)^2+(27-31)^2+(37-31)^2+(28-31)^2+(29-31)^2+(29-31)^2}{9-1}}}$$

$$=4.472$$

3) **Confidence Interval,** CI

$$31.00 \pm \frac{(2.306)(4.472)}{\sqrt{9}} = 3.438$$

Sample D1

1) **Mean,** $\bar{x}$

$$\frac{29+40+26+31+20+18+25}{7} = 27.00$$

2) **Standard deviation,** s

$$\sqrt{\frac{(29-27)^2+(40-27)^2+(26-27)^2+(31-27)^2+(20-27)^2+(18-27)^2+(25-27)^2}{7-1}}$$

$$=7.348$$

3) **Confidence Interval,** CI

$$27.00 \pm \frac{(2.447)(7.348)}{\sqrt{7}} = 6.796$$

Sample A2

1) **Mean,** $\bar{x}$

$$\frac{12+11+10+11+12+11+11+10+11+10}{10} = 11.00$$

2) **Standard deviation,** s

$$\sqrt{\frac{(12-11)^2+(11-11)^2+(10-11)^2+(11-11)^2+(12-11)^2+(11-11)^2+(11-11)^2+(10-11)^2+(11-11)^2+(11-11)^2}{10-1}}$$

$$=0.667$$

3) **Confidence Interval,** CI

$$11.00 \pm \frac{(2.262)(0.667)}{\sqrt{10}} = 0.477$$

Sample B2

1) **Mean,** $\bar{x}$

$$\frac{23+24+22+23+24+23+27+25+23+23}{10} = 23.70$$

2) **Standard deviation,** s

$$\sqrt{\frac{(23-23.7)^2+(24-23.7)^2+(22-23.7)^2+(23-23.7)^2+(24-23.7)^2+(23-23.7)^2+(27-23.7)^2+(25-23.7)^2+(23-23.7)^2+(23-23.7)^2}{10-1}}$$

$$=1.418$$

3) **Confidence Interval,** CI

$$23.70 \pm \frac{(2.262)(1.418)}{\sqrt{10}} = 1.014$$

Sample C2

1) **Mean,** $\bar{x}$

$$\frac{10+11+10+10+10+12+11+9+11}{9} = 10.44$$

2) **Standard deviation,** s

$$\sqrt{\frac{(10-10.44)^2+(11-10.44)^2+(10-10.44)^2+(10-10.44)^2+(10-10.44)^2+(12-10.44)^2+(11-10.44)^2+(9-10.44)^2+(11-10.44)^2}{9-1}}$$

$$=0.882$$

3) **Confidence Interval,** CI

$$10.44 \pm \frac{(2.306)(0.882)}{\sqrt{9}} = 0.678$$

Sample D2

1) **Mean,** $\bar{x}$

$$\frac{10+12+9+9+11+10+11+10+11+9}{10} = 10.20$$

2) **Standard deviation,** s

$$\sqrt{\frac{(10-10.2)^2+(12-10.2)^2+(9-10.2)^2+(9-10.2)^2+(11-10.2)^2+(10-10.2)^2+(11-10.2)^2+(10-10.2)^2+(11-10.2)^2+(9-10.2)^2}{10-1}}$$

$$=1.033$$

3) **Confidence Interval,** CI

$$10.20 \pm \frac{(2.262)(1.033)}{\sqrt{10}} = 0.739$$

Sample A3

1) **Mean,** $\bar{x}$

$$\frac{22+19+18+19+22+21+23+21+21+21}{10} = 20.70$$

2) **Standard deviation,** s

$$\sqrt{\frac{(22-20.7)^2+(19-20.7)^2+(18-20.7)^2+(19-20.7)^2+(22-20.7)^2+(21-20.7)^2+(23-20.7)^2+(21-20.7)^2+(21-20.7)^2+(21-20.7)^2}{10-1}}$$

$$=1.567$$

3) **Confidence Interval,** CI

$$20.70 \pm \frac{(2.262)(1.567)}{\sqrt{10}} = 1.121$$

Sample B3

1) **Mean,** $\bar{x}$

$$\frac{58+52+54+51+50+57+55+55+60+56}{10} = 54.80$$

2) **Standard deviation,** s

$$\sqrt{\frac{(58-54.8)^2+(52-54.8)^2+(54-54.8)^2+(51-54.8)^2+(50-54.8)^2+(57-54.8)^2+(55-54.8)^2+(55-54.8)^2+(60-54.8)^2+(56-54.8)^2}{10-1}}$$

$$=3.155$$

3) **Confidence Interval,** CI

$$54.8 \pm \frac{(2.262)(3.155)}{\sqrt{10}} = 2.257$$

Sample C3

1) **Mean,** $\bar{x}$

$$\frac{14+14+14+17+14+13+18+15+14+17}{10} = 15.00$$

2) **Standard deviation,** s

$$\sqrt{\frac{(14-15)^2+(14-15)^2+(14-15)^2+(17-15)^2+(14-15)^2+(13-15)^2+(18-15)^2+(15-15)^2+(14-15)^2+(17-15)^2}{10-1}}$$

$$=1.700$$

3) **Confidence Interval,** CI

$$15.00 \pm \frac{(2.262)(1.7)}{\sqrt{10}} = 1.216$$

Sample J1

1) **Mean,** $\bar{x}$

$$\frac{19+20+20+19+23+20+18+22+20+22}{10} = 20.30$$

2) **Standard deviation,** s

$$\sqrt{\frac{(19-20.3)^2+(20-20.3)^2+(20-20.3)^2+(19-20.3)^2+(23-20.3)^2+(20-20.3)^2+(18-20.3)^2+(22-20.3)^2+(20-20.3)^2+(22-20.3)^2}{10-1}}$$

$$=1.567$$

3) **Confidence Interval,** CI

$$20.30 \pm \frac{(2.262)(1.567)}{\sqrt{10}} = 1.121$$

Sample K1

1) **Mean,** $\bar{x}$

$$\frac{9+9+10+10+9+9+9+10+10}{9} = 9.44$$

2) **Standard deviation,** s

$$\sqrt{\frac{(9-9.44)^2+(9-9.44)^2+(10-9.44)^2+(10-9.44)^2+(9-9.44)^2+(9-9.44)^2+(9-9.44)^2+(10-9.44)^2+(10-9.44)^2}{9-1}}$$

$$=0.527$$

3) **Confidence Interval,** CI

$$9.44 \pm \frac{(2.306)(0.527)}{\sqrt{9}} = 0.405$$

Sample M1

1) **Mean,** $\bar{x}$

$$\frac{9+10+9+11+10+10+9+11+9+12}{10} = 10.00$$

2) **Standard deviation,** s

$$\sqrt{\frac{(9-10)^2+(10-10)^2+(9-10)^2+(11-10)^2+(10-10)^2+(10-10)^2+(9-10)^2+(11-10)^2+(9-10)^2+(12-10)^2}{10-1}}$$

$$=1.054$$

3) **Confidence Interval,** CI

$$10.00 \pm \frac{(2.262)(1.054)}{\sqrt{10}} = 0.754$$

Sample J2

1) **Mean,** $\bar{x}$

$$\frac{30+33+33+33+30+30+30+29+31+33}{10} = 30.90$$

2) **Standard deviation,** s

$$\sqrt{\frac{(30-30.9)^2+(33-30.9)^2+(33-30.9)^2+(33-30.9)^2+(30-30.9)^2+(30-30.9)^2+(30-30.9)^2+(29-30.9)^2+(31-30.9)^2+(33-30.9)^2}{10-1}}$$

$$=1.524$$

3) **Confidence Interval,** CI

$$30.90 \pm \frac{(2.262)(1.524)}{\sqrt{10}} = 1.090$$

Sample K2

1) **Mean,** $\bar{x}$

$$\frac{10+10+13+11+11+11+10+10+10+12}{10} = 10.80$$

2) **Standard deviation,** s

$$\sqrt{\frac{(10-10.8)^2+(10-10.8)^2+(13-10.8)^2+(11-10.8)^2+(11-10.8)^2+(11-10.8)^2+(10-10.8)^2+(10-10.8)^2+(10-10.8)^2+(12-10.8)^2}{10-1}}$$

$$=1.033$$

3) **Confidence Interval,** CI

$$10.80 \pm \frac{(2.262)(1.033)}{\sqrt{10}} = 0.739$$

Sample L2

1) **Mean,** $\bar{x}$

$$\frac{21+20+20+22+21+23+23+20+21+21}{10} = 21.20$$

2) **Standard deviation,** s

$$\sqrt{\frac{(21-21.2)^2+(20-21.2)^2+(20-21.2)^2+(22-21.2)^2+(21-21.2)^2+(23-21.2)^2+(23-21.2)^2+(20-21.2)^2+(21-21.2)^2+(21-21.2)^2}{10-1}}$$

$$=1.135$$

3) **Confidence Interval,** CI

$$21.20 \pm \frac{(2.262)(1.135)}{\sqrt{10}} = 0.812$$

Sample M2

4) **Mean,** $\bar{x}$

$$\frac{30+31+28+35+28+31+33+33+31+31}{10} = 31.10$$

5) **Standard deviation,** s

$$\sqrt{\frac{(30-31.1)^2+(31-31.1)^2+(28-31.1)^2+(35-31.1)^2+(28-31.1)^2+(31-31.1)^2+(33-31.1)^2+(33-31.1)^2+(31-31.1)^2+(31-31.1)^2}{10-1}}$$

$$=2.183$$

6) **Confidence Interval,** CI

$$31.10 \pm \frac{(2.262)(2,183)}{\sqrt{10}} = 1.562$$

APPENDIX G

a) Sample A1

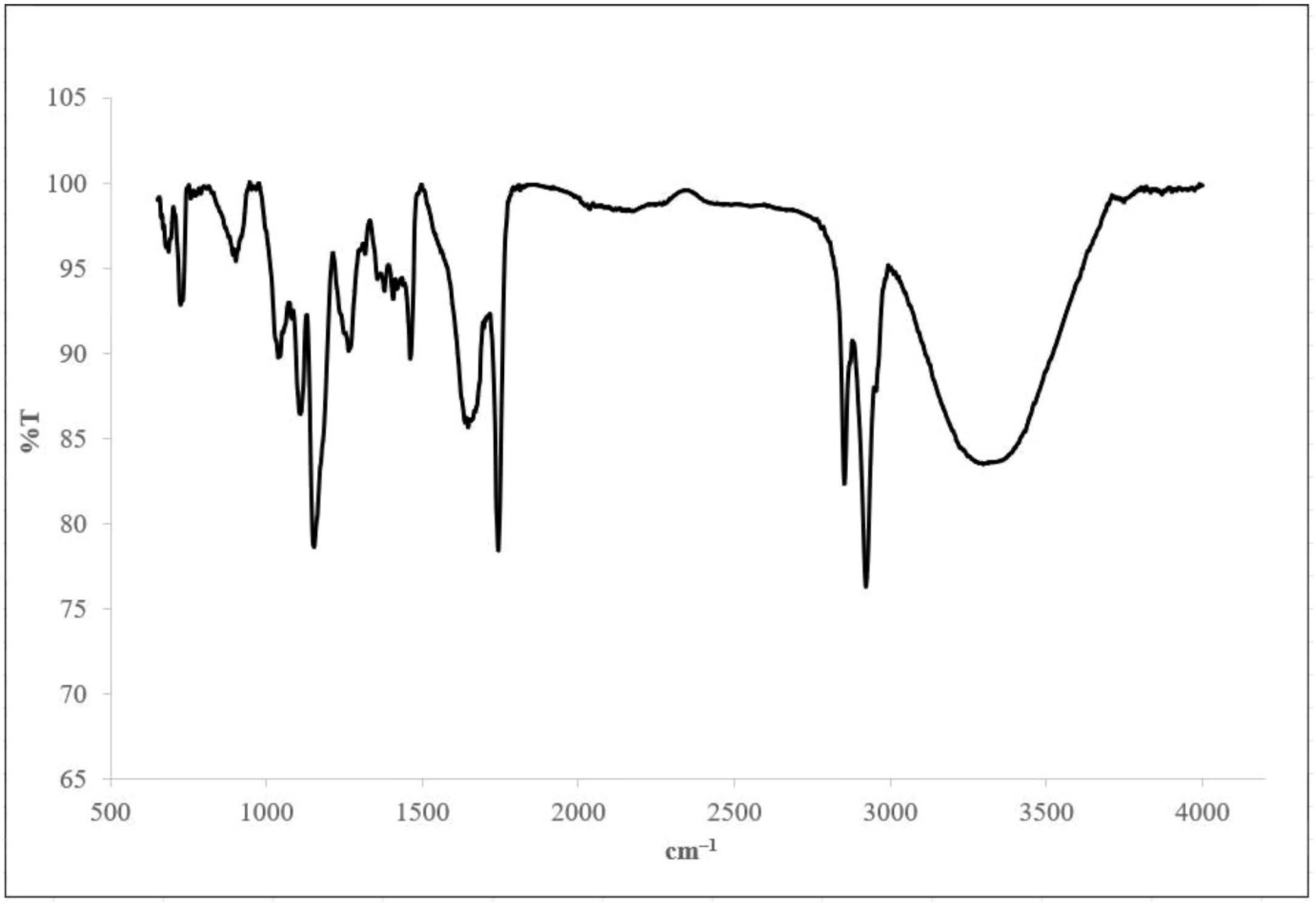

b) Sample B1

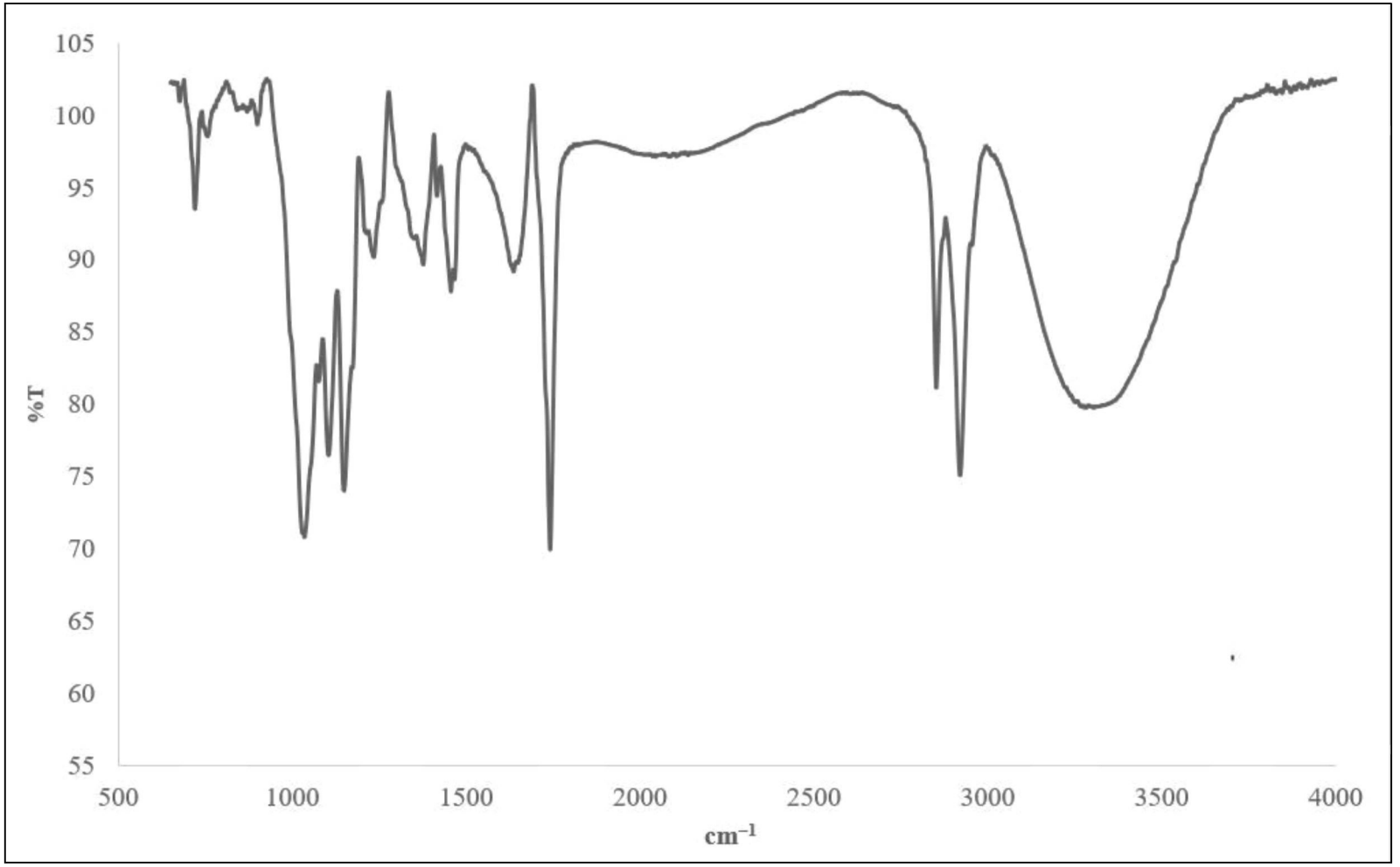
105
100
95
90
85
80
75
70
65
60
55
%T
500
1000
1500
2000
2500
3000
3500
4000
cm⁻¹

c) **Sample C1**

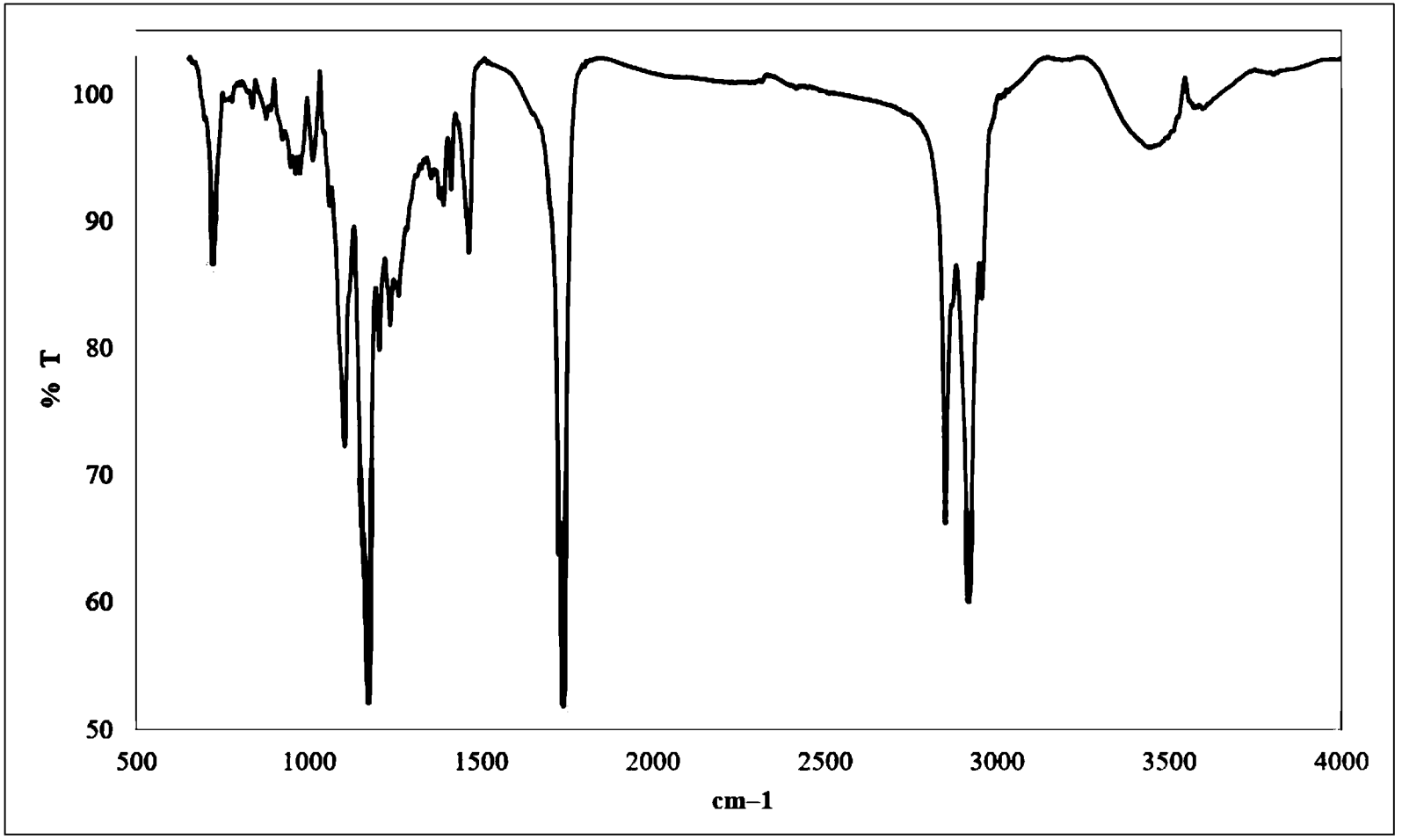

d) Sample D1

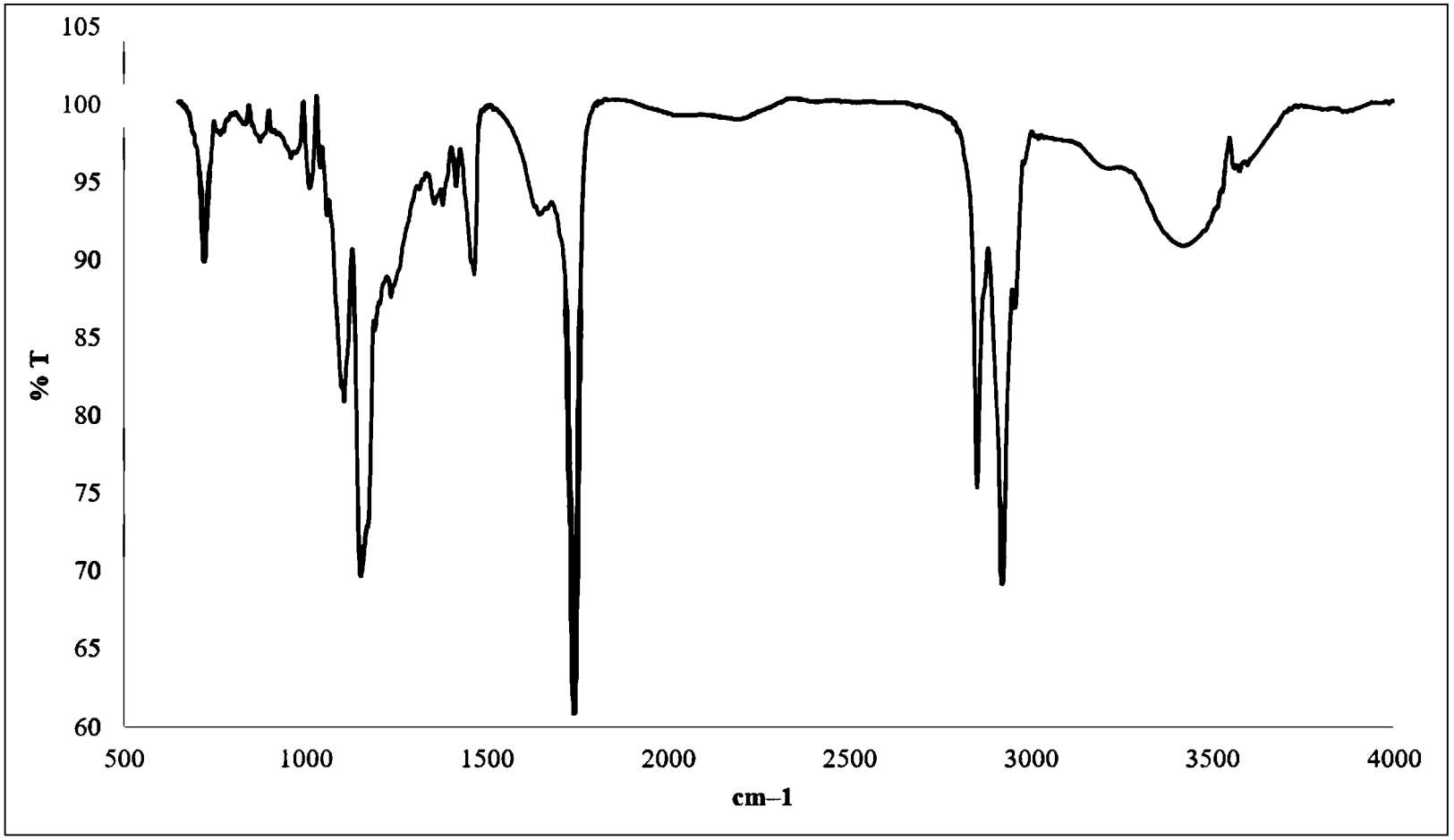
105
100
95
90
85
80
75
70
65
60
% T
500
1000
1500
2000
2500
3000
3500
4000
cm–1

e) Sample A2

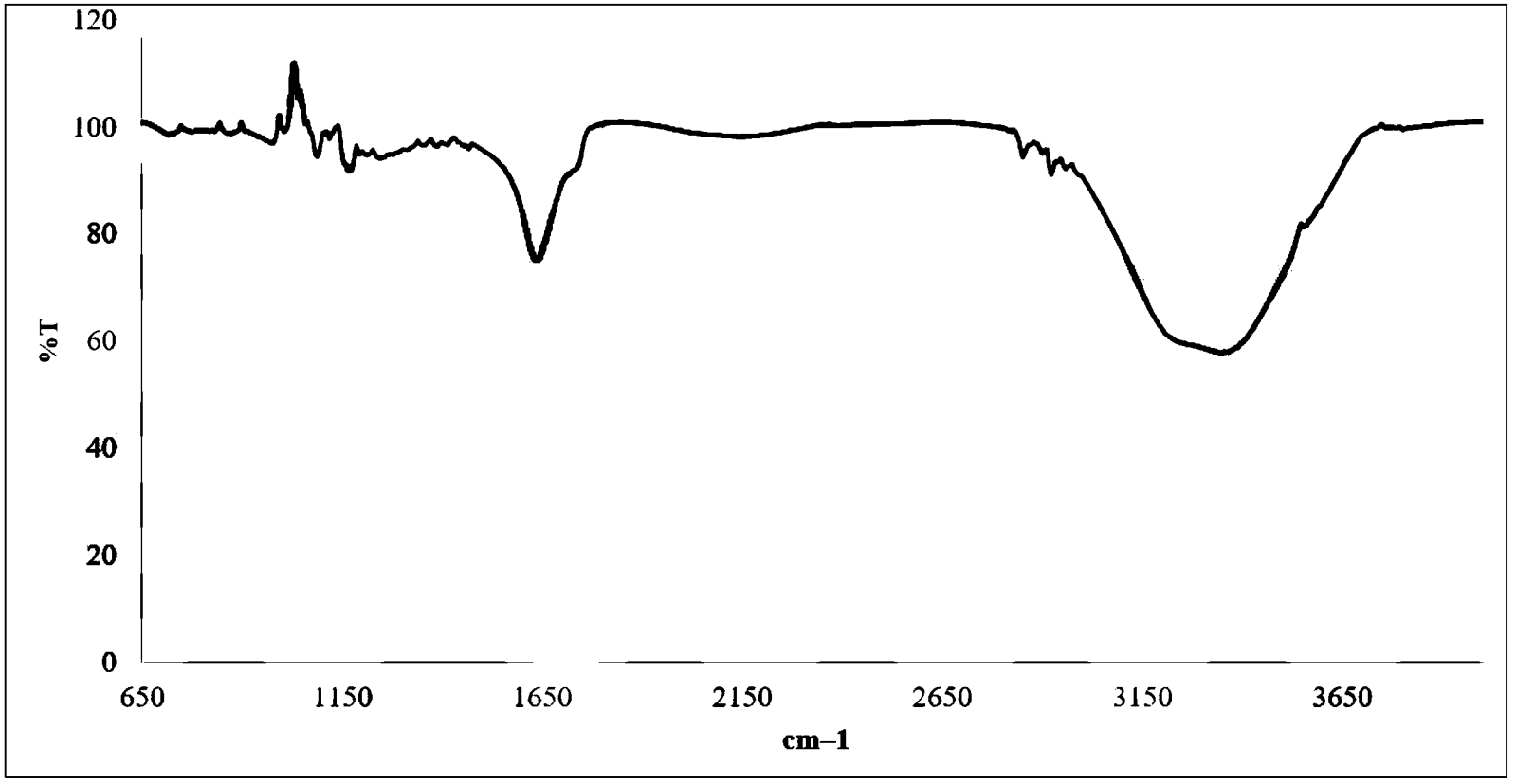

f) Sample B2

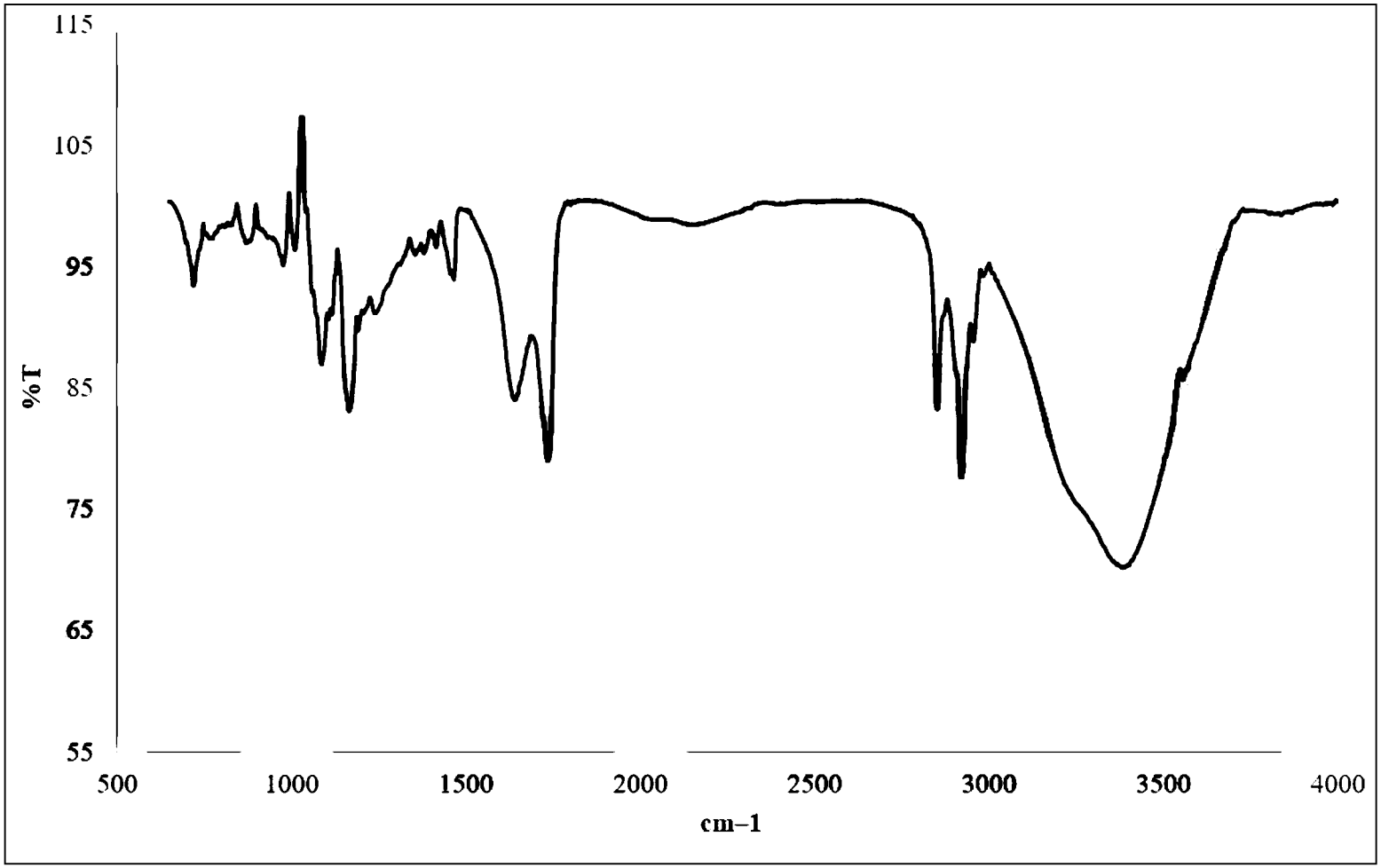
115
105
95
85
75
65
55
%T
500
1000
1500
2000
2500
3000
3500
4000
cm−1

g) Sample C2

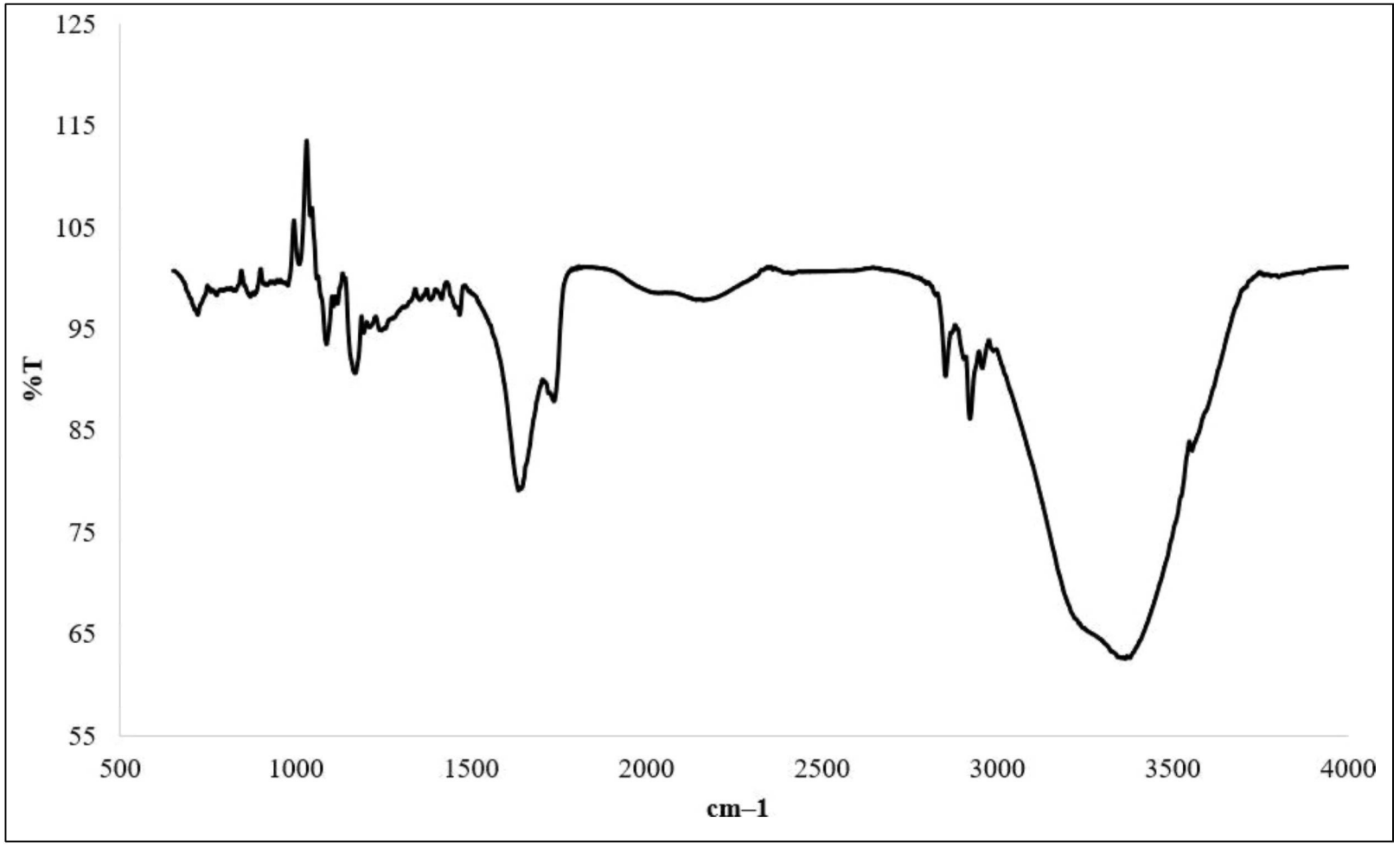
125
115
105
95
85
75
65
55
%T
500
1000
1500
2000
2500
3000
3500
4000
cm–1

h) Sample D2

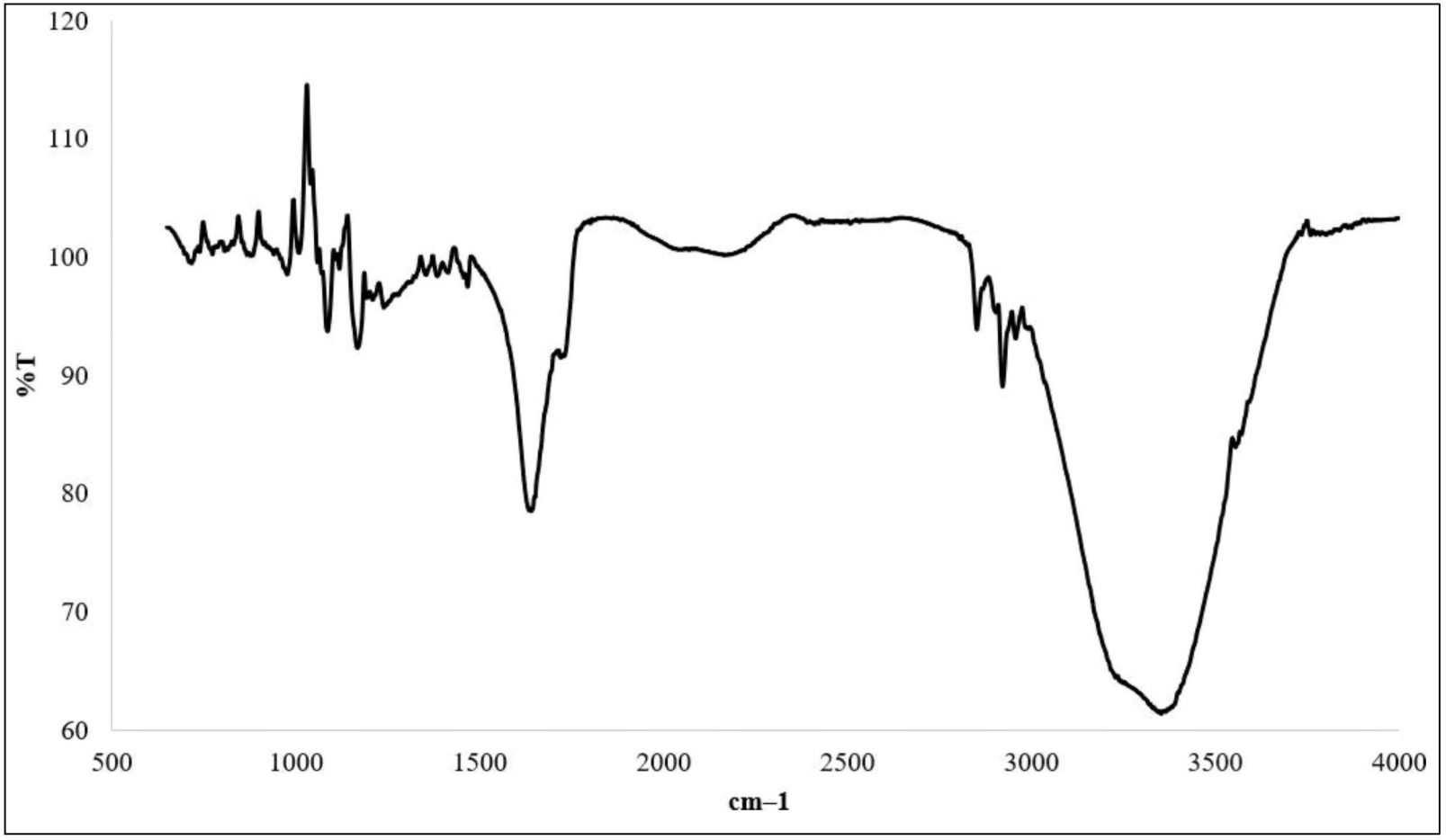
120
110
100
90
80
70
60
%T
500
1000
1500
2000
2500
3000
3500
4000
cm–1

i) **Sample A3**

j) Sample B3

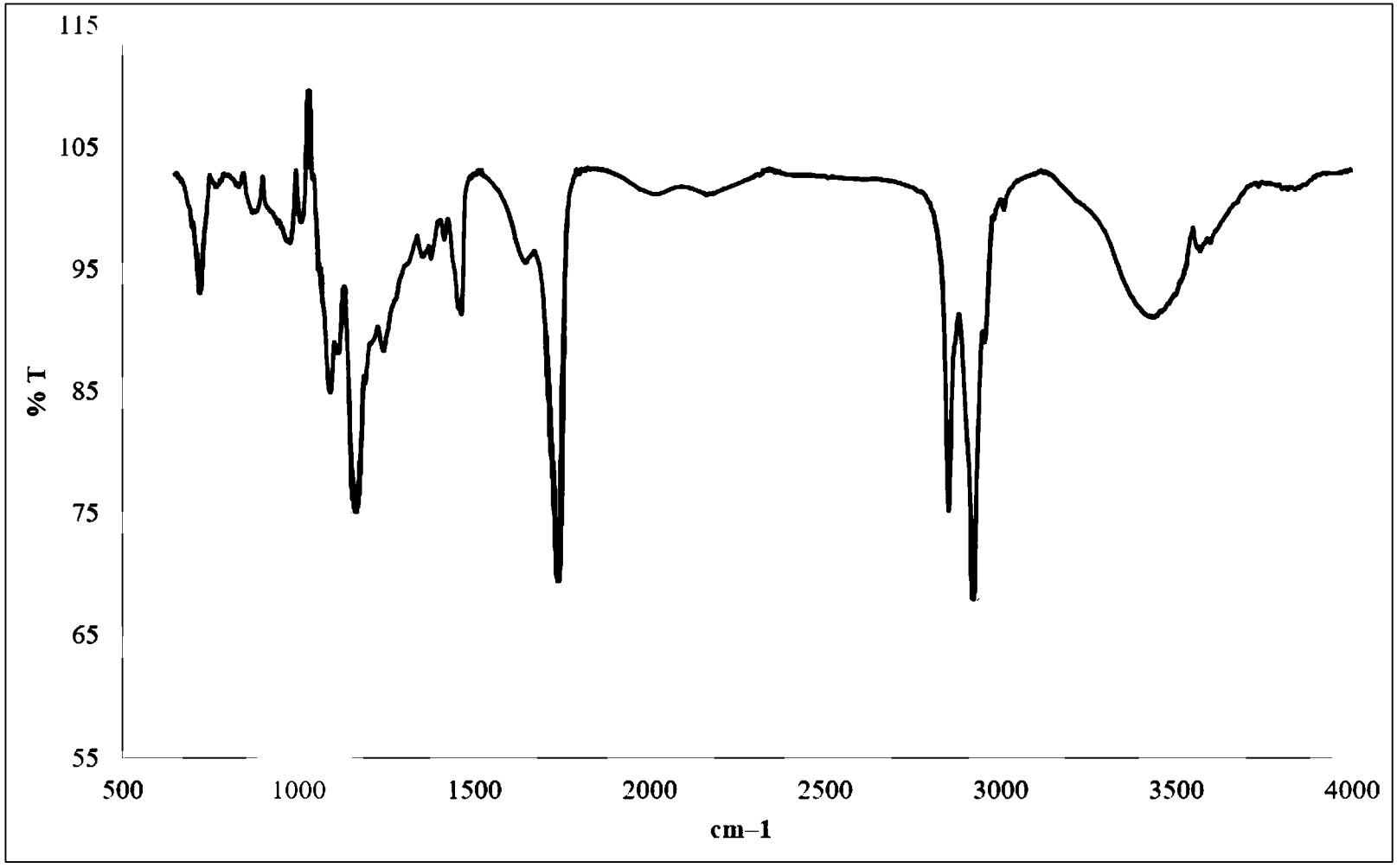
115
105
95
85
75
65
55
% T
500
1000
1500
2000
2500
3000
3500
4000
cm–1

k) Sample C3

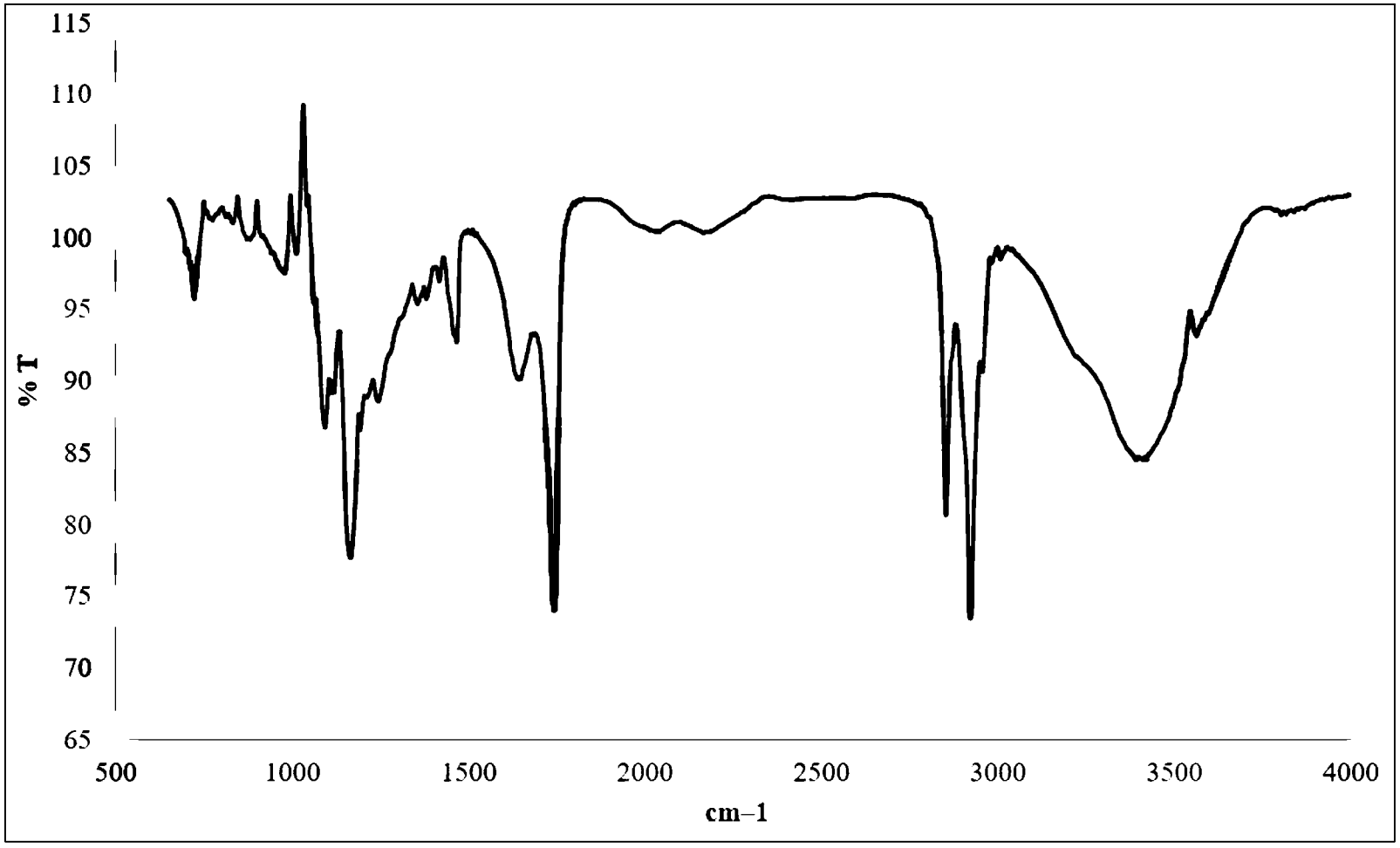
115
110
105
100
95
90
85
80
75
70
65
% T
500
1000
1500
2000
2500
3000
3500
4000
cm–1

l) **Sample D3**

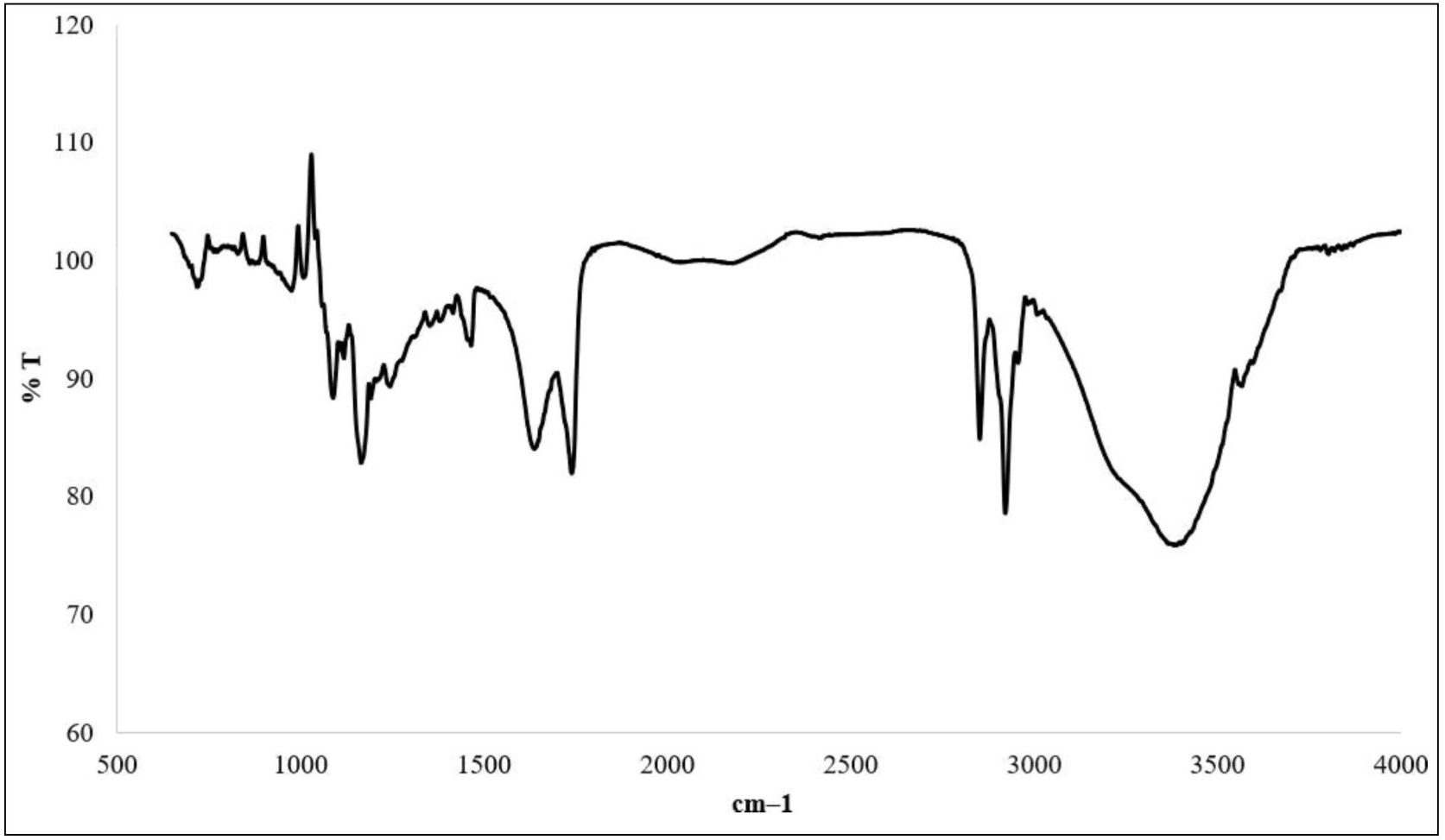
120
110
100
90
80
70
60
% T
500
1000
1500
2000
2500
3000
3500
4000
cm–1

m) Sample J1

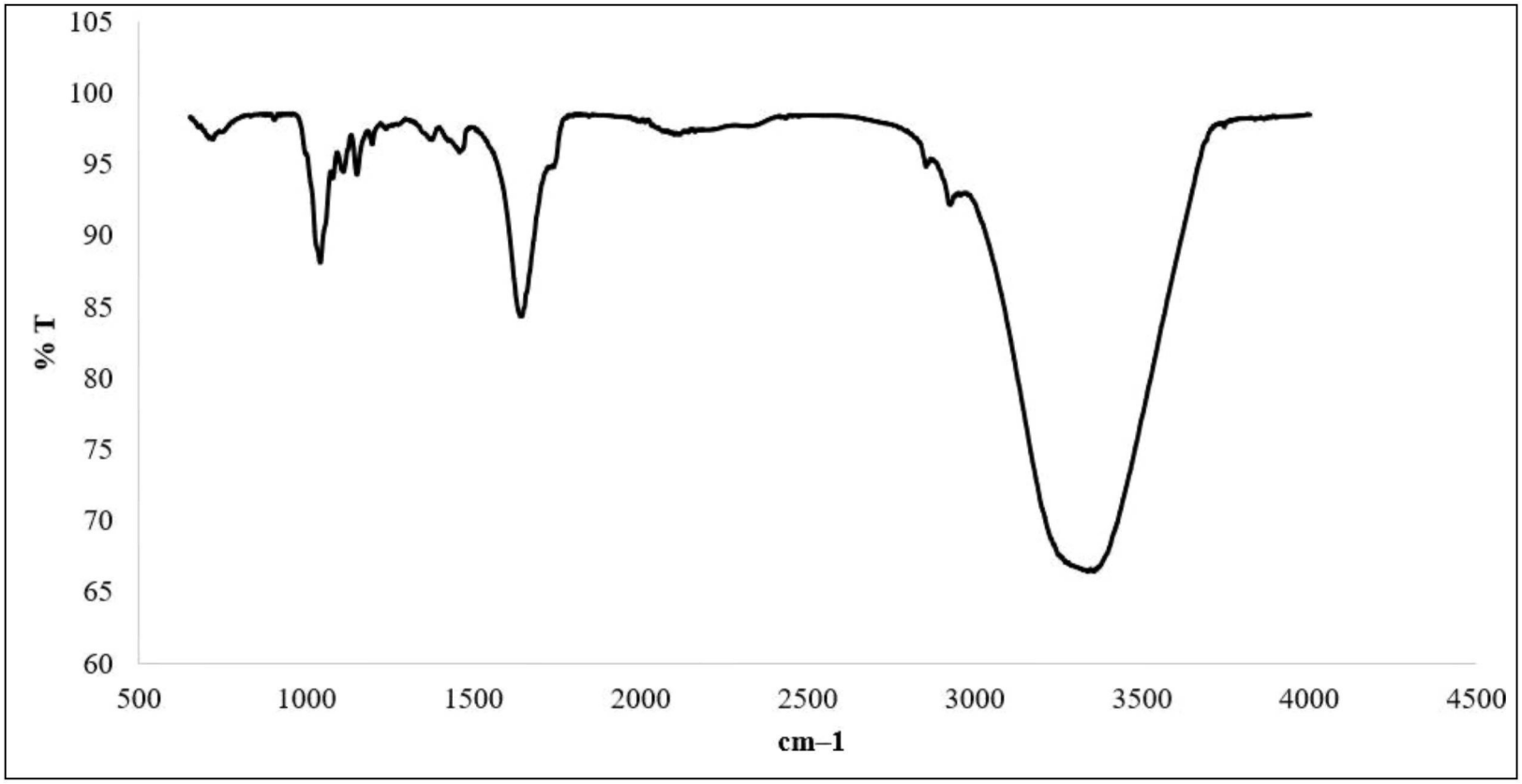
105
100
95
90
85
80
75
70
65
60
% T
500
1000
1500
2000
2500
3000
3500
4000
4500
cm–1

n) Sample K1

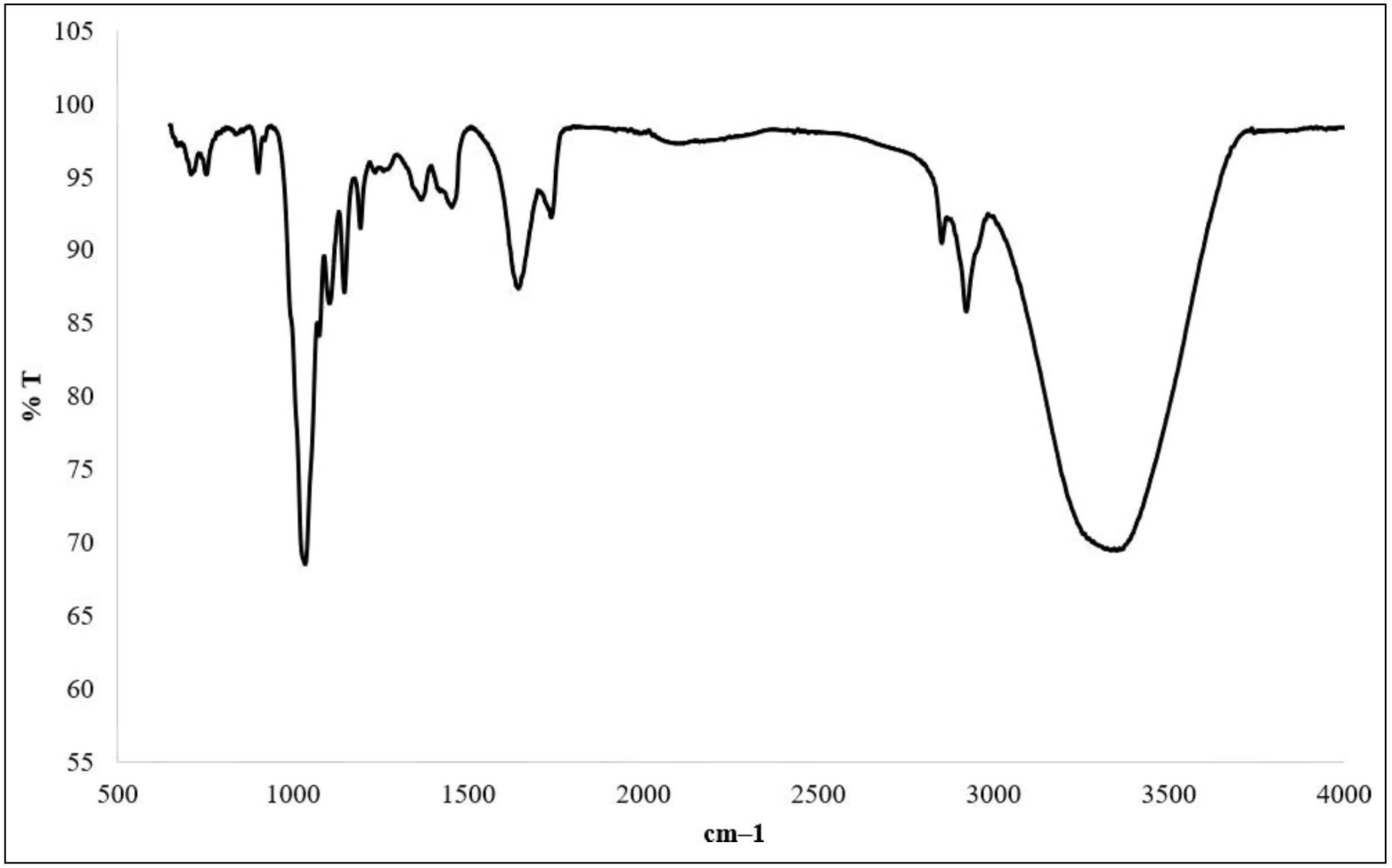
105
100
95
90
85
80
75
70
65
60
55
% T
500
1000
1500
2000
2500
3000
3500
4000
cm–1

o) Sample L1

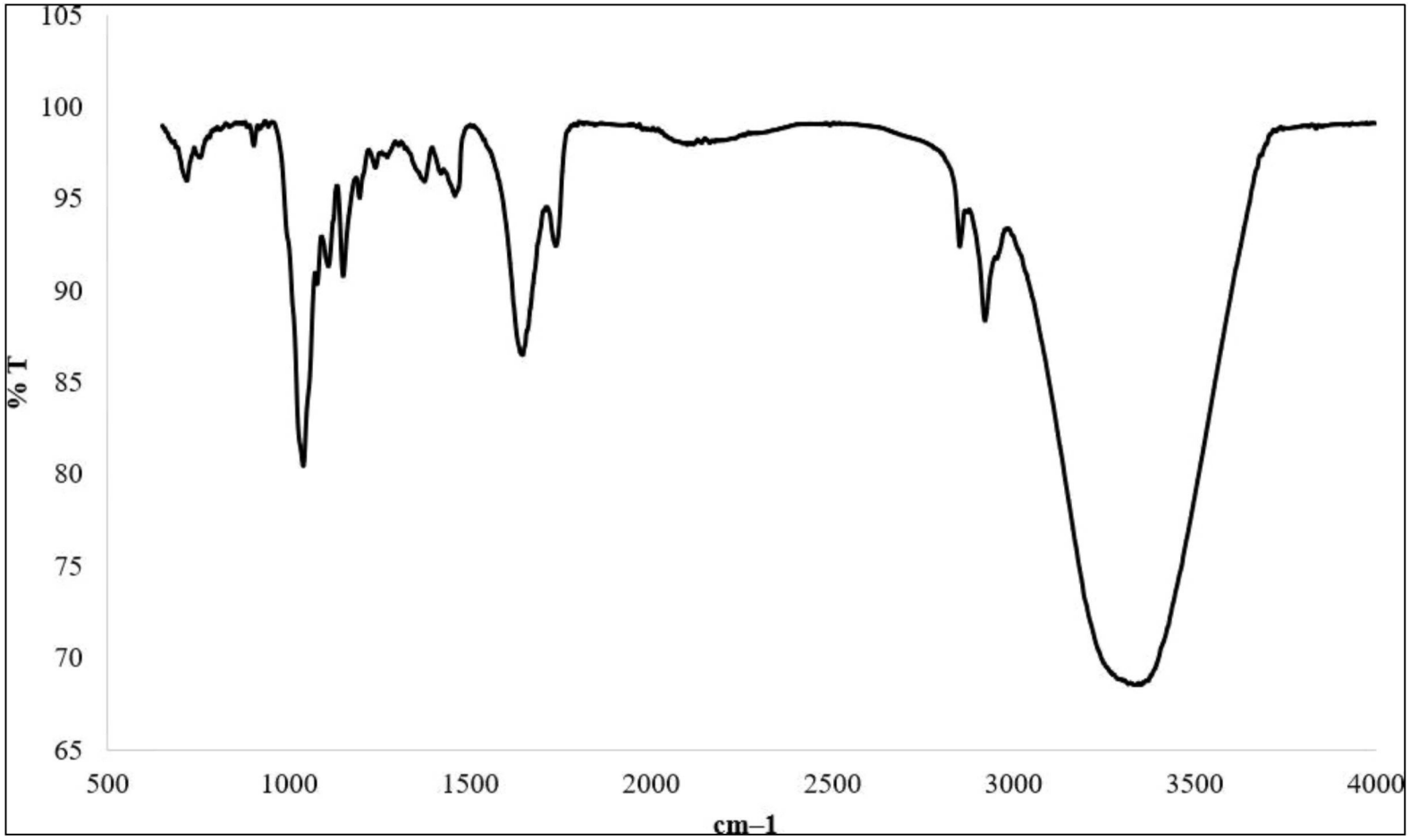
105
100
95
90
85
80
75
70
65
% T
500
1000
1500
2000
2500
3000
3500
4000
cm–1

p) Sample M1

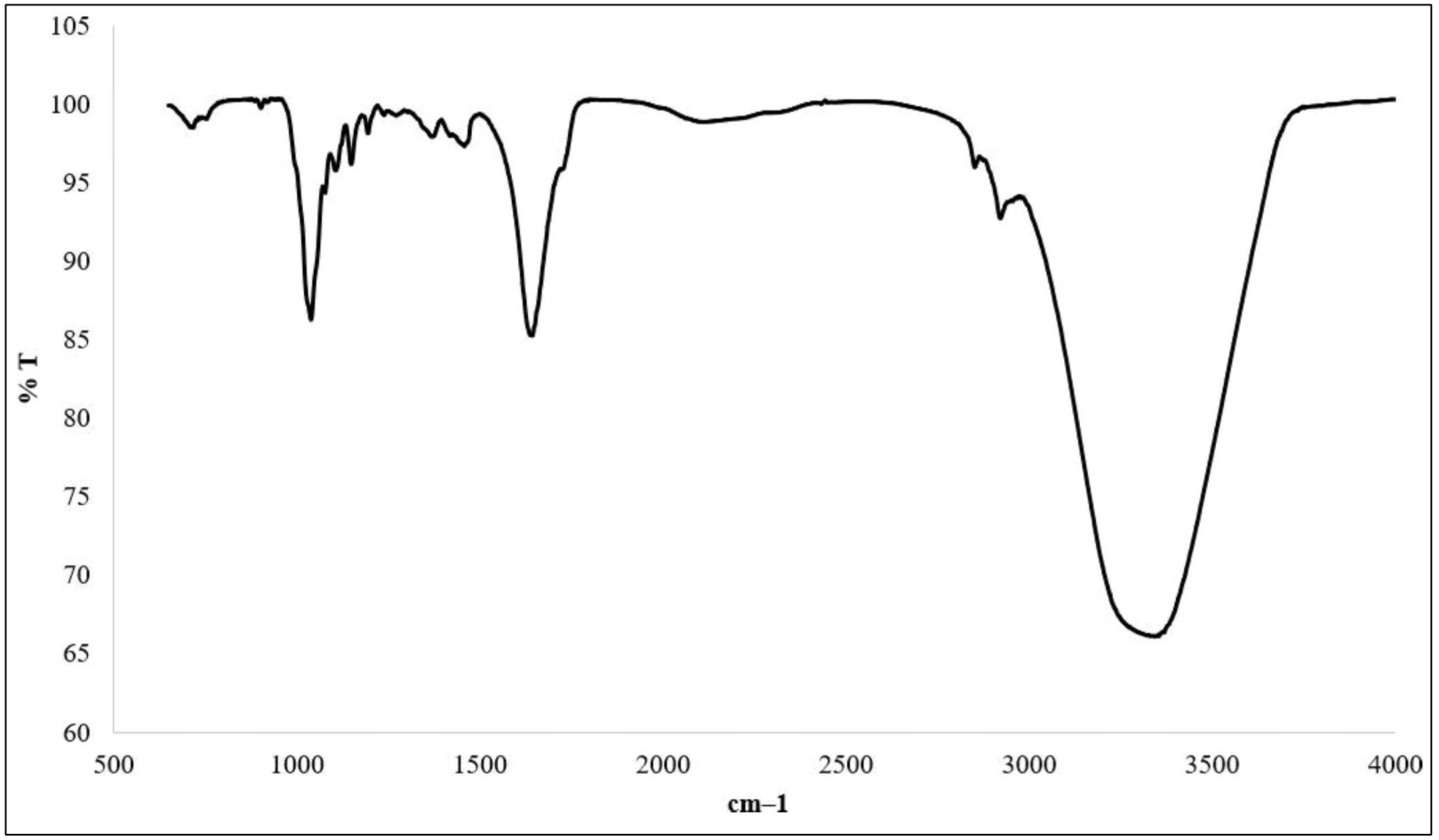
105
100
95
90
85
80
75
70
65
60
% T
500
1000
1500
2000
2500
3000
3500
4000
cm–1

q) **Sample J2**

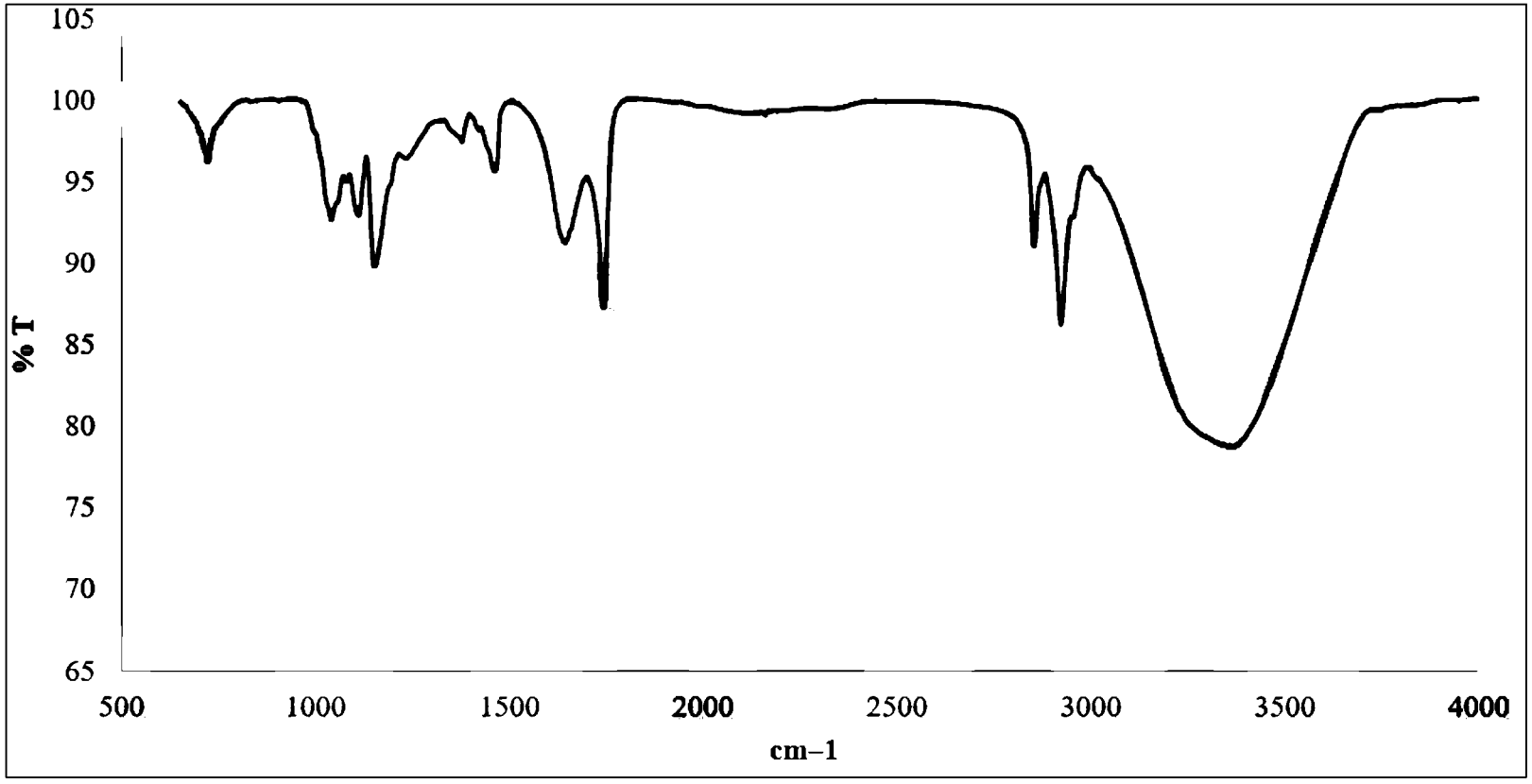
105
100
95
90
85
80
75
70
65
% T
500
1000
1500
2000
2500
3000
3500
4000
cm–1

r) Sample K2

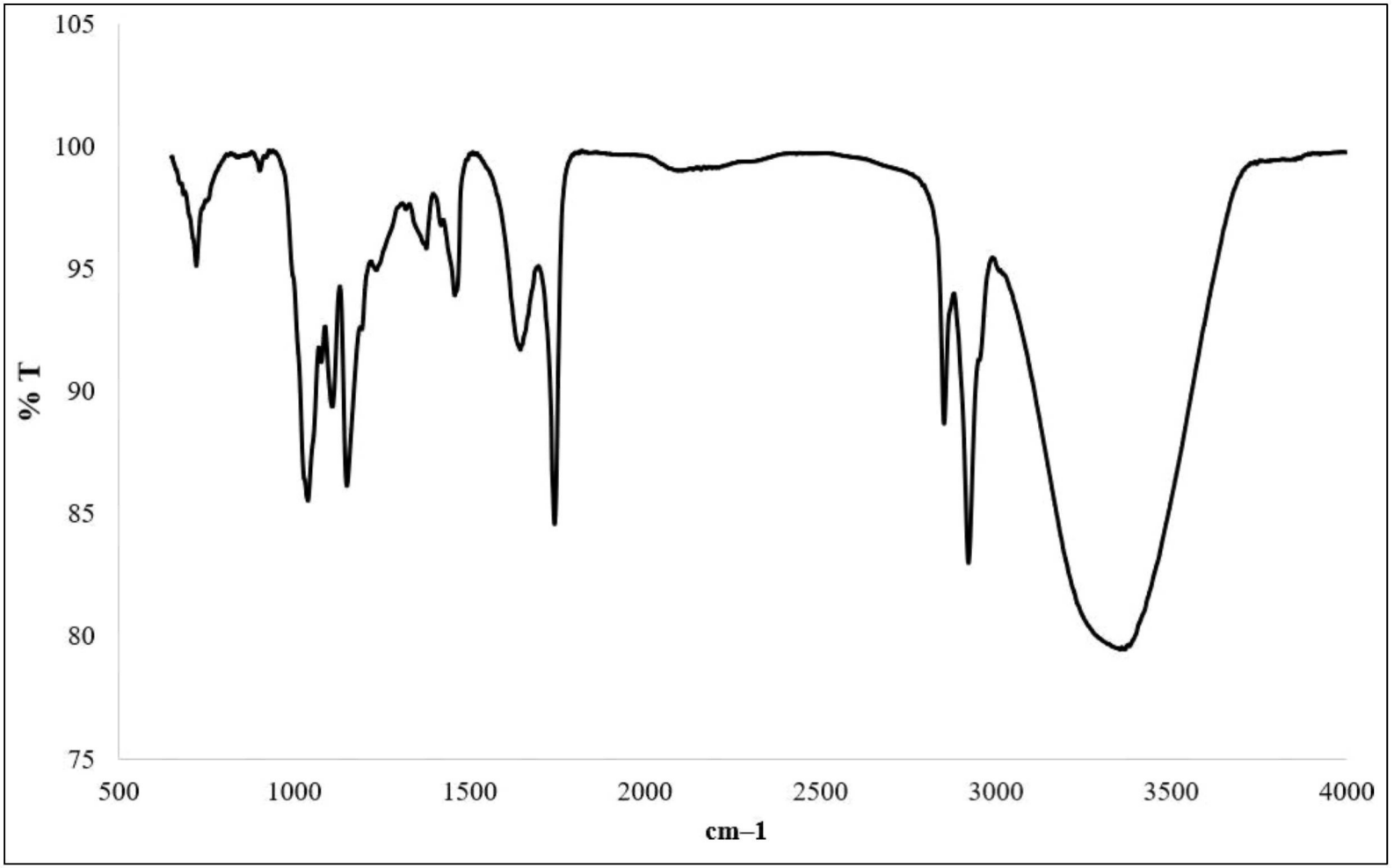
105
100
95
90
85
80
75
% T
500
1000
1500
2000
2500
3000
3500
4000
cm–1

s) Sample L2

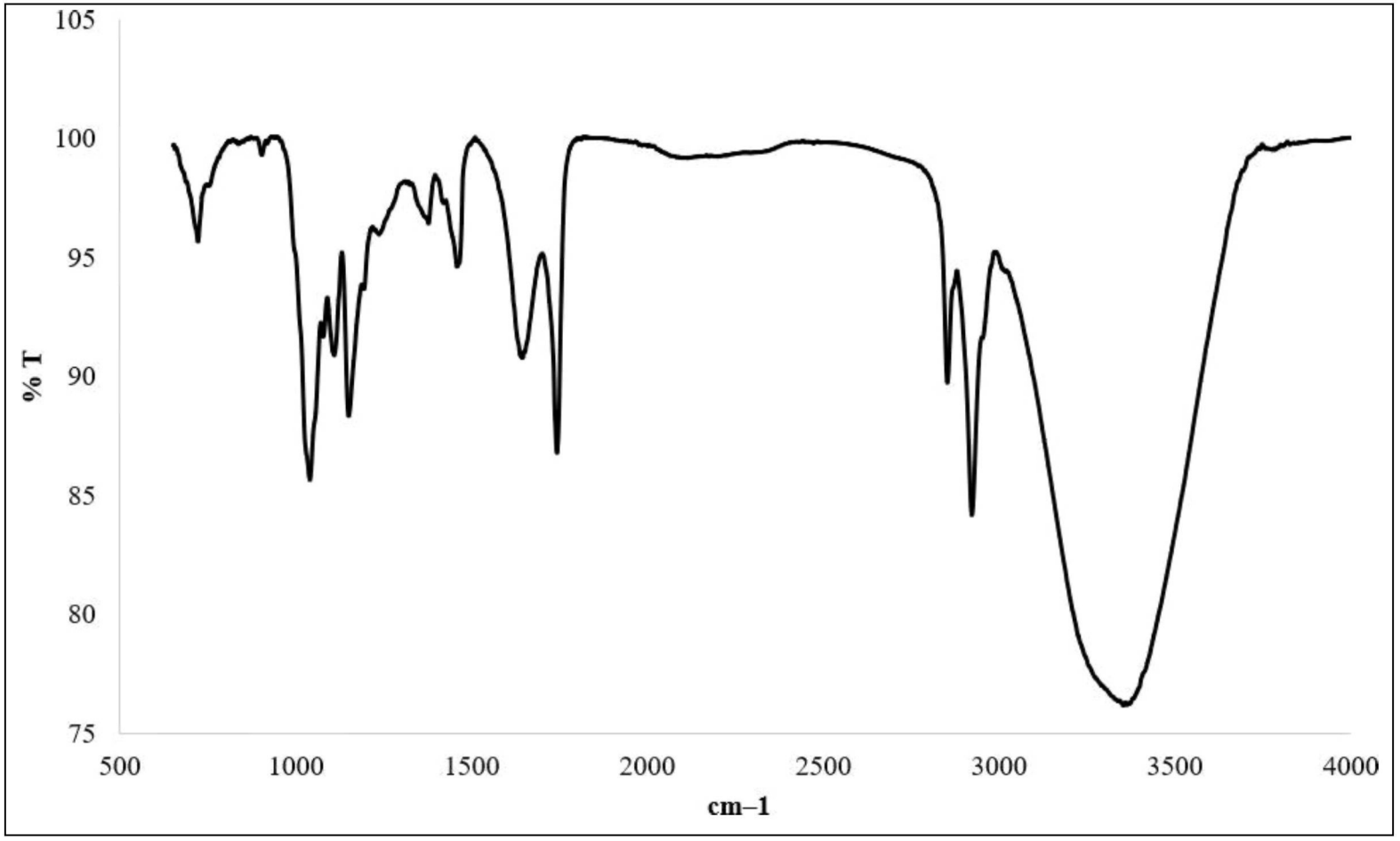
105
100
95
90
85
80
75
% T
500
1000
1500
2000
2500
3000
3500
4000
cm–1

t) Sample M2

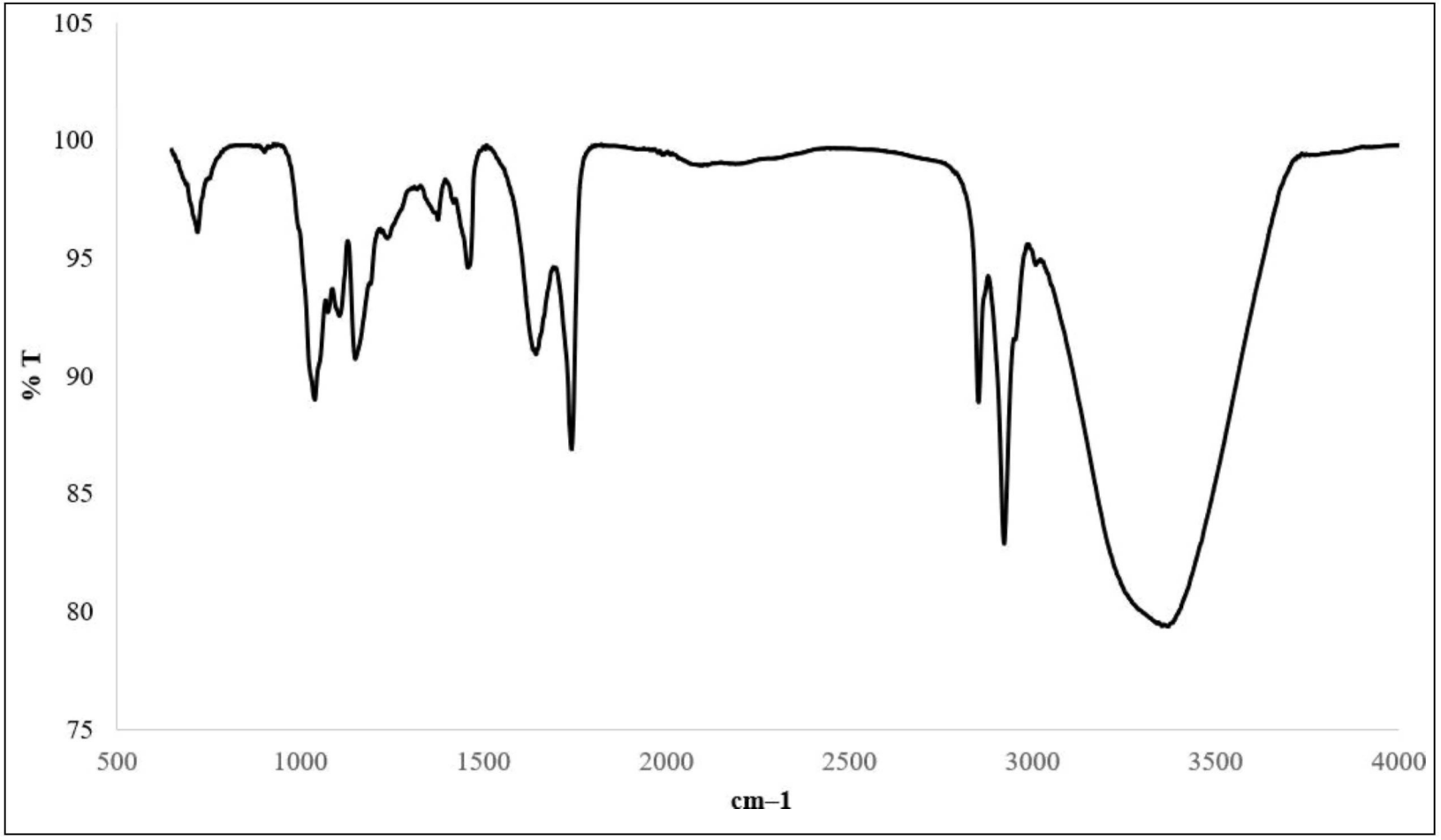
105
100
95
90
85
80
75
% T
500
1000
1500
2000
2500
3000
3500
4000
cm–1

APPENDIX H

Temperature (30 ˚C)						
Day	1	6	12	18	24	30
SAMPLE L1						

SAMPLE M1						
SAMPLE K2						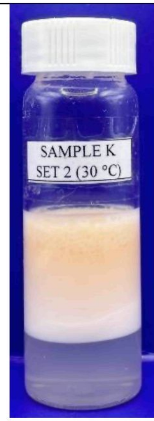

<table>
<tr>
<td>SAMPLE L2</td>
<td> 
</td>
<td> 
</td>
<td> 
</td>
<td> 
</td>
<td> 
</td>
<td> 
</td>
</tr>
</table>

Temperature (35 ˚C)						
Day	1	6	12	18	24	30
SAMPLE L1						
SAMPLE M1						

SAMPLE K2						
SAMPLE L2						

Temperature (40 ˚C)						
Day	1	6	12	18	24	30
SAMPLE L1						
SAMPLE M1						

SAMPLE K2						
SAMPLE L2						

Temperature (45 ˚C)						
Day	1	6	12	18	24	30
SAMPLE L1						
SAMPLE M1						

<table>
<tr><td>SAMPLE K2</td>
<td>  </td>
<td>  </td>
<td>  </td>
<td>  </td>
<td>  </td>
<td>  </td></tr>
<tr><td>SAMPLE L2</td>
<td>  </td>
<td>  </td>
<td>  </td>
<td>  </td>
<td>  </td>
<td>  </td></tr>
</table>

Temperature (60 ˚C)						
Day	1	6	12	18	24	30
SAMPLE L1						
SAMPLE M1				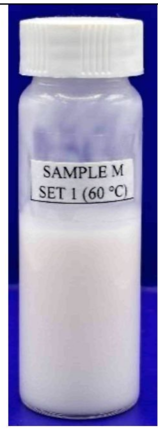		

SAMPLE K2		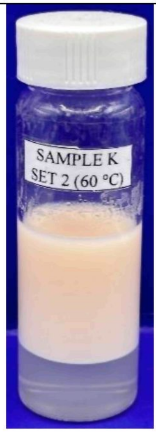			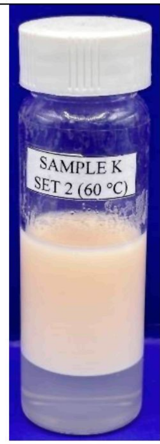	
SAMPLE L2						

APPENDIX I

Temperature (30 ˚C)							
SAMPLE L1		SAMPLE M1		SAMPLE K2		SAMPLE L2	
Before	After	Before	After	Before	After	Before	After
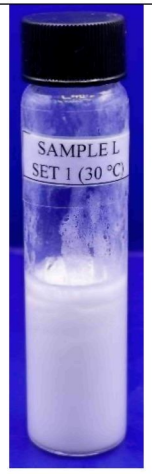							

Temperature (35 °C)							
SAMPLE L1		SAMPLE M1		SAMPLE K2		SAMPLE L2	
Before	After	Before	After	Before	After	Before	After
							

Temperature (40 ˚C)							
SAMPLE L1		SAMPLE M1		SAMPLE K2		SAMPLE L2	
Before	After	Before	After	Before	After	Before	After
							

Temperature (45 ˚C)							
SAMPLE L1		SAMPLE M1		SAMPLE K2		SAMPLE L2	
Before	After	Before	After	Before	After	Before	After
							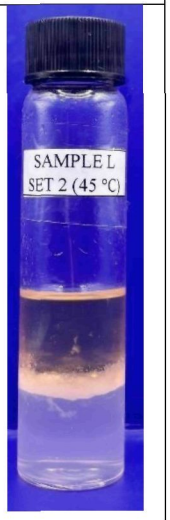

Temperature (60 ˚C)							
SAMPLE L1		SAMPLE M1		SAMPLE K2		SAMPLE L2	
Before	After	Before	After	Before	After	Before	After
		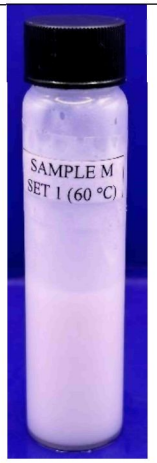					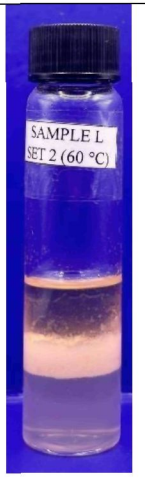

APPENDIX J

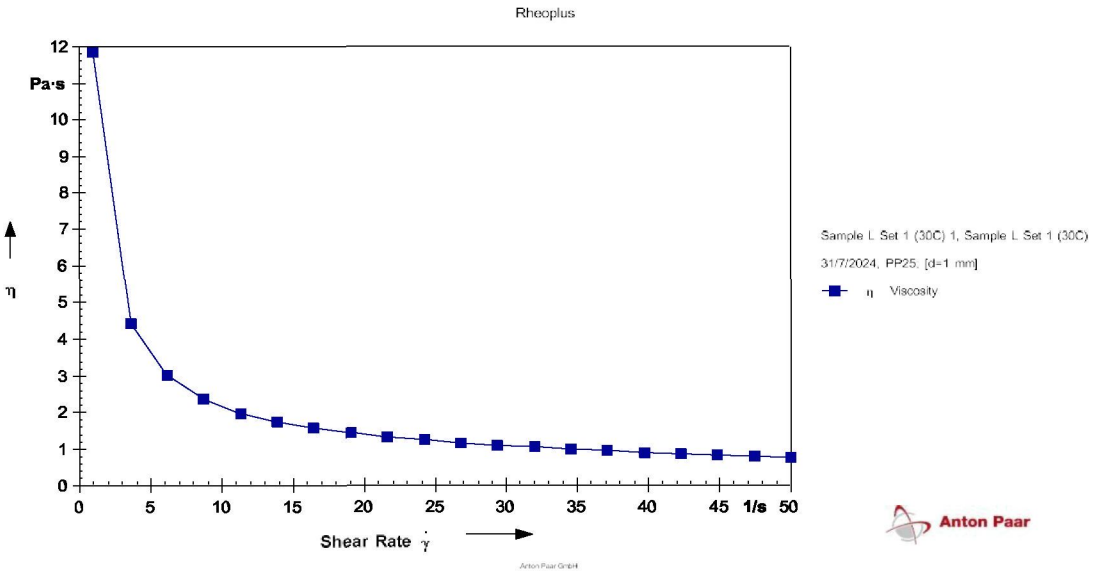

Sample L1 (30 ℃)

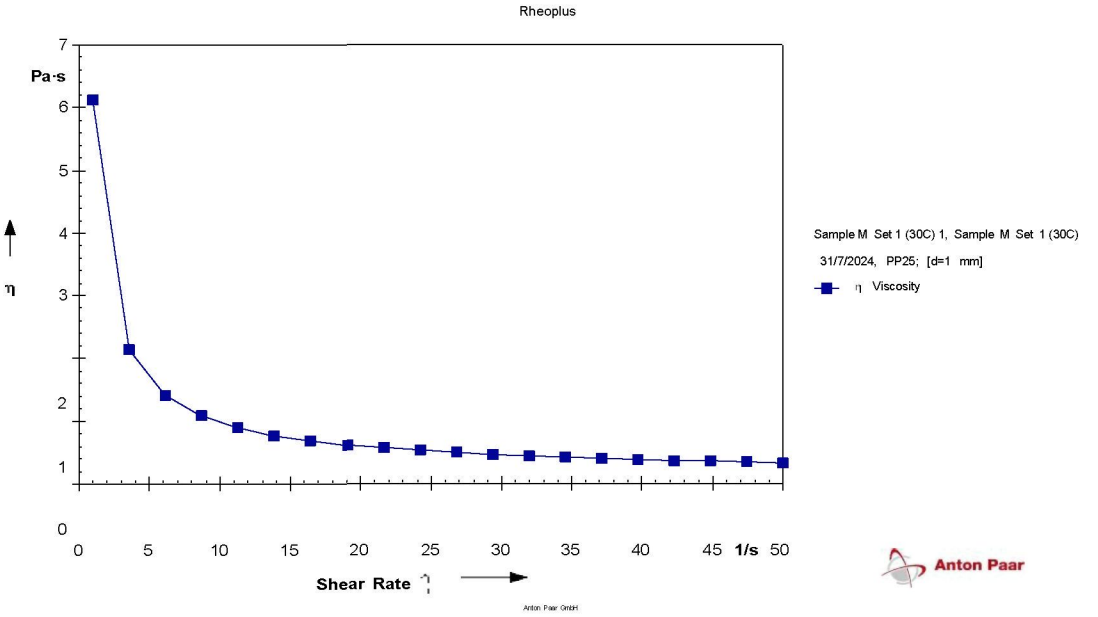

Sample M1 (30 ℃)

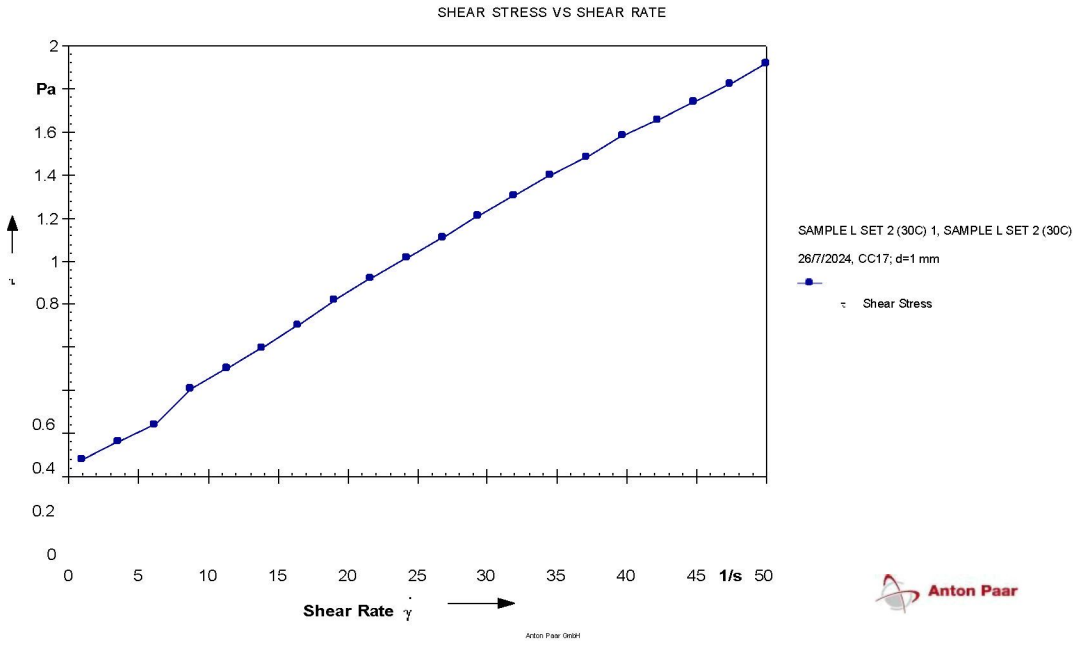

Sample K2 (30 ˚C)

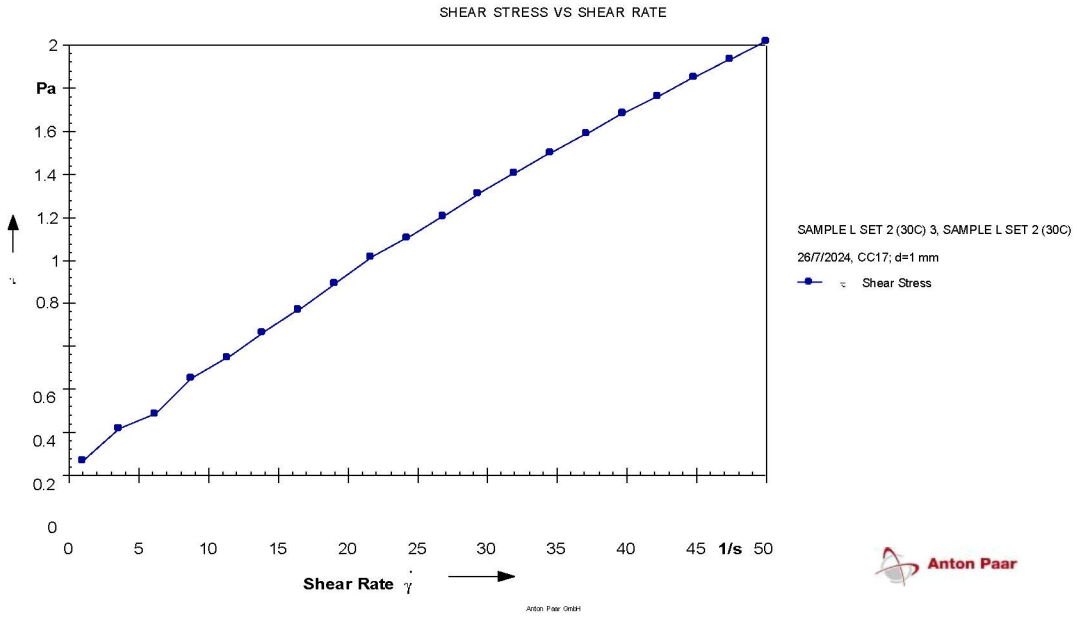

Sample L2 (30 ˚C)

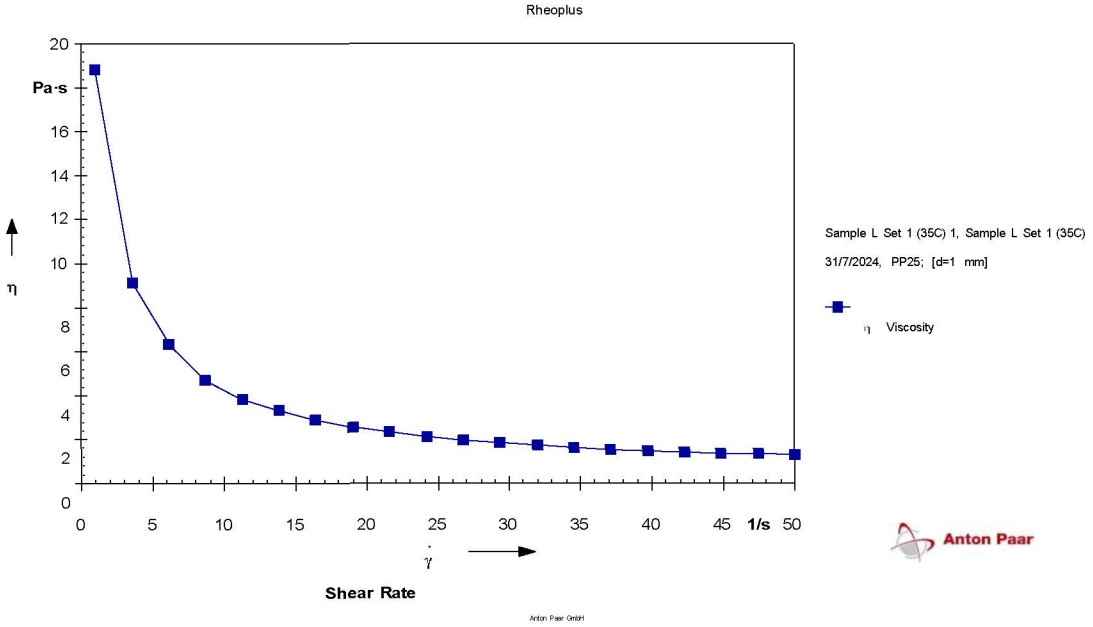

Sample L1 (35 ˚C)

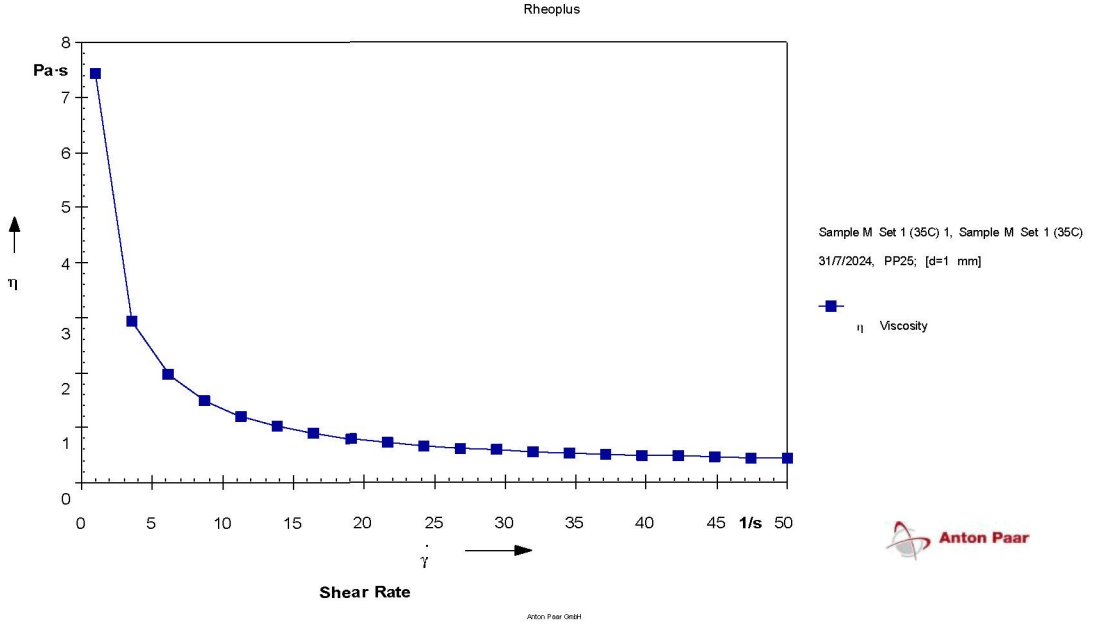

Sample M1 (35 ˚C)

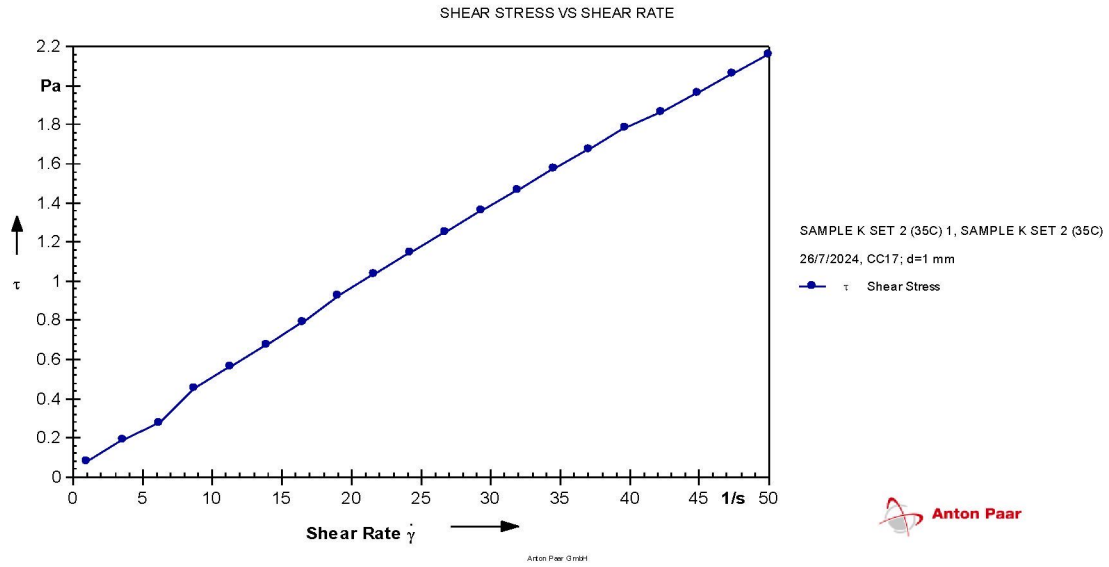

Sample K2 (35 °C)

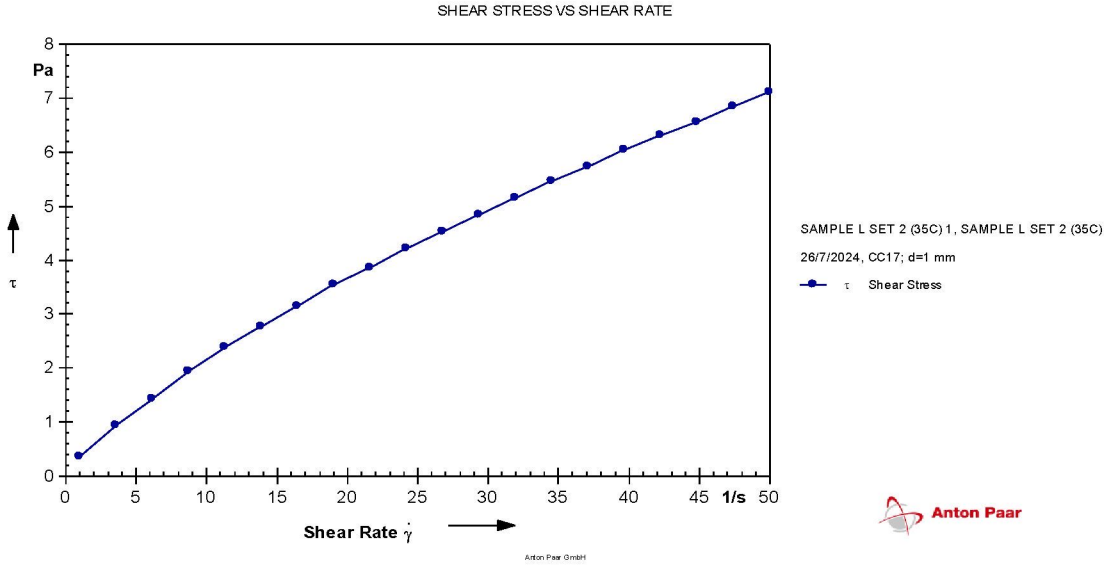

Sample L2 (35 °C)

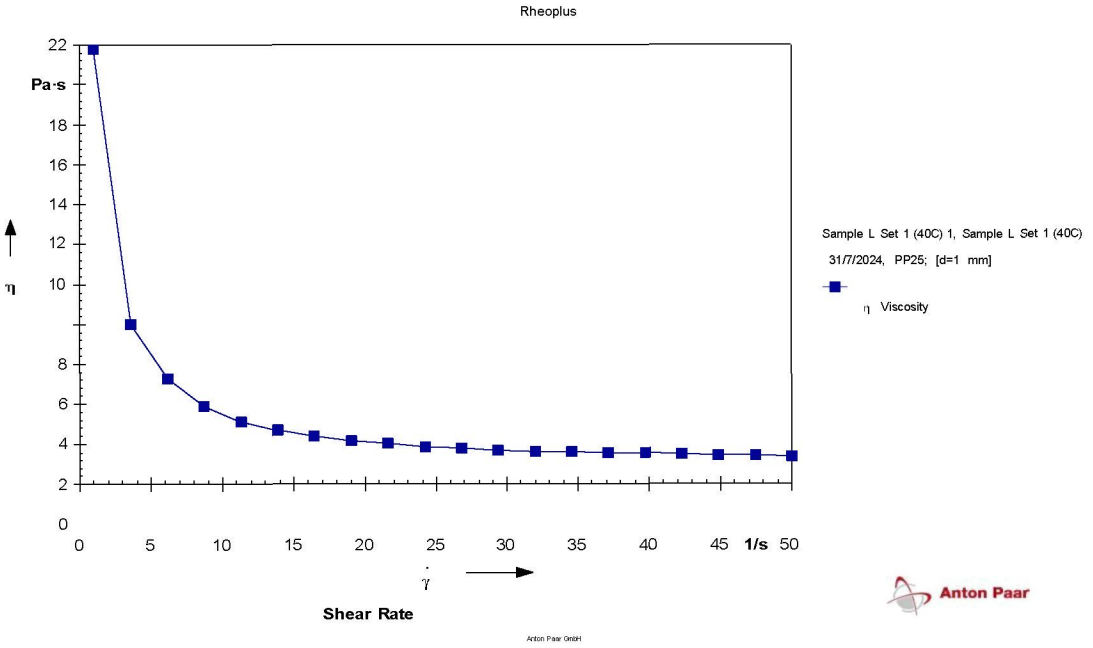

Sample L1 (40 ℃)

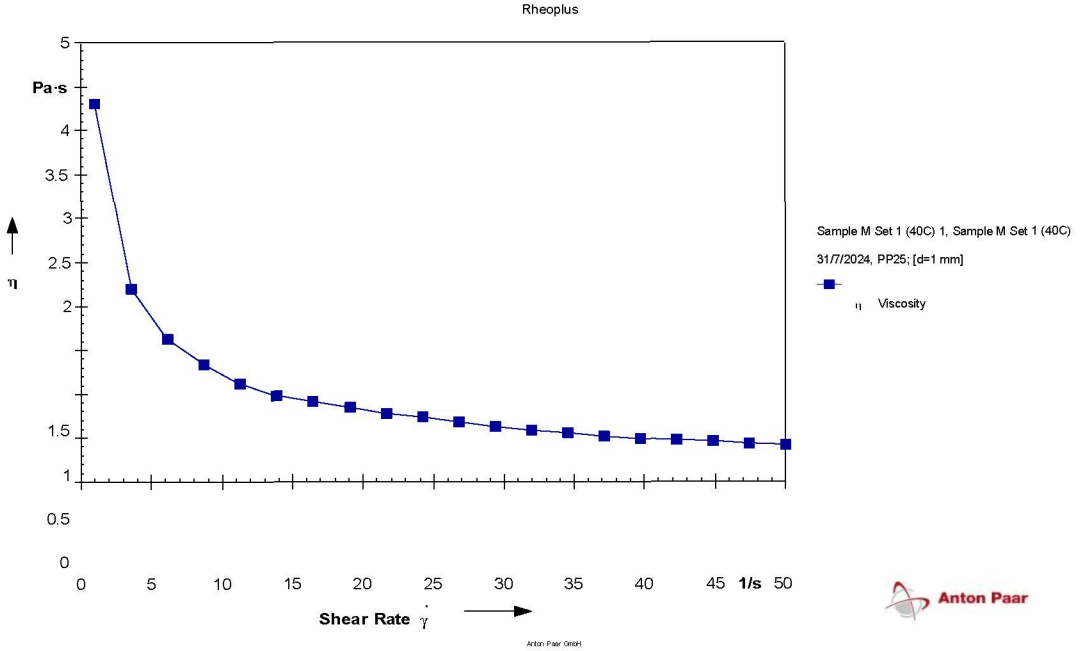

Sample M1 (40 ℃)

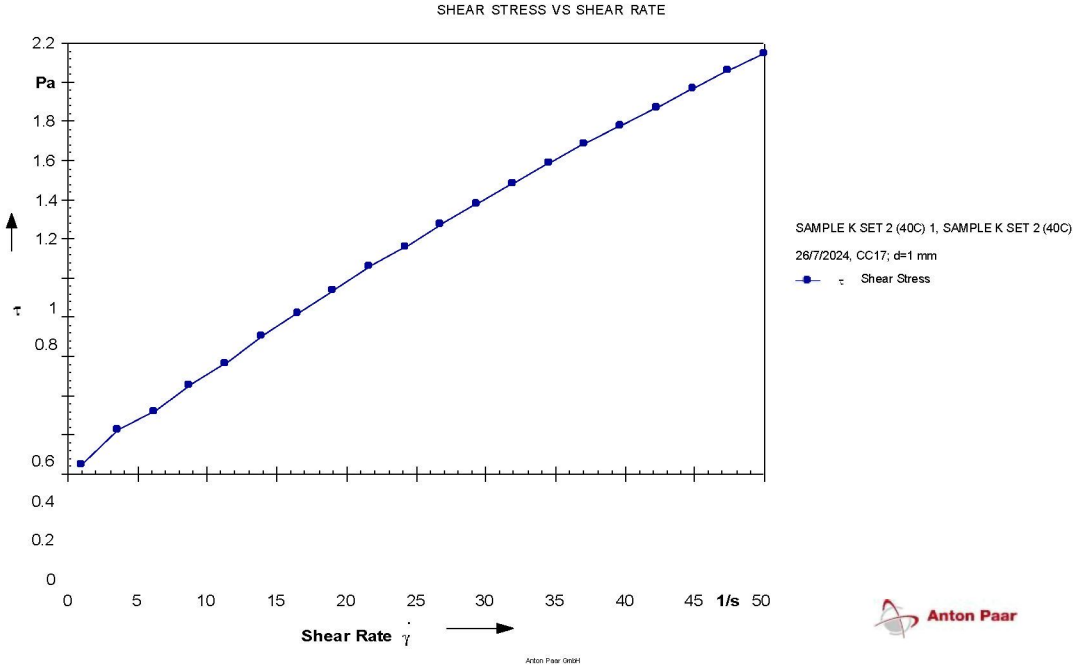

Sample K2 (40 ˚C)

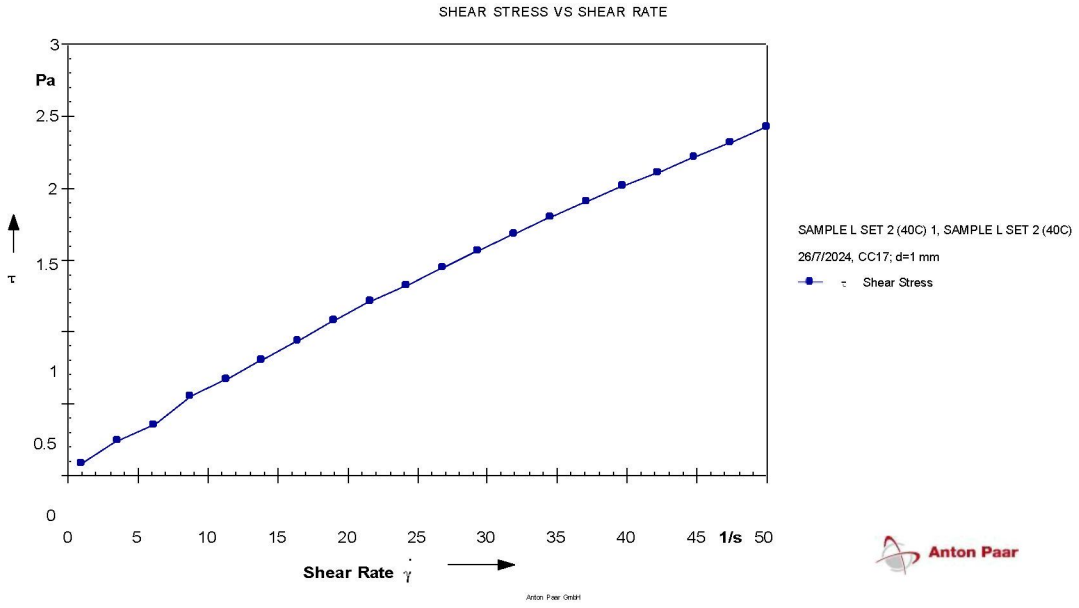

Sample L2 (40 ˚C)

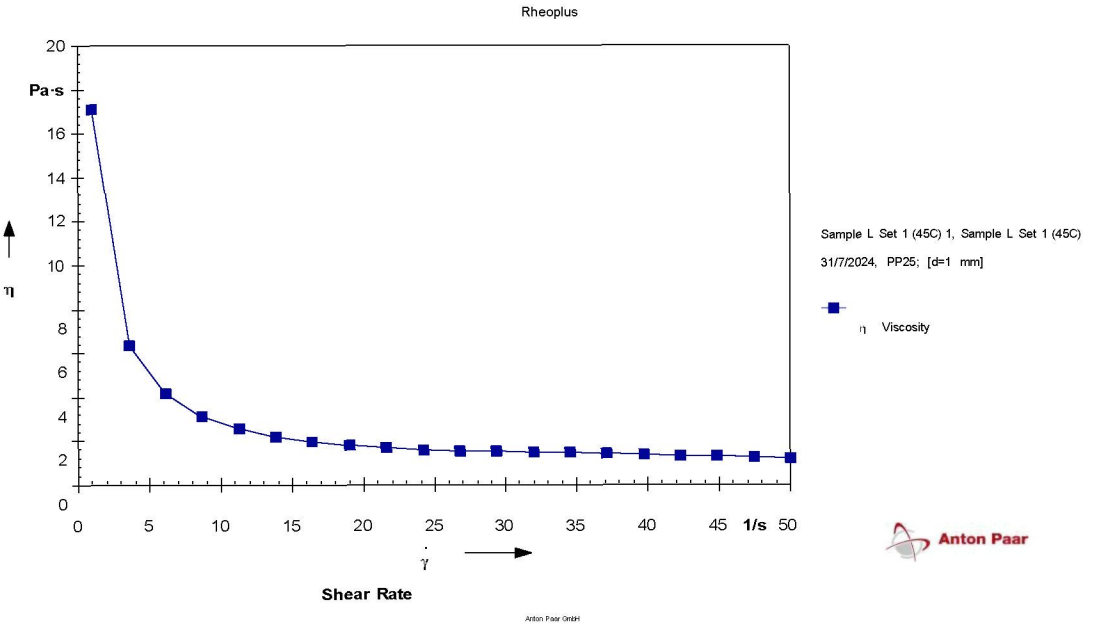

Sample L1 (45 °C)

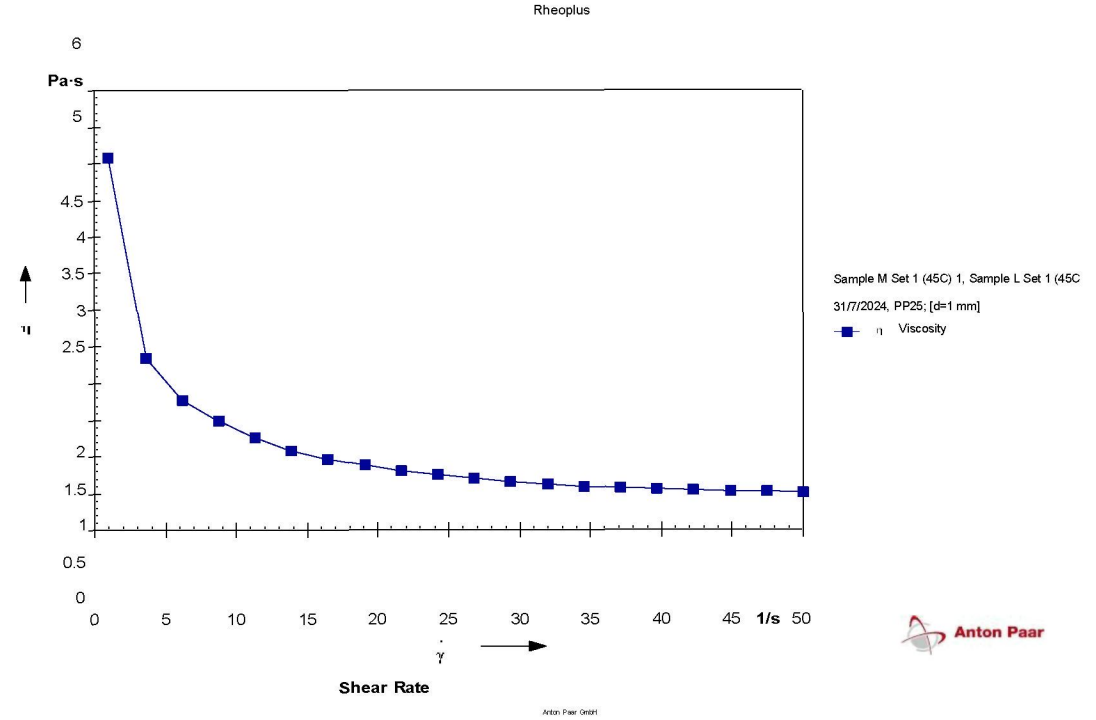

Sample M1 (45 °C)

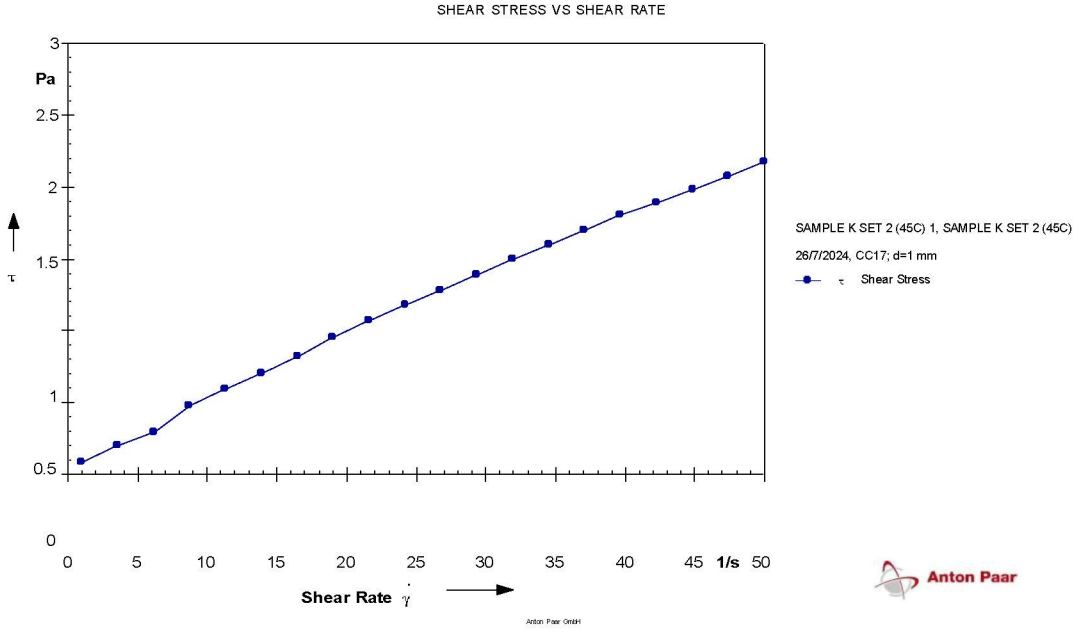

Sample K2 (45 ˚C)

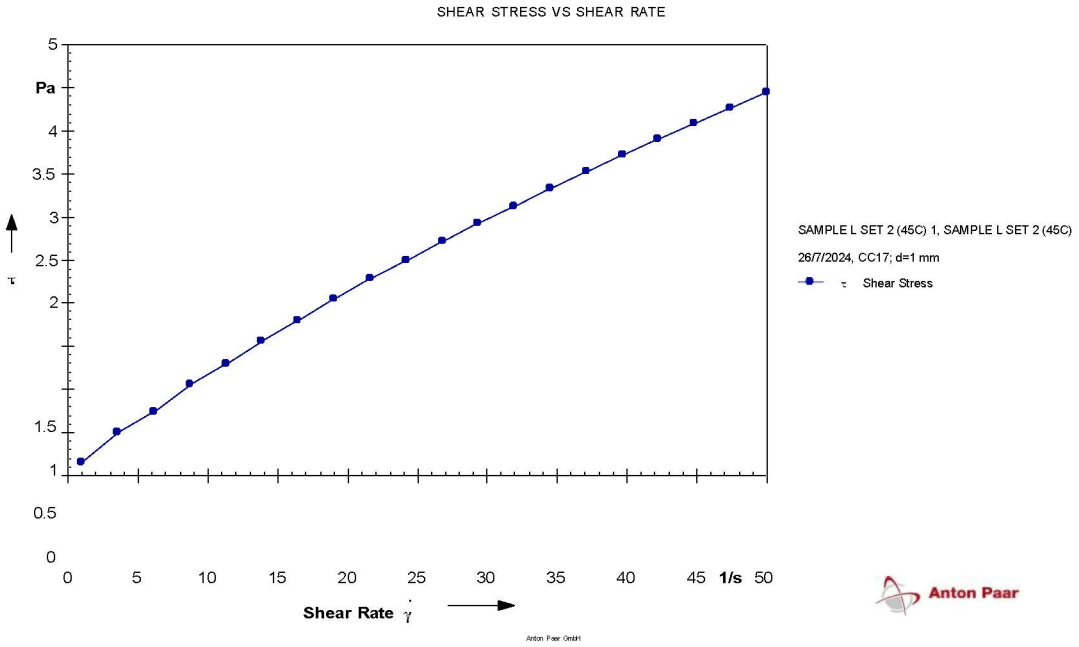

Sample L2 (45 ˚C)

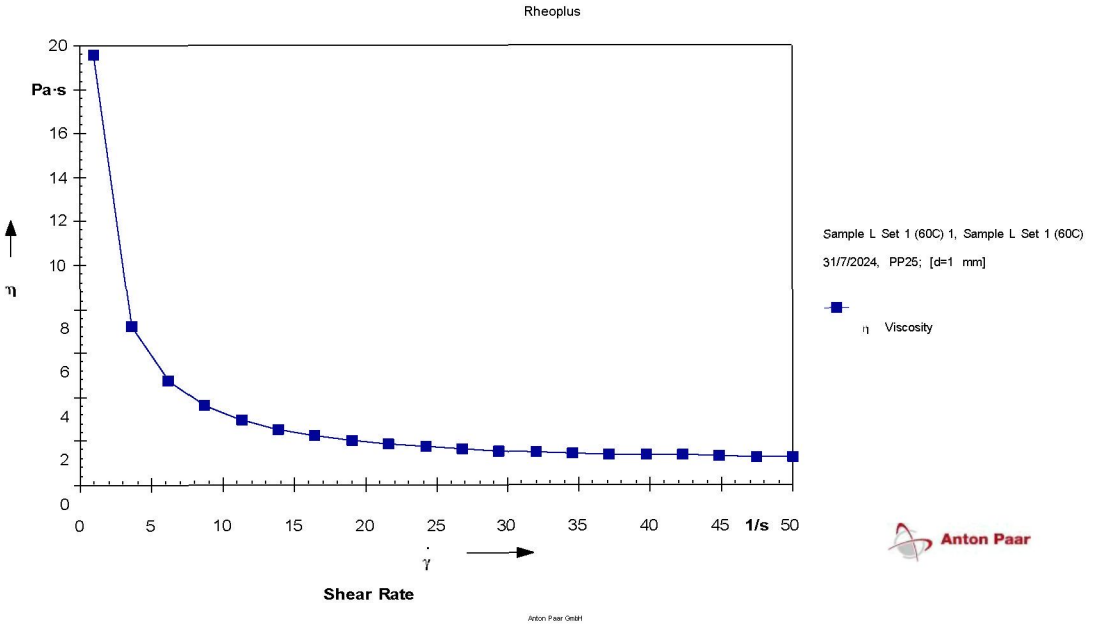

Sample L1 (60 ˚C)

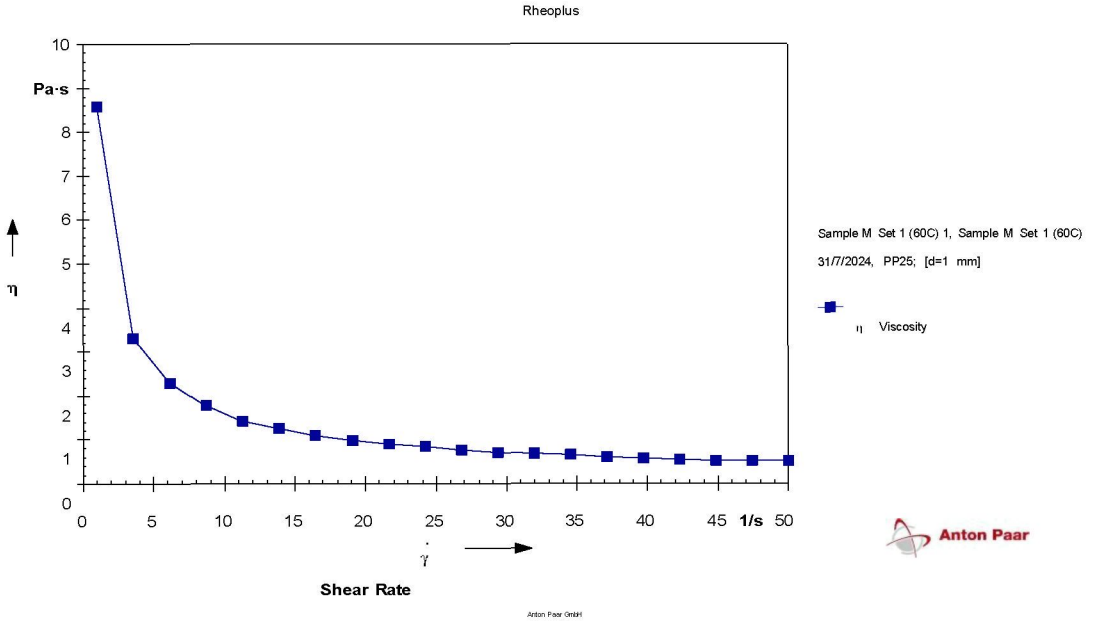

Sample M1 (60 ˚C)

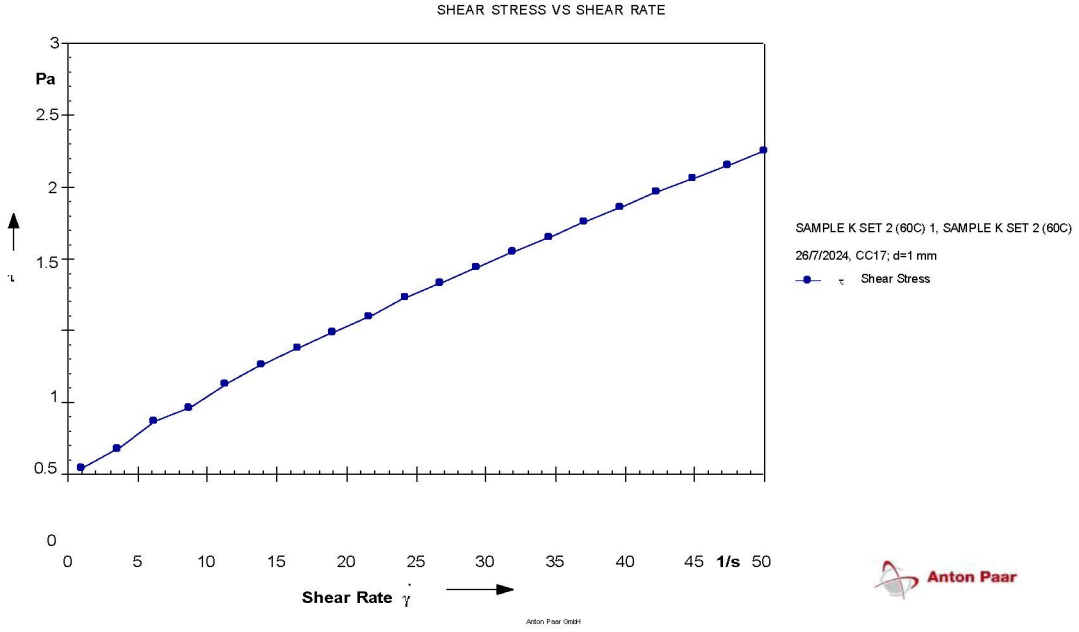

Sample K2 (60 ˚C)

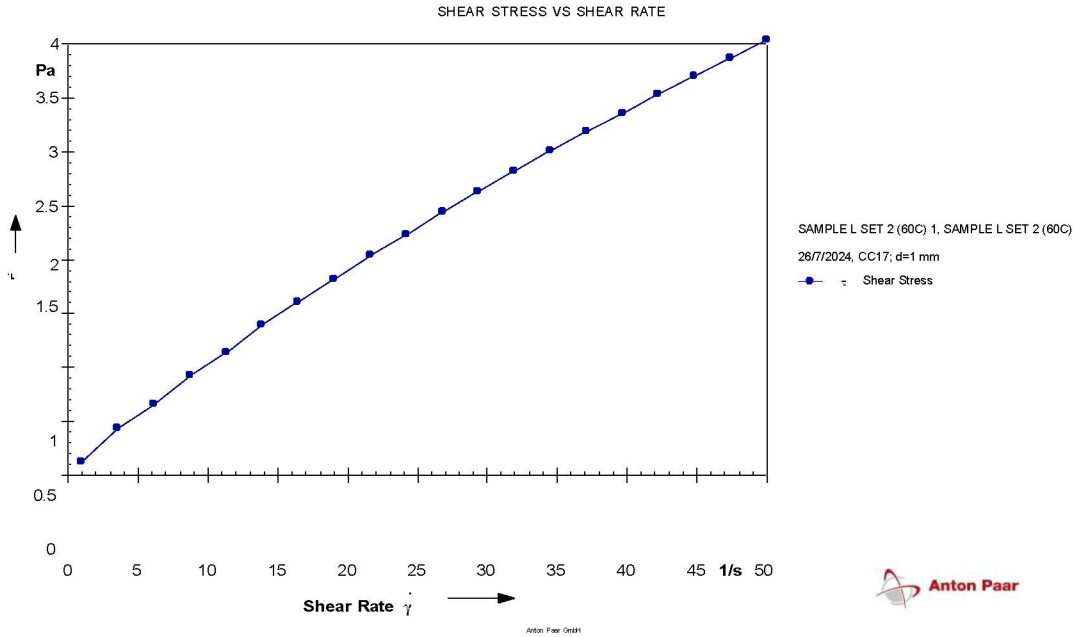

Sample L2 (60 ˚C)

APPENDIX K

Sample M1 (30 ˚C)

1) **Mean,** $\bar{x}$

$$\frac{13+14+9+12+12+11+12+14+13+13}{10} = 12.30$$

2) **Standard deviation,** s

$$\sqrt{\frac{(13-12.3)^2+(14-12.3)^2+(9-12.3)^2+(12-12.3)^2+(12-12.3)^2+(11-12.3)^2+(12-12.3)^2+(14-12.3)^2+(13-12.3)^2+(13-12.3)^2}{10-1}}$$

$$=1.494$$

3) **Confidence Interval,** CI

$$12.30 \pm \frac{(2.262)(1.494)}{\sqrt{10}} = 1.069$$

Sample K2 (30 ˚C)

1) **Mean,** $\bar{x}$

$$\frac{16+16+15+20+22+21+20+22+16+20}{10} = 18.80$$

2) **Standard deviation,** s

$$\sqrt{\frac{(16-18.8)^2+(16-18.8)^2+(15-18.8)^2+(20-18.8)^2+(22-18.8)^2+(21-18.8)^2+(20-18.8)^2+(22-18.8)^2+(16-18.8)^2+(20-18.8)^2}{10-1}}$$

$$=2.741$$

3) **Confidence Interval,** CI

$$18.80 \pm \frac{(2.262)(2.741)}{\sqrt{10}} = 1.961$$

Sample L2 (30 ˚C)

1) **Mean,** $\bar{x}$

$$\frac{38+35+37+35+36+38+35+35+38+38}{10} = 36.50$$

2) **Standard deviation,** s

$$\sqrt{\frac{(38-36.5)^2+(35-36.5)^2+(37-36.5)^2+(35-36.5)^2+(36-36.5)^2+(38-36.5)^2+(35-36.5)^2+(35-36.5)^2+(38-36.5)^2+(38-36.5)^2}{10-1}}$$

$$=1.434$$

3) **Confidence Interval,** CI

$$36.50 \pm \frac{(2.262)(1.434)}{\sqrt{10}} = 1.026$$

Sample M1 (35 ˚C)

1) **Mean,** $\bar{x}$

$$\frac{11+10+9+10+9+9+9+9+9+9}{10} = 9.40$$

2) **Standard deviation,** s

$$\sqrt{\frac{(11-9.4)^2+(10-9.4)^2+(9-9.4)^2+(10-9.4)^2+(9-9.4)^2+(9-9.4)^2+(9-9.4)^2+(9-9.4)^2+(9-9.4)^2+(9-9.4)^2}{10-1}}$$

$$=0.699$$

3) **Confidence Interval,** CI

$$9.40 \pm \frac{(2.262)(0.699)}{\sqrt{10}} = 0.500$$

Sample K2 (35 ˚C)

1) **Mean,** $\bar{x}$

$$\frac{20+21+21+23+20+20+23+20+23+21}{10} = 21.20$$

2) **Standard deviation,** s

$$\sqrt{\frac{(20-21.2)^2+(21-21.2)^2+(21-21.2)^2+(23-21.2)^2+(20-21.2)^2+(20-21.2)^2+(23-21.2)^2+(20-21.2)^2+(23-21.2)^2+(21-21.2)^2}{10-1}}$$

$$=1.317$$

3) **Confidence Interval,** CI

$$21.2 \pm \frac{(2.262)(1.317)}{\sqrt{10}} = 0.942$$

Sample L2 (35 ˚C)

1) **Mean,** $\bar{x}$

$$\frac{15+17+15+15+14+13+14+15+18+18}{10} = 15.50$$

2) **Standard deviation,** s

$$\sqrt{\frac{(15-15.4)^2+(17-15.4)^2+(15-15.4)^2+(15-15.4)^2+(14-15.4)^2+(13-15.4)^2+(14-15.4)^2+(15-15.4)^2+(18-15.4)^2+(18-15.4)^2}{10-1}}$$

$$=1.713$$

3) **Confidence Interval,** CI

$$15.50 \pm \frac{(2.262)(1.713)}{\sqrt{10}} = 1.22$$

Sample M1 (40 ˚C)

1) **Mean,** $\bar{x}$

$$\frac{8+8+8+8+8+8+9+9+8+8}{10} = 8.20$$

2) **Standard deviation,** s

$$\sqrt{\frac{(8-8.2)^2+(8-8.2)^2+(8-8.2)^2+(8-8.2)^2+(8-8.2)^2+(8-8.2)^2+(9-8.2)^2+(9-8.2)^2+(8-8.2)^2+(8-8.2)^2}{10-1}}$$

$$=0.422$$

3) **Confidence Interval,** CI

$$8.20 \pm \frac{(2.262)(0.422)}{\sqrt{10}} = 0.302$$

Sample K2 (40 ˚C)

1) **Mean,** $\bar{x}$

$$\frac{17+18+15+17+18+17+17+18+16+17}{10} = 17.00$$

2) **Standard deviation,** s

$$\sqrt{\frac{(17-17)^2+(18-17)^2+(15-17)^2+(17-17)^2+(18-17)^2+(17-17)^2+(17-17)^2+(18-17)^2+(16-17)^2+(17-17)^2}{10-1}}$$

$$=0.943$$

3) **Confidence Interval,** CI

$$15.00 \pm \frac{(2.262)(1.7)}{\sqrt{10}} = 0.674$$

Sample L2 (40 ˚C)

1) **Mean,** $\bar{x}$

$$\frac{12+15+15+16+13+13+13+14+13+13}{10} = 13.70$$

2) **Standard deviation,** s

$$\sqrt{\frac{(12-13.7)^2+(15-13.7)^2+(15-13.7)^2+(16-13.7)^2+(13-13.7)^2+(13-13.7)^2+(13-13.7)^2+(14-13.7)^2+(13-13.7)^2+(13-13.7)^2}{10-1}}$$

$$=1.252$$

3) **Confidence Interval,** CI

$$13.70 \pm \frac{(2.262)(1.252)}{\sqrt{10}} = 0.895$$

Sample L1 (45 ˚C)

1) **Mean,** $\bar{x}$

$$\frac{8+9+8+9+8+7+7+6+7+7}{10} = 7.60$$

2) **Standard deviation,** s

$$\sqrt{\frac{(8-7.6)^2+(9-7.6)^2+(8-7.6)^2+(9-7.6)^2+(8-7.6)^2+(7-7.6)^2+(7-7.6)^2+(6-7.6)^2+(7-7.6)^2+(7-7.6)^2}{10-1}}$$

$$=0.966$$

3) **Confidence Interval,** CI

$$7.60 \pm \frac{(2.262)(0.966)}{\sqrt{10}} = 0.691$$

Sample M1 (45 ˚C)

1) **Mean,** $\bar{x}$

$$\frac{8+9+9+7+9+6+7+8+9+7}{10} = 7.90$$

2) **Standard deviation,** s

$$\sqrt{\frac{(8-7.9)^2+(9-7.9)^2+(9-7.9)^2+(7-7.9)^2+(9-7.9)^2+(6-7.9)^2+(7-7.9)^2+(8-7.9)^2+(9-7.9)^2+(7-7.9)^2}{10-1}}$$

$$=1.101$$

3) **Confidence Interval,** CI

$$7.90 \pm \frac{(2.262)(1.101)}{\sqrt{10}} = 0.787$$

Sample K2 (45 ˚C)

1) **Mean,** $\bar{x}$

$$\frac{23+23+23+25+23+25+23+25+22+25}{10} = 23.70$$

2) **Standard deviation,** s

$$\sqrt{\frac{(23-23.7)^2+(23-23.7)^2+(23-23.7)^2+(25-23.7)^2+(23-23.7)^2+(25-23.7)^2+(23-23.7)^2+(25-23.7)^2+(22-23.7)^2+(25-23.7)^2}{10-1}}$$

$$=1.160$$

3) **Confidence Interval,** CI

$$23.70 \pm \frac{(2.262)(1.160)}{\sqrt{10}} = 0.829$$

Sample L2 (45 ˚C)

1) **Mean,** $\bar{x}$

$$\frac{14+14+13+16+14+15+15+15+16+16}{10} = 14.80$$

2) **Standard deviation,** s

$$\sqrt{\frac{(14-14.8)^2+(14-14.8)^2+(13-14.8)^2+(16-14.8)^2+(14-14.8)^2+(15-14.8)^2+(15-14.8)^2+(15-14.8)^2+(16-14.8)^2+(16-14.8)^2}{10-1}}$$

$$=1.033$$

3) **Confidence Interval,** CI

$$14.80 \pm \frac{(2.262)(1.033)}{\sqrt{10}} = 0.739$$

Sample L1 (60 ˚C)

1) **Mean,** $\bar{x}$

$$\frac{8+8+9+8+7+9+7+8+8+8}{10} = 8.00$$

2) **Standard deviation,** s

$$\frac{\sqrt{(8-8)^2+(8-8)^2+(9-8)^2+(8-8)^2+(7-8)^2+(9-8)^2+(7-8)^2+(8-8)^2+(8-8)^2+(8-8)^2}}{10-1}$$

$$=0.667$$

3) **Confidence Interval,** CI

$$8.00 \pm \frac{(2.262)(0.667)}{\sqrt{10}} = 0.477$$

Sample M1 (60 ˚C)

1) **Mean,** $\bar{x}$

$$\frac{8+9+7+9+7+7+7+9+8+7}{10} = 7.80$$

2) **Standard deviation,** s

$$\sqrt{\frac{(8-7.8)^2+(9-7.8)^2+(7-7.8)^2+(9-7.8)^2+(7-7.8)^2+(7-7.8)^2+(7-7.8)^2+(9-7.8)^2+(8-7.8)^2+(7-7.8)^2}{10-1}}$$

$$=0.919$$

3) **Confidence Interval,** CI

$$7.80 \pm \frac{(2.262)(0.919)}{\sqrt{10}} = 0.657$$

Sample K2 (60 ˚C)

1) **Mean,** $\bar{x}$

$$\frac{19+21+20+19+17+20+21+21+18+18}{10} = 19.40$$

2) **Standard deviation,** s

$$\sqrt{\frac{(19-19.4)^2+(21-19.4)^2+(20-19.4)^2+(19-19.4)^2+(17-19.4)^2+(20-19.4)^2+(21-19.4)^2+(21-19.4)^2+(18-19.4)^2+(18-19.4)^2}{10-1}}$$

$$=1.430$$

3) **Confidence Interval,** CI

$$19.40 \pm \frac{(2.262)(1.430)}{\sqrt{10}} = 1.023$$

Sample L2 (60 ˚C)

1) **Mean,** $\bar{x}$

$$\frac{17+18+20+21+20+18+17+20+17+20}{10} = 18.80$$

2) **Standard deviation,** s

$$\sqrt{\frac{(17-18.8)^2+(18-18.8)^2+(20-18.8)^2+(21-18.8)^2+(20-18.8)^2+(18-18.8)^2+(17-18.8)^2+(20-18.8)^2+(17-18.8)^2+(20-18.8)^2}{10-1}}$$

$$=1.549$$

3) **Confidence Interval,** CI

$$18.80 \pm \frac{(2.262)(1.549)}{\sqrt{10}} = 1.108$$

AUTHOR'S PROFILE

Muhammad Afif Syazani obtained his Bachelor of Science (Hons.) in Chemistry from Universiti Teknologi MARA (UiTM) and is currently pursuing a Master of Science in Chemistry at the same institution. His postgraduate research focuses on the stability of virgin coconut oil-in-water emulsions using mixed surfactants, specifically nonethylene glycol (MEG), Span 20, and Span 80. The study integrates both experimental and computational approaches to assess the physicochemical and molecular behavior of emulsions. He has gained practical experience in emulsion formulation and characterization techniques, including phase separation analysis, centrifugation testing, thermal cycling, and droplet size observation using optical microscopy. In addition, he is proficient in the use of a pendant drop tensiometer for interfacial tension measurements, a rotational rheometer for rheological profiling, and contact angle analysis to study surface interactions. Complementing his experimental work, Afif has also developed expertise in molecular dynamics (MD) simulations using GROMACS, involving model construction, energy minimization, system equilibration under NVT and NPT ensembles, and trajectory analysis. Prior to his postgraduate studies, he worked as a Quality Control Laboratory Analyst at Century Chemical Works, where he was involved in routine quality assessments, raw material verification, and instrumental analysis.

List of Publication:

Afif, M., Rozani, S., Amani, H., Hamid, A., Hadzir, N. M., Alif, M., Latif, M., & Som, A. M. (2024). Virgin Coconut Oil-Based Emulsion And Its Benefits: A Review. In *Malaysian Journal of Analytical Sciences* (Vol. 28).

Afif, M., Rozani, S., Amani, H., Hamid, A., Hadzir, N. M., Alif, M., Latif, M., & Som, A. M. (2024). Evaluation Of Virgin Coconut Oil-In-Water Emulsion Stability: Insights From Creaming Index And Polarised Light Microscopy Analyses. *Malaysian Journal of Microscopy*, 2024(20), 174–185.

Afif, M., Rozani, S., Amani, H., Hamid, A., Hadzir, N. M., Syaabani, M., Rafie, M., Alif, M., Latif, M., Fadilla, B. M., Said, Z., & Saidur, R. (2025). Enhanced Thermal Stability of Virgin Coconut Oil-in-Water Emulsions using Mixed Surfactants: Impact on Droplet Size and Phase Separation. *Journal of Advanced Research in Micro and Nano Engineering Journal Homepage: Journal of Advanced Research in Micro and Nano Engineering*, *42*(1), 30–57.

PERPUSTAKAAN TUN ABDUL RAZAK
BAHAGIAN SUMBER RUJUKAN UNIVERSITI (BSRU)

BORANG PENYERAHAN BAHAN HARTA INTELEK UiTM

UiTM's Intellectual Property Submission Form

Nama (*Name*) : MUHAMMAD AFIF SYAZANI BIN ROZANI

Fakulti/Pusat Akademik/Bahagian : FAKULTI SAINS GUNAAN
Faculty / Academic Centres / Department

No. Telefon (Pejabat / Hp) : _____
Telephone No. (Office / handphone)

E-mel (E-mail) : afifsyazani29@gmail.com

Tarikh (*Date*) : 17 MARCH 2026

Pihak Fakulti / Pusat Akademik / Bahagian / Saya bersetuju bahawa dokumen dan tajuk yang disenaraikan untuk dimasukkan ke dalam Repositori Institusi UiTM.
The Faculty / Academic Centres / Department / I agree that the document and titles listed below to be placed in the UiTM Institutional Repository.

JENIS BAHAN (Sila nyatakan) : THESES
Types of Material (Please specify) :

Types of Material:
Article / Book / Theses / Bulletin / Seminar / Image / Entrepreneurship / Student Project / Research Report / Industrial Training / Annual Report / Manual / Oral History / Exam Paper / Speech / Dataset / Audio / Video / Others

MAKLUMAT BAHAN *(Information of Materials)*:

Bil. *No.*	JUDUL BAHAN *Title*	HARDCOPY *(√)*	SOFTCOPY *(√)*
1.	STABILITY EVALUATION AND CHARACTERIZATION OF OIL-IN-WATER EMULSION USING METHYL-A-D-GLUCOPYRANOSIDE AND SPAN SURFACTANT SERIES WITH MOLECULARDYNAMIC SIMULATION		/

** **Sila sediakan lampiran sekiranya ruangan yang disediakan tidak mencukupi** (Please provide attachment if necessary)*

TUJUAN PENYERAHAN BAHAN (Sila tandakan √):

Purpose (Please mark √):

1. **Bahan untuk dimuat naik ke dalam Repositori Institusi UiTM:** [/]
   (Materials for uploading into the UiTM Institutional Repository (UiTM IR)):
   Fakulti / Pusat Akademik / Bahagian / Saya perlu memastikan bahawa setiap dokumen telah dibuat semakan terlebih dahulu dan tidak mengandungi sebarang maklumat sulit sebelum diserahkan kepada pihak PTAR.
   The Faculty / Academic Centres / Department must ensure that each document has been reviewed in advance and does not contain any confidential information before being submitted to PTAR).
2. **Bahan mengandungi maklumat TERHAD yang telah ditentukan oleh organisasi / badan di mana penyelidikan dijalankan:** [/]
   (Materials consisting of RESTRICTED information which has been determined by the organisation/body where the research was conducted):
   Sila nyatakan tarikh tamat embargo (jika ada)*:*
   (Please indicate the embargo expiry date (if any)):
   Embargo expiry date: Day: [ ] *Month:* [ ] *Year:* [ ]

   Nota: Embargo Expiry Date adalah tarikh tamat tempoh yang ditetapkan oleh penulis di mana pada atau selepas tarikh ini, bahan tersebut akan dipaparkan secara langsung di Repositori Institusi UiTM dan ianya boleh diakses.
   Note: Embargo Expiry Date *is the date that an author or a publisher imposed embargo expires. On and after this date, this document will be accessible in UiTM Institutional Repository.*
3. **Bahan boleh diakses secara teks penuh dan terbuka.** [/]
   (Materials can be accessed in full text via open access).
4. **Bahan dipinjamkan sementara untuk tujuan pendigitalan dan akan dikembalikan semula kepada pemilik.** [/]
   (Materials are on temporary loan for digitization and will be returned to the owner).

Pemberitahuan: Jika Repositori Institusi UiTM menerima bukti pelanggaran hak cipta, bahan yang berkaitan akan dikeluarkan serta-merta.
(Notification: If UiTM Institutional Repository receives proof of copyright violation, the relevant item will be removed immediately).

PERAKUAN:

Declaration:

Saya / kami akan bertanggungjawab ke atas bahan yang diserahkan untuk pendigitalan dan muat naik ke dalam Repositori Institusi UiTM.
I / we will be responsible for the materials submitted for digitization and uploaded into UiTM Institutional Repository.

Tandatangan Pemohon
Applicant Signature
Tarikh (*Date*): 17 MARCH 2026

Tandatangan dan Cap ~~Ketua Jabatan /~~
~~*Head of Division / Department /*~~ *Supervi*
Tarikh (*Date*):

CHM. DR HAIRUL AMANI BT ABDUL HAMID
Senior Lecturer
Faculty of Applied Sciences
Universiti Teknologi MARA
40450 Shah Alam
Selangor, Malaysia

UNTUK KEGUNAAN PEJABAT (*For office use*) 17 MARCH 2026

DITERIMA OLEH / *Received By* :
TANDATANGAN / *Signature* :
TARIKH / *Date* :

DISAHKAN OLEH / Certified *By* :
TANDATANGAN / *Signature* :
TARIKH / *Date* :